



**HAL**  
open science

# Experimental study and modelling on methane hydrates crystallization under flow from a water-oil dispersion at high water cut

Trung-Kien Pham

► **To cite this version:**

Trung-Kien Pham. Experimental study and modelling on methane hydrates crystallization under flow from a water-oil dispersion at high water cut. Other. Université de Lyon, 2018. English. NNT : 2018LYSEM012 . tel-02869624

**HAL Id: tel-02869624**

**<https://theses.hal.science/tel-02869624>**

Submitted on 16 Jun 2020

**HAL** is a multi-disciplinary open access archive for the deposit and dissemination of scientific research documents, whether they are published or not. The documents may come from teaching and research institutions in France or abroad, or from public or private research centers.

L'archive ouverte pluridisciplinaire **HAL**, est destinée au dépôt et à la diffusion de documents scientifiques de niveau recherche, publiés ou non, émanant des établissements d'enseignement et de recherche français ou étrangers, des laboratoires publics ou privés.



N°d'ordre NNT : 2018LYSEM012

**THESE de DOCTORAT DE L'UNIVERSITE DE LYON**  
opérée au sein de  
**l'Ecole des Mines de Saint-Etienne**

**Ecole Doctorale N° 488**  
**Sciences, Ingénierie, Santé**

**Spécialité de doctorat** : Génie des Procédés  
**Discipline** : DS8 Sciences pour l'ingénieur

Soutenue publiquement le 26/06/2018, par :  
**Trung-Kien PHAM**

---

**ETUDE EXPERIMENTALE ET MODELISATION DE LA CRISTALLISATION  
D'HYDRATES DE METHANE EN ECOULEMENT A PARTIR D'UNE  
DISPERSION EAU-HUILE A FORT POURCENTAGE D'EAU**

**EXPERIMENTAL STUDY AND MODELLING ON METHANE HYDRATES  
CRYSTALLIZATION UNDER FLOW FROM A WATER-OIL DISPERSION  
AT HIGH WATER CUT**

---

Devant le jury composé de :

Christelle GOUTAUDIER	Professeure, Université Claude Bernard - Lyon 1, Lyon, France	Présidente
Didier DALMAZZONE	Professeur, ENSTA ParisTech, Palaiseau, France	Rapporteur
Antonin CHAPOY	Senior Research Fellow, Heriot-Watt University, Edinburgh, United Kingdom	Rapporteur
Jean-Michel HERRI	Professeur, École Nationale Supérieure des Mines de Saint-Étienne, Saint-Étienne, France	Directeur de thèse
Ana CAMEIRAO	Professeure, École Nationale Supérieure des Mines de Saint-Étienne, Saint-Étienne, France	Co-Directrice de thèse
Philippe GLENAT	Ingénieur de Recherche, TOTAL-CSTJF, Pau, France	Invité

**Spécialités doctorales**  
 SCIENCES ET GENIE DES MATERIAUX  
 MECANIQUE ET INGENIERIE  
 GENIE DES PROCEDES  
 SCIENCES DE LA TERRE  
 SCIENCES ET GENIE DE L'ENVIRONNEMENT

**Responsables**  
 K. Wolski Directeur de recherche  
 S. Drapier, professeur  
 F. Gruy, Maître de recherche  
 B. Guy, Directeur de recherche  
 D. Grailot, Directeur de recherche

**Spécialités doctorales**  
 MATHEMATIQUES APPLIQUEES  
 INFORMATIQUE  
 SCIENCES DES IMAGES ET DES FORMES  
 GENIE INDUSTRIEL  
 MICROELECTRONIQUE

**Responsables**  
 O. Roustant, Maître-assistant  
 O. Boissier, Professeur  
 J.C. Pinoli, Professeur  
 X. Delorme, Maître assistant  
 Ph. Lalevée, Professeur

**EMSE : Enseignants-chercheurs et chercheurs autorisés à diriger des thèses de doctorat (titulaires d'un doctorat d'État ou d'une HDR)**

ABSI	Nabil	CR	Génie industriel	CMP
AUGUSTO	Vincent	CR	Image, Vision, Signal	CIS
AVRIL	Stéphane	PR2	Mécanique et ingénierie	CIS
BADEL	Pierre	MA(MDC)	Mécanique et ingénierie	CIS
BALBO	Flavien	PR2	Informatique	FAYOL
BASSEREAU	Jean-François	PR	Sciences et génie des matériaux	SMS
BATTON-HUBERT	Mireille	PR2	Sciences et génie de l'environnement	FAYOL
BEIGBEDER	Michel	MA(MDC)	Informatique	FAYOL
BLAYAC	Sylvain	MA(MDC)	Microélectronique	CMP
BOISSIER	Olivier	PR1	Informatique	FAYOL
BONNEFOY	Olivier	MA(MDC)	Génie des Procédés	SPIN
BORBELY	Andras	MR(DR2)	Sciences et génie des matériaux	SMS
BOUCHER	Xavier	PR2	Génie Industriel	FAYOL
BRODHAG	Christian	DR	Sciences et génie de l'environnement	FAYOL
BRUCHON	Julien	MA(MDC)	Mécanique et ingénierie	SMS
CAMEIRAO	Ana	MA(MDC)	Génie des Procédés	SPIN
CHRISTIE	Frédéric	PR	Science et génie des matériaux	SMS
DAUZERE-PERES	Stéphane	PR1	Génie Industriel	CMP
DEBAYLE	Johan	MR	Sciences des Images et des Formes	SPIN
DEGEORGE	Jean-Michel	MA(MDC)	Génie industriel	Fayol
DELAFOSSÉ	David	PR0	Sciences et génie des matériaux	SMS
DELORME	Xavier	MA(MDC)	Génie industriel	FAYOL
DESRAYAUD	Christophe	PR1	Mécanique et ingénierie	SMS
DJENZIAN	Thierry	PR	Science et génie des matériaux	CMP
DOUCE	Sandrine	PR2	Sciences de gestion	FAYOL
DRAPIER	Sylvain	PR1	Mécanique et ingénierie	SMS
FAUCHEU	Jenny	MA(MDC)	Sciences et génie des matériaux	SMS
FAVERGEON	Loïc	CR	Génie des Procédés	SPIN
FEILLET	Dominique	PR1	Génie Industriel	CMP
FOREST	Valérie	MA(MDC)	Génie des Procédés	CIS
FRACZKIEWICZ	Anna	DR	Sciences et génie des matériaux	SMS
GARCIA	Daniel	MR(DR2)	Sciences de la Terre	SPIN
GAVET	Yann	MA(MDC)	Sciences des Images et des Formes	SPIN
GERINGER	Jean	MA(MDC)	Sciences et génie des matériaux	CIS
GOEURIOT	Dominique	DR	Sciences et génie des matériaux	SMS
GONDRAN	Natacha	MA(MDC)	Sciences et génie de l'environnement	FAYOL
GONZALEZ FELIU	Jesus	MA(MDC)	Sciences économiques	FAYOL
GRAILLOT	Didier	DR	Sciences et génie de l'environnement	SPIN
GROSSEAU	Philippe	DR	Génie des Procédés	SPIN
GRUY	Frédéric	PR1	Génie des Procédés	SPIN
GUY	Bernard	DR	Sciences de la Terre	SPIN
HAN	Woo-Suck	MR	Mécanique et ingénierie	SMS
HERRI	Jean Michel	PR1	Génie des Procédés	SPIN
KERMOUCHE	Guillaume	PR2	Mécanique et Ingénierie	SMS
KLOCKER	Helmut	DR	Sciences et génie des matériaux	SMS
LAFOREST	Valérie	MR(DR2)	Sciences et génie de l'environnement	FAYOL
LERICHE	Rodolphe	CR	Mécanique et ingénierie	FAYOL
MALLIARAS	Georges	PR1	Microélectronique	CMP
MOLIMARD	Jérôme	PR2	Mécanique et ingénierie	CIS
MOUTTE	Jacques	CR	Génie des Procédés	SPIN
NEUBERT	Gilles			FAYOL
NIKOLOVSKI	Jean-Pierre	Ingénieur de recherche	Mécanique et ingénierie	CMP
NORTIER	Patrice	PR1	Génie des Procédés	SPIN
O CONNOR	Rodney Philip	MA(MDC)	Microélectronique	CMP
OWENS	Rosin	MA(MDC)	Microélectronique	CMP
PERES	Véronique	MR	Génie des Procédés	SPIN
PICARD	Gauthier	MA(MDC)	Informatique	FAYOL
PIJOLAT	Christophe	PR0	Génie des Procédés	SPIN
PINOLI	Jean Charles	PR0	Sciences des Images et des Formes	SPIN
POURCHEZ	Jérémy	MR	Génie des Procédés	CIS
ROUSSY	Agnès	MA(MDC)	Microélectronique	CMP
ROUSTANT	Olivier	MA(MDC)	Mathématiques appliquées	FAYOL
SANAUR	Sébastien	MA(MDC)	Microélectronique	CMP
STOLARZ	Jacques	CR	Sciences et génie des matériaux	SMS
TRIA	Assia	Ingénieur de recherche	Microélectronique	CMP
VALDIVIESO	François	PR2	Sciences et génie des matériaux	SMS
VIRICELLE	Jean Paul	DR	Génie des Procédés	SPIN
WOLSKI	Krzystof	DR	Sciences et génie des matériaux	SMS
XIE	Xiaolan	PR0	Génie industriel	CIS
YUGMA	Gallian	CR	Génie industriel	CMP

## DEDICATION

This thesis work is dedicated to my beloved son **Hoang Quan**, to my lovely daughter **Khanh Chi** and especially to my wife **Hoang Thu** who has always been beside, supported and encouraged me with endless love and firmly believed that I could overcome this challenging Ph.D. research.

## ACKNOWLEDGEMENTS

I would like to thank the following individuals who have significantly contributed to this Ph.D. thesis. This research work would not have been possible without their total support and gentle encouragement.

I would like to express my deepest thanks and my sincere appreciation to my supervisors: **Prof. Jean-Michel HERRI** and **Prof. Ana CAMEIRAO** who accepted me to do Ph.D. research as a member of Gas Hydrate Dynamics Centre, École Nationale Supérieure des Mines de Saint-Étienne (ENSM-SE). I gratefully acknowledge their continuous encouragement and generous support in my research journey with the excellent advice, valuable guidance, endless patience and profound knowledge. They have been leading me to the world of gas hydrate and flow assurance and inspiring me to do science in this field. Truly, I have benefited so much from their expertise supervision and excellent ideas and I have greatly appreciated these. Honestly, it was my honor and fortune to work with them and in a very friendly, international, and dynamic hydrate research team in SPIN Centre, ENSM-SE which helped me to be more mature in the research career.

I am grateful to **Mr. Philippe GLENAT** from TOTAL E&P who has always accompanied me on the Archimède-3 project to support me in overcoming the obstacles to my research. Importantly, his fruitful comments, periodic meeting discussions and perspectives were very helpful for me to progress my research and deeper understand the experimental results and the gas hydrate management strategies in flow assurance in the industrial scale. Indeed, I have much profited from his professional expertise and knowledge. It was my great privilege to work on the scientific project with the famous and global company as TOTAL and I had so much valuable and professional experience through doing research in an international environment which has shaped me as a researcher.

I would like to thank the thesis committee members: **Mr. Didier DALMAZZONE**, **Mr. Antonin CHAPOY**, and **Ms. Christelle GOUTAUDIER** for the acceptance to evaluate my Ph.D. work. I highly appreciate their useful suggestions and constructive comments which helped to improve the quality of this study.

I would like to thank the technicians and personnel in SPIN and SMS-MPE laboratory of ENSM-SE: **Mr. Fabien CHAUVY**, **Mr. Jean-Pierre POYET**, **Mr. Marc ROUVIERE**, **Mr. Richard DROGO**, **Mr. Jérôme MANCUSO**, **Mr. Pierre-Jacques LIOTIER**, **Mme. Andrée-Aimée TOUCAS**, and **Mme. Marie-Claude BARTHOLIN** who have been always available to help me solve problems in scientific articles, informatics, and experimental techniques.

To my Brazilian friend, **Ms. Aline MENDES-MELCHUNA**, the former Ph.D. student at ENSM-SE, the postdoctoral researcher in Colorado School of Mines, I would like to thank her for all things that she has done for me: from the beginning of Ph.D. research with the introduction to Archimède project background, careful instruction to manipulate the flowloop, data analysis, and discussion to the end of my Ph.D. thesis with manuscript review and feedback. I would say that she is one of my best friends. I also would like to thank **Mr. Carlos LANGE-BASSANI** and **Mr. Vinicius RODRIGUES DE ALMEIDA** (the new Brazilian Ph.D. students) for their help and advice in modelling and corrections to the thesis, who will continue my work for the next phase of the research project with TOTAL.

To my colleagues and friends in the Gas Hydrate Dynamics Team and SPIN Centre at ENSM-SE, I would like to thank **Mr. Jérôme DOUZET**, **Mr. Son HO-VAN**, **Mr. Thang LE**, **Mr. Saheb MAGHSOODLOOBABAKHANI**, and **Mr. Hubert FAURE** who have helped me not only for solving daily problems in the experimentation, discussion of experimental results, writing and revisions to the dissertation but also for the great moments with them to relax with very funny and joking stories after a period of research hard working time. Moreover, I would like to thank the Chinese sabbatical Associate Professor **Dr. Wuchang WANG**, the former Vietnamese Ph.D. student at ENSM-SE **Dr. Du LE-QUANG**, and the Brazilian postdoctoral researcher **Dr. Rafael CHARIN** for the useful advice and discussion on my experimental planning. Additionally, I would like to thank all the internship, Master, Ph.D. students as well as the staff, personnel, lecturers, professors in SPIN Centre and in ENSM-SE for their useful and kind support and friendly advice.

To all my friends, colleagues (in Hanoi University of Mining and Geology) and grand family (my parents, my sister, and my brother, etc.) in Vietnam, I would like to thank and acknowledge their long-distance support and encouragement. They have helped me accomplish my responsibility in Vietnam by the best manners during the period of my Ph.D. research in France.

To my small family in France, I am grateful to my son **Hoang Quan PHAM**, my daughter **Hoang Khanh Chi PHAM**, and my wife **Thi Thu (PHAM) HOANG** for their endless love, unconditional support, and firm belief in my research career. The most beautiful words are dedicated to my wife for being with me through this challenging research journey and for encouraging me in the tough moments. Without these, I would not have achieved this goal.

I would like to express my sincere gratitude to **TOTAL E&P** for the financial support in the Archimède-3 project and their approval for publishing this thesis. Furthermore, I would like to acknowledge the contribution to technical support and reviewing this manuscript from the members of TOTAL and ENSM-SE. Thanks to funding from **Gas Hydrate Dynamics Centre, SPIN Laboratory,**

**École Nationale Supérieure des Mines de Saint-Étienne, ARMINES, and TOTAL E&P**, my research findings had the opportunities to present at several national and international conferences.

Finally, I would like to sincerely acknowledge **the Vietnam International Education Development (VIED), Ministry of Education and Training (MOET), Vietnamese Government** for the financial support through the Ph.D. scholarship program 911 and **Hanoi University of Mining and Geology** for allowing and supporting me to study Ph.D. abroad.

## TABLE OF CONTENTS

DEDICATION .....	A
ACKNOWLEDGEMENTS .....	C
TABLE OF CONTENTS .....	i
LIST OF FIGURES .....	vii
LIST OF TABLES .....	xv
NOMENCLATURE.....	xvi
LIST OF ABBREVIATIONS.....	xx
INTRODUCTION .....	xxiii
INTRODUCTION (IN FRENCH) .....	xxv
CHAPTER 1. LITERATURE REVIEW.....	1
1.1. Gas hydrate background .....	1
1.2. Gas hydrate issue in flow assurance .....	4
1.2.1. High-dosage (thermodynamic) hydrate inhibitors (THIs).....	5
1.2.2. Low-dosage hydrate inhibitors (LDHIs) .....	7
1.2.2.1. Kinetic hydrate inhibitors (KHIs).....	8
1.2.2.2. Hydrate Anti-Agglomerants (AA-LDHIs) .....	9
1.3. Emulsions and suspensions .....	11
1.3.1. Surfactants.....	11
1.3.2. Emulsions.....	12
1.3.2.1. Rheology of emulsions .....	13
1.3.2.2. Relative viscosity of emulsions.....	13
1.3.3. Hydrate formation and agglomeration in emulsion systems.....	15
1.3.3.1. Hydrate formation/dissociation and their effects on the emulsion stability.....	15
1.3.3.2. Agglomeration/deposition and plugging mechanisms.....	19
1.3.4. Rheology of water/oil/hydrate suspension.....	20
1.3.4.1. Relative viscosity models of suspension .....	21
1.3.4.2. Relative pressure drop models of suspension .....	24
1.4. Hydrate formation on the surface of gas bubbles .....	25
1.5. Multiphase flow and mass transfer in oil and gas pipelines .....	28
1.5.1. Single-phase flow .....	28

1.5.2.	Two-phase Gas-Liquid flow .....	28
1.5.3.	Two-phase Liquid-Liquid flow .....	29
1.5.4.	Three-phase Solid-Liquid-Liquid flow .....	30
1.5.5.	Mass transfer and coefficient of gas transfer ( $k_{La}$ ) .....	30
1.6.	Hydrate formation and plugging in the multiphase flowlines .....	32
1.6.1.	Oil and water-dominated systems .....	32
1.6.2.	Kinetic models of hydrate formation/deposition and plugging in pipelines.....	35
1.7.	Highlights and Conclusions.....	37
1.8.	Remarques et Conclusions (in French).....	38
CHAPTER 2. FLOWLOOP APPARATUS AND EXPERIMENTAL METHODOLOGY .....		39
2.1.	Archimède flowloop system.....	39
2.1.1.	Flowloop circulation .....	39
2.1.2.	Gas-lift riser and separator.....	41
2.1.3.	Compression system (ballasts).....	43
2.1.4.	Moineau pump .....	44
2.1.5.	Cooling systems.....	45
2.1.6.	Instruments .....	45
2.1.6.1.	Gas injection and compensation system.....	45
2.1.6.2.	Temperature/pressure and pressure drop sensors .....	46
2.1.6.3.	Flowmeter and densitometer.....	47
2.1.6.4.	FBRM probe.....	48
2.1.6.5.	PVM probe.....	51
2.2.	Interfacial tension measurement.....	52
2.3.	Materials.....	53
2.4.	Experimental procedure.....	53
2.4.1.	Experimental protocol with gas-lift system.....	53
2.4.1.1.	Dispersion .....	54
2.4.1.2.	Hydrate crystallization/dissociation .....	54
2.4.2.	Experimental protocol with Moineau pump with and without gas-lift system .....	55
2.4.2.1.	Dispersion and rheological study of dispersion.....	55
2.4.2.2.	Gas transfer and hydrate formation/dissociation.....	55
2.4.3.	Shutdown and restart tests.....	56
2.5.	Data acquisition and analysis .....	56

2.6.	Measurements and calculations .....	57
2.6.1.	Measurements .....	57
2.6.2.	$K_L a$ calculation .....	57
2.6.3.	Water conversion and hydrate volume.....	57
2.6.4.	Rate of crystallization .....	58
2.7.	Highlights.....	58
2.8.	Remarques (in French) .....	58
CHAPTER 3. EXPERIMENTAL RESULTS WITH GAS-LIFT (BUBBLES) IN THE RISER .....		59
3.1.	Experimental tests.....	59
3.2.	Liquid - Liquid dispersion.....	60
3.2.1.	Stability and average chord lengths of dispersion .....	61
3.2.2.	Total chord counts of dispersion.....	61
3.3.	Hydrate formation and transport in pipelines .....	63
3.4.	Effects of water cut/additive and salt on hydrate formation and transportability .....	66
3.4.1.	Effect of water cut.....	67
3.4.1.1.	Experiments with pure water.....	67
3.4.1.2.	Experiments with additive.....	69
3.4.1.3.	Experiments with salt.....	71
3.4.1.4.	Experiments with additive and salt .....	73
3.4.2.	Effect of additive and salt.....	75
3.4.2.1.	In high water cut systems.....	75
3.4.2.2.	In low water cut systems.....	81
3.5.	Role of gas bubbles in water and oil continuous phase.....	84
3.6.	Proposed mechanisms .....	85
3.7.	Highlights and Conclusions.....	88
3.8.	Remarques et Conclusions (in French).....	90
CHAPTER 4. EXPERIMENTAL RESULTS WITH A MOINEAU PUMP WITH AND WITHOUT GAS-LIFT IN THE RISER .....		92
4.1.	Experimental tests.....	92
4.2.	Dispersion and rheological study .....	94
4.2.1.	Water-oil dispersion .....	94
4.2.2.	Rheological study of dispersion.....	97
4.3.	Hydrate formation and transport in flowlines .....	97

4.4.	Overview of hydrate slurry transport phenomena in high water cut systems .....	100
4.5.	Quick and slow (agglomeration and deposition) heterogeneity of hydrate slurry flow .....	103
4.6.	Effect of gas hydrate formation on flowing .....	107
4.7.	Effect of hydrate formation on the stability of liquid-liquid dispersion.....	108
4.8.	Effect of velocity.....	110
4.9.	Effect of water cut.....	112
4.10.	Effect of additive .....	113
4.11.	Effect of salt.....	116
4.12.	Effect of combination of additive and salt on hydrate transportability.....	118
4.12.1.	Experiments with 80%WC .....	118
4.12.2.	Experiments with 100%WC .....	121
4.13.	Effect of pressure .....	124
4.14.	Stability of hydrate slurry (SDR Tests).....	126
4.15.	Morphology of hydrate particles.....	130
4.15.1.	Hydrate morphology at 70 and 80%WC.....	130
4.15.2.	Hydrate morphology at 100%WC.....	133
4.16.	Highlights and Conclusions.....	137
4.17.	Remarques et Conclusions (in French).....	139
<b>CHAPTER 5. PROPOSED MECHANISMS AND RELATIVE PRESSURE DROP MODEL IN HIGH WATER CUT SYSTEMS.....</b>		<b>141</b>
5.1.	Proposed mechanisms at 100%WC.....	141
5.1.1.	Quick and slow heterogeneity of hydrate slurry .....	141
5.1.2.	Low and high flowrate plugging mechanisms .....	142
5.1.3.	Role of salt to enhance the performance of additive .....	143
5.2.	Relative pressure drop model developed .....	144
5.2.1.	Effect of velocity.....	147
5.2.2.	Effect of water cut.....	148
5.2.3.	Effect of additive .....	149
5.2.4.	Effect of salt.....	152
5.2.5.	Effect of pressure .....	153
5.2.6.	Effect of hydrate formation on the stability of suspension .....	154
5.2.7.	Evaluation of model developed.....	155
5.3.	Highlights and Conclusions.....	157

5.4. Remarques et Conclusions (in French).....	158
CONCLUSIONS AND PERSPECTIVES.....	159
CONCLUSIONS ET PERSPECTIVES (IN FRENCH).....	163
LIST OF PUBLICATIONS .....	166
REFERENCES .....	167
APPENDIX .....	175
Appendix A – Composition of Kerdane® used.....	175
Appendix B – Water conversion calculation .....	175
Appendix C – Hydrate volume fraction calculation.....	176
Appendix D – Rate of crystallization.....	176
Appendix E – Interfacial tension measurement .....	177
Appendix F – Stability and average chord length of dispersion (Gas-lift protocol) .....	179
Appendix G – Experimental results (density & flowrate) with Gas-lift protocol.....	185
Appendix H – Rheological study of dispersion with 80%WC (Moineau pump protocol).....	188
Appendix I – Experimental results (density & flowrate) with Moineau pump protocol (with and without gas-lift system).....	196
Appendix J – Gas transfer coefficient ( $k_L a$ ).....	205
ABSTRACT .....	207
RÉSUMÉ (IN FRENCH) .....	208



## LIST OF FIGURES

Figure 1. 1: Subsea pipelines (a) (Oilstates, 2017) and hydrate accumulation obtained from the pig-catcher (b) (Petrobras, Brazil). .....	4
Figure 1. 2: Water cut evolution over the period of 10 years of oil and gas production (Gluyas, 2003).5	5
Figure 1. 3: Pressure versus temperature diagram showing a typical operation condition curve of subsea flowline and hydrate equilibrium curve at different methanol concentrations; adapted from Sloan and Koh (2008). Points on the operation condition curve of offshore flowline indicate distance (in kilometers) from the wellhead.....	6
Figure 1. 4: The structures of mono-tail (left) and twin-tail (right) quaternary ammonium surfactant (AA-LDHI). R is butyl or pentyl; R' is a long alkyl chain and X- is an anion (M. A. Kelland, Svartaas, Øvsthus, Tomita, & Chosa, 2006). .....	8
Figure 1. 5: Anti-agglomeration mechanism with surfactants (Sun & Firoozabadi, 2015). .....	10
Figure 1. 6: Different types and structures of surfactants (Kumar et al., 2015). .....	11
Figure 1. 7: (Upper) The two simplest kinds of emulsions: oil-in-water (O/W) and water-in-oil (W/O). (Lower) The next level of complexity: water-in-oil-in-water (W/O/W) and oil-in-water-in-oil (O/W/O). The droplet sizes have been greatly exaggerated (Schramm, 2005). .....	13
Figure 1. 8: Mechanism for hydrate formation of a water droplet. Step 1: a thin porous hydrate film formed around the water droplet. Step 2: film growth. Step 3: water droplet completely converted to hydrate (Taylor, Miller, et al., 2007). .....	15
Figure 1. 9: Hydrate formation and dissociation from a W/O emulsion (1): (a) initial emulsion; (b) agglomerated hydrate particles; (c) dissociated droplets; (d) final O/W emulsion (inversion has taken place); and (e) final W/O emulsion and from an O/W emulsion (2): (a) initial emulsion; (b) after hydrate formation; and (c) final emulsion after dissociation of gas hydrate emulsion (Greaves et al., 2008).....	16
Figure 1. 10: Mass transfer at the gas-oil interface and through a water droplet during hydrate formation in oil continuous phase (D. J. Turner et al., 2009).....	17
Figure 1. 11: Schematic of hydrate cohesion through a capillary liquid bridge: embracing angle ( $\alpha$ ); capillary bridge width ( $\chi$ ); contact angle ( $\theta_p$ ); external contact angle ( $\theta_s$ ); liquid bridge immersion depth ( $d$ ); particle separation distance ( $H$ ); and particle radius ( $R$ ) (Aman et al., 2012). .....	20
Figure 1. 12: Proposed mechanisms of the hydrate formation on the bubble surface: (a) without SDS and (b) with SDS (Tajima et al., 2010). .....	27
Figure 1. 13: Gas bubble behaviors with gas hydrates in rising process: (a) gas bubble dispersed in water; (b) hydrate formed on the surface of gas bubble; (c) hydrate shell formed; (d) hydrate cracks; and (e) hydrate particles (C. Li & Huang, 2016). .....	28
Figure 1. 14: Different types of gas-liquid flow patterns in a vertical pipe (Morgado, 2016).....	29
Figure 1. 15: Flow patterns of liquid-liquid flow (Trallero et al., 1997). .....	29
Figure 1. 16: Flow regimes for slurry flow in a horizontal pipeline (Brennen, 2005).....	30
Figure 1. 17: Conceptual model for hydrate formation in oil-dominated multiphase flow systems (D J Turner, 2006).....	32
Figure 1. 18: Conceptual picture for hydrate formation in water-dominated systems consisting of gas and water phase (Zerpa, 2013). .....	33
Figure 1. 19: Conceptual picture for hydrate formation in water-dominated systems consisting of gas, water, and oil phase (Zerpa, 2013). .....	33

Figure 1. 20: Topological model of crystallization under flowing without AA-LDHI (1): (a, b) high water cut; (c, d) intermediary water cut; and (e, f) low water cut and with AA-LDHI (2): (a, b) high water cut and (c, d) low water cut (Melchuna et al., 2016). .....	35
Figure 2. 1: Schematic of the Archimède flowloop: simplified with “gas-lift” system (above, on the left) and with Moineau pump (below, on the right); modified and adapted from (Mendes-Melchuna, 2016) and (Fidel-Dufour, 2004). .....	40
Figure 2. 2: Archimède flowloop in the SPIN laboratory: (a) vertical section and (b) horizontal section. ....	41
Figure 2. 3: Structure and dimension (a)/photo (b) of the separator in the Archimède flowloop. ....	42
Figure 2. 4: Ballast system using for liquid and gas circulation in the Archimède flowloop: (a) installation and (b) operational principle; adapted from (Fidel-Dufour, 2004). ....	43
Figure 2. 5: Moineau® pump: (a) installation; (b) structure; and (c) pathway of fluids (or suspension); provided from PCM, Inc (Pump, 2017). ....	44
Figure 2. 6: Gas compensation system in the Archimède flowloop. ....	46
Figure 2. 7: Pressure drop sensors: (a) PD, PD1, PD2, PD3 and (b) PD4; installed in the Archimède flowloop. ....	47
Figure 2. 8: A basic Coriolis meter (a); the principle of measurement (b) (Tom O’Banion, 2013); and (c) Coriolis meter installed in the Archimède flowloop. ....	48
Figure 2. 9: FBRM probe: the principle of measurement (a, b); typical experimental result (c); and probe orientation installation (d) in the Archimède flowloop (Mettler-Toledo, 2007). ....	50
Figure 2. 10: PVM probe: structure and principle of measurement (a, b); hydrate formation (c); hydrate dissociation (d); and probe orientation installation (e) in the Archimède flowloop. ....	51
Figure 2. 11: Three steps of IFT measurement of DCAT (DataPhysics Instruments GmbH, 2006). ....	52
Figure 3. 1: FBRM total number of chord counts during the dispersion process of the experiments with 30%WC; 30%WC-0.01%AA-LDHI; 30%WC-NaCl; and 30%WC-NaCl with 0.01-0.05-0.1-0.5%AA-LDHI. ....	61
Figure 3. 2: FBRM total number of chord length during the dispersion process of the experiment with 80%WC; 80%WC-0.01%AA-LDHI; 80%WC-NaCl; and 80%WC-NaCl-0.01%AA-LDHI. ....	62
Figure 3. 3: FBRM total number of chord length during the dispersion process of the experiment with 90%WC; 90%WC-0.01%AA-LDHI; 90%WC-NaCl; and 90%WC-NaCl-0.01%AA-LDHI. ....	62
Figure 3. 4: A typical experiment in low water cut systems (30%WC-NaCl without AA-LDHI). To enhance hydrate formation, the system had to stop and restart 3 times to reinject methane gas up to 75 bar at minutes of 14; 95; and 121 (see protocol). PD and PD4 are pressure drops in the horizontal line and in the separator, respectively. ....	64
Figure 3. 5: A typical experiment in high water cut systems (90%WC-NaCl without AA-LDHI). To enhance hydrate formation, the system had to stop and restart once to reinject methane gas up to 75 bar at minutes of 16.5 and 18.5 respectively (see protocol). PD and PD4 are pressure drops in the horizontal line and in the separator, respectively. ....	65

Figure 3. 6: PVM images of gas hydrate formation: (a) 90%WC without AA-LDHI and salt; (b) 90%WC-NaCl without AA-LDHI; (c) 90%WC with 0.01% AA-LDHI; (d) 80%WC without AA-LDHI and salt; (e) 30%WC without AA-LDHI and salt; and (f) 30%WC-NaCl with 0.01% AA-LDHI.....	66
Figure 3. 7: Experimental results with pure water: (a) PD and PD4; (b) FBRM chord counts (0-100 $\mu$ m); and (c) FBRM chord counts (100-1000 $\mu$ m) as a function of hydrate volume fraction at 100-90-80-30%WC. ....	69
Figure 3. 8: Experimental results with additive: (a) PD and PD4; (b) FBRM chord counts (0-100 $\mu$ m); and (c) FBRM chord counts (100-1000 $\mu$ m) as a function of hydrate volume fraction at 100-90-80%WC. ....	71
Figure 3. 9: Experimental results with salt: (a) PD and PD4; (b) FBRM chord counts (0-100 $\mu$ m); and (c) FBRM chord counts (100-1000 $\mu$ m) as a function of hydrate volume fraction at 100-90-80%WC. ....	73
Figure 3. 10: Experimental results with both salt and additive: (a) PD and PD4; (b) FBRM chord counts (0-100 $\mu$ m); and (c) FBRM chord counts (100-1000 $\mu$ m) as a function of hydrate volume fraction at 100-90-80%WC.....	75
Figure 3. 11: Experimental results at 100%WC: (a) PD and PD4; (b) FBRM chord counts (0-100 $\mu$ m); and (c) FBRM chord counts (100-1000 $\mu$ m) as a function of hydrate volume fraction. ....	77
Figure 3. 12: Experimental results at 90%WC: (a) PD and PD4; (b) FBRM chord counts (0-100 $\mu$ m); and (c) FBRM chord counts (100-1000 $\mu$ m) as a function of hydrate volume fraction. ....	79
Figure 3. 13: Experimental results with 80%WC: (a) PD and PD4; (b) FBRM chord counts (0-100 $\mu$ m); and (c) FBRM chord counts (100-1000 $\mu$ m) as a function of hydrate volume fraction. ....	81
Figure 3. 14: Experimental results with 30%WC: (a) PD and (b) PD4 as a function of hydrate volume fraction. A sudden decrease or increase in PD and/or PD4 is because of stop and restart the ballast system (to increase pressure in the flowloop).....	82
Figure 3. 15: Experimental results with 30%WC: FBRM chord counts (a: 0-10 $\mu$ m; b: 10-100 $\mu$ m; and c: 100-1000 $\mu$ m) as a function of hydrate volume fraction. ....	84
Figure 3. 16: Conceptual models for hydrate formation and plugging in the gas-lift riser and separator without AA-LDHI: (a, b) in high water cut systems and (c, d) in low water cut systems. ....	86
Figure 3. 17: Conceptual models for hydrate formation and plugging in the experiment with 30%WC-0.01%AA-LDHI. ....	87
Figure 4. 1: FBRM total chord counts during the dispersion process of the experiments with 80%WC; 80%WC-1%AA-LDHI; 80%WC-NaCl; and 80%WC-NaCl-1%AA-LDHI (at 85%LV and 150L.h <sup>-1</sup> ).....	96
Figure 4. 2: FBRM total chord counts during the dispersion process of the experiments with 80%WC; 80%WC-1%AA-LDHI; 80%WC-NaCl; and 80%WC-NaCl-1%AA-LDHI (at 85%LV and 400L.h <sup>-1</sup> ).....	96
Figure 4. 3: FBRM total chord counts during the dispersion process of the experiments with 70-80%WC at 100%LV: 70%WC-200L.h <sup>-1</sup> ; 80%WC-200L.h <sup>-1</sup> ; 70%WC-400L.h <sup>-1</sup> ; and 80%WC-400L.h <sup>-1</sup> .....	97
Figure 4. 4: Typical temperature (T7: temperature in the horizontal line); flowrate; and density during a crystallization experiment [100%WC-0.5%AA-LDHI-85%LV-75bar] at 400L.h <sup>-1</sup> .....	98
Figure 4. 5: Typical pressure drop (in the horizontal line); pressure drop in the separator (PD4); and pressure during a crystallization experiment [100%WC-0.5%AA-LDHI-85%LV-75bar] at 400L.h <sup>-1</sup> .....	98
Figure 4. 6: Typical FBRM chord counts during a crystallization experiment [100%WC-0.5%AA-LDHI-85%LV-75bar] at 400L.h <sup>-1</sup> .....	99

Figure 4. 7: PVM images of gas hydrate formation and plugging for the experiment with 100%WC-0.5% AA-LDHI at 400L.h <sup>-1</sup> and 85%LV[(a): beginning of hydrate formation, 5.4 min; (b): during crystallization, 26.4 min; and (c): plugging, 65.4 min].	100
Figure 4. 8: FBRM chord counts as a function of hydrate volume in the experiment with 100%WC-1%AA-LDHI-85%LV-400L.h <sup>-1</sup> -75bar.	104
Figure 4. 9: Temperature; flowrate; and density as a function of hydrate volume in the experiment with 100%WC-1%AA-LDHI-85%LV-400L.h <sup>-1</sup> -75bar.	104
Figure 4. 10: Pressure drops in the flowloop as a function of hydrate volume in the experiment with 100%WC-1%AA-LDHI-85%LV-400L.h <sup>-1</sup> -75bar.	105
Figure 4. 11: FBRM chord counts; pressure drops; and density as a function of hydrate volume in the experiment with 100%WC-NaCl-85%LV-400L.h <sup>-1</sup> -75bar.	106
Figure 4. 12: PVM images of gas hydrate formation (before and after deposition) for the experiment with 100%WC-1% AA-LDHI at 400L.h <sup>-1</sup> and 85%LV[(a): before hydrate deposition and (b): after hydrate deposition].	106
Figure 4. 13: PVM images of gas hydrate formation (before and after deposition) for the experiment with 100%WC-NaCl at 400L.h <sup>-1</sup> and 85%LV [(a): before hydrate deposition and (b): after hydrate deposition].	107
Figure 4. 14: Flowrate and pressure drop of the experiment with 80%WC-NaCl-85%LV-150L.h <sup>-1</sup> -75bar.	107
Figure 4. 15: Flowrate and pressure drop of the experiment with 80%WC-NaCl-1%AA-LDHI-85%LV-150L.h <sup>-1</sup> -75bar.	108
Figure 4. 16: Density-pressure drop (a) and FBRM chord counts (b) of the experiment with 80%WC-NaCl-1%AA-LDHI-85%LV-400L.h <sup>-1</sup> -75bar.	109
Figure 4. 17: Effect of velocity on pressure drop and average rate of crystallization [the experiments with 100%WC-0.5%AA-LDHI-85%LV-75bar at 150 and 400L.h <sup>-1</sup> ].	110
Figure 4. 18: Effect of velocity on FBRM chord counts [the experiments with 100%WC-0.5%AA-LDHI-85%LV-75bar at 150 (a) and 400 (b) L.h <sup>-1</sup> ].	111
Figure 4. 19: Effect of water cut on pressure drop and average rate of crystallization [the experiments with 80 and 100%WC-NaCl-85%LV-400L.h <sup>-1</sup> -75bar].	112
Figure 4. 20: Effect of water cut on FBRM chord counts [the experiments with 80%WC (a) and 100%WC (b)-NaCl-85%LV-400L.h <sup>-1</sup> -75bar].	113
Figure 4. 21: Effect of additive on pressure drop and average rate of crystallization [the experiments with 100%WC-0-0.5-1%AA-LDHI-85%LV-150L.h <sup>-1</sup> -75bar].	114
Figure 4. 22: Effect of additive on FBRM chord counts [the experiments with 100%WC-0 (a)-0.5 (b)-1 (c) %AA-LDHI-85%LV-150L.h <sup>-1</sup> -75bar].	116
Figure 4. 23: Effect of salt on pressure drop and average rate of crystallization [the experiments with 100%WC-85%LV-150L.h <sup>-1</sup> -75bar without and with NaCl].	117
Figure 4. 24: Effect of salt on FBRM chord counts [the experiments with 100%WC-85%LV-150L.h <sup>-1</sup> -75bar without (a) and with (b) NaCl].	118
Figure 4. 25: Effect of a combination of salt and additive on pressure drop and average rate of crystallization [the experiments with 80%WC-85%LV-75bar-400L.h <sup>-1</sup> with NaCl - with 1%AA-LDHI - with NaCl and 1%AA-LDHI].	119

Figure 4. 26: Effect of a combination of salt and additive on FBRM chord counts [the experiments with 80%WC-85%LV-75bar-400L.h <sup>-1</sup> with NaCl (a) - with 1%AA-LDHI (b) - with NaCl and 1%AA-LDHI (c)]. .....	121
Figure 4. 27: Effect of a combination of salt and additive on pressure drop and average rate of crystallization [the experiments with 100%WC-85%LV-75bar-400L.h <sup>-1</sup> with NaCl - with 1%AA-LDHI - with NaCl and 1%AA-LDHI].....	122
Figure 4. 28: Effect of a combination of salt and additive on FBRM chord counts [the experiments with 100%WC-85%LV-75bar-400L.h <sup>-1</sup> with NaCl (a) - with 1%AA-LDHI (b) - with NaCl and 1%AA-LDHI (c)]. .....	124
Figure 4. 29: Effect of pressure on pressure drop and average rate of crystallization [the experiments with 100%WC-2%AA-LDHI-85%LV-400L.h <sup>-1</sup> at 70bar and 75bar]. .....	125
Figure 4. 30: Effect of pressure on FBRM chord counts [the experiments with 100%WC-2%AA-LDHI-85%LV-400L.h <sup>-1</sup> at 70bar (a) and 75bar (b)]. .....	126
Figure 4. 31: Shutdown and restart tests for the experiment with 100%WC-2%AA-LDHI-85%LV-400L.h <sup>-1</sup> -70bar: (a) pressure drop, hydrate volume, and flowrate; (b) density, pressure, and temperature; and (c) FBRM chord counts.....	128
Figure 4. 32: Shutdown and restart tests for the experiment with 100%WC-NaCl-1%AA-LDHI-85%LV-150L.h <sup>-1</sup> -75bar: (a) pressure drop, hydrate volume, and flowrate; (b) density, pressure, and temperature; and (c) FBRM chord counts.....	129
Figure 4. 33: PVM images of gas hydrate formation and plugging for the experiment with 70%WC at 400L.h <sup>-1</sup> and 100%LV [(a) 3 min and (b) 8 min after gas hydrate formation]. .....	130
Figure 4. 34: PVM images of gas hydrate formation and plugging for the experiment with 80%WC at 150L.h <sup>-1</sup> and 85%LV [(a) 0.5 min and (b) 2 min after gas hydrate formation]. .....	131
Figure 4. 35: PVM images of gas hydrate formation and plugging for the experiment with 80%WC at 400L.h <sup>-1</sup> and 85%LV [(a) 118.4 min and (b) 257.4 min after gas hydrate formation]. .....	131
Figure 4. 36: PVM images of gas hydrate formation and plugging for the experiment with 80%WC-1%AA-LDHI at 400L.h <sup>-1</sup> and 85%LV [(a) 5.7 min and (b) 25.7 min after gas hydrate formation]. .....	132
Figure 4. 37: PVM images of gas hydrate formation and plugging for the experiment with 80%WC-NaCl at 150L.h <sup>-1</sup> and 85%LV [(a) 7.1 min and (b) 10.1 min after gas hydrate formation].....	132
Figure 4. 38: PVM images of gas hydrate formation and plugging for the experiment with 80%WC-NaCl at 400L.h <sup>-1</sup> and 85%LV [(a) 29.4 min and (b) 40.3 min after gas hydrate formation].....	133
Figure 4. 39: PVM images of gas hydrate formation and plugging for the experiment with 80%WC-NaCl-1%AA-LDHI at 400L.h <sup>-1</sup> and 85%LV [(a) 138.8 min and (b) 163.8 min after gas hydrate formation]. .....	133
Figure 4. 40: PVM images of gas hydrate formation and plugging for the experiment with 100%WC at 150L.h <sup>-1</sup> , 75bar and 85%LV [(a) 0.7 min and (b) 1.7 min after gas hydrate formation]. .....	134
Figure 4. 41: PVM images of gas hydrate formation and plugging for the experiment with 100%WC-0.05%AA-LDHI at 150L.h <sup>-1</sup> and 90%LV [(a) 288.4 min and (b) 320.4 min after gas hydrate formation]. .....	134
Figure 4. 42: PVM images of gas hydrate formation and plugging for the experiment with 100%WC-1%AA-LDHI at 400L.h <sup>-1</sup> and 85%LV [(a) 22.8 min and (b) 24.8 min after gas hydrate formation]. .....	134

Figure 4. 43: PVM images of gas hydrate formation and plugging for the experiment with 100%WC-NaCl at 150L.h <sup>-1</sup> and 85%LV [(a) 2.5 min; (b) 3.5 min; (c) 4.5 min; and (d) 5.5 min after gas hydrate formation].	135
Figure 4. 44: PVM images of gas hydrate formation and plugging for the experiment with 100%WC-NaCl at 400L.h <sup>-1</sup> and 85%LV [(a) 52 min and (b) 157 min after gas hydrate formation].	135
Figure 4. 45: PVM images of gas hydrate formation and plugging for the experiment with 100%WC-NaCl-1%AA-LDHI at 150L.h <sup>-1</sup> and 85%LV [(a) 1.5 min and (b) 269 min after gas hydrate formation].	136
Figure 4. 46: PVM images of gas hydrate formation and plugging for the experiment with 100%WC-NaCl-1%AA-LDHI at 400L.h <sup>-1</sup> and 85%LV [(a) 53 min and (b) 93.5 min after gas hydrate formation].	136
Figure 5. 1: Mechanism of quick (a) and slow (b) heterogeneity of hydrate slurry.	142
Figure 5. 2: Mechanism of hydrate slurry plugging at low (a) and high (b) flowrate.	143
Figure 5. 3: Proposed mechanism of hydrate particle-AA-LDHI-salt interaction in preventing plug.	144
Figure 5. 4: Fully (a) and partially (b) converted hydrate particle; different hydrate agglomerate structures (c-d); homogeneous (e) and heterogeneous (f) hydrate suspension flow.	147
Figure 5. 5: Effect of velocity on relative pressure drop [the experiments with 100%WC-1%AA-LDHI-85%LV-75bar: 150L.h <sup>-1</sup> (a) and 400L.h <sup>-1</sup> (b)].	148
Figure 5. 6: Effect of water cut on relative pressure drop [the experiments with NaCl-1%AA-LDHI-85%LV-400L.h <sup>-1</sup> -75bar: 80%WC (a) and 100%WC (b)].	149
Figure 5. 7: Effect of additive on relative pressure drop [the experiments with 100%WC-85%LV-400L.h <sup>-1</sup> -75bar: 0.5% (a) - 1% (b) - 2% (c) AA-LDHI].	151
Figure 5. 8: Effect of additive on relative pressure drop [the experiments with 100%WC-NaCl-85%LV-400L.h <sup>-1</sup> -75bar: 0% (a) - 1% (b) AA-LDHI].	152
Figure 5. 9: Effect of salt on relative pressure drop [the experiments with 100%WC-1%AA-LDHI-85%LV-150L.h <sup>-1</sup> -75bar: without (a) and with salt (b)].	153
Figure 5. 10: Effect of pressure on relative pressure drop [the experiments with 100%WC-2%AA-LDHI-85%LV-400L.h <sup>-1</sup> : 70bar (a) and 75bar (b)].	154
Figure 5. 11: Effect of hydrate formation on the stability of suspension (relative pressure drop) at 80%WC-NaCl-1%AA-LDHI-85%LV-400L.h <sup>-1</sup> -75bar.	155
Figure F. 1: Pressure drop (solid line) and average chord length (dashed line) during the dispersion of the experiments without additive and salt.	179
Figure F. 2: Pressure drop (solid line) and average chord length (dashed line) during the dispersion of the experiments with additive.	180
Figure F. 3: Pressure drop (solid line) and average chord length (dashed line) during the dispersion of the experiments with salt.	181
Figure F. 4: Pressure drop (solid line) and average chord length (dashed line) during the dispersion of the experiments with both salt and additive.	182
Figure F. 5: Pressure drop (solid line) and average chord length (dashed line) during the dispersion of the experiments with both salt and additive with 30%WC.	183
Figure F. 6: PVM images of different mixtures during the dispersion process at 4.5±0.5°C and 1 bar: (a) 90%WC-NaCl without AA-LDHI; (b) 90%WC-NaCl with 0.01% AA-LDHI; (c) 80%WC-NaCl without	

AA-LDHI; (d) 80%WC-NaCl with 0.01% AA-LDHI; (e) 30%WC without AA-LDHI and salt; (f) 30%WC-NaCl without AA-LDHI; (g) 30%WC-NaCl with 0.05%AA-LDHI; and (h) 30%WC-NaCl with 0.5% AA-LDHI.  
 ..... 184

Figure G. 1: Experimental results with the gas-lift protocol (density and flowrate as a function of hydrate volume fraction) with 100%WC. .... 185  
 Figure G. 2: Experimental results with the gas-lift protocol (density and flowrate as a function of hydrate volume fraction) with 90%WC. .... 186  
 Figure G. 3: Experimental results with the gas-lift protocol (density and flowrate as a function of hydrate volume fraction) with 80%WC. .... 186  
 Figure G. 4: Experimental results with the gas-lift protocol: (a) density and (b) flowrate as a function of hydrate volume fraction) with 30%WC. .... 187

Figure H. 1: Rheological study of the experiment with 80%WC-85%LV: (a) flowrate, average chord length, and FBRM total chord counts and (b) pressure drop and density. .... 189  
 Figure H. 2: PVM images of dispersion in the rheological study of the experiment with 80%WC-85%LV: (a) 120L.h<sup>-1</sup> and (b) 400L.h<sup>-1</sup>. .... 189  
 Figure H. 3: Rheological study of the experiment with 80%WC-1%AA-LDHI-85%LV: (a) flowrate, average chord length, and FBRM total chord counts and (b) pressure drop and density. .... 190  
 Figure H. 4: PVM images of dispersion in the rheological study of the experiment with 80%WC-1%AA-LDHI-85%LV: (a) 120L.h<sup>-1</sup>; (b) 200L.h<sup>-1</sup>; (c) 300L.h<sup>-1</sup>; and (d) 400L.h<sup>-1</sup>. .... 191  
 Figure H. 5: Rheological study of the experiment with 80%WC-NaCl-85%LV: (a) flowrate, average chord length, and FBRM total chord counts and (b) pressure drop and density. .... 192  
 Figure H. 6: PVM images of dispersion in the rheological study of the experiment with 80%WC-NaCl at 85%LV: (a) 120L.h<sup>-1</sup> and (b) 400L.h<sup>-1</sup>. .... 193  
 Figure H. 7: Rheological study of the experiment with 80%WC-NaCl-1%AA-LDHI-85%LV: (a) flowrate, average chord length, and FBRM total chord counts and (b) pressure drop and density. .... 194  
 Figure H. 8: PVM images of dispersion in the rheological study of the experiment with 80%WC-NaCl-1%AA-LDHI-85%LV: (a) 120L.h<sup>-1</sup> and (b) 400L.h<sup>-1</sup>. .... 195

Figure I. 1: Experimental results (a-l) with the Moineau pump protocol (density and flowrate as a function of hydrate volume fraction) with 100%WC. .... 201  
 Figure I. 2: Experimental results (a-e) with the Moineau pump protocol (density and flowrate as a function of hydrate volume fraction) with 80%WC. .... 204



## LIST OF TABLES

Table 1. 1: Crystalline cavities and structures of clathrate hydrates (Sloan & Koh, 2008). .....	2
Table 2. 1: Important operation parameters and dimensions of the Archimède flowloop.....	41
Table 3. 1: Experimental conditions and results with the gas-lift system at 75 bar and $4.5\pm 0.5^{\circ}\text{C}$ .....	60
Table 4. 1: Experimental conditions and results with the Moineau pump (with and without gas-lift system). .....	93
Table 4. 2: Characteristics of dispersion systems at $4.5\pm 0.5^{\circ}\text{C}$ and 1 bar (before methane injection).	95
Table 4. 3: Summary of hydrate slurry transport phenomena in high water cut systems. ....	101
Table 4. 4: Driving force of the experiments with and without salt at an experimental temperature of $5^{\circ}\text{C}$ . .....	102
Table 4. 5: Kinetics parameters of the experimental tests with Moineau pump and gas-lift system.	102
Table 5. 1: Important parameters ( $K_v$ , $R^2$ , and $\bar{R}(t)$ ) of the experimental tests to develop relative pressure drop model. ....	156
Table A. 1: Chemical composition and properties of Kerdane® .....	175
Table E. 1: The interfacial tension (IFT) of water and Kerdane® without and with 0.01%AA-LDHI. ....	177
Table J. 1: Gas transfer coefficients at different pressures and $4.5\pm 0.5^{\circ}\text{C}$ with the Moineau pump protocol (before crystallization).....	205

## NOMENCLATURE

Symbol	Description	Unity
$a$	mass transfer surface area per volume of liquid or consistency ratio or a factor	$[\text{cm}^{-1}]$ or $[-]$
$A$	cross-sectional area	$[\text{m}^2]$
$A_{CH_4}$	amount of methane gas consumed	$[\text{mol}]$
$ACL$	average chord length	$[\mu\text{m}]$
$A_f$	final number of mol of methane gas consumed (the time once the curve attained platform)	$[\text{mol}]$
$A_{GL}$	total interfacial area in the reactor or surface of the gas-liquid interface	$[\text{m}^2]$
$A_p$	interfacial area	$[\text{m}^2]$
$A_t$	number of mol of methane gas consumed at the time (t)	$[\text{mol}]$
$C$	concentration in the volume of liquid	$[\text{mol}\cdot\text{cm}^{-3}]$
$C^*$	interfacial concentration	$[\text{mol}\cdot\text{L}^{-1}]$
$C_{AA-LDHI}$	dosage of AA-LDHI	wt.% of water
$C_b$	concentration in the liquid bulk	$[\text{mol}\cdot\text{L}^{-1}]$
$C_{ext}$	interfacial concentration at the gas-liquid equilibrium	$[\text{mol}\cdot\text{L}^{-1}]$
$C_{NaCl}$	dosage of NaCl	$\text{gNaCl}\cdot\text{L}^{-1}(\text{H}_2\text{O})$
$C_w^0$	initial molar concentration of water	$[\text{mol}]$
$d$	liquid bridge immersion depth	$[\text{m}]$
$d_A$	aggregate diameter	$[\text{m}]$
$d_{A,max}$	maximum size of aggregate	$[\text{m}]$
$d_p$	particle diameter	$[\text{m}]$
$D$	diameter of pipe	$[\text{m}]$
$f$	fugacity of the dissolved gas or Fanning friction factor or fractal dimension	$[\text{MPa}]$ or $[-]$
$f_{eq}$	equilibrium fugacity	$[\text{MPa}]$
$F_A$	capillary force or inter-particle cohesion force	$[\text{N}]$
$G_G$	mass flux of air (gas)	$[\text{kg}\cdot\text{s}^{-1}\cdot\text{m}^{-2}]$

$G_L$	mass flux of water (liquid)	[kg.s <sup>-1</sup> .m <sup>-2</sup> ]
$H$	particle separation distance	[m]
$HV$	hydrate volume fraction	[%] or [-]
$IFT$	interfacial tension	[mN.m <sup>-1</sup> ]
$j_G$	gas volumetric flux	[m.s <sup>-1</sup> ]
$j_L$	liquid volumetric flux	[m.s <sup>-1</sup> ]
$k$	constant or self-crowding factor or additional exponent coefficient	[-]
$k_L$	mass transfer constant at the gas-liquid interface	[m.s <sup>-1</sup> ]
$k_L a$	mass transfer coefficient at the gas-liquid interface	[s <sup>-1</sup> ]
$K$	ratio of the viscosity of the dispersed phase ( $\mu_D$ ) to that of the continuous phase ( $\mu_C$ )	[-]
$K^*$	kinetic constant	[-]
$K_0$	factor that considers the presence of surfactant adsorbed on the surface of the dispersed droplets	[-]
$K_v$	(structural) effective volume fraction factor	[-]
$L$	length of pipe between two points of pressure drop measurement	[m]
$LV$	liquid volume fraction	[%]
$m_w^i$	initial mass of water in the mixture	[g]
$M_w$	molecular weight	[g.mol <sup>-1</sup> ]
$M_2$	second moment of the population density function	[-]
$n$	number of moles of gas consumed in hydrate formation or behavior ratio or new degree of freedom	[mol] or [-]
$n_{cell}$	number of cells of hydrate structure I	[-]
$n_{CH_4}$	number of mol of methane consumed for hydrate formation	[mol]
$n_{crw}$	number of mol of water converted to hydrate	[mol]
$n_w^i$	initial number of mol of water in the mixture	[mol]
$N$	number of hydrate particles	[-]
$N_{Avogadro}$	Avogadro number	[6.022x10 <sup>23</sup> mol <sup>-1</sup> ]

$N_{crw}$	number of water molecules converted to hydrate	[-]
$P$	pressure	[bar] or [MPa]
$P_{eq}$	equilibrium pressure	[bar] or [MPa]
$P_{exp}$	experimental pressure	[bar] or [MPa]
$PD$	pressure drop	[bar] or [mbar]
$Q$	flowrate	[m <sup>3</sup> .h <sup>-1</sup> ] or [L.h <sup>-1</sup> ]
$r$	speed of dissolution or mass transfer	[mol.s <sup>-1</sup> ]
$R$	ideal gas constant or particle radius	[J.K <sup>-1</sup> .mol <sup>-1</sup> ] or [m]
$R^*$	harmonic mean radius of the particle pair	[m]
$R^2$	coefficient of multiple determination	[-]
$Re$	Reynolds' Number	[-]
$R(t)$	crystallization rate	[%HV.min <sup>-1</sup> ]
$\bar{R}(t)$	average crystallization rate	[%HV.min <sup>-1</sup> ]
$R(t)^{MAX}$	crystallization rate maximum	[%HV.min <sup>-1</sup> ]
$RPD$ or $\Delta P_r$	relative pressure drop	[-]
$t$	time	[s]
$t_0$	initial time	[s]
$T$	temperature	[°C or K]
$T_{eq}$	equilibrium temperature	[°C or K]
$T_{exp}$	experimental temperature	[°C or K]
$u$	velocity	[m.s <sup>-1</sup> ]
$U_G$	superficial velocity of gas	[m.s <sup>-1</sup> ]
$U_L$	superficial velocity of liquid	[m.s <sup>-1</sup> ]
$v_m$	molar volume of the hydrate particles	[m <sup>3</sup> .mol <sup>-1</sup> ]
$V_{cell}$	volume of one hydrate cell ( $S_i$ )	[m <sup>3</sup> .cell <sup>-1</sup> ]
$V_G$	gas volume	[cm <sup>3</sup> ]
$V_H$	hydrate volume	[m <sup>3</sup> ]
$V_L$	liquid volume	[cm <sup>3</sup> ]
$V_{total}$	total volume of the mixture	[m <sup>3</sup> ]

$WC$	water cut or water fraction	[%]
$x_b$	gas mole fraction in the liquid bulk in equilibrium with the hydrate phase	[-]
$x_{int}$	gas mole fraction in the liquid in equilibrium with the gas at the interface	[-]
$Z$	compressibility factor	[-]

### Greek Letters

$\alpha$	embracing angle	[degrees]
$\dot{\gamma}$	shear rate	[s <sup>-1</sup> ]
$\gamma$	water–oil interfacial tension	[mN.m <sup>-1</sup> ]
$\Delta P$	pressure drop or driving force	[bar]
$\Delta T$	driving force or sub-cooling	[bar] or [°C]
$\eta$	water conversion	[%]
$[\eta]$	intrinsic viscosity	[-]
$\theta_p$	contact angle	[degrees]
$\theta_s$	external contact angle	[degrees]
$\mu$	apparent dynamic viscosity of emulsion or suspension	[Pa.s]
$\mu_0$	viscosity of the dispersing liquid	[Pa.s]
$\mu_r$	relative viscosity of emulsion or suspension	[-]
$\mu_C$	continuous phase dynamic viscosity	[Pa.s]
$\mu_E$	dynamic viscosity of emulsion	[Pa.s]
$\mu_S$	suspension dynamic viscosity	[Pa.s]
$\rho$	density	[kg.m <sup>-3</sup> ]
$\rho_G$	mass density of the gas phase	[kg.m <sup>-3</sup> ]
$\rho_L$	mass density of the flowing (liquid) phase	[kg.m <sup>-3</sup> ]
$\sigma$	surface (interfacial) tension	[mN.m <sup>-1</sup> ]
$\tau$	shear stress	[Pa]
$v$	velocity of flow	[m.s <sup>-1</sup> ]
$\Phi$	real volume fraction of dispersed (solid) phase	[-]
$\Phi^*$	dispersed phase volume fraction for which the relative viscosity	[-]

$\mu_r = \mu_E/\mu_C$  reaches 100

$\Phi_{eff}$	effective volume fraction	[-]
$\Phi_{max}$	maximum volume fraction to which particles can pack or the packing concentration of randomly packed spheres	[-]
$\chi$	capillary bridge width	[m]

## LIST OF ABBREVIATIONS

AA-LDHI	Anti-Agglomerant – Low Dosage Hydrate Inhibitor
ATR-FTIR	Attenuated Total Reflection– Fourier Transform Infrared
CAPEX	Capital Expenditure
CFD	Computational Fluid Dynamic
CLD	Chord Length Distribution
CMC	Critical Micelle Concentration
DEG	Diethylene Glycol
DEPO.	Deposition
ENSM-SE	École Nationale Supérieure des Mines de Saint-Étienne
F	Foam or Flowrate
FBRM	Focused Beam Reflectance Measurement
G	Gas
GL	Gas-Lift
H	Hydrate
IFP	French Petroleum Institute
KHI	Kinetic Hydrate Inhibitor
L	Liquid
MEG or EG	Mono-ethylene Glycol or Ethylene Glycol
MeOH	Methanol
OPEX	Operational Expenditure
O/W	Oil-in-Water Emulsion
O/W/O	Oil-in-Water in Oil Emulsion
PBM	Population Balance
PVCap	Poly-N-vinylcaprolactam

PVM	Particle Video Microscope
QAS	Quaternary Ammonium Salts
rp	Repeated
rpm	revolutions per minute
S <sub>I</sub> , S <sub>II</sub> , and S <sub>H</sub>	Hydrate Structure I, II, and H
SDR	Shutdown and Restart
SDS	Sodium Dodecyl Sulfate
ST	Stratified smooth flow
ST&MI	Stratified flow with Mixing at the Interface
TEG	Tri-ethylene Glycol
THI	Thermodynamic Inhibitor
W/O	Water-in-Oil Emulsion
W/O/W	Water-in-Oil in Water Emulsion
W/O/W/O	Water-in-Oil in Water-in-Oil Emulsion
vol.%	Percent (in volume)
wt.%	Percent (in mass)



## INTRODUCTION

*Nothing great was ever achieved without enthusiasm.*

*Ralph Waldo Emerson*

Gas (clathrate) hydrates are ice-like crystalline structures composed of molecular water cages stabilized by methane, ethane, propane, etc. at low temperature and high-pressure conditions (Sloan & Koh, 2008). Today, oil and gas fields gradually become mature which is reflected on the increase in the amount of water produced (water cut), as a result, hydrates might have more chance to form. Furthermore, offshore systems mainly containing crude oil, natural gas, and water always operate at low temperature and high pressure which are favoring conditions for gas hydrate formation and agglomeration. Gas hydrate is a great concern in flow assurance which may become a potential hazard (plug) to the oil and natural gas transportation flowlines. There are several chemical strategies to manage this hydrate plug risk including the addition of thermodynamic inhibitors (THIs), or low dosage hydrate inhibitors (LDHIs): kinetic hydrate inhibitors (KHIs) and anti-agglomerants (AA-LDHIs). The most traditional method to prevent gas hydrates is thermodynamic inhibition (e.g., using methanol or glycols) which shifts the hydrate equilibrium conditions to higher pressure and lower temperature. However, the severe conditions (higher pressure, lower temperature, higher acid gas content, and higher water cut) in oil and gas transportation make thermodynamic mitigation less acceptable because of the high amount of THIs used. To reduce the cost, LDHIs are used at a low dosage (1-2 wt.%) compared to the THIs. The fact that KHIs can delay the nucleation or growth of hydrate formation while AA-LDHIs allow the hydrate formation but help to maintain hydrate particles finely dispersed in production fluids.

Few researchers have addressed the problems of gas hydrate formation, agglomeration, and transport in high water cut systems in the presence of gas bubbles, salt, and commercial anti-agglomerants at low dosage hydrate inhibitor (AA-LDHIs) using a pilot scale flowloop. This poorly understood knowledge is because of the complicated nature and the stability of emulsion during hydrate crystallization and also due to effects of hydrate formation on multiphase flow and vice versa. This is also due to the unpredictable behaviors of AA-LDHIs to prevent plug in different oil and gas transport conditions (the presence of salt, type of oil, water cut, velocity, etc.).

The aim of this present work is to deeper understand kinetics of hydrate crystallization and transportability in pipelines from emulsion or dispersion (especially in high water cut systems), with and without salt and AA-LDHIs, by using the PVM (Particle Video Microscope) and FBRM (Focused Beam Reflectance Measurement) probes. In other words, the objective of this research is to bring a new understanding of the kinetics of methane hydrate formation, agglomeration, deposition, and

plugging from emulsion (dispersion) systems in pipelines and to understand the role of commercial additives (AA-LDHs) in dispersing hydrate particles to prevent plugging. The flowloop experiments were carried out in low and high water cut systems, with different flowrates, different amount of salt and AA-LDHs using a Moineau pump and/or gas-lift system in LGF laboratory, PEG department, SPIN center, École Nationale Supérieure des Mines de Saint-Étienne, France. The results obtained from the flowloop experiments help to find new insights and to propose conceptual mechanisms of gas hydrate formation, agglomeration, deposition, and plugging in flowlines at low and high water cuts. Additionally, a model was developed to predict the relative pressure drop of hydrate slurry in oil and gas pipelines.

The thesis is constituted by 05 chapters highlighted as follows:

**Chapter 1 (Literature Review)** provides bibliography related to the main topics of this thesis including gas hydrates in flow assurance, emulsion, gas hydrate formation, agglomeration, deposition, plugging, anti-agglomeration, rheology of emulsion and suspension, multiphase flow, flow patterns, and mass transfer in subsea flowlines.

**Chapter 2 (Flowloop Apparatus and Experimental Methodology)** presents the Archimède flowloop apparatus and experimental methodology used in this work. Moreover, several important measurements and calculations are described meticulously.

**Chapter 3 (Experimental Results with Gas-Lift (Bubbles) in the Riser)** focuses on the flowloop experimental results with gas-lift protocol using Kerdane<sup>®</sup> oil with and without salt and/or AA-LDHs from low to high water cuts. The proposed mechanisms of hydrate formation, agglomeration, deposition, and plugging with and without AA-LDHs at different continuous phases are described in presence of gas bubbles.

**Chapter 4 (Experimental Results with a Moineau Pump with and without Gas-Lift in the Riser)** illustrates the flowloop experimental results with a Moineau pump protocol using Kerdane<sup>®</sup> oil with and without salt and/or AA-LDHs in high water cut systems and at different flowrates. In this protocol, occasionally, the gas-lift system is used to co-work with the Moineau pump to launch hydrate nucleation and/or enhance hydrate formation in pipelines.

**Chapter 5 (Proposed Mechanisms and Relative Pressure Drop Model in High Water Cut Systems)** describes several conceptual models for hydrate formation and transport phenomena and also a relative pressure drop model. These models are proposed and developed based on the flowloop experimental results in high water cut systems with Moineau pump protocol.

**Finally, conclusions** are summarized and **perspectives** are proposed for further research.

## INTRODUCTION (IN FRENCH)

*Rien de grand n'a jamais été accompli sans enthousiasme.*

*Ralph Waldo Emerson*

Les hydrates de gaz (ou hydrates de clathrate) sont des structures cristallines semblables à de la glace. Ils sont constitués de cages d'eau moléculaires stabilisées par des gaz d'hydrocarbures légers (méthane, éthane, propane, etc.) à basse température et à haute pression (Sloan & Koh, 2008). Aujourd'hui, les champs de pétrole et de gaz deviennent progressivement mûrs et provoquent une augmentation de la quantité d'eau produite (fraction d'eau), ce qui a pour conséquence que des hydrates ont plus de chance de se former. Les systèmes sous-marins contenant principalement du pétrole brut, du gaz naturel et de l'eau fonctionnent toujours à basse température et à haute pression, ce qui favorise les conditions de formation et d'agglomération des hydrates de gaz, provoquant des bouchons dans les pipelines. L'hydrate de gaz est une grande préoccupation dans le domaine de l'étude des écoulements. Il peut devenir un risque potentiel pour le transport de pétrole et de gaz naturel une fois formé dans les lignes de production. Il existe plusieurs stratégies de type chimiques pour gérer ce risque notamment l'ajout d'inhibiteurs thermodynamiques (THIs) ou d'inhibiteurs d'hydrates à faible dose (LDHIs) en tant qu'inhibiteurs de l'hydrate cinétique (KHIs) ou antiagglomérants (AA-LDHIs). La méthode la plus classique pour empêcher la formation des hydrates de gaz est l'inhibition thermodynamique (par exemple en utilisant du méthanol ou des glycols) qui déplace les conditions d'équilibre de l'hydrate à une pression plus élevée et à une température plus basse. Cependant, les conditions sévères (pressions plus élevées, températures plus basses, teneur plus élevée en gaz acides et fraction d'eau plus élevée) dans le transport du pétrole et du gaz rendent l'atténuation thermodynamique moins acceptable en raison de la quantité élevée de THI utilisée. Pour réduire le coût, les LDHIs sont utilisés à une très petite quantité par rapport aux THIs. En outre, les KHIs peuvent retarder la nucléation ou la croissance des hydrates tandis que les AA-LDHIs permettent la formation d'hydrates mais aident à maintenir les particules d'hydrate finement dispersées dans les fluides de production.

Peu de chercheurs ont abordé des problèmes de la formation d'hydrates de gaz, à l'agglomération et au transport à haute fraction d'eau en présence de bulles de gaz, de sel et d'antiagglomérants commerciaux à faible dose d'inhibiteur d'hydrate (AA-LDHIs). Ceci est dû à la nature compliquée et à la stabilité de l'émulsion pendant la cristallisation mais aussi à cause de l'effet de la formation d'hydrates sur l'écoulement multiphasique et vice versa. Ceci est également dû aux comportements imprévisibles des AA-LDHIs pour éviter bouchage en différentes conditions de transport de pétrole et de gaz (présence de sel, type d'huile, fraction d'eau, vitesse, etc.).

Le but de ce travail est de comprendre plus en profondeur la cinétique de cristallisation et de transportabilité des pipelines à partir de l'émulsion (à différentes fractions d'eau, en particulier à forte teneur) avec ou sans du sel et AA-LDHIs, en utilisant les sondes PVM (Particle Video Microscope) et FBRM (Focused Beam Reflectance Measurement). En d'autres termes, l'objectif de ce travail est d'apporter une nouvelle compréhension de la cinétique de la cristallisation, de l'agglomération, du dépôt et du colmatage des hydrates dans les pipelines et du rôle des additifs commerciaux dans la dispersion des particules d'hydrates. Les expériences sur la boucle Archimède ont été réalisées pour des fractions d'eau faibles à élevées, à différents débits, avec et sans sel et/ou AA-LDHI en utilisant la pompe Moineau et/ou les conditions de gaz-lift. Ces expérimentations ont eu lieu dans le laboratoire LGF, centre SPIN, École Nationale Supérieure des Mines de Saint-Étienne, France. Les résultats obtenus à partir d'expériences en boucle d'écoulement aident à trouver de nouvelles idées et à proposer un mécanisme conceptuel et modèle de formation, d'agglomération, de dépôt et de bouchage des hydrates de gaz dans les conduites pétrolières.

Ce manuscrit est constitué de 5 chapitres :

**Chapitre 1 (Revue de la Littérature)** fournit une bibliographie sur les principaux sujets de cette thèse, y compris la formation des hydrates de gaz, les études d'écoulement, les émulsions, l'agglomération, les dépôts, les bouchages, l'anti-agglomération, les écoulements poly-phasiques, les modèles d'écoulement avec et sans hydrate de gaz et le transfert de masse dans les écoulements sous-marins.

**Chapitre 2 (Dispositif de la Boucle et Méthodologie Expérimentale)** présente le dispositif utilisé (la boucle Archimède) et la méthodologie expérimentale appliquée lors de ces travaux. De plus, plusieurs mesures et calculs importants sont décrits.

**Chapitre 3 (Résultats Expérimentaux avec le Système de Gaz-Lift)** se concentre sur les résultats expérimentaux de la boucle avec protocole du gaz-lift utilisant de l'huile (Kerdane®) avec et sans sel et/ou AA-LDHI de faible à forte fraction d'eau. Un mécanisme de formation, d'agglomération, de dépôt et de bouchage d'hydrate est proposé et décrit en présence de bulles de gaz.

**Chapitre 4 (Résultats Expérimentaux avec la pompe Moineau sans et avec le Système de Gaz-Lift)** illustre les résultats expérimentaux avec protocole à pompe Moineau utilisant du Kerdane® avec ou sans sel et/ou AA-LDHI à forte fraction d'eau et à différents débits (et utilisant occasionnellement le système du gaz-lift pour lancer la nucléation d'hydrates et améliorer la formation d'hydrates dans les pipelines).

**Chapitre 5 (Mécanismes proposés et modèle de perte de charge relative pour les systèmes à forte fraction d'eau)** décrit plusieurs modèles conceptuels pour les phénomènes de formation et de transport des hydrates ainsi que le modèle de perte de charge relative. Ces modèles sont proposés et développés sur la base de résultats expérimentaux de la boucle sur des systèmes à forte fraction d'eau avec protocole à pompe Moineau.

**Finalement**, dans une dernière partie, sont résumées les conclusions de ces travaux et sont proposées des perspectives pour des prochaines études.

# CHAPTER 1. LITERATURE REVIEW

*In science, the credit goes to the man who convinces the world,  
not to the man to whom the idea first occurs.*

*Francis Darwin*

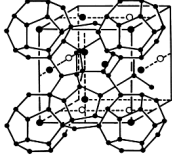
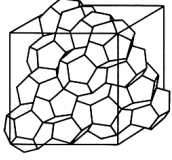
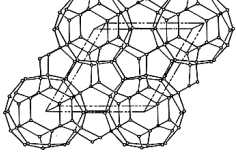
This chapter introduces the important definitions related to gas hydrate and flow assurance domain. In particular, the hydrate risk management strategies in oil and gas transportation are discussed. Emulsion, gas hydrate formation and agglomeration in emulsion, and hydrate suspensions are presented. Viscosity models of dispersion and suspension are summarized. Gas hydrate formation on the surface of gas bubbles is discussed. Multiphase flow and mass transfer which play a vital role in hydrate formation process are also reported. Finally, hydrate formation and transport in multiphase flow systems and hydrate kinetic models are presented.

## 1.1. Gas hydrate background

Gas (clathrate) hydrates are ice-like crystalline structures composed of molecular water cages stabilized for example by light hydrocarbon (methane, ethane, propane, etc.) at low temperature and high-pressure conditions (Sloan & Koh, 2008). The gas molecules (guests) are present inside cages (hosts) formed by water molecules bounded by hydrogen bonds and stabilized due to van der Waal's forces.

There are three different main crystalline types of hydrate structure:  $S_I$ ,  $S_{II}$ , and  $S_H$ , as shown in Table 1. 1. These structures are formed by five polyhedra where the vertices are the oxygen atoms of the water molecules and the edges represent hydrogen bonds. According to Jeffrey (1984), the polyhedra  $n_i^{m_i}$  has  $m_i$  faces of kind  $i$  containing  $n_i$  edges. The fit of the guest molecule within the water cage determines the crystal structure. In contrast with structures  $S_I$  and  $S_{II}$ , structure  $S_H$  requires two different guest molecules to form hydrate: a small one such as methane and a larger one with the size larger than 7.4 Å (cycloheptane, etc.). In oil and gas transportation, the hydrate structure I formed with light gases (e.g., methane or ethane) while heavier components (e.g., propane and iso-butane) are hydrate formers for the hydrate structure II. The presence of gas and water in the proper conditions (low temperature and high pressure) makes hydrate formation possible. Gas hydrate formation presents two stages including nucleation and growth depending on mass and heat transfer and intrinsic kinetics. Hydrate dissociation can be encountered once the temperature and pressure conditions become softer (Sloan & Koh, 2008).

**Table 1. 1: Crystalline cavities and structures of clathrate hydrates (Sloan & Koh, 2008).**

Hydrate structure	$S_I$		$S_{II}$		$S_H$		
Ideal Unit Cell Formula	 6X.2Y.±6 H <sub>2</sub> O		 8X.16Y.136 H <sub>2</sub> O		 1X.3Y.2Z.34 H <sub>2</sub> O		
Description	$5^{12}$	$5^{12}6^{-2}$	$5^{12}$	$5^{12}6^4$	$5^{12}$	$4^35^66^3$	$5^{12}6^8$
Cavity	Small	Large	Small	Large	Small	Medium	Large
Lattice Parameter, Å	a=12		a=17.30		a=12.26, c=10.17		
Number of Cavities	2	6	16	8	3	2	1
Average Cavity Radius, Å	3.95	4.33	3.91	4.73	3.91 <sup>b</sup>	4.06 <sup>b</sup>	5.71 <sup>b</sup>
Coordination Number <sup>a</sup>	20	24	20	28	20	20	36
<p>(a) Number of oxygens at the periphery of each cavity; X and Y refer to large voids and 12-hedra, respectively.</p> <p>(b) Estimates of structure H cavities from geometric models; Z is the <math>4^35^66^3</math> cavity.</p>							

Several remarkable hydrate growth models are described as follows:

Englezos (1987) proposed a kinetic model of methane and ethane hydrate formation. According to this model, the hydrate formation experiences three stages: (1) diffusion of the guest molecule from the gas-liquid interface to the liquid bulk; (2) diffusion of the guest molecule from the liquid bulk to the hydrate-solution interface; (3) reaction of water and guest molecule at the hydrate-solution interface. The driving force for gas hydrate formation is attributed to the difference between the fugacity of the dissolved gas (at the operating temperature and pressure),  $f$ , and the three-phase equilibrium fugacity at the experimental temperature  $f_{eq}$ . The growth rate can be expressed as follows:

$$\left(\frac{dn}{dt}\right)_p = K^* A_p (f - f_{eq}) \quad (1.1)$$

Where the term  $t$  is time,  $A_p$  is the interfacial area,  $n$  is the number of moles of gas consumed during hydrate formation, and  $K^*$  is the kinetic constant associated with steps (2) and (3) of the above proposed mechanism. In this model, they assumed that spherical particles are homogeneously distributed in the reactor and the overall reaction rate is obtained by the integration of the above equation.

The kinetic model of Skovborg and Rasmussen (1993) was based on the model of Englezos (1987). The gas consumption rate is proposed by the following equation:

$$\frac{dn}{dt} = k_L A_{GL} C_w^0 (x_{int} - x_b) \quad (1.2)$$

Where the term  $t$  is time,  $k_L$  is the mass transfer coefficient at the gas-liquid interface,  $x_{int}$  is the gas mole fraction in the liquid in equilibrium with the gas at the interface,  $x_b$  is the gas mole fraction in the liquid bulk in equilibrium with the hydrate phase for the operating conditions,  $C_w^0$  is the initial molar concentration of water,  $A_{GL}$  is total interfacial area in the reactor, and  $n$  is the number of moles of gas consumed during hydrate formation. These authors proposed that all resistance to mass transfer during hydrate formation is in the diffusion of the dissolved gas from the gas-liquid interface to the liquid. They also stated that this model is very sensitive to errors in the calculation of the driving force.

According to the proposed model of Herri (1999), the reactor is divided into two distinct zones: (1) the interfacial region, with a diminutive thickness, where only primary nucleation takes place due to high supersaturation; (2) the liquid bulk, where crystals growth occurs but primary nucleation is also possible, depending on supersaturation. The main variables of the systems are the population density function the bulk zone  $f(R, t)$  and the concentration  $C_b(t)$  in dissolved methane in the bulk zone;  $t$  denotes the time and  $R$  the equivalent particle radius. The system dynamic behavior is basically described by two different equations, as follows:

(1) The population balance equation of the hydrate crystals:

$$\frac{\partial f}{\partial t} + G \left( \frac{\partial f}{\partial R} \right) = B'(R) - D'(R) \quad (1.3)$$

This is assumed that the growth rate  $G$ ,  $G = (dR/dt)$ , is independent of the grain size. The birth term  $B'(R)$  is the contribution of primary nucleation, secondary nucleation, breakage, and agglomeration. The death term  $D'(R)$  is mainly due to the agglomeration.

(2) The mass balance equation in dissolved methane in the bulk zone:

$$\frac{dC_b}{dt} = k_L a (C_{ext} - C_b) - \frac{4\pi \cdot G M_2}{v_m} \quad (1.4)$$

Where  $v_m$  is the molar volume of the hydrate particles,  $M_2$  is the second moment of the population density function,  $a$  is the mass transfer surface area per volume of liquid ( $\text{cm}^{-1}$ ),  $k_L$  is the

mass transfer coefficient ( $\text{cm}\cdot\text{s}^{-1}$ ),  $C_b$  is the methane concentration in the bulk of the liquid, and  $C_{ext}$  is the interfacial concentration imposed by the gas/liquid equilibrium.

## 1.2. Gas hydrate issue in flow assurance

Flow assurance can be defined as the application of different methods to ensure that the fluids in pipelines are continuously transported from the offshore wellhead to the production platform, refinery or gas markets. Major issues in flow assurance involve plugging and deposition from gas hydrates, waxes, halite, inorganic scales and asphaltenes (Rao, 2013). Gas hydrate formation is a great concern in flow assurance (Figure 1. 1). This represents a potential hazard (plug) to oil and natural gas transportation once deep-sea pipelines operate in favorable conditions to form hydrate (low temperature and high pressure) as seen in Figure 1. 3. In fact, hydrates form at the interface between the two phases (oil/water, gas/water), rather than the body of liquid water or the body of gaseous phase (Sloan et al., 2010). Especially, in recent years, the amount of water produced significantly increased because the oil and gas fields have become mature as shown in Figure 1. 2 (Gluyas, 2003). Oil and gas companies are producing an average of three barrels of water for each barrel of oil in their depleting reservoirs and spending more than \$40 billion to tackle with a huge amount of water (Bailey, 2000). In addition, from Schlumberger's data, today, the water cut in the reservoirs can reach very high value.

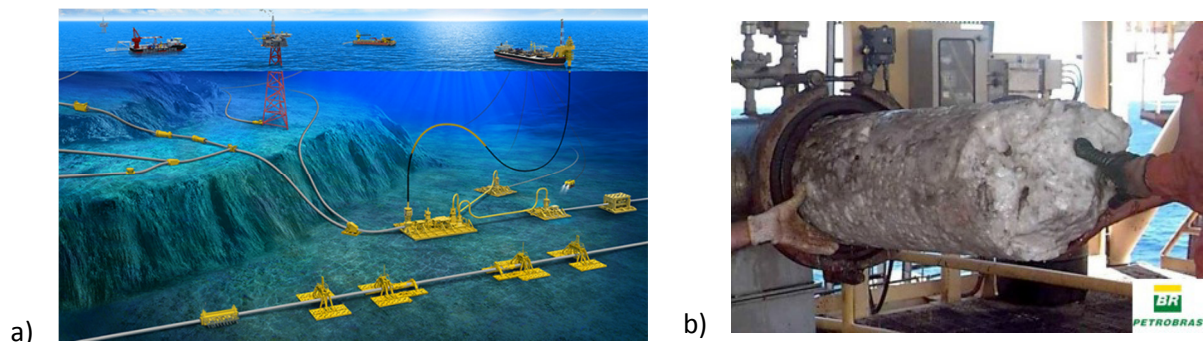


**Figure 1. 1: Subsea pipelines (a) (Oilstates, 2017) and hydrate accumulation obtained from the pig-catcher (b) (Petrobras, Brazil).**

Generally, up to date, hydrates can be prevented via a combination of the following methods (Sloan & Koh, 2008):

1. Physical (thermal or mechanical) methods: controlling pressure, temperature, and composition of the system (removal of water in oil and gas production prior to transport); line burial with wellhead heat addition; (electrical or hot water) heated pipelines and insulation.

2. Chemical methods: Thermodynamic Hydrate Inhibitors (THIs) or Low Dosage Hydrate Inhibitors (LDHIs): Kinetic Inhibitors or Anti-Agglomerants (AAs).

Among these hydrate preventing methods mentioned above, the most widely used ones are the addition of thermodynamic inhibitors, kinetic hydrate inhibitors, and commercial anti-agglomerants or low dosage hydrate inhibitors due to their low cost. The most traditional method employed to prevent gas hydrates is thermodynamic inhibition which shifts the hydrate equilibrium conditions to tougher conditions to form hydrates at higher pressure and lower temperature. However, a higher amount of THIs used at more severe conditions (deepwater, higher acid gas contents, higher water cuts, long tie-backs, etc.) in oil and gas transportation makes thermodynamic prevention less competitive due to the higher cost of THI injection. To reduce the cost or save CAPEX (facilities, pipe and pump) and OPEX (purchase, transportation and regeneration of additives), a large number of KHIs and/or AA-LDHIs are developed and used at a low dosage (<2 wt.%) compared to THIs (up to 20 wt.%). In fact, KHIs may delay the nucleation or growth of hydrate formation while AA-LDHIs allow forming hydrate but help to maintain hydrate particles dispersed and avoiding the plug in flowlines. These LDHIs are innovative and alternative technologies to thermodynamic inhibitors for preventing the plug in subsea-pipelines.

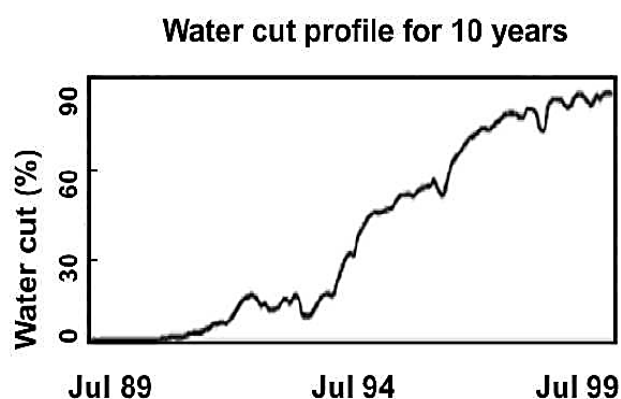


**Figure 1. 2: Water cut evolution over the period of 10 years of oil and gas production (Gluyas, 2003).**

Hydrate plugs prevented by thermodynamic (time-independent) or kinetic (time-dependent) or anti-agglomeration approaches are shown in the following sections of 1.2.1 and 1.2.2.

### **1.2.1. High-dosage (thermodynamic) hydrate inhibitors (THIs)**

Several additives are applied to gas hydrate formation and plugging prevention, including alcohols (methanol, ethanol, etc.), glycols (MEG, DEG, TEG, etc.) and some salts (NaCl, CaCl<sub>2</sub>, MgCl<sub>2</sub>, etc.). Among alcohols applied to prevent plug, methanol is the most widely used inhibitor because of its cost and its effectiveness. Katz, (1959) indicated that the inhibition capability of alcohols increases

with volatility, i.e., methanol > ethanol > isopropanol. Figure 1. 3 shows the hydrate-forming region in the pressure versus temperature diagram and the depth of the flowline from the deep-sea wellhead to the platform, accordingly to the different methanol concentrations added to the system. Without THI, the risk of hydrate formation is high. Because of hot fluid in the reservoir, up to 15 km from the subsea wellhead, hydrate formation is prevented in the oil and gas transport pipelines. In the range of 15 to 72 km from the wellhead, the oil and gas system enters hydrate formation zone due to a lower temperature in the deep ocean. However, an addition of methanol at a concentration higher than 20 wt.% could totally inhibit forming hydrate and prevent plugging (Sloan et al., 2010) and (Zerpa, 2013).

In the mechanisms of thermodynamic inhibitors, the glycols and alcohols present hydrogen bonding chance with water through hydroxyl groups. Besides, salt dissolves in solution as ions and interacts with the dipoles of the water molecules with a much stronger Coulombic bond than either the hydrogen bond or the van de Waals forces. The robust bond of water with salt ions inhibits hydrate formation and water is attracted to ions more than water is attracted to build the hydrate structure. Generally, thermodynamic inhibitors increase the competition for water molecules by the dissolved inhibitor molecules or ion through hydrogen bonding (for alcohols or glycols), or via Coulombic forces (for salt ions) (Sloan & Koh, 2008).

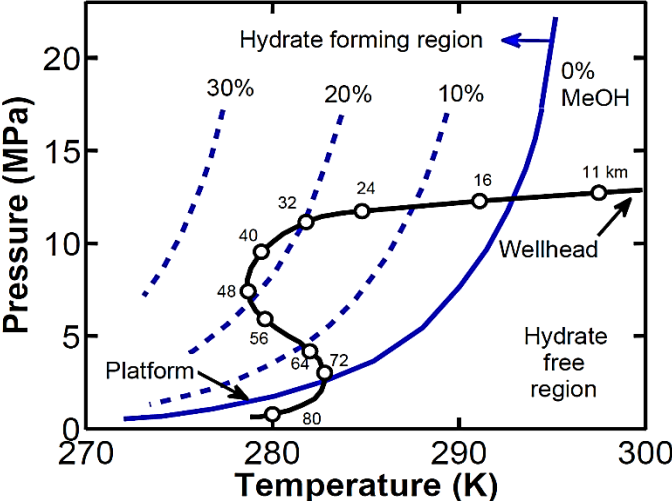


**Figure 1. 3: Pressure versus temperature diagram showing a typical operation condition curve of subsea flowline and hydrate equilibrium curve at different methanol concentrations; adapted from Sloan and Koh (2008). Points on the operation condition curve of offshore flowline indicate distance (in kilometers) from the wellhead.**

However, as mentioned above, severe conditions in oil and gas transportation make thermodynamic prevention less acceptable economically and feasible technically. The recent strategy to manage hydrate risk is based on using low dosage hydrate inhibitors as KHIs and AA-LDHIs. The most attractive hydrate risk management is by means of AA-LDHIs which allow hydrates to form (impossible to avoid hydrate formation at hard operational conditions) and disperse these hydrate particles to avoid plugging in flowlines.

### **1.2.2. Low-dosage hydrate inhibitors (LDHIs)**

In the last 10–15 years, LDHIs have been developed and can be significantly cheaper than other methods used. LDHIs are divided into two main groups: kinetic inhibitors (KHIs) and anti-agglomerants (AA-LDHIs). Their action relates to the surface or interfacial phenomena. Commercial KHIs are principally based on specific classes of the water-soluble polymer. Unlike AA-LDHIs, KHIs can also be used in gas lines where there is no liquid hydrocarbon phase (M. A. Kelland, Svartaas, Øvsthus, Tomita, & Chosa, 2006). Kinetic inhibitors have been shown to be active at significantly lower concentrations than thermodynamic inhibitors. Generally, anti-agglomerants used in preventing hydrate plugs are surface-active substances (surfactants). Besides, another kind of hydrate inhibitors is natural hydrate inhibitor encountered in several types of crude oils. Polar compounds present in crude oil, such as asphaltenes, resins or naphthenic acids, are known to enable stabilization of water in oil (W/O) emulsions (Foredal, 1996).

LDHIs are added at low concentrations, approximately 0.1–1.0 wt.% active concentration. This can be contrasted with the 15–20 wt.% needed for thermodynamic inhibitors such as methanol, glycols or salts (M. A. Kelland, 2006). The two different types of additives may have different field application ranges related to performance, field conditions, fluid properties, the properties of the additives and also environmental impact. It is generally considered that the AA-LDHIs can work at higher sub-cooling than KHIs. Therefore, for deep water applications, AA-LDHI is the unique class of LDHIs that can be deployed (M. A. Kelland, Svartaas, Øvsthus, Tomita, & Chosa, 2006). Shell's AA-LDHIs are now fully commercial and applied to a number of fields, several in the Gulf of Mexico and elsewhere such as the Dutch sector of the North Sea. These AA-LDHIs are based on quaternary ammonium surfactants with two or 3 butyl or pentyl groups attached to the quaternary ammonium nitrogen atom (Figure 1. 4). These quaternary groups are known to attach strongly to hydrate crystal surfaces. The surfactants may compose of two hydrophobic tails (oil-soluble AA-LDHIs) (Klomp, 1999) or a single tail (water-soluble AA-LDHIs) (Klomp, 1995). Several service companies to date have quaternary surfactant AA-LDHIs in their portfolio of LDHIs (M. A. Kelland, Svartaas, Øvsthus, Tomita, & Chosa, 2006). The actual performance of LDHIs is not only dependent on the composition of the

liquid hydrocarbon phase but also on other factors as pressure, salinity, other additives, and mixing (M. A. Kelland, 2006).

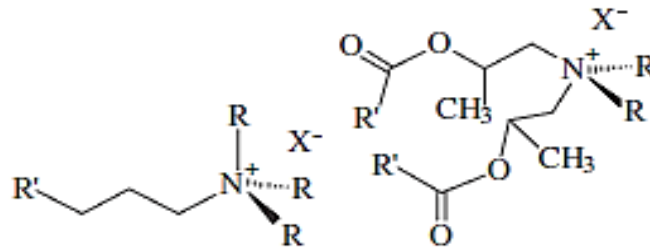


**Figure 1. 4: The structures of mono-tail (left) and twin-tail (right) quaternary ammonium surfactant (AA-LDHI). R is butyl or pentyl; R' is a long alkyl chain and X- is an anion (M. A. Kelland, Svartaas, Øvsthus, Tomita, & Chosa, 2006).**

#### 1.2.2.1. Kinetic hydrate inhibitors (KHIs)

Kinetic hydrate inhibitors are generally low molecular weight polymers which are water-soluble and added to the water phase to prevent hydrate formation and plug in pipelines. The KHIs in the water phase are then removed at a platform or onshore (Sloan & Koh, 2008). Some typical kinetic inhibitors are poly-N-vinylcaprolactam (PVCap) and poly-N-vinylpyrrolidone (PVP). These inhibitors act possibly by bonding to the hydrate surface and preventing significant crystal nucleation and growth for a period of time which is longer than the free water residence time in a pipeline. Kinetic inhibitors' action is limited at a long period of time, low temperature, and high pressure because with enough long time, the crystal growth can be important enough to cause line plugs (Sloan & Koh, 2008). In addition, KHIs are considered only to be effective at a sub-cooling (the difference between the system temperature and the hydrate equilibrium temperature) of less than 8.3<sup>0</sup>C (Colombel et al., 2009) and (M. A. Kelland, 2006) and less effective at shut-in conditions.

The hydrate kinetic inhibition mechanism is not fully understood. Some scientists suggest this mechanism is to prevent hydrate nucleation (M. A. Kelland, 2006). However, there is evidence to support that hydrate kinetic inhibitors inhibit the growth (Larsen, 1997). This apparent conflict is due to the definition of the size at which crystal nucleation stops and growth begins. To tackle this confusion, one may consider growth to occur after the critical nucleus size is achieved. The key to the function of these KHI polymers is that they adsorb on the surface of the hydrate particles. As the polymer KHI chains are adsorbed more closely together on the crystal surface, it becomes more difficult for the hydrate crystal to grow between them (Sloan & Koh, 2008).

Because of limitations of KHIs as mentioned above, it is highly important to develop and adopt another generation of LHDIs which can address the disadvantages of KHIs: hydrate anti-agglomerants (AA-LDHIs) as discussed in section 1.2.2.2.

#### **1.2.2.2. Hydrate Anti-Agglomerants (AA-LDHIs)**

Recently, AA-LDHIs have been investigated extensively because of their high performance at severe conditions and CAPEX and OPEX savings. Anti-agglomerants (AA-LDHIs) are long molecules (surfactants) that reduce particles cohesion and typically provide a relatively stable water-in-oil emulsion (Sloan & Koh, 2008). There are two common types of AA-LDHIs: (1) firstly, the French Petroleum Institute (IFP) type (polymeric) that provides a special kind of water in oil emulsion and restrict hydrate particles to water droplets, preventing agglomeration (Behar, 1991) and (2) secondly, the Shell type (Klomp, 1995) that is designed to adsorb on the hydrate surfaces. This AA-LDHI has a hydrate-philic head group(s) to lower growth rate and long hydrophobic tail(s) to help disperse hydrate particles in oil phase by creating oil-wet hydrate surface. In oil external phase systems, there are three ways of preventing hydrate plugs: (1) prevent hydrate nucleation, (2) prevent hydrate growth, and (3) prevent agglomeration of hydrate particles, as a result, plugs will not form (Sloan & Koh, 2008). Anklam (2008) deduced that an effective anti-agglomerant must be that: (1) reduces the size of hydrate particles, (2) decreases the interfacial tension between water and oil phase and (3) changes the wettability of hydrate surface to oil-wet by mean of increasing contact angle through the water phase.

According to the theory of capillary force forming by the liquid bridge, if the interfacial tension between oil and water reduces, the capillary force among hydrate particles proportionally decreases leading to prevention of hydrate particle agglomeration. Thanks to surfactants adsorbed onto the hydrate particle surface, the hydrate particles can be prevented from others or from water droplets, because of changing the wettability of hydrate particles as shown in Figure 1. 5 (M. Sun, 2015).

Generally, anti-agglomerants allow hydrates to form but prevent the agglomeration and deposition of hydrate crystals such that transportable, non-agglomerated and viscous hydrate slurry is formed in a liquid hydrocarbon phase (Huo et al., 2001). Anti-agglomerants can be considered as bridge compounds that keep apart the normally aggregated hydrate particles which keep suspended in the oil phase without aggregation. The anti-agglomerants are capable of preventing a new water phase which forms a capillary bridge between hydrate particles; as a result, the particles will not attract each other. The most common AA-LDHIs based on quaternary ammonium surfactants (one

end of the molecule attached to the hydrate structure and the other end of the long chain dissolved in the oil phase) are widely used and commercially available but a series of new surfactants for anti-agglomeration are discovered recently (M. A. Kelland, Svartaas, Øvsthus, Tomita, & Chosa, 2006); (M. A. Kelland, Svartaas, Øvsthus, Tomita, & Mizuta, 2006); (M. A. Kelland, 2008) and (Sloan & Koh, 2008). Zanota et al., (2005), in their study, used the Quaternary Ammonium Salts (QAS) as hydrate plug inhibitors. They revealed that all the QAS tested in his work exhibited some kinetic inhibitions and/or anti- agglomeration effectiveness. A new active agent with low concentration (0.2 wt.% of water) shows high efficiency at a full range of water to oil ratios (M. Sun & Firoozabadi, 2013). AA-LDHs have been reported to be ineffective beyond a water cut of 50 vol.% (M. a Kelland, 2006). However, several studies revealed that AA-LDHs are positive for high water cut systems (Alapati et al., 2008); (Azarinezhad et al., 2008) and (Gao, 2009).

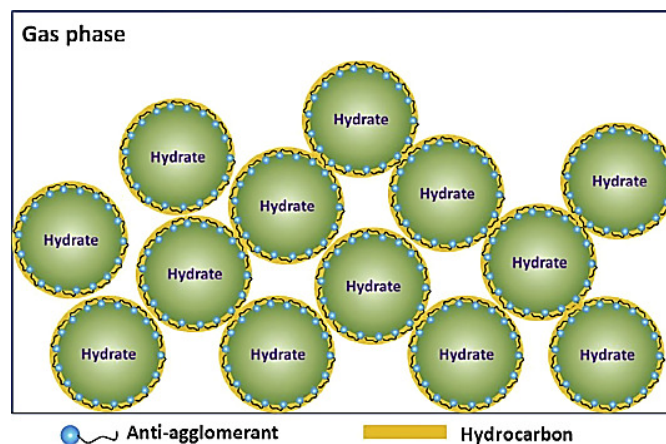


**Figure 1. 5: Anti-agglomeration mechanism with surfactants (Sun & Firoozabadi, 2015).**

The addition of alcohol and salt as co-surfactants can improve or decrease the anti-agglomeration performance depending on the types of these co-surfactants and range of these concentrations. York (2008) proposed that an addition of salt (NaCl or MgCl<sub>2</sub>) causes agglomeration of hydrates. On the contrary, a positive effect of salt on the efficiency of AA-LDHI was observed by (Azarinezhad et al., 2008); (Kelland, 2009); (Gao, 2009); (Moradpour, 2011); (Chua & Kelland, 2013); (Nagappayya et al., 2015); (Zhao et al., 2016) and (Dong et al., 2017). In addition, the effect of alcohol co-surfactant on the activity of anti-agglomerants was also investigated. York and Firoozabadi, (2008) showed that the methanol alcohol co-surfactants might help with anti-agglomeration. This was also in accord with the study of Gao, (2009).

### 1.3. Emulsions and suspensions

Emulsion is frequently encountered during the transportation of crude oil due to the presence of water in oil & natural gas production. In the presence of emulsifiers (surfactants), emulsions will be stable in some ways. Depending on the water fraction and the amount of gas, the multiphase systems in pipelines may include oil external phase (W/O), water external phase (O/W), and gas-dominated systems. Emulsions in the presence of dispersed solids (e.g., hydrates, waxes, etc.) become suspensions which are the main concerns in flow assurance.

#### 1.3.1. Surfactants

Surface-active agents (or surfactants) are amphiphilic compounds which are composed of two functional groups: a hydrophilic (polar or water soluble) group and a lipophilic (hydrophobic, non-polar) group. As their definition, surfactant molecules exhibit a double affinity for both polar and non-polar substances. Surfactants are divided into several groups based on the hydrophilic functional group dissolved in water or their moieties as follows: anionic, cationic, non-ionic and amphoteric (or zwitterionic) as shown in Figure 1. 6. Anionic surfactants possess a hydrophilic head with a negative charge which is associated with an inorganic metal positive (cationic) charge (e.g., sodium). Cationic surfactants contain a hydrophilic part with a positive charge associated with an inorganic negative (anionic) charge (chloride, bromide, etc.). Non-ionic surfactants have no electrical charges in their functional groups. Amphoteric surfactants have both oppositely charged (cationic and anionic) groups in their hydrophilic parts (Zerpa, 2013). The exceptional category of surfactant possibly is zwitterionic one in which it contains both cationic and anionic functional heads.

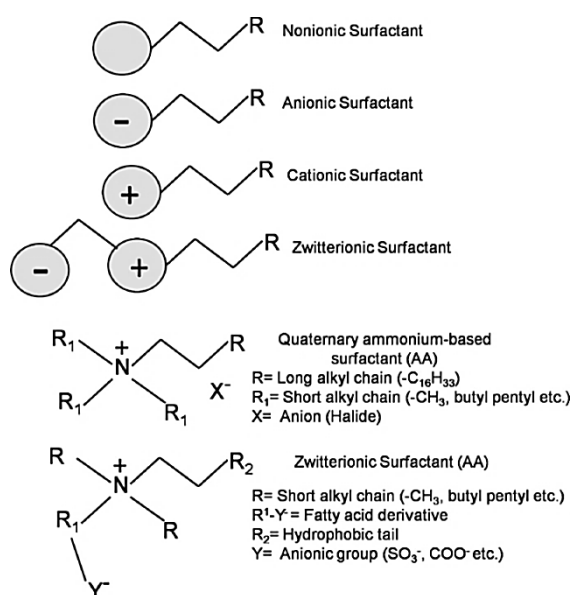


Figure 1. 6: Different types and structures of surfactants (Kumar et al., 2015).

The balance between the lipophilic and hydrophilic group characteristic will determine the behavior of each surfactant molecule. Particularly, the water-soluble or oil-soluble characteristics of surfactant molecules depend on the property of hydrophilic or hydrophobic groups (or the length of hydrocarbon chain). The presence of surfactants can modify the interfacial tension and the contact angle between phases and wettability of solids surface. Moreover, in water, they can aggregate (or self-associate) to form many types of structures with different shapes and orientations (called micelles) (Zerpa, 2013) and (Kumar et al., 2015). The surfactant concentration at which the first micelle is established is known as the critical micelle concentration (CMC), this is detected from a sudden change of some variables, including surface tension, viscosity, electrical conductivity, and density (Preston W.C, 1948).

In fact, surfactants have many applications to chemical engineering, food, and oil/gas industries as in stabilizing the emulsion, enhancing surface activity, foaming, wetting, flow assurance, oil and gas storage and transportation, etc. In gas hydrate industry, surfactants are used for diverse purposes, different types of surfactants can impact differently on the kinetics of hydrate formation (induction time and growth rate) in positive (enhancement) or negative (inhibition) way.

### **1.3.2. Emulsions**

Emulsion is a liquid-liquid colloidal dispersion system in which at least two immiscible liquid phases are required. The dispersed phase is referred to internal phase and the external phase is continuous phase. For almost all of the emulsions, one liquid is water and the other is hydrocarbon or oil (Schramm, 2005). In oil and gas flowlines, there is a large amount of water frequently co-existing with oil and gas due to crude oil production methods. As a result, water or oil will easily disperse together inducing emulsions. Some common surface-active components in crude oil are asphaltenes, resins with organic acids and bases, naphthenic acids, and carboxylic acids, among many others (Sjoblom et al., 2003). The two main simple kinds of emulsions in subsea pipelines are water-in-oil (W/O) and oil-in-water (O/W) emulsions. Besides, some complicated emulsions (so-called double or multiple emulsions) may be encountered as water-in-oil in water (W/O/W) or oil-in-water in oil (O/W/O) or even water-in-oil in water-in-oil (W/O/W/O) as shown in Figure 1. 7 (Schramm, 2005). These multiple emulsions may consist of only one, several or a large number of internal droplets. Sometimes, emulsion inversion phenomena also occur in particular conditions (the presence of solids, the increase in the amount of the dispersing liquid, and the coalescence of dispersing droplets, with or without surfactants). Emulsion inversion can be explained by two following mechanisms: catastrophic inversion and transitional inversion. The first one occurs if the dispersed fraction volume exceeds a critical value. The latter term appears when the system HLB

(hydrophilic-lipophilic balance) is changed (including salinity, surfactant type, temperature, etc.) and the water and oil volumetric fraction remain constant (Sjöblom, 2006).

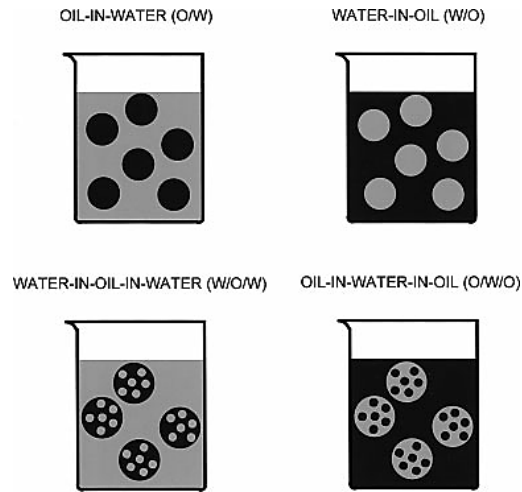


**Figure 1. 7: (Upper) The two simplest kinds of emulsions: oil-in-water (O/W) and water-in-oil (W/O). (Lower) The next level of complexity: water-in-oil-in-water (W/O/W) and oil-in-water-in-oil (O/W/O). The droplet sizes have been greatly exaggerated (Schramm, 2005).**

### 1.3.2.1. Rheology of emulsions

Emulsion properties, such as emulsion type, droplet size distribution, the stability, and rheology depend mostly on the following variables: composition of the oil, the salinity of the aqueous phase, nature and concentration of the surfactant, and temperature. Rheology of emulsion concerns the behavior of emulsion as Newtonian or non-Newtonian fluids. In general, the shear stress ( $\tau$ ), shear rate ( $\dot{\gamma}$ ) and viscosity of emulsion ( $\mu$ ) can be described by two following Ostwald relationship:

$$\tau = a\dot{\gamma}^n \quad \text{and} \quad \mu = a\dot{\gamma}^{n-1} \quad (1.5)$$

Where  $a$  is the consistency ratio and  $n$  is the behavior ratio; if  $n < 1$ , the fluid is pseudoplastic (or *shear-thinning*, lower apparent viscosity at higher shear rates); if  $n = 1$ , the fluid is Newtonian (the shear stress is directly proportional to the shear rate, constant viscosity) and if  $n > 1$ , the fluid is called dilatant (or *shear-thickening*, higher apparent viscosity at higher shear rates).

### 1.3.2.2. Relative viscosity of emulsions

The viscosity is an important characteristic of emulsion and it depends on these following factors: the viscosity of internal and external phase, the volume fraction of the dispersed phase, the droplet size distribution, emulsifiers, temperature, pressure, and shear rate. The relative viscosity of emulsion ( $\mu_r$ ) can be defined as the ratio of the viscosity of the emulsion ( $\mu_e$ ) to that of the

continuous phase ( $\mu_c$ ):  $\mu_r = \mu_E/\mu_c$ . Einstein, (1906, 1911) proposed the relative viscosity of emulsion ( $\mu_r$ ) as following:

$$\mu_r = \frac{\mu_E}{\mu_c} = 1 + 2.5\Phi \quad (1.6)$$

Where  $\phi$  is the volume of the dispersed phase ( $\phi < 2\%$ ) and this equation is valid if there is no interaction between the droplets.

Taylor (1932) suggested another expression with a small concentration of dispersed (spherical and tiny) drops as follows:

$$\mu_r = \frac{\mu_E}{\mu_c} = 1 + \frac{2.5(K + 0.4)}{K + 1}\Phi \quad (1.7)$$

Where  $K$  is defined as the ratio of the viscosity of the dispersed phase ( $\mu_D$ ) to that of the continuous phase ( $\mu_c$ ):  $K = \mu_D/\mu_c$ . This model is valid for very dilute emulsions. If  $K = \mu_D/\mu_c \gg 1$  ( $K$  tends to infinity) for the dispersions of spherical solids particles then we obtained the Einstein equation. Pal and Rhodes (1985) proposed the correlation for relative viscosity of emulsion as follows:

$$\mu_r = \frac{\mu_E}{\mu_c} = \left[ 1 + \frac{\Phi/\Phi^*}{1.187 - \Phi/\Phi^*} \right]^{2.5} \quad (1.8)$$

Where  $\phi^*$  is the dispersed phase volume fraction for which the relative viscosity  $\mu_r = \mu_E/\mu_c$  reaches 100. This value is determined experimentally for different systems ( $\phi^* \sim 0.66-0.81$ ). Additionally, it is recommended that the correlation should be used only in the concentration range of  $\phi/\phi^* < 1$ .

Pal (2000) also developed a viscosity-concentration equation for emulsions of nearly spherical droplets as below:

$$(\mu_r)^{-\frac{2}{5}} \left( \frac{2\mu_r + 5K}{2 + 5K} \right)^{\frac{-3}{5}} = 1 - K_0\Phi \quad (1.9)$$

Where  $K_0$  is a factor that considers the presence of surfactant adsorbed on the surface of the dispersed droplets. Indeed,  $K_0$  is constant for a certain emulsion system. However, it probably is not the same for every emulsion system and depends on: (1) the nature of the surfactant, (2) the concentration of the surfactant, and (3) the chemical nature of the dispersed and continuous phases. In this work, the presence of surfactant could cause an appreciable attraction of the continuous

phase molecules to the surface of the droplets. Consequently, the effective dispersed phase concentration ( $\phi_{\text{eff}}$ ) is higher than the true concentration of the emulsion ( $\phi$ ) and thus  $\phi_{\text{eff}} = K_o\phi$ , where  $\phi_{\text{eff}}$  is the effective volume fraction;  $\phi$  is the real volume fraction of the dispersed phase and  $K_o \sim 1.166-2.072$ .

In this present work, a study on the rheological properties of emulsion not only provides useful information on the stability and micro-structure of the emulsion but also plays a crucial role in predicting the gas hydrate formation and agglomeration in the emulsion.

### 1.3.3. Hydrate formation and agglomeration in emulsion systems

Mechanisms of hydrate formation and transport in emulsion systems might be different from those in pure water systems. The hydrate formation and dissociation may also affect the emulsion stability. The capillary forces formed by the liquid bridges between hydrate particles and between hydrate particles and pipe surface are the main reasons for hydrate agglomeration, deposition, and plugging.

#### 1.3.3.1. Hydrate formation/dissociation and their effects on the emulsion stability

Høiland et al., (2005) indicated that the presence of hydrate particles caused a strong effect on emulsion stability. In this work, the particle wettability is a crucial parameter for emulsion property. As a result, a reduction of inversion point is because of water-wet hydrates while an increase is by dint of oil-wet hydrates. Taylor et al., (2007) proposed a mechanism of hydrate film growth in the hydrocarbon/water interface using video microscopy and gas consumption. This indicated that an aqueous phase supplied hydrate former to the initial hydrate growth, and free gas phase supplied hydrate former in the hydrate film thickening. According to this work, the hydrate formation from a water droplet underwent three steps as follows in Figure 1. 8: 1) the formation of thin hydrate film covered the water droplet interface, 2) inside core film growth, and 3) full bulk conversion of hydrate shell.

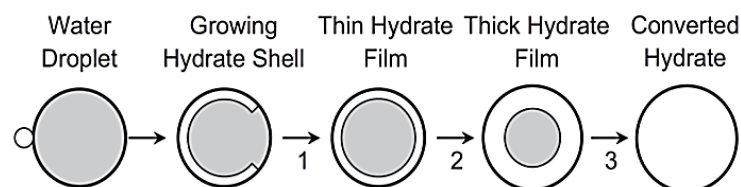


**Figure 1. 8: Mechanism for hydrate formation of a water droplet. Step 1: a thin porous hydrate film formed around the water droplet. Step 2: film growth. Step 3: water droplet completely converted to hydrate (Taylor, Miller, et al., 2007).**

Lachance et al., (2008) investigated the effect of hydrate formation and dissociation on emulsion stability using differential scanning calorimetry. They concluded that hydrate formation and dissociation destabilized W/O emulsions in oil with a low fraction of asphaltene. At a high content of asphaltene in oil, they resisted the destabilization of the emulsion. They also developed a new hydrate-induced destabilization model for both formation and dissociation steps which contribute to insight into the effect of hydrate on emulsion stability. Greaves et al., (2008) indicated that hydrate formation and dissociation from water-in-oil (W/O) emulsions destabilized the emulsion, with the final emulsion formulation favoring a water continuous state following re-emulsification. Hence, following dissociation, the W/O emulsion formed a multiple o/W/O emulsion (60 vol% water) or inverted at even higher water cuts, forming an oil-in-water (O/W) emulsion (68 vol% water) as shown in Figure 1. 9.

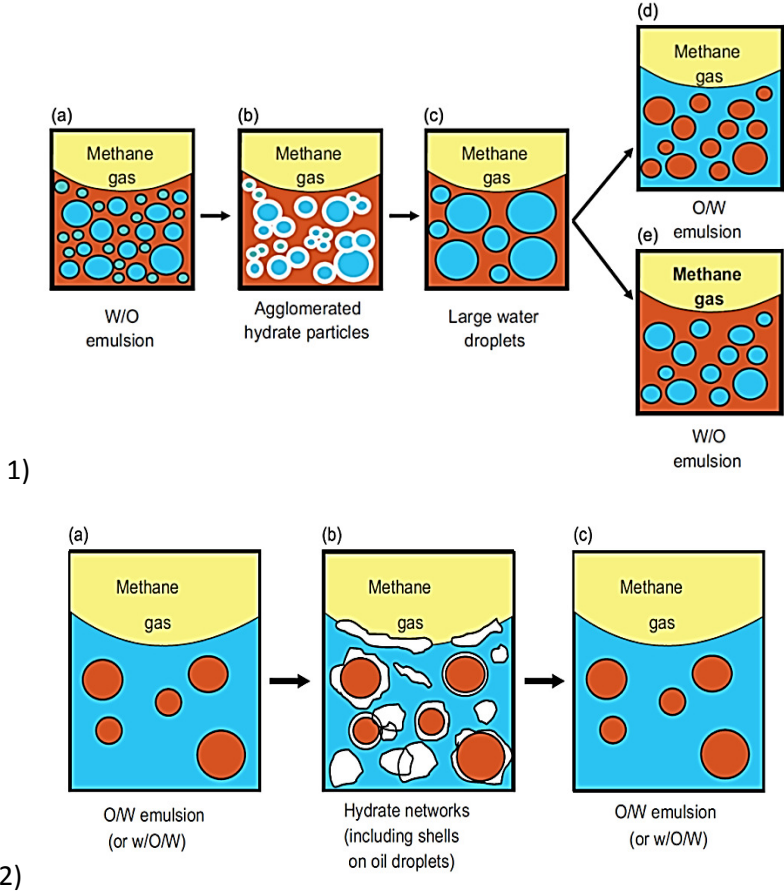


**Figure 1. 9: Hydrate formation and dissociation from a W/O emulsion (1): (a) initial emulsion; (b) agglomerated hydrate particles; (c) dissociated droplets; (d) final O/W emulsion (inversion has taken place); and (e) final W/O emulsion and from an O/W emulsion (2): (a) initial emulsion; (b) after hydrate formation; and (c) final emulsion after dissociation of gas hydrate emulsion (Greaves et al., 2008).**

In low water cut systems or oil continuous phase (W/O emulsion), hydrate formed at the water/oil interface forming hydrate thin film on the water droplet. This shell was fully converted to hydrate by several stages in the presence of gas dissolved in the oil phase as shown in Figure 1. 10. Moreover, the droplet size distribution was maintained during hydrate formation. In this mechanism, the methane in the gas phase transfers to the oil phase through the gas–oil interface. Methane diffuses then to the oil-water interface to form hydrate. During hydrate formation, the methane concentration is depleted at the hydrate/water droplet surface, though the growing hydrate shell limits the rate of methane penetration from the oil to the water to form more hydrate. In these stages, water droplets act as individual reactors (Douglas J. Turner et al., 2009). Turner et al., (2005) proposed a kinetic model including formation and dissociation rate and relative viscosity of the hydrate slurry. In addition, Turner et al., (2009) developed a model for gas hydrate formation in the emulsion. This model proposed the growth of hydrate in oil, in which gas hydrate forms on the surface of the water droplet and followed by additional conversion to its core. This model proposed several steps for hydrate growth, including: (1) Methane transfer into the oil phase from the vapor phase (2) Methane diffuses into the water/hydrate phase from the oil phase, and (3) Hydrate shell growth. Dalmazzone et al., (2009) studied the kinetics of methane formation in water-in-oil emulsion using a high-pressure differential scanning calorimetry. Furthermore, a model was proposed for the kinetics of hydrate formation in a water droplet dispersed in oil continuous phase. This model was based on crystal growth theory coupled with a statistically normal distribution of induction times representing the global phenomenon.

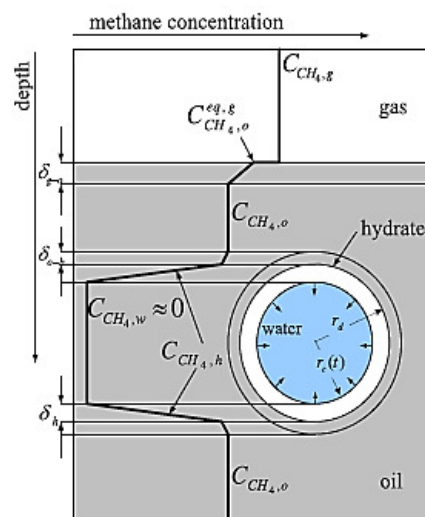


**Figure 1. 10: Mass transfer at the gas-oil interface and through a water droplet during hydrate formation in oil continuous phase (D. J. Turner et al., 2009).**

In high water cut systems or water continuous phase (O/W emulsion), the mechanism of gas hydrate formation is different from the one in W/O emulsion. Hydrate film forms on the exterior of the oil droplet and grows over the time. Some hydrate particles could be formed freely in the free liquid water. Interestingly, gas hydrates may be formed in the gas phase with water evaporated in appropriate conditions (low temperature and high pressure). However, there are only a few hydrate cages forming in the body of the gas because there are very few water molecules to make significant amounts of the host crystal structure in the bulk gas (Sloan et al., 2010).

Recently, Shi et al., (2011) proposed that gas hydrates also form on the exterior of water droplet dispersed in oil. In other words, an outward hydrate growth shell is formed once water permeates through the hydrate shell from the core of the water droplets. Talatori and Barth (2011) conducted the experiments with 50%WC (water in oil emulsion) and at 80%WC (oil in water emulsion). The results of this study showed that the rate of crystallization at oil continuous phase is higher than the one at water continuous phase. At 80%WC, the growth experienced two steps: the rate of formation in the first step was slower than that in the second step which is the same as the one at 50%WC. The change of formation rate was because of phase inversion. Karanjkar et al., (2012) studied the formation of cyclopentane hydrate in an emulsion and also concluded that hydrate formation occurs primarily at the interface between water droplets and the oil continuous phase with 40%WC. Without surfactants, a strong hydrate shell formed around the water droplet limiting transport of hydrate former to the free water which still trapped inside the hydrate layer. In the presence of oil-soluble surfactants, the hydrate crystals were much smaller. They suggested that hydrate formation apparently proceeds in three stages: 1) nucleation, 2) surface growth, and 3) radical growth. They also proposed a mechanism for hydrate formation.

Mu et al., (2014) investigated the kinetics of hydrate formation from pure methane in water-in-oil emulsions. The experimental results revealed that the higher water cut, the higher hydrate growth rate. A mathematical model considering the heat transfer and surface reaction was developed for the formation kinetics of methane hydrates in the emulsion. Li et al., (2015) also studied the kinetics of methane hydrate formation in water-in-oil emulsion system and showed that the increase in hydrate formation rate corresponds to the increase in the agitation rate. A mathematical model of hydrate formation kinetics was proposed based on crystal growth theory and the mass transfer. Sohn et al., (2015) studied hydrate plug formation from low to high water cut in the presence of thermodynamic and kinetic inhibitors in a high-pressure autoclave system. A simple model for hydrate growth in water-and oil-continuous systems was also developed to predict hydrate growth rate.

### 1.3.3.2. Agglomeration/deposition and plugging mechanisms

Agglomeration is the process in which particles assembly to form larger particles or agglomerates. Deposition might take place on the surface immersed in suspension. This surface is macroscopic dimension comparing to the particle. In term of mechanistic view, deposition on the solid surface may be considered as particle-particle agglomeration (M. Elimelech, J. Gregory, 1995).

Austvik et al., (2000) suggested that the plug structures in pipelines are porous in the presence of hydrate particles, liquid water, liquid hydrocarbon, and gas. The water liquid which is trapped between the hydrate particles is the main cause of plugging. Yang et al., (2004) observed in his study that there was a capillary cohesion of rough surfaces in the presence of bridging liquid between hydrate particles. Taylor et al., (2007a) also pointed out that capillary bridging is the dominant mechanism of cohesion between hydrate particles. Greaves et al., (2008) revealed that with W/O emulsion, hydrate formation leads to rapid agglomeration, while dissociation of these large agglomerates can lead to larger water droplets and perhaps a free water phase. The capillary force between hydrate particles may play the vital role in hydrate accumulation. Israelachvili, (2011) mentioned different geometries of liquid bridges may impact on the capillary forces of two surfaces. The capillary bridge theory was shown in the following equation (Aman et al., 2012):

$$\frac{F_A}{R^*} = 2\pi\gamma \sin(\alpha) \sin(\theta_p + \theta_s) + \frac{2\pi\gamma \cos\theta_p}{1 + \frac{H}{2d}} \quad (1. 10)$$

Where  $F_A$  is the hydrate–hydrate cohesive force normalized by the harmonic mean radius of the particle pair ( $R^*$ ),  $\gamma$  is water–oil interfacial tension and the remaining parameters are indicated in Figure 1. 11.

According to Aspenes et al., (2010), mechanism of hydrate agglomeration, deposition and plugging in pipelines is attributed to the capillary forces which are formed by a liquid bridge between hydrate particles and between hydrate particles and pipe surface. In his study, the adhesion force depends significantly on the presence of water in the system. If there is a water droplet deposited on the pipe surface, the adhesion force between the hydrate and the pipe surface is more than 10 times higher than hydrate–hydrate adhesion forces. Moreover, the presence of a water-saturated oil phase causes an increase in cohesion force between hydrate particles.

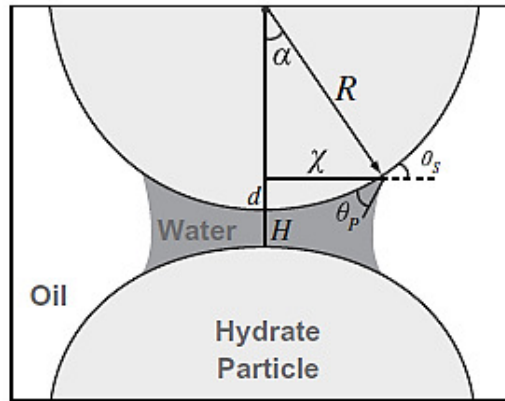


**Figure 1. 11: Schematic of hydrate cohesion through a capillary liquid bridge: embracing angle ( $\alpha$ ); capillary bridge width ( $\chi$ ); contact angle ( $\theta_p$ ); external contact angle ( $\theta_s$ ); liquid bridge immersion depth ( $d$ ); particle separation distance ( $H$ ); and particle radius ( $R$ ) (Aman et al., 2012).**

Several theoretical models have been proposed in the literature to describe the growth of particle clusters either by perikinetic aggregation (caused by Brownian motion) or by orthokinetic aggregation (caused by medium flow) (Jullien, 1990) and (Potanin, 1991). Two mechanisms of agglomeration are proposed by Emilie Colombel et al., (2010). The first one is the contact-induced agglomeration mechanism for which the crystallization-agglomeration process is described as the result of the contact between a water droplet and a hydrate particle. The second one is the shear-limited agglomeration mechanism for which the balance between hydrodynamic force and adhesive force is considered. The hydrate agglomeration mechanism is attributed to water droplets crystallization in subsequent contact with hydrate particles (Fidel-Dufour et al., 2006). Additionally, the viscosity of the hydrate slurry is a function of the agglomerate size (Camargo, 2002).

#### **1.3.4. Rheology of water/oil/hydrate suspension**

In the presence of solids (hydrate particles) in fluids (emulsion or dispersion), the rheological properties of flow shift significantly because of co-existence of three phases (water/oil/hydrate) in the pipelines. Particularly, this would lead to the effect of fine solids on the viscosity of emulsion (or dispersion). The relative viscosity of emulsion/solid suspension is a function of the oil, solids and shear rate. The gas hydrate particles may aggregate and this would lead to an increase in the viscosity of flow and finally, it may cause the plugging in the pipelines. The viscosity of suspension may be predicted and calculated by different models developed by many authors in the presence of solids. In the case of hydrate formation and agglomeration in pipelines, the size of the hydrate particle agglomerates may be calculated using the model of Camargo and Palermo (2002). This model

proposed that the viscosity of hydrate slurry increases with the increase in agglomeration size. The existing models to predict the relative viscosity of suspension are briefly described in section 1.3.4.1.

#### 1.3.4.1. Relative viscosity models of suspension

Numerous models were developed to describe the relative viscosity of suspension ( $\mu_r$ ) as a function of hydrate volume. Furthermore, an effective hydrate volume fraction ( $\phi_{\text{eff}}$ ) instead of the real hydrate volume ( $\phi$ ) is considered in the model of Camargo (2002) which takes into account the liquid (oil and/or water) trapped inside the hydrate agglomerates.

- Model of Richardson (1933)

Richardson (1933) modified the model of Einstein with the factor ( $a$ ) which is normally higher than 2.5. However, this model is just valid for a low dispersed volume fraction.

$$\mu_r = \frac{\mu}{\mu_c} = e^{a\phi} \quad (1.11)$$

Where  $\mu_r$  is the relative viscosity;  $\mu$  is the apparent viscosity of suspension;  $\mu_c$  is the viscosity of continuous phase (dispersing liquid or emulsion) and  $\phi$  is the volume fraction of dispersed solid phase.

- Model of Mooney (1950)

Mooney (1950) is the first person who considered that the volume occupied by solid particles in one continuous phase is higher than the real volume of particles. This volume is related directly to the maximum volume fraction ( $\phi_{\text{max}}$ ).

$$\mu_r = \frac{\mu}{\mu_c} = e^{\frac{2.5\phi}{1-k\phi}} \quad (1.12)$$

Where  $\mu_r$  is the relative viscosity;  $\mu$  is the apparent viscosity of suspension;  $\mu_c$  is the viscosity of the continuous phase;  $\phi$  is the volume fraction of dispersed solid phase;  $k$  is a constant, the self-crowding factor, predicted only approximately by the theory ( $1.35 < k < 1.91$ ; different  $k$  for different sets of experimental data).

- Model of Brinkmann-Roscoe (1952)

Roscoe (1952) developed the correlation to predict the viscosity of Newtonian poly-dispersed system as follows:

$$\mu_r = \frac{\mu}{\mu_c} = (1 - \phi)^{-2.5} \quad (1.13)$$

Where  $\mu_r$  is the relative viscosity;  $\mu$  is the apparent viscosity of suspension;  $\mu_c$  is the viscosity of the continuous phase and  $\phi$  is the volume fraction of dispersed solid phase. For a system with the uniform size of solid particles, the correlation can be modified as follows:

$$\mu_r = \frac{\mu}{\mu_c} = (1 - 1.35\phi)^{-2.5} \quad (1.14)$$

- The model of Krieger (1972)

$$\mu_r = \frac{\mu}{\mu_c} = \left(1 - \frac{\phi}{\phi_{max}}\right)^{-[\eta]\phi_{max}} \quad (1.15)$$

The term of  $\phi_{max}$  is maximum packing volume fraction which is determined by the packing geometry depending on the particle shape and size distribution. The maximum packing volume fraction for hard spheres is often taken as 0.74 (close-packed uniform spheres) which is the value associated with random close packing. The factor  $[\eta]$  is intrinsic viscosity, normally taking  $[\eta] = 2.5$  for hard spheres. However, at high concentration, the intrinsic viscosity depends considerably on the particle-particle interactions. Hence, this value varies with experimental conditions (Quemada, 1977).

- Model of Barnea and Mizrahi (1973)

For the Newtonian suspension composed of spherical solid particles, Barnea and Mizrahi (1973) developed the correlation of viscosity as follows:

$$\mu_r = \frac{\mu}{\mu_c} = e^{\frac{2.66\phi}{1-\phi}} \quad (1.16)$$

Where  $\mu_r$  is the relative viscosity;  $\mu$  is the apparent viscosity of suspension;  $\mu_c$  is the viscosity of continuous phase and  $\phi$  is the volume fraction of dispersed solid phase.

- Model of Mills (1985)

Mills (1985) developed a model to predict the viscosity of suspensions as a function of real hydrate volume fraction and maximum hydrate volume fraction as below:

$$\mu_r = \frac{\mu}{\mu_c} = \frac{1 - \phi}{\left(1 - \frac{\phi}{\phi_{max}}\right)^2} \quad (1.17)$$

Where  $\mu_r$  is the relative viscosity;  $\mu$  is the apparent viscosity of suspension;  $\mu_c$  is the viscosity of continuous phase. This equation well adapted to hard spheres with only hydrodynamic interactions.  $\phi_{max}$  is the maximum volume fraction to which particles can pack or the packing concentration of randomly packed spheres (equal to 4/7).

- Model of Camargo-Palermo (2002)

Camargo (2002) developed a model of Mills (1985) to obtain a new model to predict the viscosity of suspensions. They defined porosity of aggregation of hydrate particles by introducing a fractal dimension ( $f$ ). The number of hydrate particles  $N$  in a fractal aggregate is as a function of  $d_A$  (aggregate diameter),  $d_p$  (particle diameter) and  $f$  as follows:

$$N = \left( \frac{d_A}{d_p} \right)^f \quad (1.18)$$

Indeed, due to fractal structure of aggregates, an effective particle hydrate volume fraction ( $\Phi_{eff}$ ) which is defined as the sum of the real volume of hydrate particles plus the trapped fluid between particles in contact is taken into account replacing the real particle hydrate volume fraction as the following equation (Mills, 1985):

$$\mu_r = \frac{\mu}{\mu_c} = \frac{1 - \Phi_{eff}}{\left(1 - \frac{\Phi_{eff}}{\Phi_{max}}\right)^2}; \quad \Phi_{max} = \frac{4}{7} \quad (1.19)$$

$$\Phi_{eff} = \Phi \left( \frac{d_A}{d_p} \right)^{(3-f)} \quad (1.20)$$

Where  $\mu_r$  is the relative viscosity and the fractal dimension is from 1.7 to 2.1 for perikinetic aggregation (caused by Brownian motion) and more compact with higher than 2 to 2.7 under shearing condition (Hoekstra et al., 1992).

Due to the flowing force applied to hydrate aggregates, they cannot grow freely. The maximum size of aggregate depends on the balance between shear stress and cohesion force ( $F_A$ ) between particles considering the hydrodynamic interaction of aggregates as follows:

$$d_{A,max} = \left[ \frac{F_A (d_p)^{2-f}}{\mu_0 \dot{\gamma}} \right]^{\frac{1}{4-f}} \quad (1.21)$$

The hydrodynamic interaction of aggregates can be taken into account by substituting the viscosity  $\mu_0$  of the dispersing liquid by the apparent viscosity of the suspension  $\mu$ . Where  $\mu$  is the apparent viscosity of suspension and  $\dot{\gamma}$  is the shear rate.

At equilibrium, it is supposed that  $d_A \sim d_{A, max}$ . The value of  $d_A/d_p$  can be obtained by solving the following equation:

$$\frac{d_A^{(4-f)}}{d_p} - \frac{F_A \left[ 1 - \frac{\Phi}{\Phi_{max}} \left( \frac{d_A}{d_p} \right)^{(3-f)} \right]^2}{d_p^2 \mu_0 \dot{\gamma} \left[ 1 - \Phi \left( \frac{d_A}{d_p} \right)^{(3-f)} \right]} = 0 \quad (1.22)$$

Finally, the viscosity of the suspension is calculated by equation (1. 19). It is noted that if  $d_A/d_p < 1$  then  $d_A$  is fixed equal to  $d_p$ .

#### 1.3.4.2. Relative pressure drop models of suspension

The friction factor ( $f$ ) is determined by these following relations based on existing theoretical work and/or experimental data as follows (Midoux, 1993):

$$f = \frac{16}{Re} \text{ for laminar flow (Fanning)} \quad (1.23)$$

$$f = aRe^{-b} \text{ for turbulent flow, Blasius (1913), where } a=0.079 \quad (1.24)$$

or 0.046 and  $b=0.25$  or  $0.20$ , respectively)

$$f = \frac{\Delta P}{L} \frac{D}{2\rho v^2} \quad (1.25)$$

Where  $Re$  is the Reynolds number which can be expressed as:

$$Re = \frac{\rho v D}{\mu} \text{ or } \mu = \frac{\rho v D}{Re} \quad (1.26)$$

$\Delta P$  is the pressure drop (Pa),  $L$  is the length of pipe between two points of pressure drop measurement (m),  $D$  is the diameter of pipe (m),  $\rho$  is the density of fluid ( $\text{kg.m}^{-3}$ ),  $v$  is the velocity of flow ( $\text{m.s}^{-1}$ ) and  $\mu$  is the viscosity of fluid (Pa.s).

Besides, the viscosity of emulsion can be estimated (in laminar regime) as following (Midoux, 1993):

$$\mu = \frac{D^2}{32} \cdot \frac{1}{v} \cdot \frac{\Delta P}{L} \quad (1.27)$$

The correlation between relative viscosity and pressure drop model of suspension in turbulent and laminar regime is described as below. In this correlation, we used relative viscosity model of Mills (1985) as described in section 1.3.4.1 and using the term  $\phi_{eff}$  instead of  $\phi$  (Camargo,

2002) and (Moradpour et al., 2011). The relative pressure drop (RPD) is defined as the instantaneous pressure drop (after hydrate nucleation) divided by the initial pressure drop (before hydrate nucleation).

- In laminar regime:

$$\Delta P = \frac{2fL\rho v^2}{D} \rightarrow \frac{\Delta P_{(t)}}{\Delta P_{(t_0)}} = \frac{f(t)}{f(t_0)} = \frac{Re_{(t_0)}}{Re_{(t)}} = \frac{\mu_{(t)}}{\mu_{(t_0)}} \quad (1.28)$$

$$\frac{\Delta P_{(t)}}{\Delta P_{(t_0)}} = \frac{\mu_{(t)}}{\mu_{(t_0)}} = \frac{1 - \Phi_{eff}}{\left[1 - \left(\frac{\Phi_{eff}}{\Phi_{max}}\right)\right]^2} \quad (1.29)$$

- In turbulent regime:

$$\Delta P = \frac{2fL\rho v^2}{D} \rightarrow \frac{\Delta P_{(t)}}{\Delta P_{(t_0)}} = \frac{f(t)}{f(t_0)} = \frac{Re_{(t)}^{-b}}{Re_{(t_0)}^{-b}} = \left(\frac{Re_{(t)}}{Re_{(t_0)}}\right)^{-b} = \left(\frac{\mu_{(t)}}{\mu_{(t_0)}}\right)^b \quad (1.30)$$

$$\frac{\Delta P_{(t)}}{\Delta P_{(t_0)}} = \left(\frac{\mu_{(t)}}{\mu_{(t_0)}}\right)^b = \left\{ \frac{1 - \Phi_{eff}}{\left[1 - \left(\frac{\Phi_{eff}}{\Phi_{max}}\right)\right]^2} \right\}^b = \frac{(1 - \Phi_{eff})^b}{\left[1 - \left(\frac{\Phi_{eff}}{\Phi_{max}}\right)\right]^{2b}} \quad (1.31)$$

#### 1.4. Hydrate formation on the surface of gas bubbles

Numerous studies on hydrate formation on the surface of gas bubbles were published. The main advantage of this method is to enhance hydrate formation by enlarging contact surface between gas and water without thermodynamic or kinetic promoters or mechanical methods such as stirring, spraying, etc. (Luo et al., 2007). Similarly, this phenomenon is encountered in the offshore oil and gas drilling blowout, the leakage of pipeline transportation and the instability of submarine gas hydrate resources and gas bubbles rising in deep water (C. Li & Huang, 2016).

Main and Bishnoi (1981) proved that reaching a specific condition, hydrate shell may form rapidly on the natural gas bubbles and shed from the interface and hydrated gas bubbles disintegrated or collapsed into large hydrate flakes. Afterwards, Gumerov and Chahine (1998) conducted their own experiments to observe and describe the dynamics of gas bubbles in hydrate formation conditions. In this work, bubbles of various unusual shapes in normal conditions were observed. Such shapes strongly depend on the rates of gas supply. At high flowrate of gas injection, the hydrate layer was mobile and seems to be aluminum paint. At lower gas flowrate, bubbles were completely covered with hydrates. After bubble detachment, they observed very strong shape deformation due to the liquid flow. The collapse of bubbles partially and completely covered by hydrates was also observed.

Gas hydrate formation on the surface of gas bubbles continued to be investigated and disclosed at a high rate of hydrate formation by (Luo et al., 2007) and (Tajima et al., 2010). Furthermore, the conceptual mechanism of hydrate formation on the surface of gas bubbles with and without additives (SDS) was presented by Tajima et al., (2007) as shown in Figure 1. 12. In this mechanism, the morphology of the hydrate film and its characteristics were significantly changed with increasing the SDS concentration which was attributed to SDS molecules adsorbed on the interface of bubbles and water. In the absence of SDS, the homogeneous and rigid hydrate shell was formed. However, in the presence of SDS, rougher and heterogeneous hydrate shell was formed but easily collapsed. According to Luo (2007), hydrate formation rate on the surface of the rising bubble was high, however, the formed hydrate shell was not broken up easily. The hydrate shell-covered bubbles tended to agglomerate rather than fuse into the bigger ones. This kind of behavior of hydrate shell hindered the further formation of hydrate and lowered consumption rate of methane. Moreover, Sun (2007) studied the morphology of three-dimensional growth of hydrate shell covering the gas bubble in water or an aqueous surfactant solution. The results revealed that the roughness of the hydrate surface was affected by the time elapsed and the magnitude of driving force. They also developed a kinetic model to correlate the growth rates of hydrate film.

Sato (2013) from his experiment confirmed that a thin methane hydrate film is formed on the bubble surface and it changes the motion of the bubble in fluid significantly (zigzag). The zigzag motion of the methane hydrate bubbles (contrary to the spiral motion of methane bubbles) changed with Reynolds number. Additionally, the shape of the methane hydrate bubble was transformed from spherical to ellipsoidal. The same phenomenon was observed in the behavior of a bubble with a surfactant. Chen et al., (2013) performed methane hydrate formation on suspended gas bubbles in water. In this study, methane gas was gradually injected into a counter-flowing water column and they observed a solid hydrate shell formed instantly once a certain methane concentration was reached and witnessed a full hydrate shell on suspended gas bubbles. They also found that the hydrated bubbles were not stable and this leads to dispersed hydrate particles in water.

Recently, Warzinski et al., (2014) presented high-definition, experimental observations of complex surficial mechanisms governing methane bubble hydrate formation. Their new findings are synergistic feedbacks between bubble hydrodynamics, hydrate morphology, and coverage characteristics. Effect of SDS and PVCap on the morphology of methane-propane hydrate forming on the gas bubble was investigated by (S. Y. Lee et al., 2014). In this study, with pure water, smooth hydrate film was formed at first on the bubble surface and became rough later. In the presence of SDS, significant changes in morphology were observed and the gas bubble was not fully covered by

hydrate film once the SDS concentration increased. In the PVCap solution, hydrate crystals formed on the bubble surface and spread out the whole surface. Morphology of hydrate film formed on the gas bubble/water interface with different gas mixtures was revealed by microscopic visual methods by S.-L. Li et al., (2014). This work contributed new observations and insights of hydrate film textures with different gas compositions and degree of sub-cooling.

The cohesion force of methane hydrates was measured and mentioned in the recent study of Sato (2016). In this work, there was little force between two methane hydrate samples to detach in the water. Additionally, the adhesion of methane bubbles to the pipe wall depends on whether the bubbles are broken up or not. However, the breakup behavior of the bubbles covered with methane is still unknown. Another mechanism of hydrate formation on the surface of gas bubble was proposed in the model of Li and Huang (2016) as shown in Figure 1. 13.

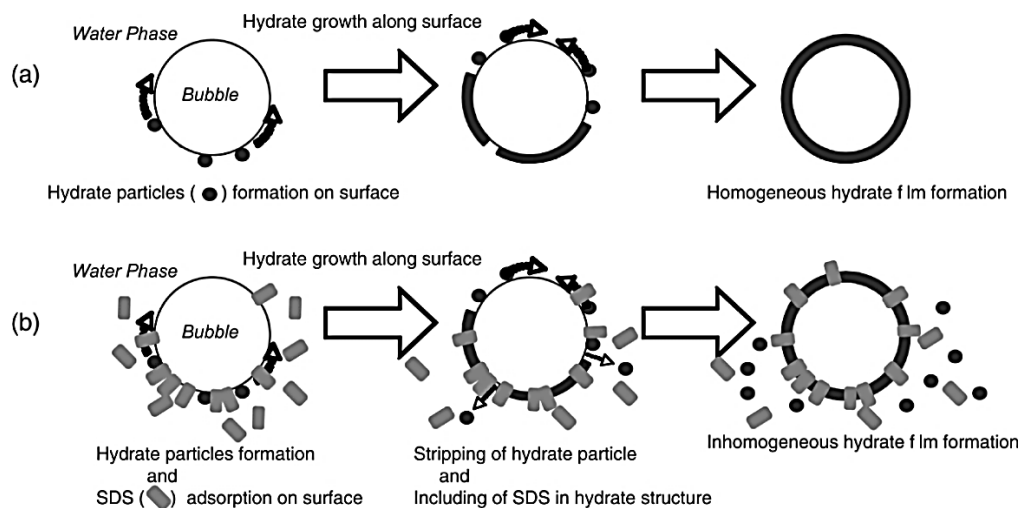


**Figure 1. 12: Proposed mechanisms of the hydrate formation on the bubble surface: (a) without SDS and (b) with SDS (Tajima et al., 2010).**

Concerning gas bubble size, Main and Bishnoi (1981) published that the sizes of the gas bubbles were in the range of 8-27 mm in diameter generated in an opposing water flow to simulate the process of gas bubbles ascending in deep water. When gas blows out in deep sea water, gas bubbles appear in radii of 0.5–5 mm (Leifer & Patro, 2002). In the presence of additives, the size decreases with increasing of AA-LDHI while without AA-LDHI is about 4 mm in diameter (Tajima et al., 2010). Sato et al., (2013) revealed that the diameter of the methane hydrate bubble changed from 3.8 to 7.8 mm which corresponds to 555 to 1155 of Reynolds number. Li and Huang (2016), in their model of gas bubbles with gas hydrates rising in deep water, used the range of 1.5-5 mm in diameter of gas bubbles released at depths of 1000-2000m.

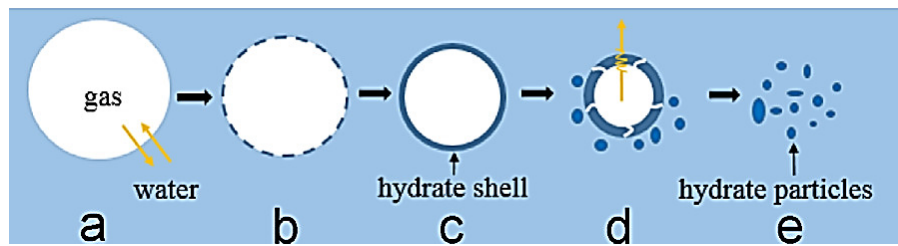


**Figure 1. 13: Gas bubble behaviors with gas hydrates in rising process: (a) gas bubble dispersed in water; (b) hydrate formed on the surface of gas bubble; (c) hydrate shell formed; (d) hydrate cracks; and (e) hydrate particles (C. Li & Huang, 2016).**

## **1.5. Multiphase flow and mass transfer in oil and gas pipelines**

This section will describe the different types of flow in subsea pipelines. Generally, multiphase flow is encountered in oil and gas production from the reservoir to the platform. Mass transfer which plays a key role in hydrate crystallization in flowlines will be also discussed.

### **1.5.1. Single-phase flow**

The single phase term represents either gas or liquid phase. In this study, single phase flow is in horizontal and vertical lines of the flowloop in the experiments with 100%WC before hydrate crystallization. In oil and gas industry, more than one phase (multiphase) flow is encountered in almost cases. All of the multiphase flows and related definitions are shown in the following sections of 1.5.2; 1.5.3 and 1.5.4.

### **1.5.2. Two-phase Gas-Liquid flow**

In this study, two-phase gas-liquid flow is in the separator where gas and liquid are separated or in the riser in which gas is injected at the bottom of the gas-lift system. The Gas-Liquid flow regime is mainly dependent on the flowrate, liquid properties, geometry and inclination of the flowline.

In vertical gas-liquid flow, injecting gas at low flowrate at the bottom of tube leads to a random distribution of small bubbles in the liquid continuous phase, so-called bubbly flow. Increasing of gas velocity causes coalescence between gas bubbles. As a result, larger bubbles with bullet shape (Taylor bubbles) are formed. This slug flow is characterized by Taylor bubbles separated by liquid slugs that may contain small, dispersed bubbles in it. The increase in gas flowrate leads to coalescence of Taylor bubbles resulting semi-annular and annular flow. As a consequence of a further increase in the gas flowrate, the liquid becomes dispersed within the continuous gas phase in a mist flow. Several main types of gas-liquid flow patterns in a vertical line are shown in Figure 1. 14 (Morgado, 2016).

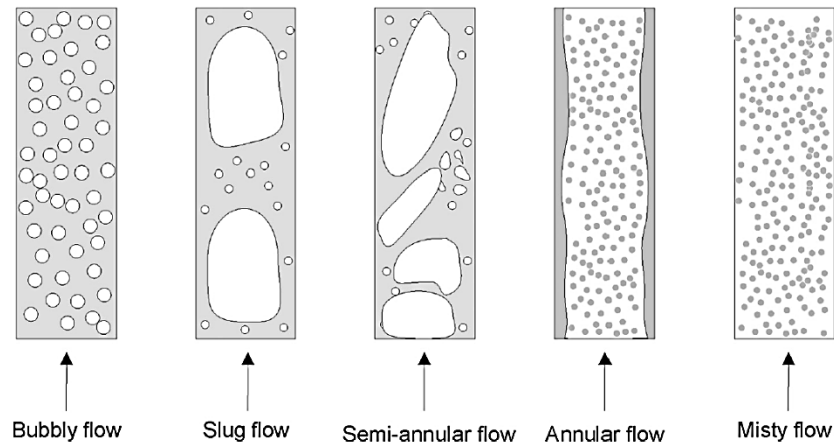


Figure 1. 14: Different types of gas-liquid flow patterns in a vertical pipe (Morgado, 2016).

### 1.5.3. Two-phase Liquid-Liquid flow

In this present work, two-phase liquid-liquid flow is encountered in the vertical and horizontal lines of the flowloop for the experiments in the presence of oil. Trallero (1997) classified liquid-liquid flow into the following categories as shown in Figure 1. 15:

- *Stratified flow*: Two liquid phases are separated by the density. The heavier liquid phase flows at the bottom of the pipe while the lighter one moves on the upper part of the tube. This flow regime can be divided into two sub-categories:
  - + Stratified smooth flow (ST): at a low flowrate of oil and water.
  - + Stratified flow with mixing at the interface (ST&MI): at a higher flowrate of oil and water.

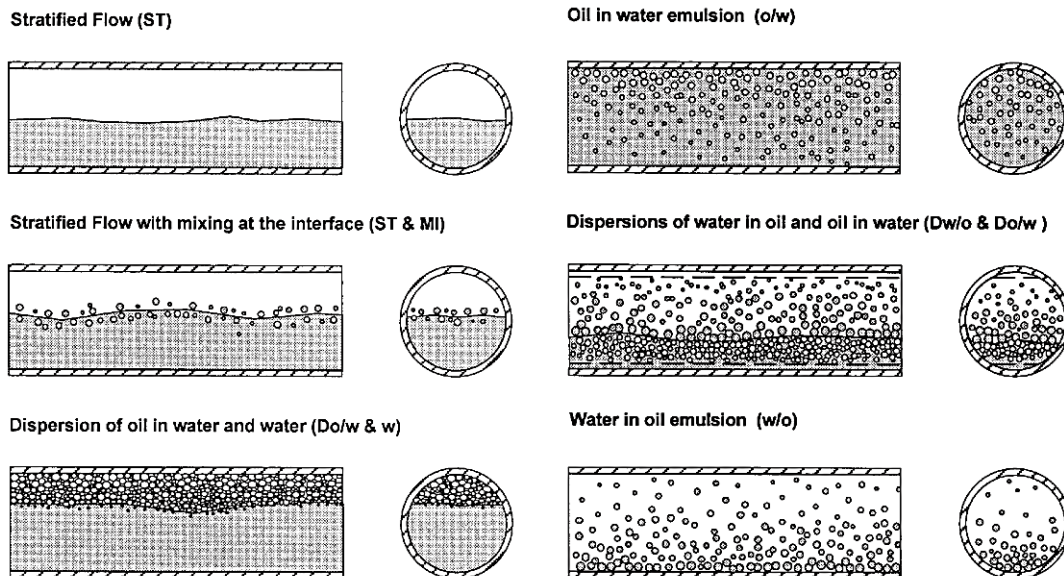


Figure 1. 15: Flow patterns of liquid-liquid flow (Trallero et al., 1997).

- *Dispersed flow*: several flow regimes are observed as below:
  - + Dispersion of oil in water and water (Do/w&w) and oil in water emulsion (o/w).
  - + Dispersion of water in oil and oil in water (Dw/o&Do/w) and water in oil emulsion (w/o).

#### 1.5.4. Three-phase Solid-Liquid-Liquid flow

Once hydrate formed in the flowloop, two-phase liquid-liquid flow will become three phase solid-liquid-liquid flow. Brennen (2005) proposed the main flow regimes of solid/liquid mixture flow in a horizontal line as presented in Figure 1. 16. In this contribution, when the solid particles are small or their settling velocity is supposed to much less than the turbulent mixing velocities in the fluid. Additionally, the volume fraction of solids is low or moderate, the flow will be well-mixed or dispersed. This is defined as the *homogeneous* flow regime (Figure 1. 16) which typically only appears in practical slurry pipelines if all the particle sizes are uniform of tens of microns or less. Once larger particles are present, vertical gradients will occur in the concentration and the regime is termed *heterogeneous*. Furthermore, the larger particles will tend to settle faster and so a vertical size gradient will also occur. The limit of this heterogeneous flow regime occurs when the particles form a packed bed in the bottom of the pipe. When a packed bed grows, the flow regime is known as a *saltation* flow. In this flow regime, solid aggregates may be transported in two ways: (1) the bed moves *in mass* or (2) aggregates in suspension above the bed are carried along by the suspending fluid. In this present study, the solid-gas-liquid-liquid flow is in the separator or in the riser (with gas-lift protocol) once hydrate formed. Moreover, the solid-liquid-liquid flow is encountered in the horizontal and vertical lines of the flowloop at the onset time of hydrate formation.

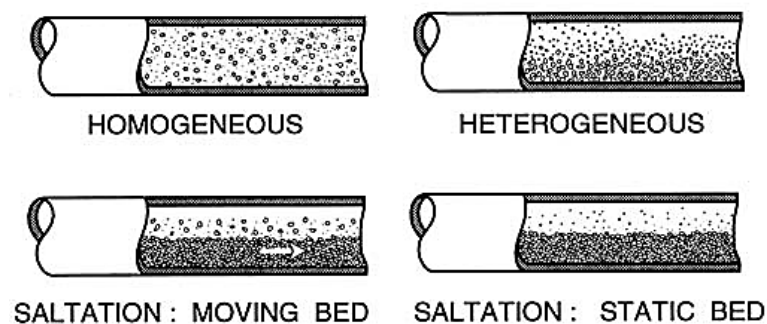


Figure 1. 16: Flow regimes for slurry flow in a horizontal pipeline (Brennen, 2005).

#### 1.5.5. Mass transfer and coefficient of gas transfer ( $k_L a$ )

The rate of methane consumption (solubility) into liquid depending mainly on mass transfer coefficient in liquid and mass transfer area per volume of liquid is expressed as the following equation (J. M. Herri, 1996):

$$r = k_L a (C_{ext} - C) V_L \quad (1.32)$$

Where  $r$  is the speed of dissolution or mass transfer [ $\text{mol.s}^{-1}$ ],  $a$  is contact surface between methane gas and liquid per liquid volume ( $\text{cm}^{-1}$ ),  $V_L$  is the liquid volume [ $\text{cm}^3$ ] and  $k_L$  is the coefficient of mass transfer near liquid [ $\text{cm.s}^{-1}$ ],  $C_{ext}$  is the concentration at interface [ $\text{mol.cm}^{-3}$ ] and  $C$  is the concentration in the volume of liquid [ $\text{mol.cm}^{-3}$ ].

In fact, the total methane consumption increases and reaches a plateau under imposed conditions (temperature and pressure). The rate of methane gas dissolved in liquid is linked with the rate of change in pressure as follows:

$$A_{CH_4(t)} = \frac{V_G}{R} \left( \frac{P_0}{Z_0 T_0} - \frac{P(t)}{Z(t) T(t)} \right) \quad (1.33)$$

Where  $A_{CH_4(t)}$  is the amount of methane gas consumed [mol];  $P_0$ ,  $P(t)$ ,  $T_0$ ,  $T(t)$ ,  $Z_0$ ,  $Z(t)$  are pressure, temperature and coefficient of compressibility of methane gas at initial time and instant time (t);  $R$  is the gas constant ( $8.314 \text{ J.mol}^{-1}.\text{K}^{-1}$ ) and  $V_G$  is the gas volume.

The compressibility factor of methane ( $P = [1 - 10 \text{ MPa}]$  and  $T = [0-10^\circ\text{C}]$ ) can be calculated from the following equation:

$$Z = -0,0196P[\text{MPa}] + 0,994 \quad (1.34)$$

Otherwise, we can suppose that:

$$(A_f - A_t) = (C_{ext} - C) V_L \quad (1.35)$$

Where  $A_t$  and  $A_f$  are the numbers of mol of methane gas consumed at the time (t) and the final time (the time once the curve attained platform).

The speed of consummation can be written as:

$$\frac{dA_t}{dt} = k_L a (C_{ext} - C) V_L = k_L a (A_f - A_t) \quad (1.36)$$

Integrating this equation from  $t_0$  (initial time) to  $t$ , we obtained the following equation:

$$\ln \frac{A_f}{A_f - A_t} = k_L a (t - t_0) \quad (1.37)$$

From this equation, we plot a graph of  $\ln \frac{A_f}{A_f - A_t}$  as a function of time ( $t$ ). The  $k_L a$  can be then obtained based on the slope of the graph (linear or straight line).

## 1.6. Hydrate formation and plugging in the multiphase flowlines

In oil and gas pipelines, the gas hydrate formation mechanisms are very complicated and depend on multiphase, mass and heat transfer and/or intrinsic kinetics (Douglas J. Turner et al., 2009). This section is dedicated to discussing hydrate formation and transport phenomena in dispersed multiphase flow systems. Additionally, the kinetic models of hydrate growth, deposition, and plugging in pipelines will be reported.

### 1.6.1. Oil and water-dominated systems

The oil-dominated (or low water cut) systems include oil, gas and water phase and oil is predominated, typically equal to 50 vol.% or greater (Figure 1. 17). The water is divided into small droplets dispersed in the oil phase (oil continuous phase and free water phase) by surfactants and shearing (Sloan et al., 2010). The steps for hydrate plug formation are shown in Figure 1. 17 (D J Turner, 2006):

- (1) Water disperses in an oil-continuous phase emulsion as small droplets less than 50  $\mu\text{m}$  due to oil chemistry and shearing;
- (2) Hydrate grows on the droplet rapidly in the oil-water interface;
- (3) During crystallization, crystals continue to grow as a function of mass and heat transfer. Hydrates start agglomerating by dint of free water within and between the droplets which enable strong capillary attractive forces between hydrate-covered droplets. Water droplets can also wet hydrate-covered droplets and/or be nucleated by hydrate-covered droplets;
- (4) Hydrate plug formation in pipelines is a result of coalescence of hydrate particles.

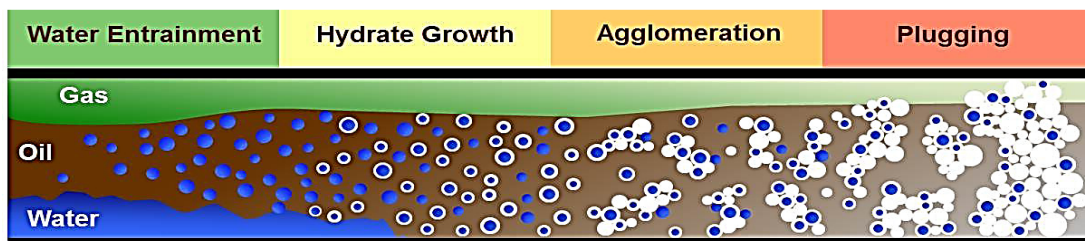


Figure 1. 17: Conceptual model for hydrate formation in oil-dominated multiphase flow systems (D J Turner, 2006).

Turner (2005) studied gas hydrate formation in emulsion both in an autoclave and flowloop but only in low water cut systems (5 vol.% - 35 vol.%) and without anti-agglomerants. Generally, the

kinetics and mechanism of methane gas hydrate formation and agglomeration/deposition in flowloop, as well as flow characteristics and rheological properties of natural gas hydrate slurry with and without anti-agglomerants in low water cut systems, were widely investigated.

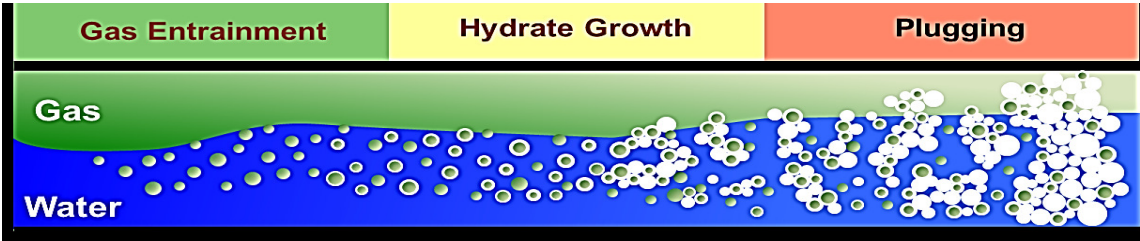


Figure 1. 18: Conceptual picture for hydrate formation in water-dominated systems consisting of gas and water phase (Zerpa, 2013).

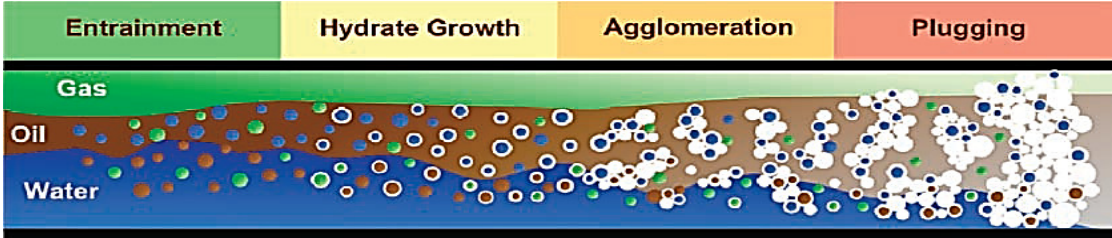
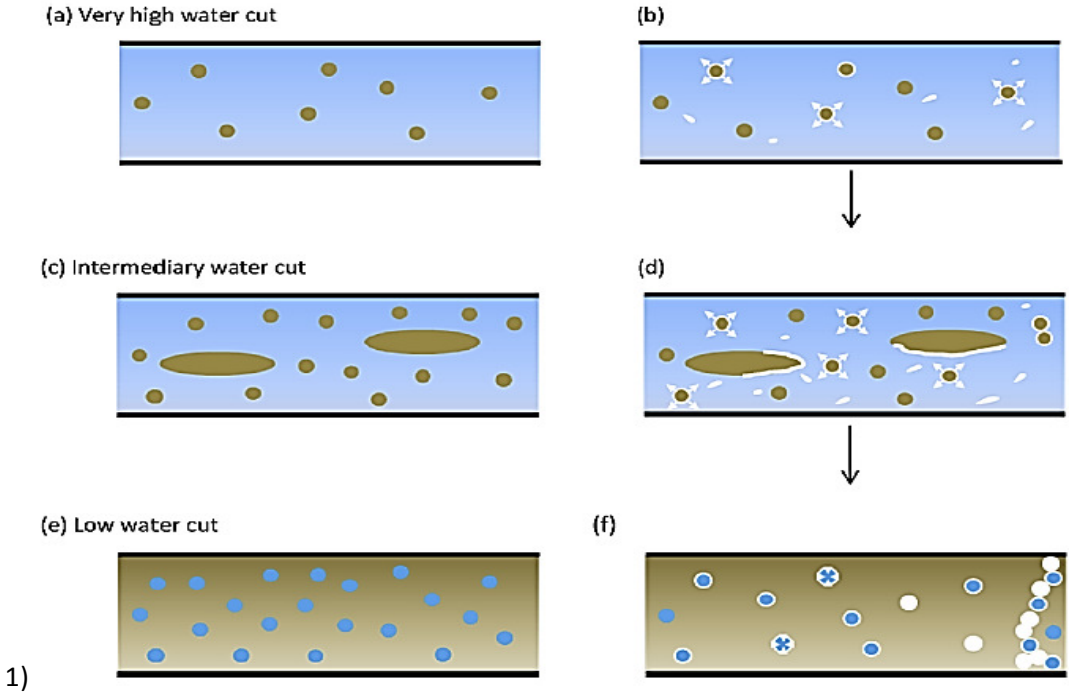


Figure 1. 19: Conceptual picture for hydrate formation in water-dominated systems consisting of gas, water, and oil phase (Zerpa, 2013).

In the water-dominated (high water cut) systems, water prevails compared to oil and gas, typically water holdup greater than 70 vol.% as shown below in Figure 1. 18. Furthermore, water can no longer be totally emulsified in the oil phase or oil may be dispersed in water continuous phase; a separate continuous water phase may exit (Figure 1. 19). The inversion of the oil phase emulsion does not commonly occur so that an external water phase remains unchanged (Sloan et al., 2010). D. Lippmann, D. KESSEL (1994) performed the hydrate formation experiments with dominated pure water, several natural gas mixtures with and without the oil phase in a stirred autoclave. All experiments without oil phase which they used a rotating autoclave showed that there were no hydrate growth and pipe wall adhesion observed in small pipes. Furthermore, hydrate deposition can be avoided by shearing in larger pipes. Plugging was by means of high friction of the huge amount of hydrate particles forming slush. Similarly, Andersson, (2000) carried out the gas hydrate slurry experiment with pure water and pure methane and natural gas mixture in a closed circulation loop in the laminar and turbulent flow. The experimental results indicated that in the turbulent regime, the pressure drop of hydrate slurry flow (up to 21% of hydrate volume fraction) was the same as that of pure water flow due to high shear separating and isolating hydrate particles from the pipe wall.

However, in the laminar flow regime, apparent viscosities of methane hydrate slurries depend on hydrate volume fraction. The increase in hydrate concentration caused increasing the slurry viscosity. Sanjeev V. Joshi et al., (2013) studied hydrate formation and plugging in 100 vol.% water cut systems in a flowloop. They also proposed a hydrate plugging mechanism as a transition from homogeneous to heterogeneous suspension flow. Generally, the hydrate formation, agglomeration, deposition, and plugging with and without anti-agglomerants in flowlines are not widely understood to date.

The study concerning gas hydrate formation and agglomeration in the Archimède flowloop (this apparatus simulates the actual conditions in the pipeline) at École Nationale Supérieure des Mines de Saint-Étienne (ENSM-SE) was firstly investigated by Fidel-Dufour et al., (2006). This work showed the rheological properties of hydrate slurry in water in dodecane emulsion with low water cut (5-30 vol.%) and in the presence of anti-agglomerants (0-0.5wt.%). In addition, a model was developed for crystallization and rheology based on the flowloop experimental data. Afterwards, Leba et al., (2010) studied the formation and agglomeration of gas hydrate particles in water in oil (Kerdane®) emulsion with low water cut (5-30 vol.%) in the presence of anti-agglomerants (0.5-1 wt.%) in the flowloop using the FBRM probe. Recently, Melchuna et al., (2016) investigated gas hydrate formation and agglomeration in the emulsion from low to high water cut, different flowrates and amount of additives (anti-agglomerants) by using FBRM and PVM probes. Topological model of crystallization under flow without AA-LDHI proposed in this study is shown in Figure 1. 20.



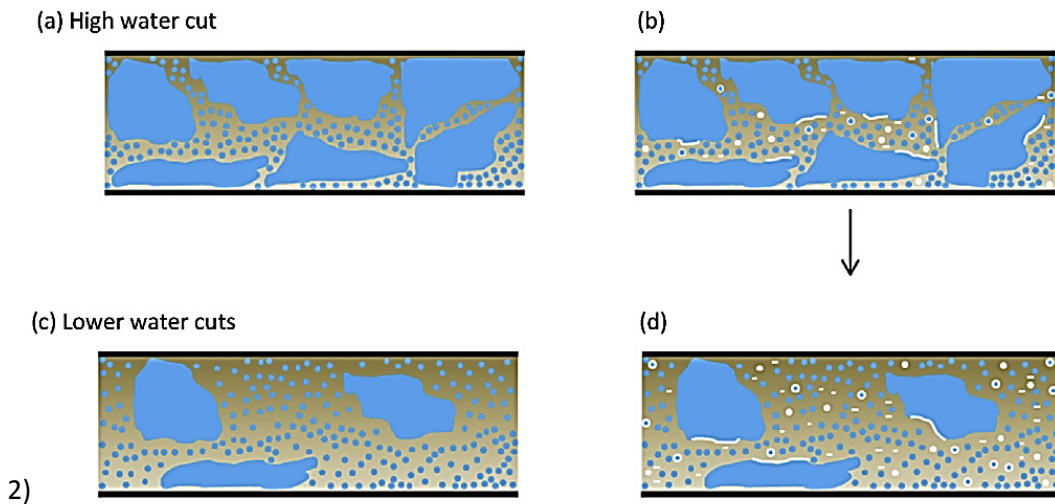


**Figure 1. 20: Topological model of crystallization under flowing without AA-LDHI (1): (a, b) high water cut; (c, d) intermediary water cut; and (e, f) low water cut and with AA-LDHI (2): (a, b) high water cut and (c, d) low water cut (Melchuna et al., 2016).**

### 1.6.2. Kinetic models of hydrate formation/deposition and plugging in pipelines

In oil-dominated (low water cut) systems, Camargo and Palermo (2002) also developed a rheological model for suspension and agglomeration of hydrate particles in an asphaltenic crude oil based on the data obtained from laboratory and flowloop scale. Davies et al., (2010) improved the model which includes hydrate formation kinetics and thermodynamics to predict plugging in industrial multiphase flowlines. Jassim et al.,(2010) developed a new model for hydrate deposition based on particle dynamics theories in gas-dominated flowlines using: (1) computational fluid dynamics (CFD) technique, (2) nucleation and growth models, and (3) a novel approach of particle migration and deposition. Wang et al., (2010) proposed a model for safe transport of hydrate slurry based on a new and non-dimensional parameter which is defined as the ratio of kinetic energy and separating energy of the hydrate particles in pipelines.

Lv et al., (2013) developed a model for an inward and outward hydrate shell growth based on the experimental data taking into account of thermodynamics, kinetics, and mass and heat transfer. Zerpa (2013) developed three kinetic models from the model of Turner (2005) for prediction of gas hydrate formation in all three multiphase flows in pipelines (oil-external phase, water-external phase, and gas-dominated systems). Chaudhari (2015) developed the methods and tools for hydrate risk assessment (hydrate risk quantification) in oil and gas production. A correlation to predict a hydrate volume at transition zone from homogeneous to heterogeneous phase was developed by Joshi, (2012) as a function of the Reynolds number, which was later improved by Grasso, (2015).

Vijayamohan (2015) proposed a plugging onset model for partially and completely dispersed systems. In this work, onset plugging hydrate volume is a function of Reynolds number, liquid loading, capillary number, and viscosity of oil and water. Balakin et al., (2016) developed and proposed a model for gas hydrate agglomeration and deposition with combined (computational fluid dynamic) CFD-PBM (population balance) technique. Model of hydrate blockage in gas-dominated systems which was developed by Wang et al., (2016), was also used for hydrate formation and deposition in deep water gas well testing work. Moreover, Wang et al., (2017) proposed a model for hydrate formation and deposition prediction in gas-dominated systems with free water. In this model, hydrate formation was considered from both liquid film and liquid droplets. Lorenzo et al., (2017) developed a model for hydrate deposition and sloughing in gas-dominant pipelines. This model allows estimating pressure and temperature along a horizontal pipeline in the presence of MEG.

## 1.7. Highlights and Conclusions

This chapter summarized the hydrate formation issues in different systems and gas hydrate in flow assurance. In details, kinetics, mechanisms, and models of hydrate formation, agglomeration, deposition and plugging in pure water and emulsion (or dispersion) systems in pipelines (and autoclave) along with hydrate formation on the gas bubble surface were outlined. Rheology of water/oil/hydrate suspension was considered with several models to predict relative viscosity of the solids-liquids suspension. The novel approach using low dosage hydrate inhibitors to prevent agglomeration and plugging was also introduced. Besides, the important factors prior to hydrate crystallization such as emulsion type, rheology of emulsion and flow patterns in multiphase flow (in horizontal and vertical flow) which impact on the hydrate formation and plugging mechanism were presented. The mass transfer which is a key factor to control hydrate formation was mentioned and quantified by the coefficient of gas transfer. Several remarkable conclusions can be highlighted from the literature review, as follows:

- (1) Limited studies and poorly understood data concerning the formation of hydrate on the surface of gas bubbles and hydrate formation, agglomeration, deposition and plugging in high water cut systems (up to 100%WC) in a pilot-scale flowloop.
- (2) Limited research was carried out on the influence of hydrate formation on multiphase flow and vice versa. Additionally, few studies have been devoted to effects of salt and anti-agglomerants on morphology and kinetics of methane hydrate formation and transportability in high water cut systems (up to 100%WC).

This present study aims to bridge the gaps mentioned above: (1) and (2), by using a flowloop to reproduce the real conditions in oil and gas transport under the deep-sea pipelines. In details, the objective of this work is to investigate hydrate formation, agglomeration, deposition and plugging, especially in high water cut systems with and without salt and AA-LDHs. Besides, the effect of hydrate crystallization on oil-water flow and vice versa will be revealed. In addition, gas hydrates formation and transport in the presence of gas bubbles with and without salt and AA-LDHs were studied by using the gas-lift system.

## 1.8. Remarques et Conclusions (in French)

Ce chapitre résume la formation d'hydrates dans différents systèmes et la problématique des hydrates de gaz dans l'étude des écoulements. Nous avons décrit en détail la cinétique, les mécanismes et les modèles de formation d'hydrates, d'agglomération, de dépôt et de bouchage dans des systèmes d'eau pure et d'émulsion (ou de dispersion) et/ou dans les pipelines ainsi que la formation d'hydrates à la surface des bulles de gaz. La rhéologie de la suspension eau/huile/hydrate a été considérée avec plusieurs modèles pour prédire la viscosité relative de la suspension solides-liquides. Une nouvelle approche utilisant des inhibiteurs d'hydrate à faible dose pour empêcher l'agglomération et le bouchage a également été introduite. Aussi, nous avons présenté les facteurs importants avant la cristallisation de l'hydrate tels que le type d'émulsion, la rhéologie de l'émulsion et les schémas d'écoulement multiphasique (en écoulement horizontal et vertical) qui ont un impact sur le mécanisme de formation d'hydrate et sur le bouchage. Le transfert de masse qui est un facteur clé pour contrôler la formation d'hydrate a été mentionné et quantifié par le coefficient de transfert de gaz.

Plusieurs conclusions peuvent être tirées de la revue de la littérature :

(1) Des études limitées et des données mal comprises concernaient la formation d'hydrates à la surface des bulles de gaz et la formation d'hydrates, l'agglomération, le dépôt et le colmatage dans les systèmes à haute teneur en eau (jusqu'à 100%WC) dans une boucle à l'échelle pilote.

(2) Un nombre limité de recherches ont été réalisées sur l'effet de la formation d'hydrates sur l'écoulement et le transport multiphasiques et vice versa. En outre, peu d'études ont été consacrées aux effets du sel et des anti-agglomérants sur la morphologie et la cinétique de la formation d'hydrate de méthane et la transportabilité dans les systèmes à haute teneur en eau (jusqu'à 100% WC).

Ce travail vise à combler les lacunes mentionnées ci-dessus : (1) et (2) en utilisant une boucle pour reproduire les conditions réelles dans le transport de pétrole et de gaz dans les pipelines sous la mer profonde. Ceci afin d'étudier la formation d'hydrates, l'agglomération, le dépôt et le bouchage, notamment dans les systèmes à haute teneur en eau avec et sans sel et AA-LDHI. Aussi, l'effet de la formation d'hydrate sur l'écoulement multiphasique et vice versa sera mis en avant. De plus, la formation et le transport d'hydrates de gaz en présence de bulles de gaz avec et sans sel et AA-LDHI seront étudiés en utilisant un système de gaz-lift.

## CHAPTER 2. FLOWLOOP APPARATUS AND EXPERIMENTAL METHODOLOGY

*Science is a way of thinking much more than  
it is a body of knowledge.*

*Carl Sagan*

This chapter aims to describe the experimental facilities, typical conditions of running tests and experimental methodology used in this study. In details, the flowloop system, materials, protocols, measurements, data acquisition, analysis, and calculations are discussed. It is noticed that all experiments are performed by two protocols (gas-lift and Moineau pump) in a flowloop located in École Nationale Supérieure des Mines de Saint-Étienne (ENSM-SE).

### 2.1. Archimède flowloop system

The experimental apparatus used in this study is named “Archimède flowloop” which reproduces the real conditions encountered in the oil and gas production and transport. This flowloop is equipped with many up-to-date sensors, probes, and instruments to investigate in detail hydrate formation, agglomeration, deposition, and plugging phenomena under flowing.

#### 2.1.1. Flowloop circulation

The experiments were performed in the Archimède flowloop (Figure 2. 1 and Figure 2. 2) at École Nationale Supérieure des Mines de Saint-Étienne, France. This flowloop was employed to test commercial additives in a pilot scale which is close to the field conditions (high pressure, low temperature and under flowing) in oil and gas industry.

This system might operate at a maximum pressure of 80 bar, temperature between 0°C and ambient temperature. A Moineau pump and/or a gas-lift system can be used to circulate the fluids in the flowloop. In this experimental work, the gas-lift was used separately and together with the Moineau pump which is described in detail in the work of (Fidel-Dufour, 2004); (Leba, 2009); (Mendes-Melchuna, 2016) implying that the flowrate depends on the viscosity of the mixture. The flowloop is designed with 38.5 m of horizontal pipe with 1 cm of diameter, a riser and a descending pipe (both of them have a height of 12.6 m and a diameter of 1.5 cm), a gas injection system, and one sapphire window. At the top of flowloop riser, there is a separator including two steps of separation (the primary and the secondary one). The total liquid volume is 11.5 L (including the volume of horizontal and vertical lines and separator). The total free gas head volume is 14.9 L (with both volume of ballasts and separator) and the gas volume of ballasts is 10L approximately. The length (L) between two points of the main pressure drop ( $\Delta P$ ) in the horizontal section is 24.08m.

Several important process parameters and dimensions of the Archimède flowloop are shown in Table 2. 1.

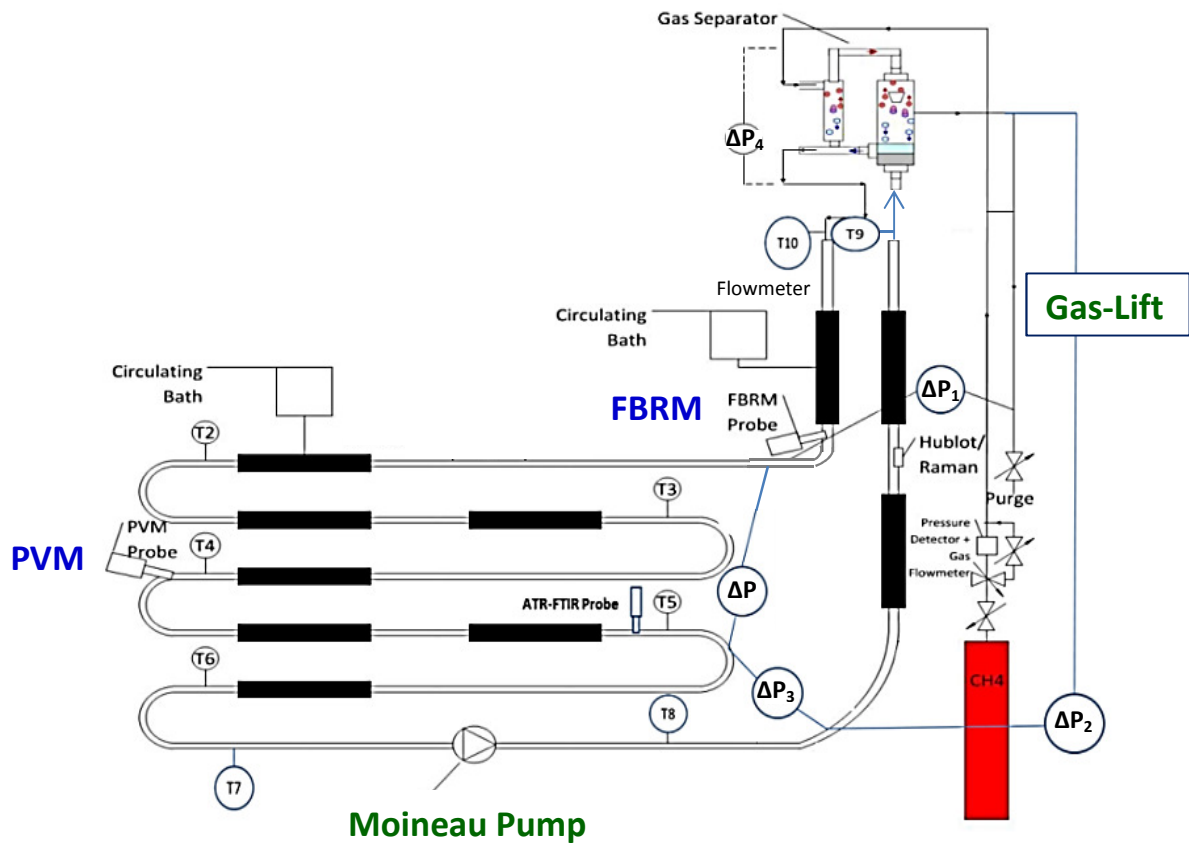


**Figure 2. 1: Schematic of the Archimède flowloop: simplified with “gas-lift” system (above, on the left) and with Moineau pump (below, on the right); modified and adapted from (Mendes-Melchuna, 2016) and (Fidel-Dufour, 2004).**

This experimental apparatus is equipped with temperature (thermocouples), pressure and pressure drop (differential pressure transducer) probes for the determination of the beginning of the crystallization and identification of the plugging troubles. The Focused Beam Reflectance Measurement (FBRM) probe is to measure particle size distribution of droplets and hydrates (via the chord counts). In addition, the Particle Video Microscope (PVM) probe helps to observe the liquid-liquid dispersion, the gas hydrate formation, and agglomeration phenomena. Furthermore, a mass flow meter is installed to measure the flowrate and density of fluid and suspension. A gas compensation system (gas flowrate meter and pressure controller) can be used to keep the total pressure at a constant value (75 bar). The cooling systems control the temperature in the flowloop at  $(4.5 \pm 0.5^\circ\text{C})$  by using the water/ethanol circulation jacket attached to the flowloop.



Figure 2. 2: Archimède flowloop in the SPIN laboratory: (a) vertical section and (b) horizontal section.

Table 2. 1: Important operation parameters and dimensions of the Archimède flowloop.

Diameter in horizontal lines [cm]	Diameter in vertical lines [cm]	Total volume of liquid [L]	Total volume of gas line and separator [L]	Total gas volume in two ballasts [L]
1	1.5	11.5	4.9	10
Temperature [°C]	Pressure [bar]	Flowrate [L.h <sup>-1</sup> ]	Protocol	Flow regime
4.5±0.5 (including 10 temperature sensors)	80 (maximum) (including 2 pressure sensors)	120-400 (including densitometer)	Gas-lift and Moineau pump	Laminar- Intermediate- Turbulent
Separators	Pressure drop sensors	FBRM probe	PVM probe	Gas compensation system
02	05	01	01	YES

### 2.1.2. Gas-lift riser and separator

The gas-lift riser is the upcoming pipe section of the Archimède flowloop which transports gas bubbles (when using ballast systems), emulsion and hydrate to the separator. In the separator, gas and liquid are separated and the liquid and hydrate return to the horizontal line through down coming pipe section. Generally, the gas-lift riser plays an important role in gas hydrate formation and

transport because of the presence of gas bubbles in this part when using ballast systems. Besides, the role of the separator is to ensure that there is no free gas phase in the horizontal lines of the flowloop.

In dimension, the gas separator has 4.53 cm of internal diameter and 2.2 m in height. There is a tube placed inside the separator with a height of 1.5 m which connects directly to the gas-lift riser. This tube works as a geyser which breaks liquid droplets into smaller ones in the separator. Consequently, this increases the contact surface between gas and liquid. The second smaller separator with an external diameter of 0.64cm aims to collect the droplets which pass through the first one. This smaller separator is connected to the descending pipe. The dimension of all parts constituting the separator is shown in Figure 2. 3.

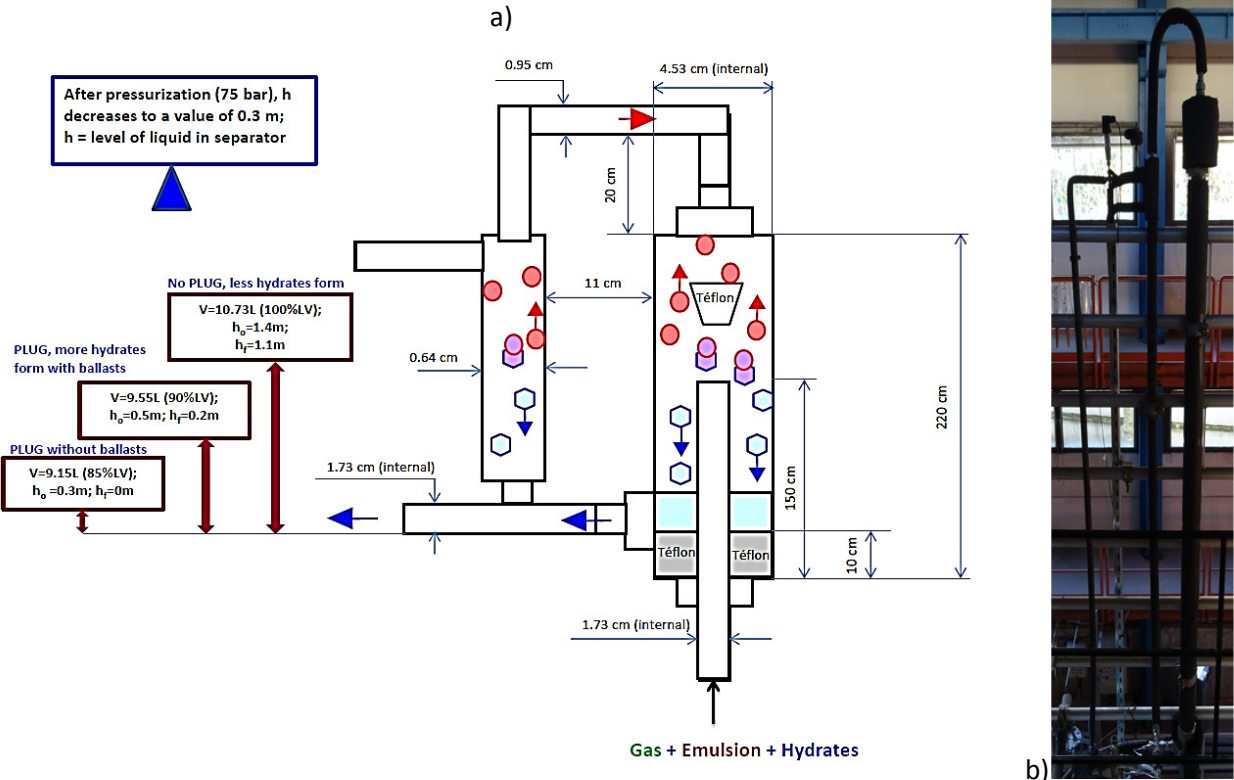


Figure 2. 3: Structure and dimension (a)/photo (b) of the separator in the Archimède flowloop.

The fact that the liquid level (or liquid volume in the flowloop) in the separator plays a vital role for hydrate formation. Particularly, if the liquid volume is of 100 vol.% (or 10.73L of liquid in the flowloop) then the average crystallization rate is very low or fewer hydrates form. The decrease in liquid volume increases the rate of hydrate formation. For example, if the liquid volume is of 90 vol.% (or 9.55L of liquid in the flowloop), the increase in average crystallization rate is witnessed. Finally, if the liquid volume is of 85 vol.% (or 9.15L of liquid in the flowloop) then the rate of crystallization reaches the highest value among the three liquid volumes mentioned above. It is supposed that the

lower liquid level in the separator liberates the geyser and this enhances the contact surface between the gas and liquid phase. It is important to note that the pressurization at 75 bar reduces the liquid level in the separator with the value of 0.3m approximately. We assumed that there are some dead legs (or free spaces) in the flowloop (possibly in the Moineau pump or purge valves, etc.) prior to pressurization.

### 2.1.3. Compression system (ballasts)

Gas-lift or so-called the ballast system is used to inject methane into the bottom of the riser and followed by methane recovery from the separator. After separation, the (methane) gas needs to be recompressed before re-injecting into the lower part of the riser. Moreover, this mechanism helps to circulate the fluid ( $0-150\text{L}\cdot\text{h}^{-1}$ , in laminar regime) in the flowloop without Moineau pump. In the flowloop, there are two ballasts (each 10L of internal volume) containing liquid water (6 liters of water per each ballast) inside at the lower part (grey one) and gas on the higher part of ballasts (green one) in Figure 2. 4. By using the gas-lift pump, water in this ballast (1) can move to another one (2). At this ballast (2), gas is compressed and injected to the lower part of the riser. On the other hand, at ballast (1) water level is decreased, as a result, gas is injected from the separator as shown in Figure 2. 1. These ballasts change their roles frequently once the pressure drop (between top and bottom) in a ballast reaches limited values (high or low level). More details on the ballast system are shown in the thesis of (Fidel-Dufour, 2004).

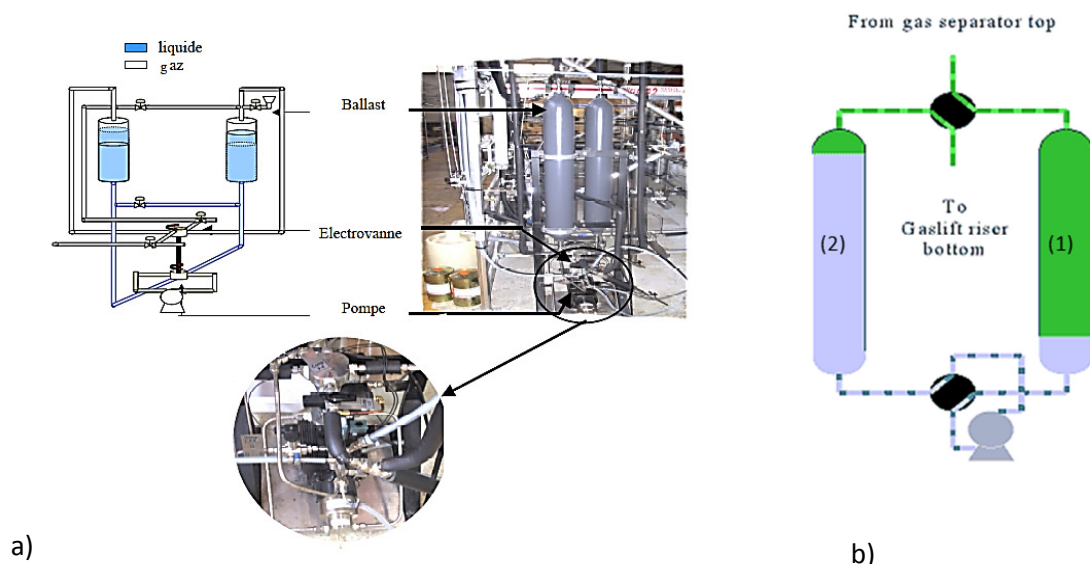
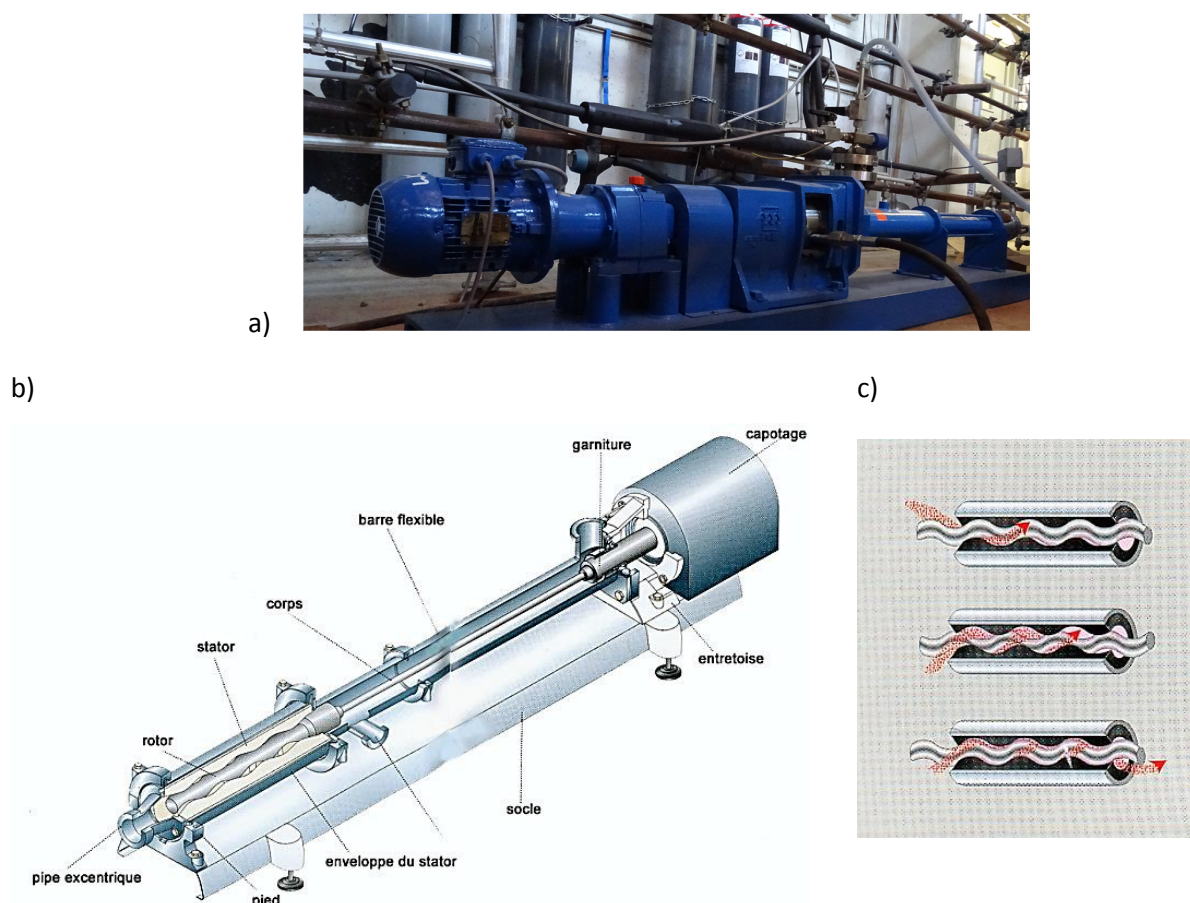


Figure 2. 4: Ballast system using for liquid and gas circulation in the Archimède flowloop: (a) installation and (b) operational principle; adapted from (Fidel-Dufour, 2004).

#### 2.1.4. Moineau pump

A Moineau® pump type MR 6120 S is installed on the Archimède flowloop provided from PCM Company (Figure 2. 5). This pump is used to circulate fluid at constant flowrate (laminar-intermediate-turbulent regime) in the flowloop at low and high pressure (from 1 up to 80 bar). The Moineau® pump is a type of progressive cavity pump consisting of a helical rotor turning inside a helical stator (PCM Instruction Manual). The rotational movement generates an axial displacement of the closed cells, transferring the product from the input to the discharge without crashing the crystal (PCM® Instruction Manual). This is a crucial factor to investigate the hydrate formation and agglomeration because the hydrate particles and agglomerates will not be destroyed by pumping.



**Figure 2. 5: Moineau® pump: (a) installation; (b) structure; and (c) pathway of fluids (or suspension); provided from PCM, Inc (Pump, 2017).**

The Moineau® pump helps in charging liquid into the flowloop, circulating and inducing dispersion with constant flowrate during rheological study and crystallization. The flowrate allowed in the flowloop ranges from 0 to 500L.h<sup>-1</sup> (however for the security, the minimum is 100L.h<sup>-1</sup> and the maximum is 400L.h<sup>-1</sup>). The pump operates at ambient temperature and recommended a maximum

pressure of 80 bar (through associated with hydraulic center working at 100 bar). A recommended maximum pressure drop once hydrate formed in the horizontal pipeline is of 12 bar.

### **2.1.5. Cooling systems**

The temperature in the flowloop is controlled by a cooling system composed of two circulating baths, provided by Huber® (Model CC 250, Polystat CC1) which circulates a coolant (a mixture of water-50 vol.% and ethanol-50 vol.%) to the heat exchanger system. In order to prevent heat losses, the entire flowloop, including the heat exchangers, is jacketed with an insulating material.

A third and smaller cooling bath, also provided by Huber® (Model Ministat) is used to refrigerate the *cold point*. We also used ethanol and water as coolants in this bath. The *cold point* (or crystallizer) is a section consisting of a small heat exchanger around a pipe (1.10 m in length with 0.635 cm of external diameter). This pipe bypasses the second loop of the horizontal section. The goal of the *cold point* is to promote the nucleation by forming ice and introduce it to the flowloop. By this, the third circulating bath is set at a lower temperature (until -25°C) than the value set for the two others circulating baths. There is the possibility of blocking the *cold point* due to the lower temperature applied. However, this does not present a risk because once this line is blocked; the liquid can still normally pass to the principal flowloop line. In fact, the temperature of the zone closed to this system is normally lower than the others from 1-2°C. Generally, we start these three cooling systems at the same time to cool down the flowloop system to  $4.5 \pm 0.5^\circ\text{C}$  before crystallization. Once hydrate formed, the third cooling system was stopped.

### **2.1.6. Instruments**

Numerous sensors, probes, and controllers are installed into the flowloop to monitor the hydrate crystallization process. These helpful instruments are to gain insights into hydrate formation and transport phenomena. Moreover, the use of these instruments together might help to confirm the experimental results.

#### **2.1.6.1. Gas injection and compensation system**

This system (provided by Brooks®) which composes of gas flow meter (Serial No: T10771/012, Model 5860) and pressure controller (Serial No: F23280-001, Model 5866), perform continuous gas injection into the flowloop until reaching desired pressure (set value of pressure, 75 bar) as shown in Figure 2. 6. This system is used to keep the pressure of crystallization process constant (by pressure controller) and to measure the amount of gas injected into the flowloop (by

gas flow meter). The gas flowrate measured is in the range of 0-20 l/min at normal condition (0°C, 1atm). Indeed, the gas flowrate is automatically converted into the normal condition in every measurement and indicated in normal units (Brooks, 2010). Methane is then injected into the flowloop at the top of the separator and solubilized into the fluid mixture.

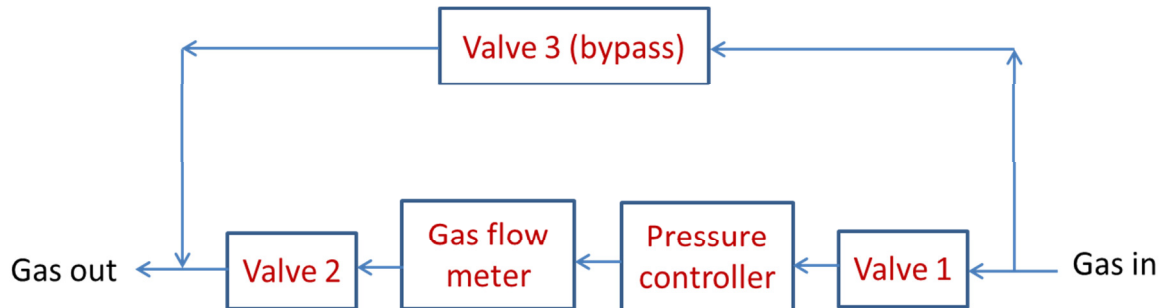


Figure 2. 6: Gas compensation system in the Archimède flowloop.

#### 2.1.6.2. Temperature/pressure and pressure drop sensors

Temperatures in every section of the flowloop are monitored by a set of temperature sensors (type PT100) distributed over the flowloop. The ambient temperature is also recorded by a temperature sensor installed outside the system.

In the top of the separator, there are two pressure sensors (provided by KELLER®) measuring the pressure inside the flowloop system (one measures pressure at the top of the separator and other one measures pressure in the purge line of the gas line). Furthermore, there is one pressure sensor in the ballast system and one in the gas line attached to the gas compensation system.

The flowloop is equipped with five pressure drop sensors (provided by ROSEMOUNT®, Model 3051) (Rosemount, 1997), as seen in Figure 2. 7. Each pressure drop sensor installed in the flowloop is explained as follows: pressure drop in the horizontal line section is given by  $\Delta P$  (from the beginning part to the middle part of horizontal line); pressure drop between the descending pipe and the gas phase (in the separator) is given by  $\Delta P1$ ; pressure drop between the riser and the gas phase (in the separator) is given by  $\Delta P2$ ; pressure drop between the middle part and the end part in the horizontal section is given by  $\Delta P3$ ; and pressure drop at the separator is given by  $\Delta P4$ . More details in the installation of temperature/pressure drop sensors are shown in Figure 2. 1.

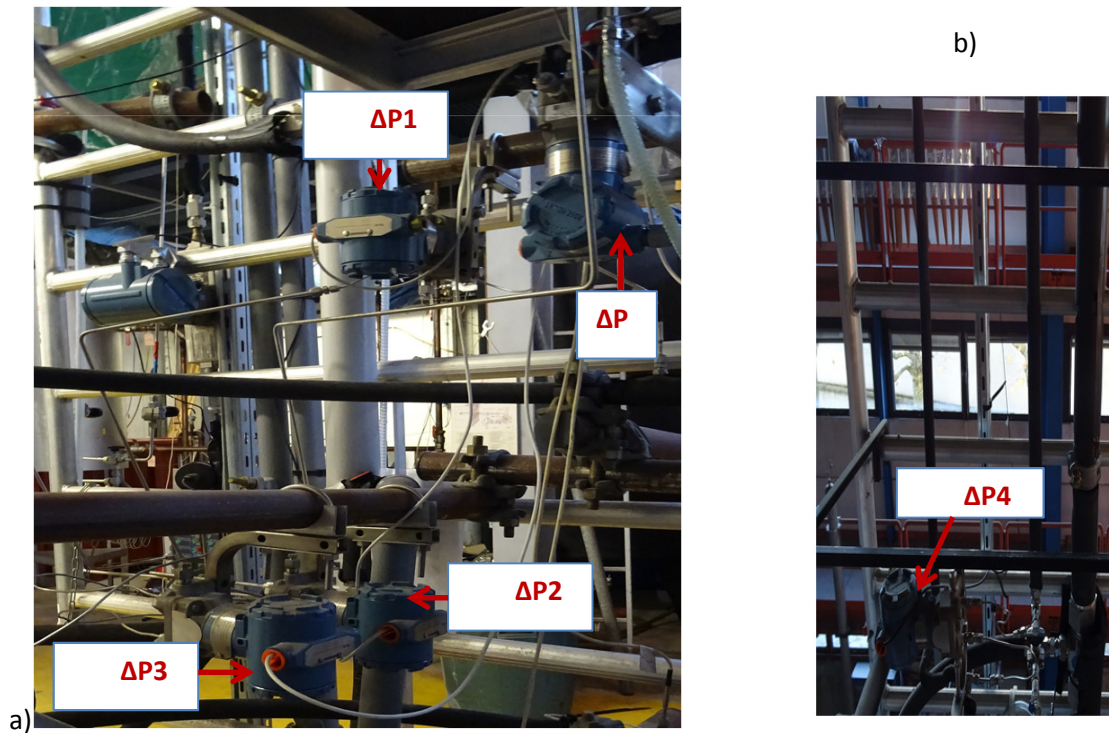
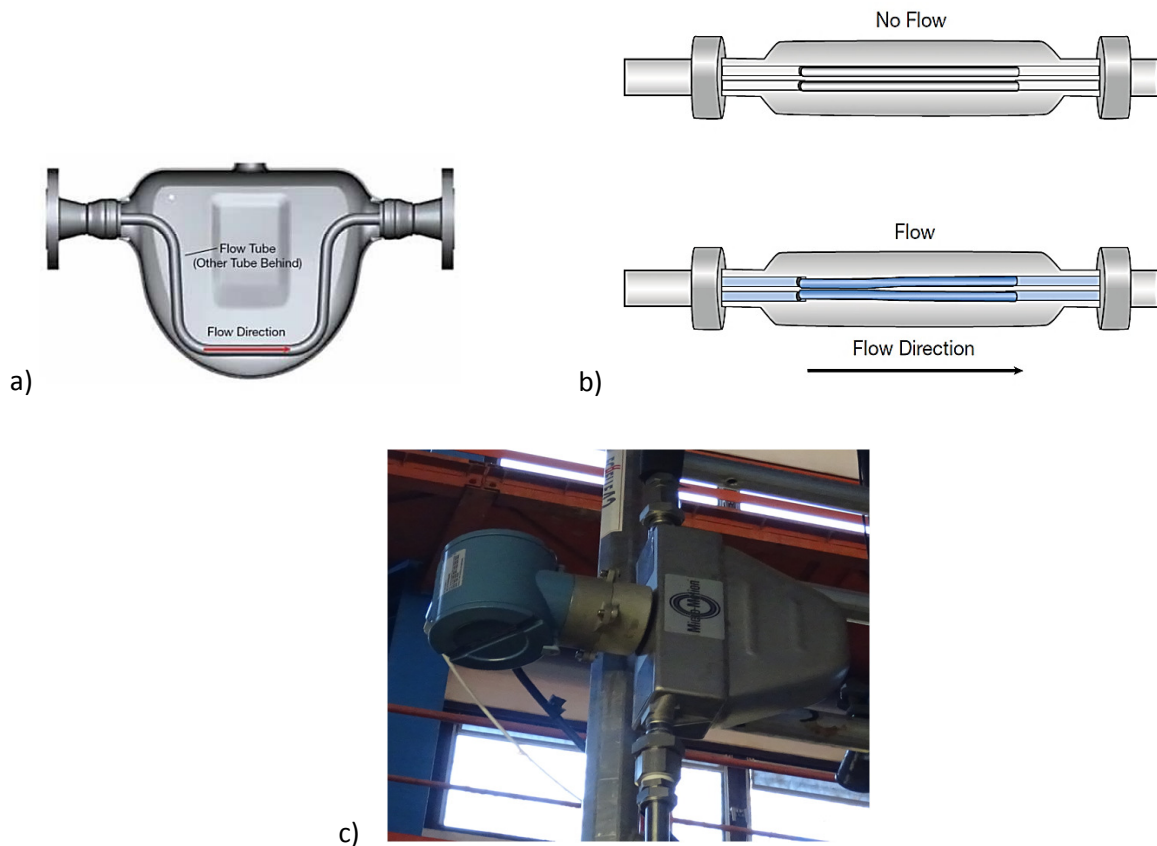


Figure 2. 7: Pressure drop sensors: (a) PD, PD1, PD2, PD3 and (b) PD4; installed in the Archimède flowloop.

### 2.1.6.3. Flowmeter and densitometer

A mass flowmeter with densimeter (provided by MICRO MOTION®) installed in the descending pipe of the flowloop allows measuring simultaneously both the flowrate (accuracy of  $\pm 0.5\%$  of rate) and the density (accuracy of  $\pm 0.01\text{g}\cdot\text{cm}^{-3}$ ) of the liquid or suspension mixture circulating in the flowloop (Figure 2. 8). The flowrate is measured based on the *Coriolis Effect*. In a Coriolis meter, the material which we aim to measure will pass through one or more oscillating tubes; the rate at which mass flow impacts on the oscillation of the tubes can be related to both mass flow and density. A basic dual-tube Coriolis meter containing two curved tubes is shown in Figure 2. 8 a. If there is no fluid passing through the tubes, they simply vibrate toward and away from each other in parallel (Figure 2. 8 b, top), and the outputs of the upstream and downstream motion sensors are in phase. However, in case of material flowing through the tubes, the *Coriolis Effect* causes the downstream side of the loop to slightly lead the upstream side, which generates a slight twist in the loops of tubing (Figure 2. 8 b, bottom). The amount of twist and hence the phase difference between the outputs of the upstream and downstream pickoff sensors varies linearly with the speed of flowing mass in the tubes. The phase is converted to time which is directly proportional to mass flowrate. This principle can be applied to a liquid, gas, or slurry. The natural vibration frequency of the tubes is determined thanks to their stiffness and mass (Tom O'Banion, 2013).

Because the fluid volume in the tubes is always constant, a change in the fluid density leads to a change in the mass in the tubes. Once the mass inside the tubes varies, the natural frequency of the tubes also varies, and this variation is detected by the pickoff sensors. The natural frequency is directly related to the fluid density inside the tubes (Tom O'Banion, 2013).



**Figure 2. 8: A basic Coriolis meter (a); the principle of measurement (b) (Tom O'Banion, 2013); and (c) Coriolis meter installed in the Archimède flowloop.**

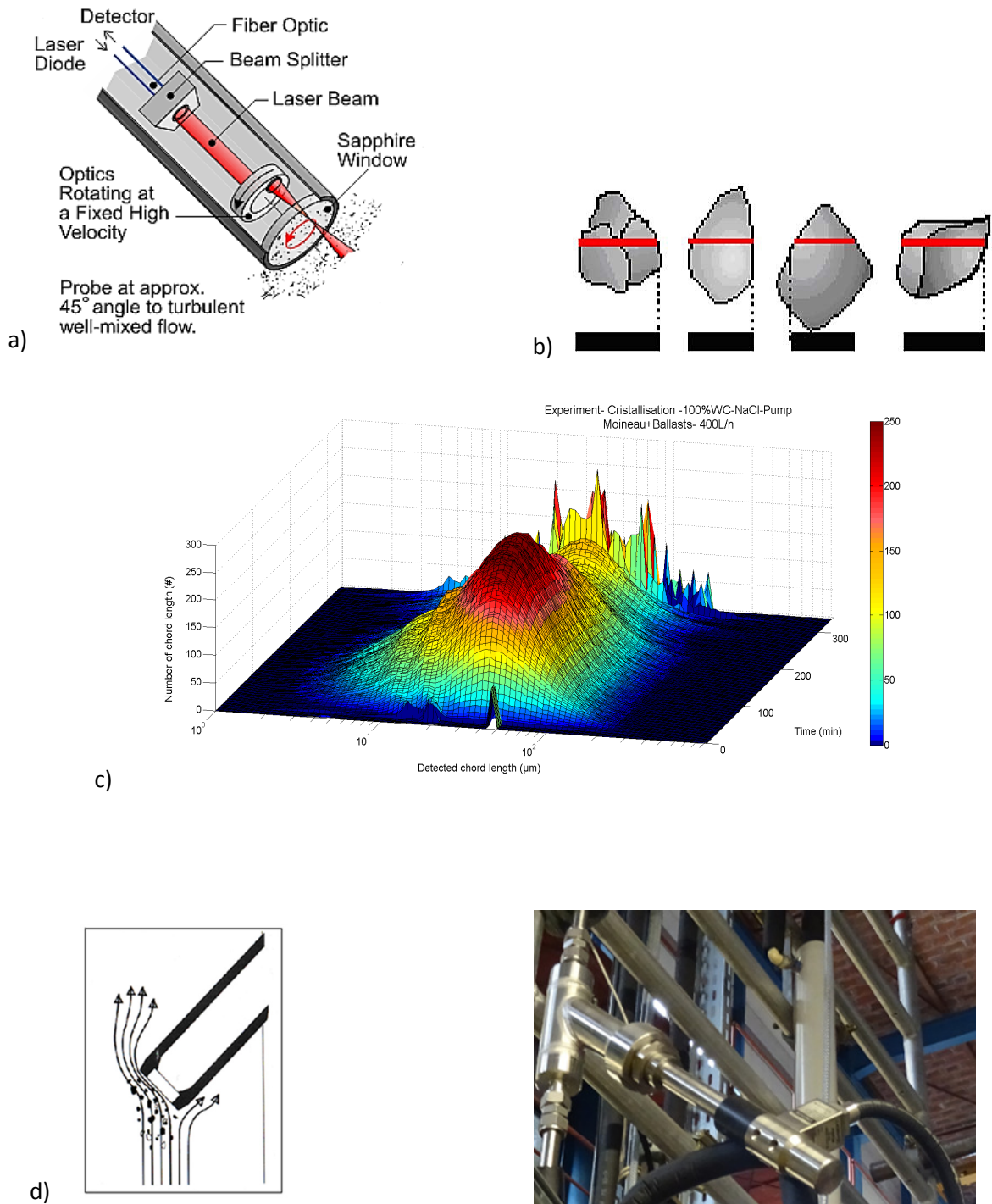
#### 2.1.6.4. FBRM probe

The Focused Beam Reflectance Measurement (FBRM) Model D600X-C22-TM probe is an in situ particle size analyzer provided by Mettler-Toledo Lasentec® (Figure 2. 9). We used this FBRM probe because of its advantages in identifying hydrate formation, agglomeration, and deposition based on a number of chord counts versus detected chord lengths.

This probe allows detecting in-process, real-time, particle size and high solids concentration particle count. In the operational principle, this apparatus emits a laser beam (with a wavelength of 785 nm) through the sapphire window of the probe which is highly focused at a point outside but close to the probe's window surface. This focused beam is then moved by optical system rotating towards a fixed path around the circumference (25 mm in tip diameter) of the probe window at a

constant and high scan speed of  $2\text{m}\cdot\text{s}^{-1}$  (2123 rpm, assuming a tip (scanning) diameter of 18 mm) (Akhfash et al., 2017). During the analysis, as particles pass by the window surface, the focused beam intersects the edge of a particle. Inversely, the particle then begins to reflect back the laser light and continues to reflect back the light until the focused beam reaches the particle's opposite edge. The reflectance laser light is collected by the FBRM optics and converted into an electronic signal. The (distance) chord length is deduced from the reflectance time multiplied by the laser scan speed. The probe is able to measure the chord lengths between 0.5 and 1000  $\mu\text{m}$  (Leba et al., 2010a) and (Mettler-Toledo, 2007). The adjustable focal point position (depending on the particle properties, (Monnier et al., 1996)) of the laser which is the standard focal length as recommended by the manufacturer was set to  $-20\ \mu\text{m}$  from the probe window.

Tens of thousands of chords per second are principally measured by the FBRM system (measurement unit of counts is of the number of chord counts per second or  $\text{s}^{-1}$ ). In this work, every 5 seconds (set value), the FBRM probe will automatically provide a CLD (Chord Length Distribution), giving the number of chord lengths counted for each chord length range (Figure 2. 9 c). The FBRM probe was equipped in the flowloop at angles of  $45^\circ$  to optimize particles or droplets passing through its window (to impinge the flow on to the window surface) and to obtain a representative sample as recommended from FBRM provider. It is highly noted that materials that do not backscatter such as pure oils in pure water and other materials that only produce spectral reflection cannot be measured properly with FBRM. Several other limitations of FBRM tool to particle characteristics (optical properties and shape of particles or backscattering effects) or to mask/shadow effects which impact on measurements were mentioned in the research of Douglas J Turner et al., (2005); M. Li, Wilkinson, & Patchigolla, (2005); Leba, (2009) and Mendes-Melchuna, (2016). The position of the FBRM probe equipped in the flowloop is on the descending section as shown in Figure 2. 1. For more information on the probe and the technique, the reader is referred to the FBRM User's Manual (FBRM, 2005) and (Mettler-Toledo, 2007).



### 2.1.6.5. PVM probe

The Particle Video Microscope (PVM) Model V819 probe is an in-situ particle size and shape (morphology) analyzer provided by Mettler-Toledo Lasentec® (Figure 2. 10). We used this PVM probe because of its advantages in identifying the morphology of hydrate particles and agglomerates during crystallization (hydrate formation, agglomeration, and deposition) based on the number of hydrate particles and agglomerates detected as well as their sizes and shapes.

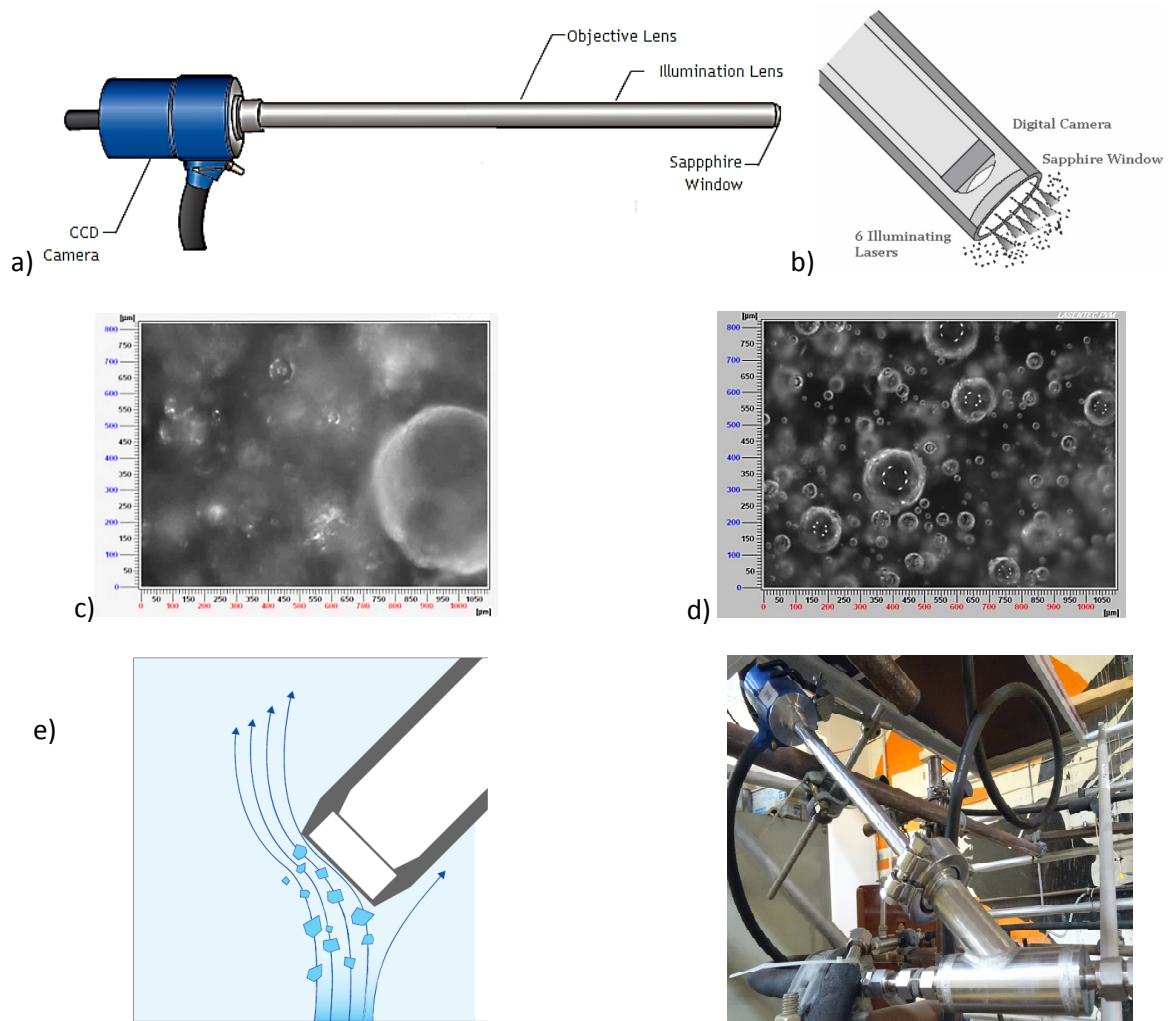


**Figure 2. 10: PVM probe: structure and principle of measurement (a, b); hydrate formation (c); hydrate dissociation (d); and probe orientation installation (e) in the Archimède flowloop.**

The PVM V819 probe is a Particle Vision Microscope that takes real-time and online images of particles and/or droplets. The PVM technology uses a high-resolution camera and internal illumination to obtain high-quality images. The probe consists of six lasers which illuminate a specific area in front of the probe face. The PVM field of view (nominal) is of  $1075\mu\text{m} \times 825 \mu\text{m}$  with a resolution of  $2\mu\text{m}$ . This technique provides visual evidence during hydrate formation and

agglomeration. It is noted that in this study, digital images are recorded automatically every 20 ( $\pm 5$ ) seconds. Figure 2. 10 shows the PVM probe description (a, b) (PVM, 2009); (Boxall et al., 2008) and images obtained from experimental results with hydrate particles formed in the emulsion (c) and hydrate particles during dissociation (d). Similar to the FBRM probe, the PVM probe was installed in the flowloop at angles of  $45^\circ$  to maximize particles or droplets passing through its window (to direct the flow onto the window surface) and to obtain a typical sample as recommend by PVM provider (Figure 2. 10 e). The PVM probe position is on the horizontal section of the flowloop as shown in Figure 2. 1. This PVM probe was used in this study as a complementary tool to FBRM technique. For more information on the probe and the technique, the reader is referred to the PVM User’s Manual (PVM, 2009).

## 2.2. Interfacial tension measurement

The objective of interfacial tension (IFT) measurement is to confirm that addition of AA-LDHI decreases significantly IFT between oil (Kerdane®) and water which impacts on the oil-water dispersion. In this measurement, we used the method of Interfacial tension with a plate of Dynamic Contact Angle Meter and Tensiometer DataPhysics (DCAT). The measurement of the interfacial tension can be carried out using ‘normal’ Wilhelmy plate PT 11, made of platinum-iridium according to DIN 53914. The small plate PT 9 or other probes in a Square, Circle, Ellipse or User defined form can be also used for this measurement (DataPhysics Instruments GmbH, 2006).

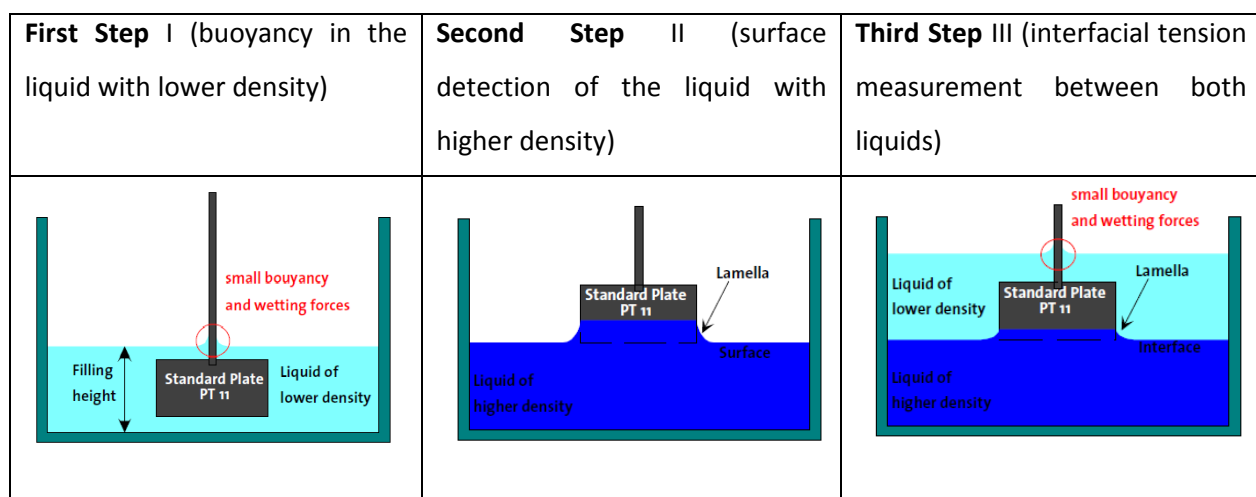


Figure 2. 11: Three steps of IFT measurement of DCAT (DataPhysics Instruments GmbH, 2006).

The measurement procedure of the interfacial tension comprises the three steps. Firstly, we measure the buoyancy of the probe in the liquid with the lower density. Secondly, the surface of the liquid with the higher density is detected. In the third step, the real measurement of the interfacial

tensions between the two not miscible liquids is conducted. All three steps are illustrated in Figure 2. 11. More details on this IFT measurement method are shown in the Operating Manual DCAT (DataPhysics Instruments GmbH, 2006). Experimental results obtained with and without AA-LDHI are shown in Appendix E.

### **2.3. Materials**

In this study, we used water (ultrapure water, provided from Millipore filter), oil (Kerdane<sup>®</sup>, provided by TOTAL FLUIDES), methane (99.99 % purity supplied by AIR LIQUID) and additive. The dispersant additive used in this work is a commercial anti-agglomerant provided by TOTAL. The additive is a water-soluble mixture, mostly composed of a natural oil-based surfactant (30 to 60 wt.%; the proprietary formula; the structure is not depicted in this study) and methanol (40 to 50 wt.%). The density of the mixture is 0.8637 g.mL<sup>-1</sup>. The commercial anti-agglomerant (AA-LDHI) was added for several experiments to test their role to prevent hydrate agglomeration and plugging in flowlines. Moreover, salt (provided by Chimie – Plus Laboratoires, 99.8% NaCl) was added into the water phase for several experiments. Kerdane<sup>®</sup> was used in this work as an oil phase because it is clear oil and this facilitates observing gas hydrate formation and plugging phenomenon by the PVM probe. Furthermore, there are no natural surfactants in this oil so we can compare the experiments without additive to those with additive.

### **2.4. Experimental procedure**

In this present work, we used two protocols to investigate hydrate formation and transport in the flowloop: (1) gas-lift and (2) Moineau pump protocol. Generally, each protocol includes dispersion, gas transfer into liquid, crystallization, and dissociation. The objective of dispersion is to disperse water-oil to produce water-oil dispersion as in the oil and gas transportation pipelines. The gas transfer step is to calculate the gas transfer coefficient ( $k_L a$ ) which determines the rate of gas transfer into fluids. This parameter ( $k_L a$ ) can impact on the rate of hydrate crystallization. Crystallization step is to understand the phenomena of gas hydrate formation, agglomeration, deposition and plugging in flowlines. Finally, we depressurize and stop cooling system to dissociate hydrate. This final step is to stop the experiments, switch the flowloop from experimental conditions to ambient conditions to empty and clean the flowloop for the next (new) experiments.

#### **2.4.1. Experimental protocol with gas-lift system**

The experimental procedure with gas-lift systems is shown in section 2.4.1.1 (water-oil dispersion) and 2.4.1.2 (hydrate crystallization/dissociation).

#### **2.4.1.1. Dispersion**

Liquid-liquid dispersions were formed by mixing water and oil without and with salt and/or commercial anti-agglomerant. The water salinity was of 30g NaCl per 1 liter of water (or 2.91 wt.% NaCl in aqueous solution, this concentration is constant for all experiments with NaCl). The AA-LDHI dosage used was in the range of 0-0.5 wt.% of water. It is noticed that the dosage of AA-LDHI for the experiments in high water cut systems is limited to 0.01 wt.%. This is because too much foam formed once the dosage of AA-LDHI is higher than 0.01 wt.%, disturbing operation of ballasts system. The range of water cuts with this protocol was of 30-80-90-100 vol.%. Because of much foam formed in the mixture with 80%WC-0.01%AA-LDHI, 5 ppm of silicone oil (M.40.165.10 provided by Huber) was added only for this experiment. The mixture was charged into the flowloop and circulated at the flowrate of  $150\text{L}\cdot\text{h}^{-1}$  approximately to induce dispersion. It is important to note that, because of the high viscosity of low water cut systems (30%WC), especially for the experiments with salt and/or AA-LDHI, the flowrate for dispersion was always in the range of  $20\text{-}115\text{L}\cdot\text{h}^{-1}$ . The circulation in the flowloop was carried out by a “gas-lift” system, injecting compressed air (at  $4.5\pm 0.5^\circ\text{C}$  and atmospheric pressure) at the bottom of the riser until reaching a stability of flowrate, FBRM chord counts, and pressure drop.

#### **2.4.1.2. Hydrate crystallization/dissociation**

Once flowrate in the flowloop was stable, the system was cooled down to  $4.5\pm 0.5^\circ\text{C}$ . Then it was pressurized up to 75 bar by injection of methane and ballast system was started (flowrate of approximately  $150\text{L}\cdot\text{h}^{-1}$  for high water cut systems and  $20\text{-}115\text{L}\cdot\text{h}^{-1}$  for low water cut systems) by a pump at 30-35% capacity (recommended). We waited for gas solubilizing in the liquid in 5-10 minutes. Then, a second injection was performed up to 75 bar (to promote hydrate formation), and gas was solubilized again by transferring into liquids but in smaller quantity. Then, the pressure was stabilized. Afterwards, gas hydrate formed which again consumed gas. During the crystallization, we monitored the gas consumption rate, flowrate and density, the pressure drop in the horizontal section and in the separator, the temperature, the FBRM and the PVM signals. To increase the amount of hydrate formation, occasionally, re-pressurization up to 75 bar was carried out for several experiments.

At the end of the experiment (when crystallization was finished, i.e., no more hydrate formed or pipe was plugged), the flowloop was depressurized gradually until the ambient pressure and the cooling system was stopped. Finally, the remaining mixture was taken out of the flowloop, which was cleaned two (or more with AA-LDHI and oil) times with tap water and final step with pure filtered

water to ensure that there was almost no oil and additive existing in the flowloop after cleaning. Normally, each cleaning time by liquid circulation in the flowloop took 30-60 minutes, depending on the amount of oil and AA-LDHI used for the experiments. It is important to note that a few numbers of chord counts (in FBRM chord counts) were observed for some experiments with 100%WC possibly due to the existence of oil in the flowloop (impossible to completely avoid oil).

#### **2.4.2. Experimental protocol with Moineau pump with and without gas-lift system**

The experimental procedure with Moineau pump with and without gas-lift systems is shown in details in section 2.4.2.1 (dispersion and rheological study of dispersion) and 2.4.2.2 (gas transfer and hydrate formation/dissociation). The purpose of the rheological study is to understand the behavior of water-oil dispersion and flow (with and without salt and/or AA-LDHI) such as droplets distribution, mean droplets size of dispersion and flow regime.

##### **2.4.2.1. Dispersion and rheological study of dispersion**

Similar to gas-lift protocol, the liquid-liquid dispersions were formed by mixing water and oil without and with salt and/or commercial anti-agglomerant. The water salinity was of 30g NaCl per 1 liter of water (or 2.91 wt.% NaCl in aqueous solution, this concentration is constant for all experiments with NaCl) and the AA-LDHI dosage used was in the range of 0-2 wt.% of water. The range of water cuts with this protocol was of 80-100 vol.%. The mixture was charged into the flowloop and circulated by Moineau pump at the flowrate of  $150\text{L}\cdot\text{h}^{-1}$  and at  $4.5\pm 0.5^\circ\text{C}$  and atmospheric pressure to induce dispersion until reaching a stability of flowrate, FBRM chord counts, and pressure drop. The liquid volume in the flowloop at 100-90-85 vol.% corresponding with 148-55-30 mbar in PD4 (pressure drop in the separator) at flowrate of  $150\text{L}\cdot\text{h}^{-1}$ , was adjusted by directly taking out the liquid from the flowloop through several purge valves.

For the rheological study, the flowrate was varied from  $120\text{L}\cdot\text{h}^{-1}$  to  $400\text{L}\cdot\text{h}^{-1}$  at ambient temperature and atmospheric pressure. The important parameters concerning in this rheological study are pressure drop, flowrate, density, PVM and FBRM chord counts.

##### **2.4.2.2. Gas transfer and hydrate formation/dissociation**

Once the flowrate in the flowloop was stable and the system was cooled down to  $4.5\pm 0.5^\circ\text{C}$ , the Moineau pump was stopped. Then, the flowloop was pressurized by the high-pressure ballast system (75 bar). At this time, balance (between the flowloop and ballast system) pressure is of 50 bar approximately, the Moineau pump was restarted and an additional injection of methane (up to 75 bar) started at a liquid flowrate of 150 or  $400\text{L}\cdot\text{h}^{-1}$ . We waited for gas solubilizing in the liquid in 5-10

minutes which helps in evaluating gas transfer coefficient (section 2.6.2 and the results are shown in Appendix J). Then, a second injection was performed up to 75 bar and started gas compensation system (or manually gas injected) to stabilize experimental pressure at 75 bar for gas hydrate formation. It is noted that the gas-lift system (co-working with Moineau pump) was started at 22% (minimum and recommended) capacity of ballast pump only if no hydrate formed for a long period of time and low average crystallization rate. In fact, the ballasts only work with Moineau pump in several minutes after hydrate formation. Nonetheless, during the hydrate crystallization, the ballasts can be restarted to enhance hydrate formation (This was performed in several experiments).

During the crystallization, the gas consumption rate, the pressure drop in the horizontal section and in the separator, the temperature, flowrate, density, the FBRM and the PVM signals were monitored. At the end of the experiment (when crystallization was finished i.e., no more hydrate formed or pipe was plugged), the flowloop was depressurized gradually until the ambient pressure and the cooling system was stopped. The procedure to empty and clean the flowloop is the same as the one mentioned above in section 2.4.1.2. It is important to note that a few numbers of chord counts (in FBRM measurements) were observed for some experiments with 100%WC possibly due to little oil is still in the flowloop (impossible to avoid oil completely).

### **2.4.3. Shutdown and restart tests**

With Moineau pump protocol, to test the stability of hydrate slurry during shutdown of flowing and to test the role of AA-LDHI to help to restart (or avoid plugging) the systems after long time shutdown period, several shutdown and restart (SDR) tests were performed with AA-LDHI. The hydrate slurry is considered as stable if the flowrate, pressure drop, density and FBRM chord counts are almost identical before and after restarting the flowloop system. It is noted that SDR tests were only conducted for the experiments without plugging. The protocol for SDR tests was as follows: (1) stopping the Moineau pump during crystallization; (2) waiting for different periods of time (10-20-30-60 minutes). It is noticed that the time for SDR tests cannot be longer due to limited experimental time (9 hours) in one day; and (3) restarting the Moineau pump to evaluate the stability of hydrate slurry in terms of flowrate, pressure drop, and density and FBRM chord counts.

## **2.5. Data acquisition and analysis**

All experimental data were recorded online by LABVIEW, V819 PVM software from METTLER-TOLEDO, LASENTEC® products, and LASENTEC® FBRM data acquisition software. The experimental data were converted to Excel (except PVM images), treated and analyzed on the computer.

## 2.6. Measurements and calculations

The important process parameters are quantified by sensor and probe measurements and also by calculations. These will be described in the following sections.

### 2.6.1. Measurements

In this study, measurements were carried out in the following processes: dispersion, rheological study, gas transfer and crystallization; including pressure, pressure drop, temperature, gas consumption, liquid flowrate, density, size (chord length), and form of droplets/hydrates (by using FBRM and PVM probes).

### 2.6.2. $K_La$ calculation

Gas transfer coefficient describes the rate of gas transferring into liquid. The calculation of  $k_La$  was described in section 1.5.5 in Chapter 1.

### 2.6.3. Water conversion and hydrate volume

Water conversion and hydrate volume are very crucial factors to evaluate the cause of plugging in pipelines once hydrate formed. The amount of hydrate formed (water conversion and hydrate volume fraction) was quantified by gas consumption (the decrease in total pressure or from the gas flowmeter in the gas compensation system). The quantity of methane consumed ( $A_{CH_4(t)}$  in mol) calculated by the difference of pressure is shown in equations (1. 33) and (1. 34) in Chapter 1. Besides, the quantity of methane consumed is calculated by gas compensation (system) method, as follows:

$$A_{CH_4(t)} = \frac{V_{CH_4(consumed)}\rho_{CH_4(at\ normal\ condition)}}{M_w} \quad (2. 1)$$

Where  $V_{CH_4}$ (consumed) is volume of methane consumed calculated from gas flowmeter [ln/min];  $\rho_{CH_4}$  (at normal condition) = 0.716 g/l (gas, 0 °C and 1atm) and  $M_w$  is molecular weight of methane [g/mol].

The water conversion and hydrate volume calculation are described (in details) in Appendix B and C. Some lattice parameters of hydrate structure I for calculation of hydrate volume can be found in Hester (2011).

#### **2.6.4. Rate of crystallization**

Hydrate growth is evaluated through the crystallization rate. The definitions of crystallization rate  $[R(t)]$ , average crystallization rate  $[\bar{R}(t)]$ , and maximum crystallization rate  $R(t)^{MAX}$  are described in details in Appendix D.

#### **2.7. Highlights**

This chapter is dedicated to describing the Archimède flowloop apparatus and its facilities to study gas hydrate formation, agglomeration, deposition and plugging. Besides, measurement of interfacial tension between oil and water with and without AA-LDHI was presented. Materials and their origins used for this work were detailed. The experimental procedure for both gas-lift and Moineau pump with and without ballast system and shutdown and restart tests were proposed to deeper understand the phenomena related to hydrate formation in pipelines. Besides, the method to acquire, measure the data and calculate the important parameters (the interfacial tension, gas transfer coefficient, water conversion, hydrate volume, rate of crystallization, etc.) was clarified in formulas and equations to quantify the experimental analysis and evaluate hydrate formation issue in flow assurance.

#### **2.8. Remarques (in French)**

Ce chapitre est consacré à la description du dispositif expérimental utilisé dans cette étude : la boucle Archimède, et à sa capacité à étudier la formation, l'agglomération, le dépôt et le bouchage des hydrates de gaz. En outre, la mesure de la tension interfaciale entre l'huile et l'eau avec et sans AA-LDHI a été présentée. L'origine et les caractéristiques des produits utilisés pour ce travail ont été détaillés. La procédure expérimentale pour les deux protocoles : gaz-lift et pompe Moineau (avec ou sans système de ballasts) incluant les opérations d'arrêt et de redémarrage a été proposée pour mieux comprendre les phénomènes liés à la formation d'hydrates dans les pipelines. Aussi, la méthode d'acquisition, de mesure des données et de calcul des paramètres importants (tension interfaciale, coefficient de transfert de gaz, conversion d'eau et volume d'hydrate, vitesse de cristallisation, etc.) a été explicitée sous forme d'équations pour quantifier l'analyse expérimentale et évaluer le problème de la formation d'hydrates en écoulement.

## CHAPTER 3. EXPERIMENTAL RESULTS WITH GAS-LIFT (BUBBLES) IN THE RISER

*The art and science of asking questions is the source of all knowledge.*

*Thomas Berger*

This chapter will focus on results and discussion of the experiments with the gas-lift system in which the flow was induced through gas injection without a volumetric pump. Methane was injected at the bottom of the riser at high pressure (75 bar) which enhanced the gas transfer (or contact surface) through bubbles dispersing into the liquid phase (water-oil dispersion). The aim of this chapter is to deeper understand hydrate crystallization and slurry transportability in pipelines at low and high water cut with and without AA-LDHI and/or salt under gas bubbles in the riser. The experiments were performed in the “Archimède” 80 bar - flowloop equipped with FBRM and PVM probes along with temperature, pressure, pressure drop, flowrate, and density sensors. In this chapter, before crystallization study, the water-oil dispersion (in the presence and absence of AA-LDHI and/or salt) and gas transfer (into liquid phase) rate ( $k_L a$ ) will be investigated. Afterwards, the effects of various parameters on methane hydrate formation and transport in flowlines will be studied, including water volume fraction (water cut), amount of commercial anti-agglomerant low dosage hydrate inhibitor (AA-LDHI), and water salinity in a mixture of oil (Kerdane®) and water.

### 3.1. Experimental tests

A total of 25 experiments (including the repeated ones) were carried out in the flowloop with the gas-lift system with different water fractions with and without AA-LDHI and/or salt. It should be noted that all experiments were conducted at an initial pressure of 75 bar, and temperature of  $4.5 \pm 0.5^\circ\text{C}$ . All experimental tests are summarized below in Table 3. 1. The period of time elapsed between the hydrate induction (starting of gas hydrate formation) and plugging is named “flowing time” in this study. Moreover, “plugging time” is defined as the moment at which the flowrate falls to zero and the gas-lift system starts to dysfunction.

**Table 3. 1: Experimental conditions and results with the gas-lift system at 75 bar and 4.5±0.5°C.**

WC	Flowrate	AA-LDHI	NaCl	Water Conversion	HV	Induction Time	Flowing Time
(%)	(L.h <sup>-1</sup> )	(wt.% of water)	(g.L <sup>-1</sup> (H <sub>2</sub> O))	(%)	(%)	(min)	(min)
100	150	0	0	1.00	1.26	1.30	1.60
	150rp(1)*	0	0	0.64	0.80	10.50	1.60
	150	0.01 (F)**	0	0.51	0.64	12.90	1.10
	150	0	30	0.96	1.19	9.40	2.40
	150	0.01(F)**	30	1.15	1.42	0.60	2.10
	150rp(1)*	0.01(F)**	30	1.48	1.84	0.75	3.10
90	150	0	0	1.41	1.58	11.50	2.10
	150	0.01(F)**	0	0.50	0.57	24.70	1.25
	150	0	30	0.93	1.04	26.60	1.50
	150	0.01(F)**	30	2.14	2.38	0.40	3.20
	150rp(1)*	0.01(F)**	30	1.80	2.01	0.40	3.20
80	150	0	0	1.07	1.07	7.10	3.50
	150	0.01(F)**	0	3.56	3.56	1.50	8.80
	150	0	30	1.20	1.19	20.40	3.00
	150	0.01(F)**	30	2.74	2.72	0.60	3.20
	150rp(1)*	0.01(F)**	30	2.81	2.78	0.50	3.10
30	115	0	0	0.86	0.32	2.50	0.42
	20-25	0.01(F)**	0	45.79	16.67	2.70	<b>NO PLUG</b>
	60	0	30	39.50	14.31	2.80	133.90
	25-40	0.01(F)**	30	27.13	9.92	2.80	46.20
	25-30rp(1)*	0.01(F)**	30	35.34	12.84	3.90	42.60
	40-50	0.05(F)**	30	29.28	10.69	3.00	36.40
	40-50rp(1)*	0.05(F)**	30	25.64	9.38	2.30	41.25
	20-40	0.10(F)**	30	31.43	11.45	3.20	116.20
30	0.50(F)**	30	20.76	7.63	2.60	<b>NO PLUG</b>	

\*rp(x): the repeated experiments; x: number of repeats; \*\*(F): Foam formed.

### 3.2. Liquid - Liquid dispersion

As mentioned in the experimental methodology, oil-water dispersion with gas-lift protocol was induced by circulation of the mixture using compressed air. Afterwards, the system was cooled

down to  $4.5\pm 0.5^{\circ}\text{C}$  and reached a stable flowrate and pressure drop before methane injection for crystallization. The main focus of this section is to understand the liquid-liquid dispersion properties (continuous phase, dispersed phase, droplets size distribution, polydispersity/mono-dispersity, homogeneity, and total chord counts of dispersion during the time) in terms of reaching a constant pressure drop and a constant average chord length of dispersed droplets.

### 3.2.1. Stability and average chord lengths of dispersion

This part is devoted to the study of stability, homogeneity and average chord length of dispersion. *Nota bene*: preliminary understanding of liquid-liquid dispersion (before crystallization) is crucial to insight into the gas hydrate formation, agglomeration/deposition, and plugging in pipelines (more details in Appendix F).

### 3.2.2. Total chord counts of dispersion

In low water cut systems, salt water was less dispersed in the oil continuous phase compared to pure water as seen in the total number of chord counts indicated in Figure 3. 1. This phenomenon can be explained by the difference of interfacial tension (IFT). In fact, the IFT of pure water-oil was smaller than that of salt water-oil as stated by (Cai et al., 1996).

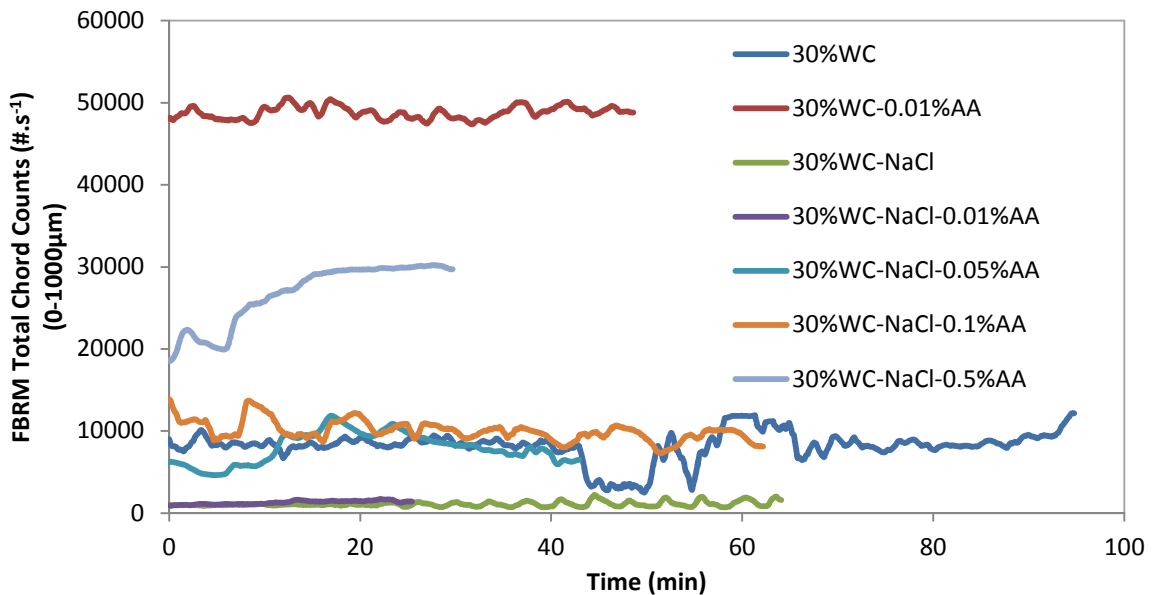


**Figure 3. 1: FBRM total number of chord counts during the dispersion process of the experiments with 30%WC; 30%WC-0.01%AA-LDHI; 30%WC-NaCl; and 30%WC-NaCl with 0.01-0.05-0.1-0.5%AA-LDHI.**

The experimental results showed that an increase in the amount of AA-LDHI declined the interfacial tension between oil and water as shown in Appendix E and Al-Sahhaf et al., (2005).

Consequently, a homogeneous dispersion and an increase in the total number of chord counts were witnessed in the experiments with AA-LDHI in both cases with and without salt (Figure 3. 1).

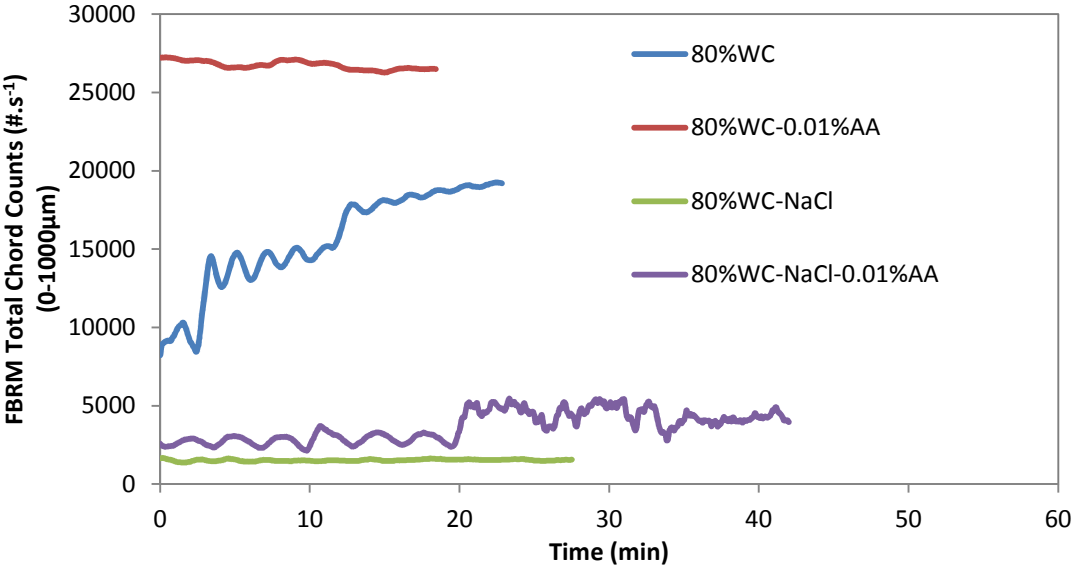


Figure 3. 2: FBRM total number of chord length during the dispersion process of the experiment with 80%WC; 80%WC-0.01%AA-LDHI; 80%WC-NaCl; and 80%WC-NaCl-0.01%AA-LDHI.

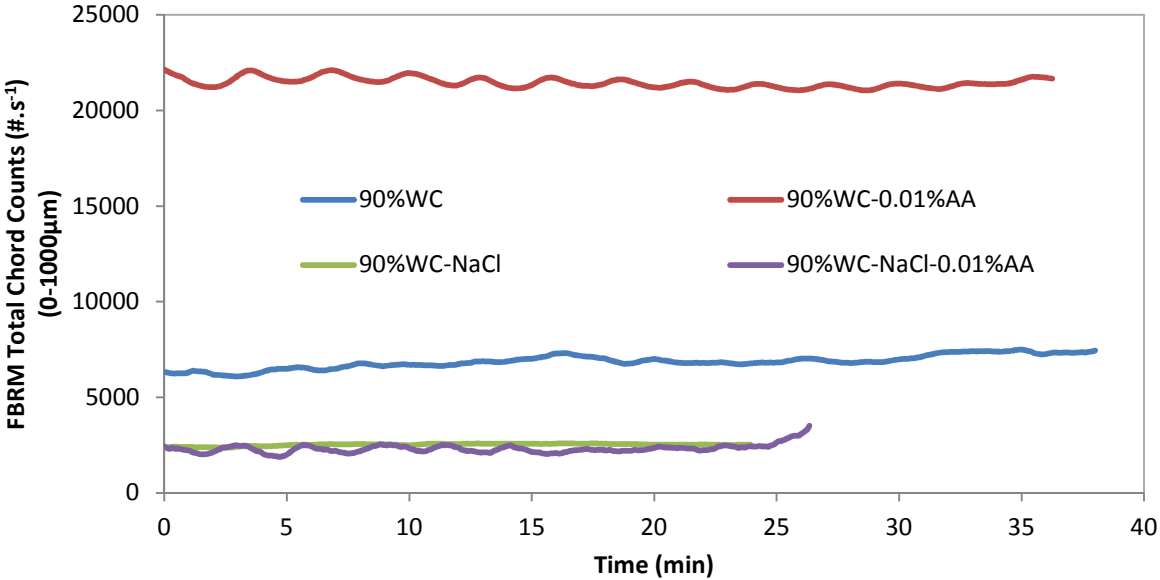


Figure 3. 3: FBRM total number of chord length during the dispersion process of the experiment with 90%WC; 90%WC-0.01%AA-LDHI; 90%WC-NaCl; and 90%WC-NaCl-0.01%AA-LDHI.

The properties of dispersion with and without AA-LDHI and/or salt observed in high water cut systems were similar to those in low water cut systems. This means that addition of salt decreased

the total chord counts of dispersion. On the contrary, the presence of AA-LDHI increased the total chord counts of dispersion. All dispersions of mixtures with 80 and 90%WC are shown in Figure 3. 2 and Figure 3. 3.

Generally, the total number of chord counts decreased by increasing water fraction with AA-LDHI. Conversely, for the experiments with salt, the total number of chord counts declined by decreasing water fraction.

### **3.3. Hydrate formation and transport in pipelines**

To represent the results in low and high water cut systems, two typical experiments with 30%WC-NaCl and 90%WC-NaCl were selected and presented in Figure 3. 4 and Figure 3. 5. This should be noted that in these experiments, to induce nucleation and maximum quantity of hydrate formation, only one-time re-injection of methane until 75 bar was necessary for high water cut systems, instead of three times for low water cut systems. During gas injection, the gas-lift system was stopped (for the security of system) until the desired pressure (75 bar) was attained (restarted system).

The beginning of gas hydrate formation can be easily identified by a temperature increase (crystallization is exothermic) and a sharp decrease in static pressure (gas consumption) (Figure 3. 4 and Figure 3. 5). This can be accompanied by an increase in pressure drop in the horizontal pipeline and/or in the separator. In addition, hydrate formation can be detected from the visualization of the PVM images (Figure 3. 6). In fact, once hydrate formed, there was a slight increase in pressure drop in horizontal sections as well as a sharp increase in pressure drop in the separator (Figure 3. 4 and Figure 3. 5). The small increase in pressure drop in the horizontal line can be attributed to the small amount of hydrate volume present in pipelines. Furthermore, an accumulation and deposition of hydrate particles in the separator were noticed. This was based on a significant increase in the pressure drop of the separator.

In high water cut systems, despite the small hydrate volume in the flowloop for each test, the plug occurred very quickly (in few minutes) after gas hydrate formation (Figure 3. 5). In low water cut systems (30%WC, Figure 3. 4), gas hydrate formed at beginning of the experiment and it took quite long time to plug (higher hydrate volume can be transported compared to high water cut systems) except the experiment without AA-LDHI and salt. It is noted that in low water cut systems, the pressure drop in separator gradually increased compared to the sudden increase in high water cut systems (Figure 3. 4 and Figure 3. 5).

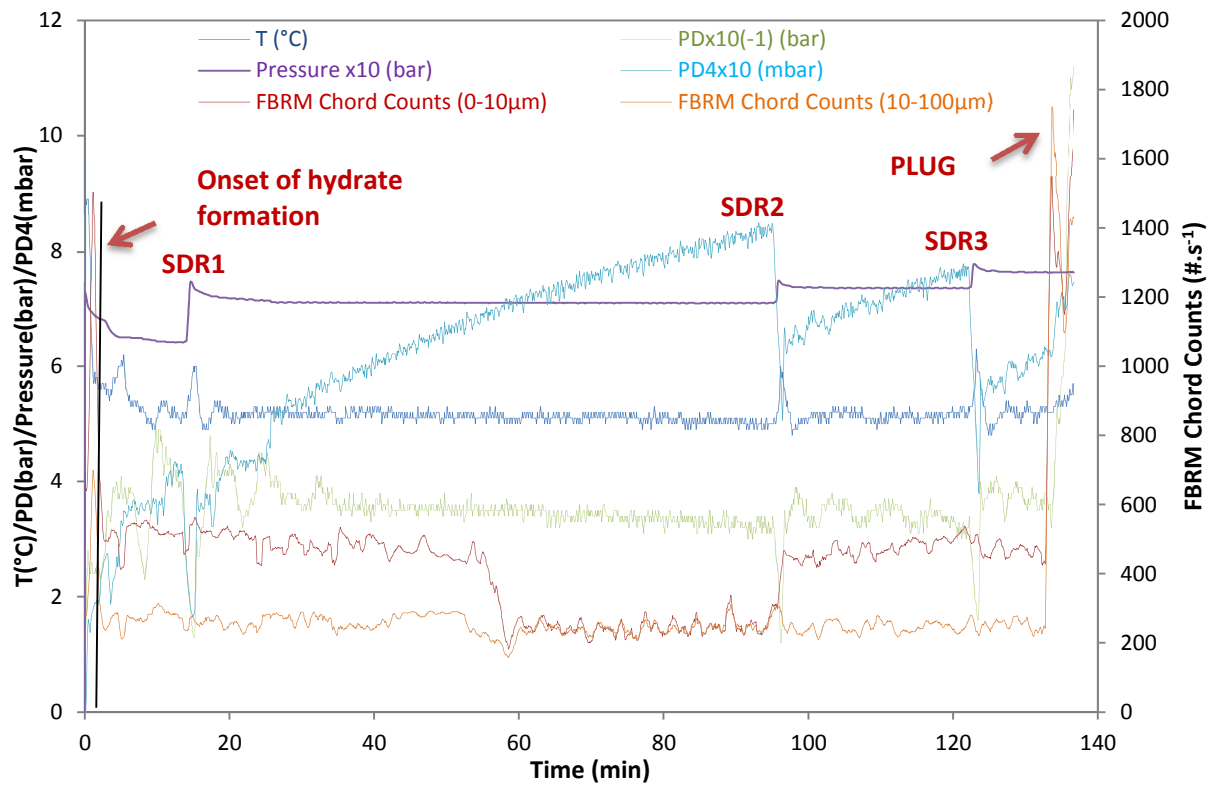


**Figure 3. 4: A typical experiment in low water cut systems (30%WC-NaCl without AA-LDHI). To enhance hydrate formation, the system had to stop and restart 3 times to reinject methane gas up to 75 bar at minutes of 14; 95; and 121 (see protocol). PD and PD4 are pressure drops in the horizontal line and in the separator, respectively.**

The difference of hydrate slurry transport between low and high water cut systems can be attributed to the different characteristics of the continuous phase. In oil continuous phase (30%WC), the water droplets dispersing in oil phase converted into hydrate with less deposition than agglomeration due to the oil-wet surface of the pipe wall. However, at plugging time, it was supposed that hydrate deposited on the wall of pipelines and separator since a significant increase in pressure drop in the horizontal line and in the separator was witnessed (Figure 3. 4). This explanation agreed with previous work (Sanjeev V. Joshi et al., 2013) which reported that agglomeration may not produce a sharp increase in pressure drop but high pressure drops were observed only once hydrate deposited on the wall of the pipe. Besides, an incremental increase in pressure drop in the separator (not a sharp increase in pressure drop in the horizontal line) was witnessed for some experiments in low water cut systems (Figure 3. 14). This was possibly due to hydrate plug occurred in the riser. In the water continuous phase, hydrates formed in the water phase and deposited more easily (less agglomeration) due to hydrate sticking tendency into the water-wet surface of the pipe wall. This can be hypothesized that gas hydrate formed in the riser with a high rate of crystallization due to the gas-

lift system which promoted a quick growth (high contact surface between gas and water in the riser and separator). In addition, hydrate particles deposited quickly on the wall of the separator and/or riser as soon as they formed (Figure 3. 5).

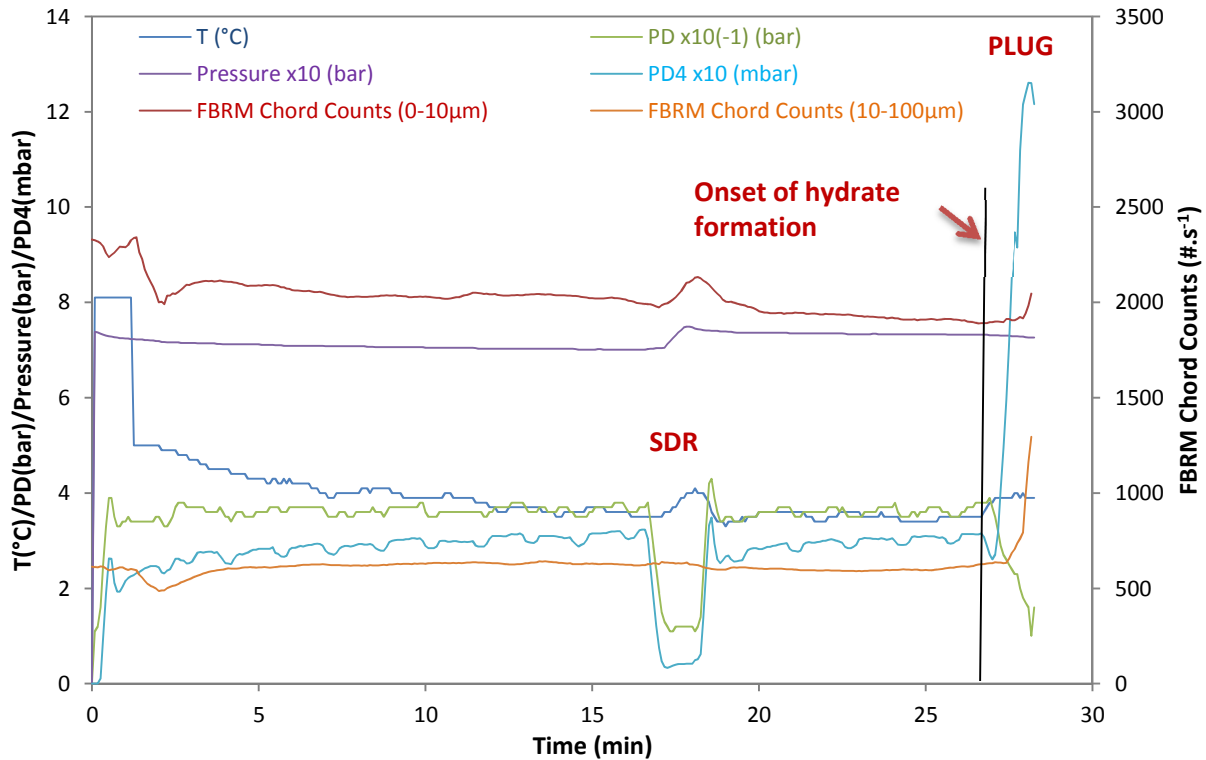


**Figure 3. 5: A typical experiment in high water cut systems (90%WC-NaCl without AA-LDHI). To enhance hydrate formation, the system had to stop and restart once to reinject methane gas up to 75 bar at minutes of 16.5 and 18.5 respectively (see protocol). PD and PD4 are pressure drops in the horizontal line and in the separator, respectively.**

From PVM images, hydrate particles with hydrate film covering droplets (Figure 3. 6 a and b) in the presence of oil were observed. In certain experiments, the agglomerates might be observed (Figure 3. 6 c, d, e, and f). In the experiments with AA-LDHI, PVM probe provided images with low quality. Therefore, it was relatively difficult to observe clearly the morphology of hydrate particles during crystallization. In low water cut systems, we did not see obviously hydrate particles possibly by oil continuous phase and AA-LDHI which prohibited PVM probe laser. Moreover, in high water cut systems, because of hydrate sticking on the separator, hydrate particles were observed only by the PVM probe at the end of crystallization (plugging time) or were not observed (in certain experiments).

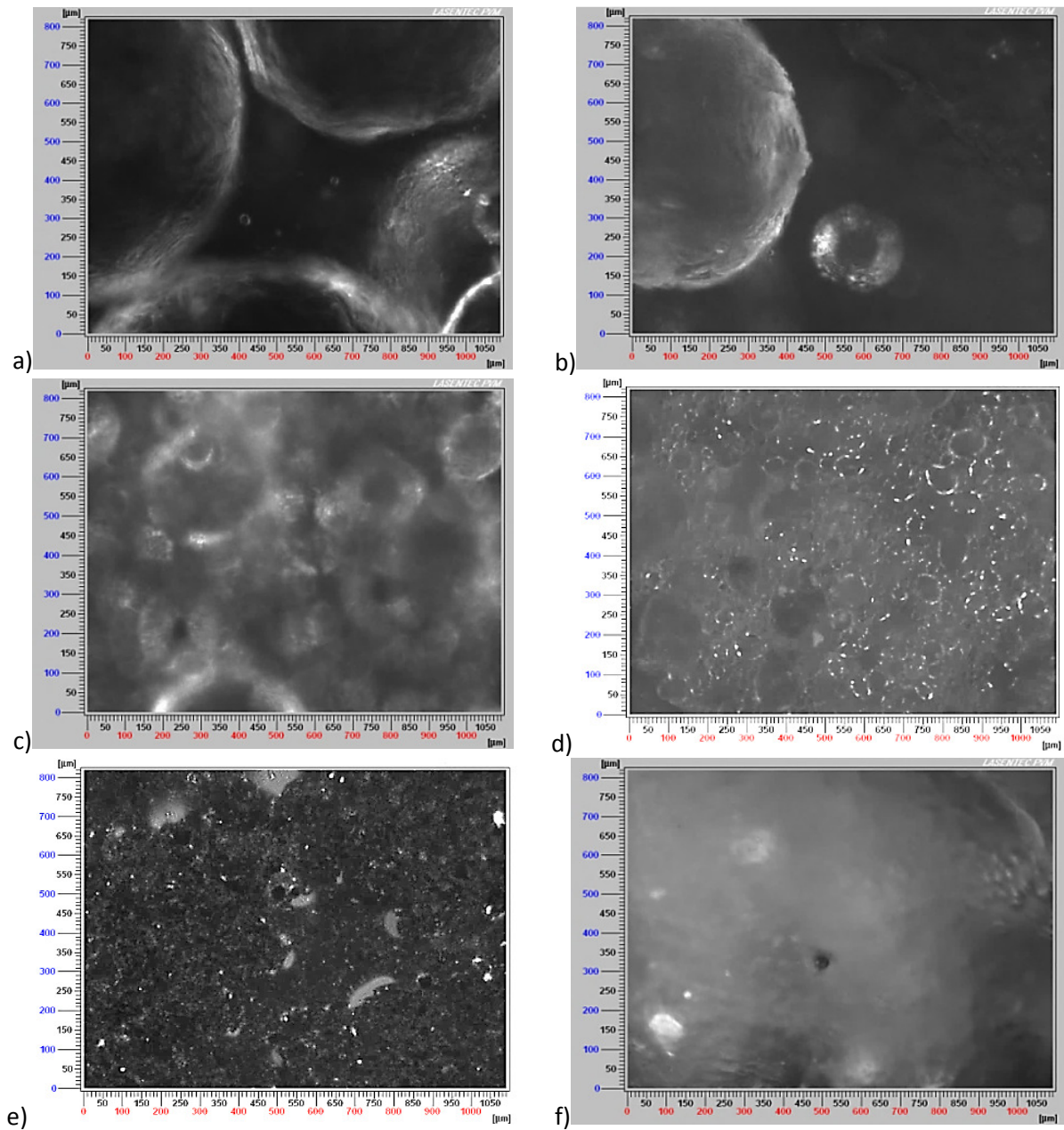


**Figure 3. 6: PVM images of gas hydrate formation: (a) 90%WC without AA-LDHI and salt; (b) 90%WC-NaCl without AA-LDHI; (c) 90%WC with 0.01% AA-LDHI; (d) 80%WC without AA-LDHI and salt; (e) 30%WC without AA-LDHI and salt; and (f) 30%WC-NaCl with 0.01% AA-LDHI.**

### **3.4. Effects of water cut/additive and salt on hydrate formation and transportability**

The experimental results in high water cut systems (Table 3. 1) showed that plugging occurred quickly after gas hydrate formation even at low hydrate volume and in the presence of AA-LDHI. In low water cut systems (Table 3. 1), higher hydrate volume fraction can be transported in the presence of AA-LDHI and/or salt compared to the one in high water cut systems. There was no plug for the experiments with 30%WC-0.01%AA-LDHI and 30%WC-NaCl-0.5%AA-LDHI. It is highlighted

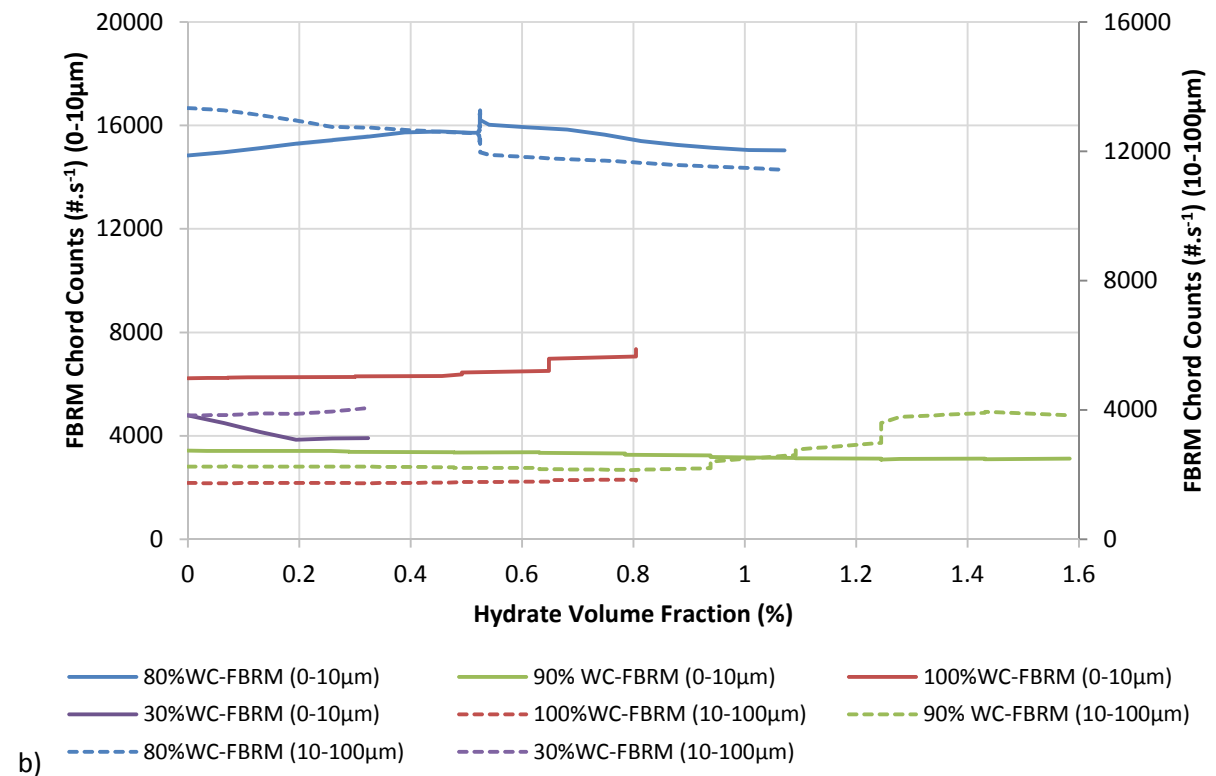
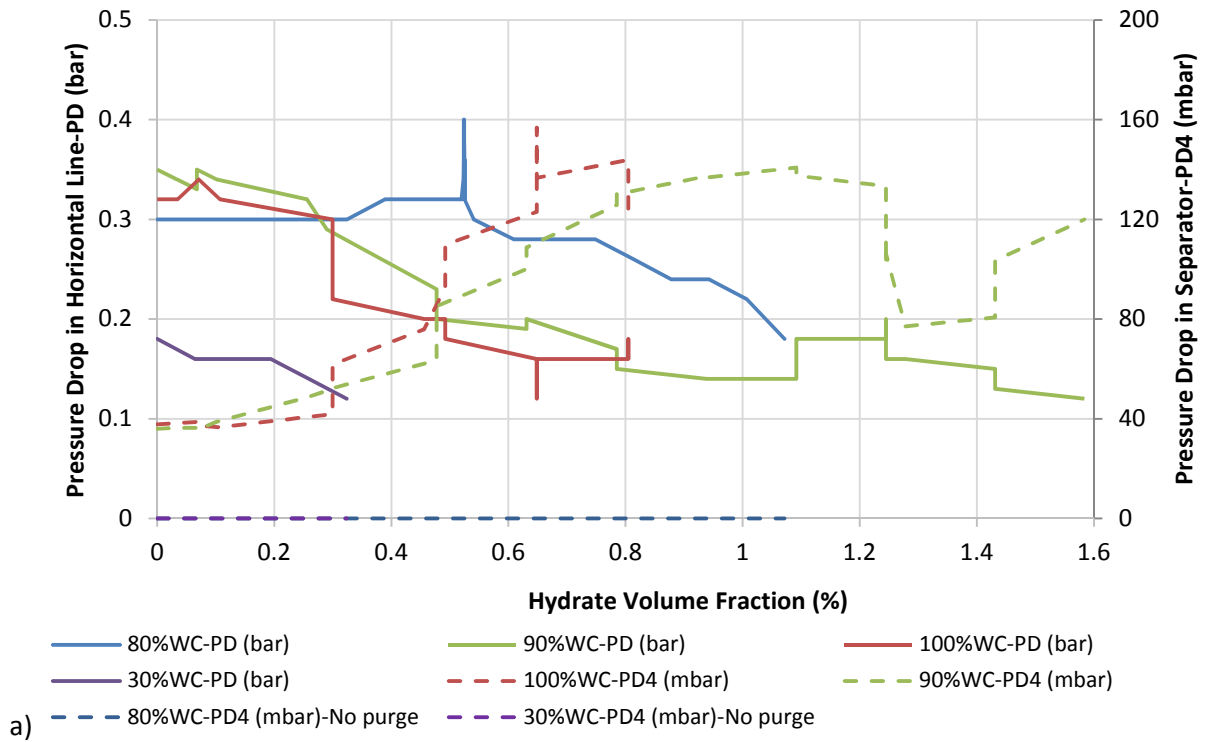
that plugging phenomenon with gas-lift protocol was not only dependent on hydrate volume present in the system but also on the way hydrates agglomerated or deposited on the separator and/or the pipe wall. In this study, effects of water cut, additives, and salt on the hydrate formation and transportability were investigated in the following sections: 3.4.1 and 3.4.2.

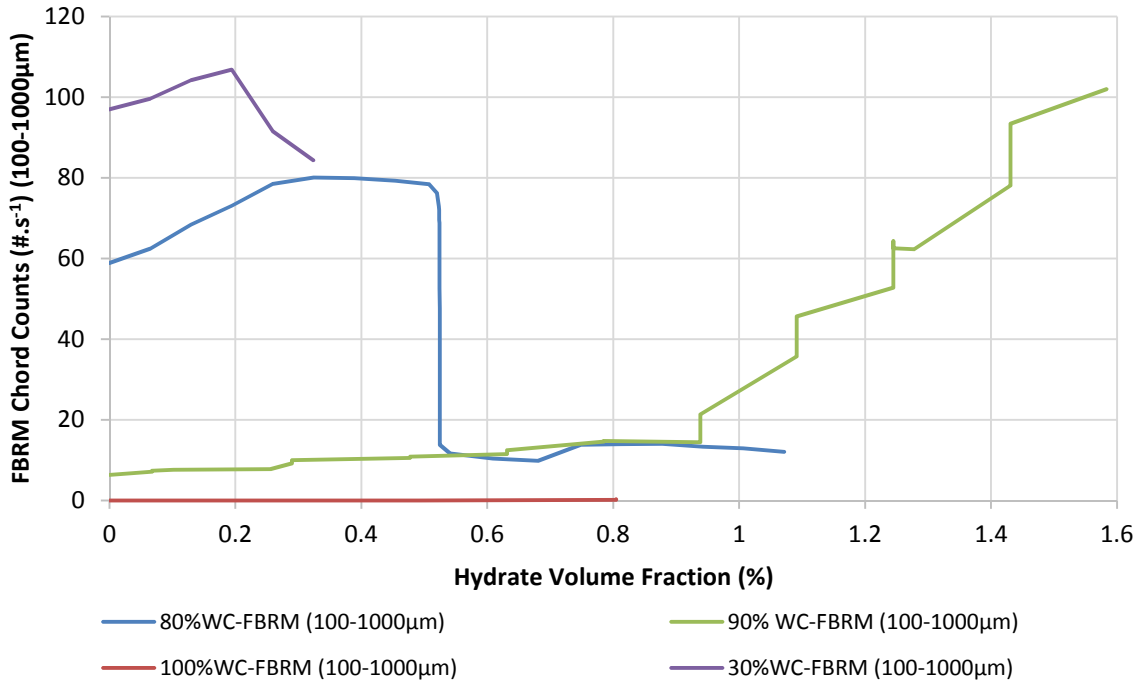
### **3.4.1. Effect of water cut**

Commonly, in low water cut systems, a higher hydrate volume transported (for the experiments with salt and AA-LDHI separately or both of salt and AA-LDHI) compared to those in high water cut systems was observed. This was interpreted by the fact that oil continuous phase played a vital role for salt and/or AA-LDHI to improve hydrate slurry transport.

#### **3.4.1.1. Experiments with pure water**

The difference between the experiments with pure water in low and high water cut systems was not remarkable (Figure 3. 7 a). This means that the plug occurred quickly after hydrate formation for all experiments with pure water. The pressure drop in the separator (PD4) increased sharply once hydrate formed. This might be due to hydrate accumulated and plugged in the separator. Once hydrate formed, the pressure drop in the horizontal line experienced a small increase (at 80%WC) due to the presence of hydrate particles. Moreover, a small decrease in pressure drop in the horizontal line was observed (at 30-90-100%WC) due to the decrease and fluctuation of flowrate (Appendix G). This probably impacted on pressure drop measurements. The change of FBRM chord counts in the experiments with 80-90%WC (Figure 3. 7 b and c) can be attributed to transport of hydrate from separator to be present in the horizontal line. This also agreed with PVM measurements (Figure 3. 6) and the increase in pressure drop in the horizontal line (Figure 3. 7 a).



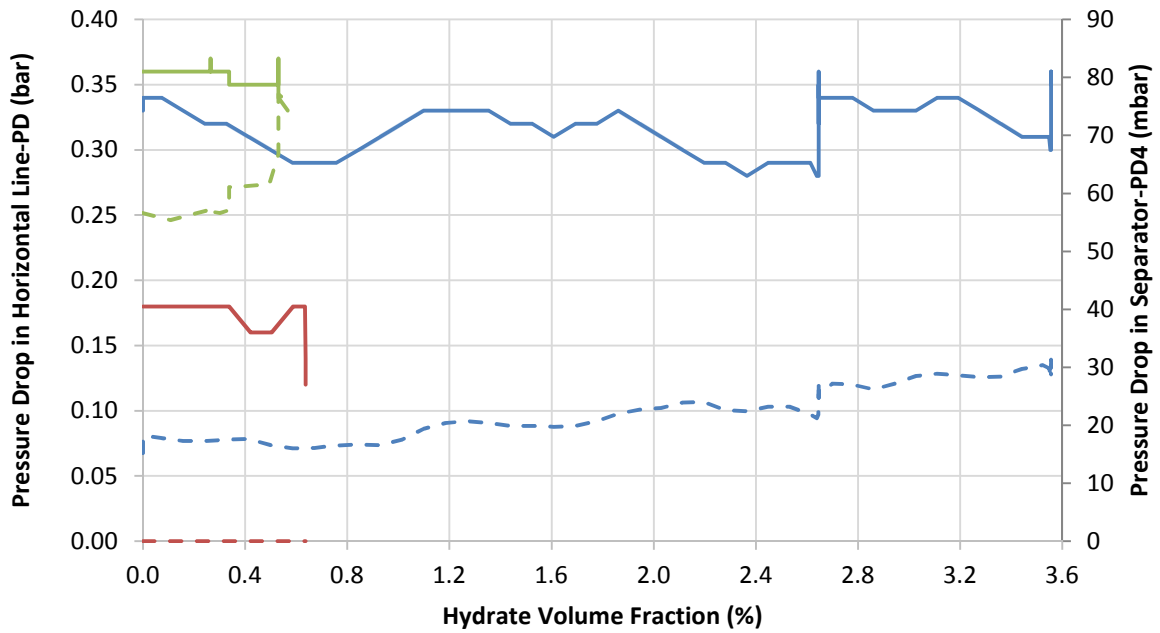


c)

**Figure 3. 7: Experimental results with pure water: (a) PD and PD4; (b) FBRM chord counts (0-100µm); and (c) FBRM chord counts (100-1000µm) as a function of hydrate volume fraction at 100-90-80-30%WC.**

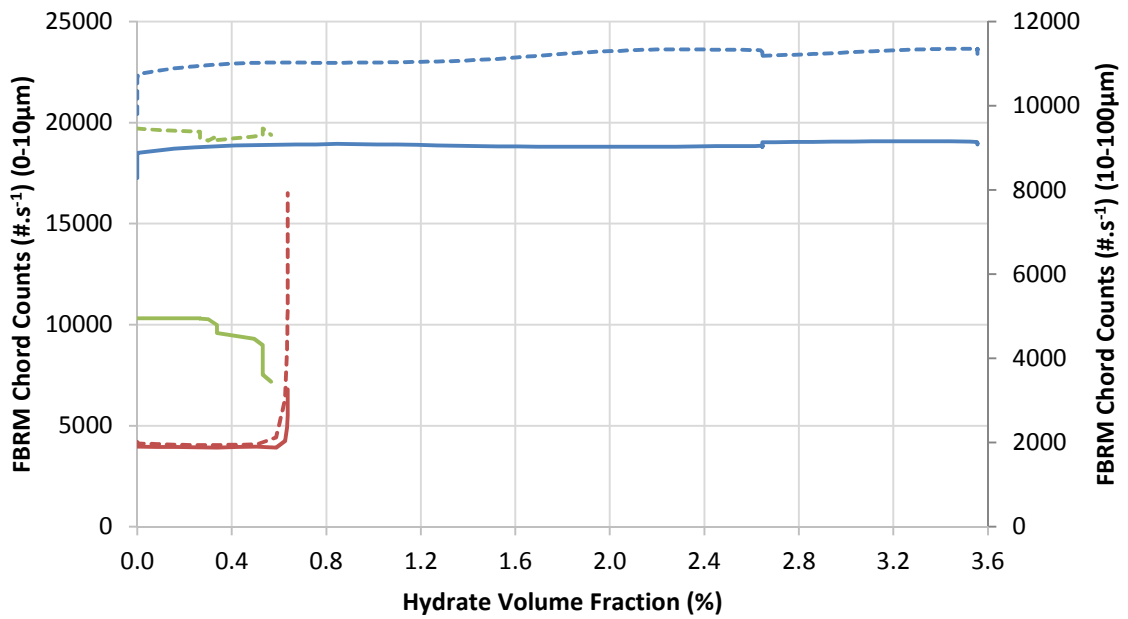
### 3.4.1.2. Experiments with additive

An adequate dosage of oil partially contributed to hydrate slurry transport in the presence of AA-LDHI in high water cut systems (Figure 3. 8 and Table 3. 1). Indeed, the experiment with 80%WC-0.01%AA-LDHI showed longer flowing time with higher hydrate volume transported than those of the experiments with 90-10%WC-0.01%AA-LDHI (Table 3. 1). The role of oil to prevent plugging in the presence of AA-LDHI has been enlightened by (Sun & Firoozabadi, 2015). They supposed that surfactants adsorbed on the hydrate surface creating hydrophobic layers which attract oil to cover the hydrate surface. This hindered collisions and/or lowered adherent forces between hydrate particles leading to prevent agglomeration and plugging. In our case, the plug still happened because of a low dosage of 0.01%AA-LDHI added. However, at 30%WC, 0.01%AA-LDHI was enough to prevent plugging up to 16.67%HV (Table 3. 1, Figure 3. 14, and Figure 3. 15). Plug occurred in the horizontal line for the experiments with 80%WC-0.01%AA-LDHI (no sharp increase in pressure drop in the separator) while this appeared in the separator for the experiments with 90 and 100%WC-0.01%AA-LDHI (a sharp increase in pressure drop in the separator). The increase in FBRM chord counts of experiments with 30-80-90-100%WC-0.01%AA-LDHI can be attributed to the presence of hydrate particles in the horizontal line (Figure 3. 8 and Figure 3. 15).



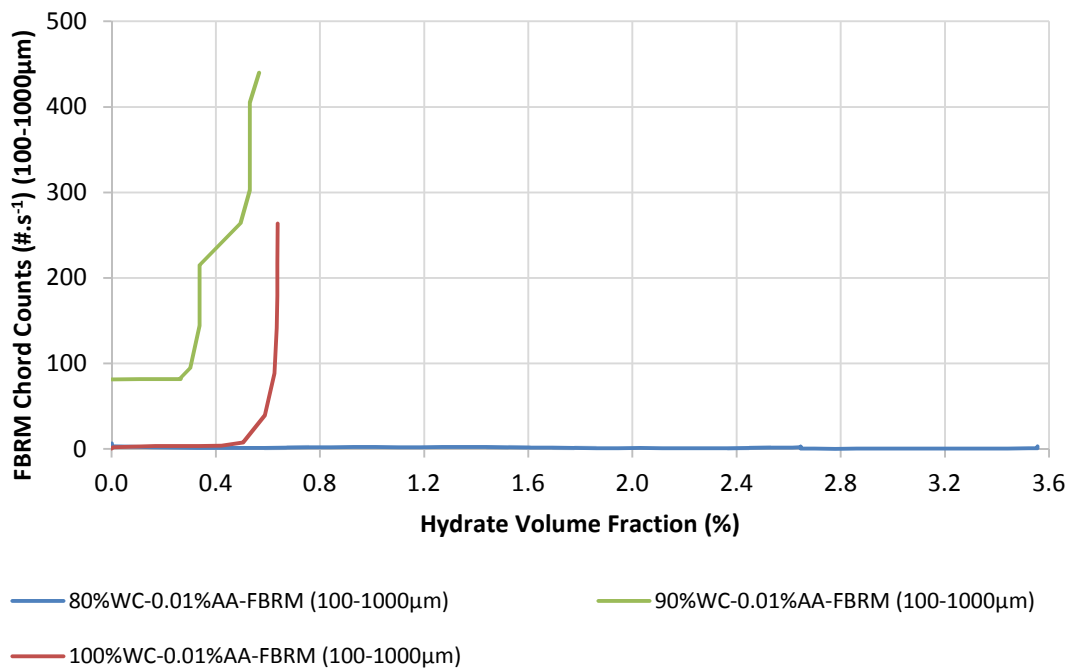
a)

- 80%WC-0.01%AA-PD (bar)
- 90%WC-0.01%AA-PD (bar)
- 100%WC-0.01%AA-PD (bar)
- - - 100%WC-0.01%AA-PD4 (mbar)-No purge
- - - 90%WC-0.01%AA-PD4 (mbar)
- - - 80%WC-0.01%AA-PD4 (mbar)



b)

- 80%WC-0.01%AA-FBRM (0-10µm)
- 90%WC-0.01%AA-FBRM (0-10µm)
- 100%WC-0.01%AA-FBRM (0-10µm)
- - - 100%WC-0.01%AA-FBRM (10-100µm)
- - - 90%WC-0.01%AA-FBRM (10-100µm)
- - - 80%WC-0.01%AA-FBRM (10-100µm)

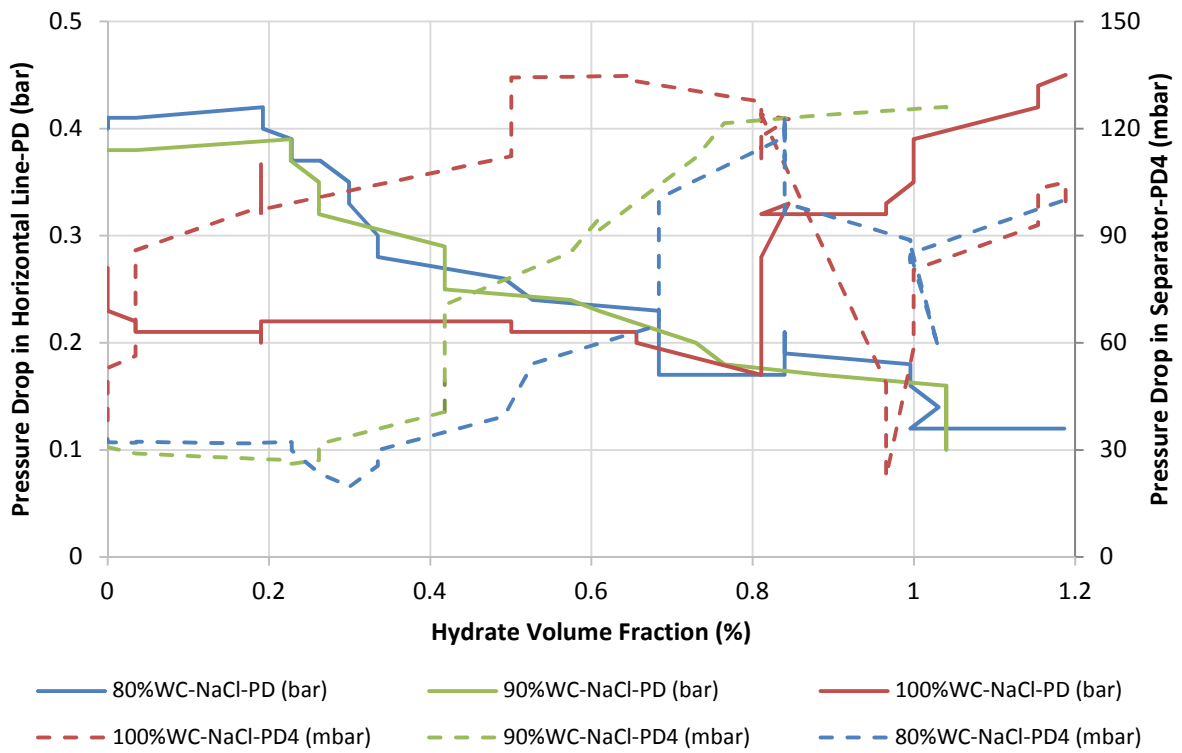


c)

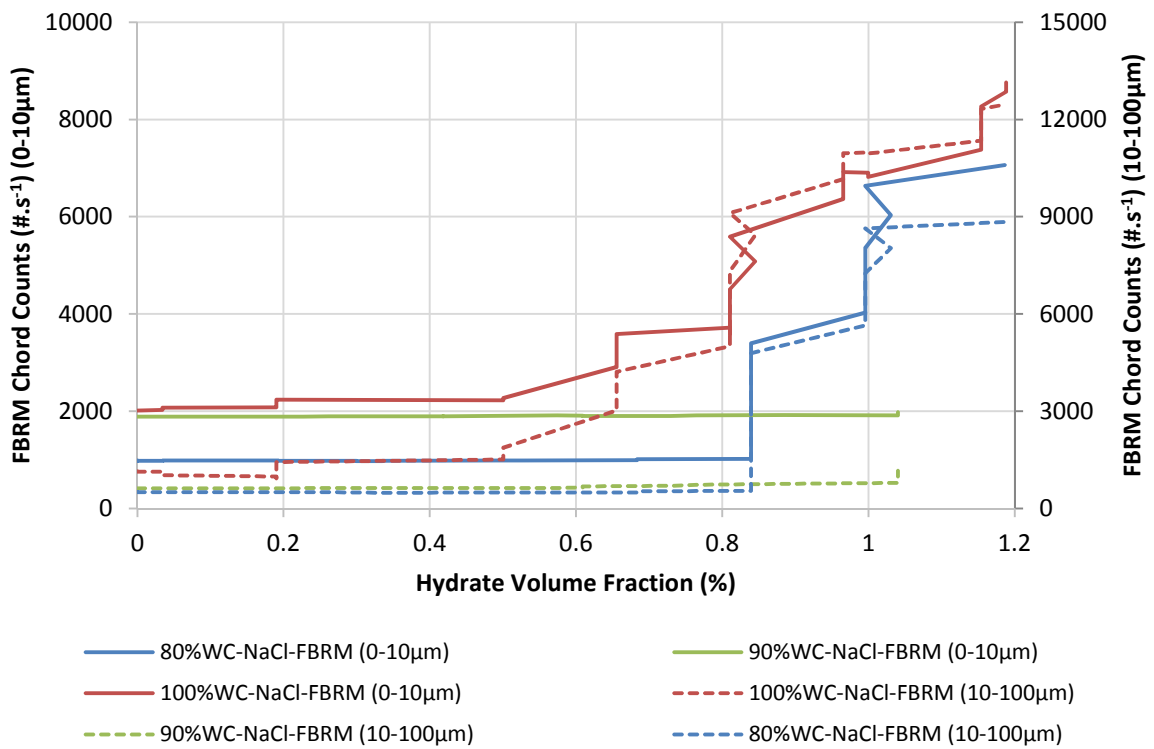
**Figure 3. 8: Experimental results with additive: (a) PD and PD4; (b) FBRM chord counts (0-100μm); and (c) FBRM chord counts (100-1000μm) as a function of hydrate volume fraction at 100-90-80%WC.**

### 3.4.1.3. Experiments with salt

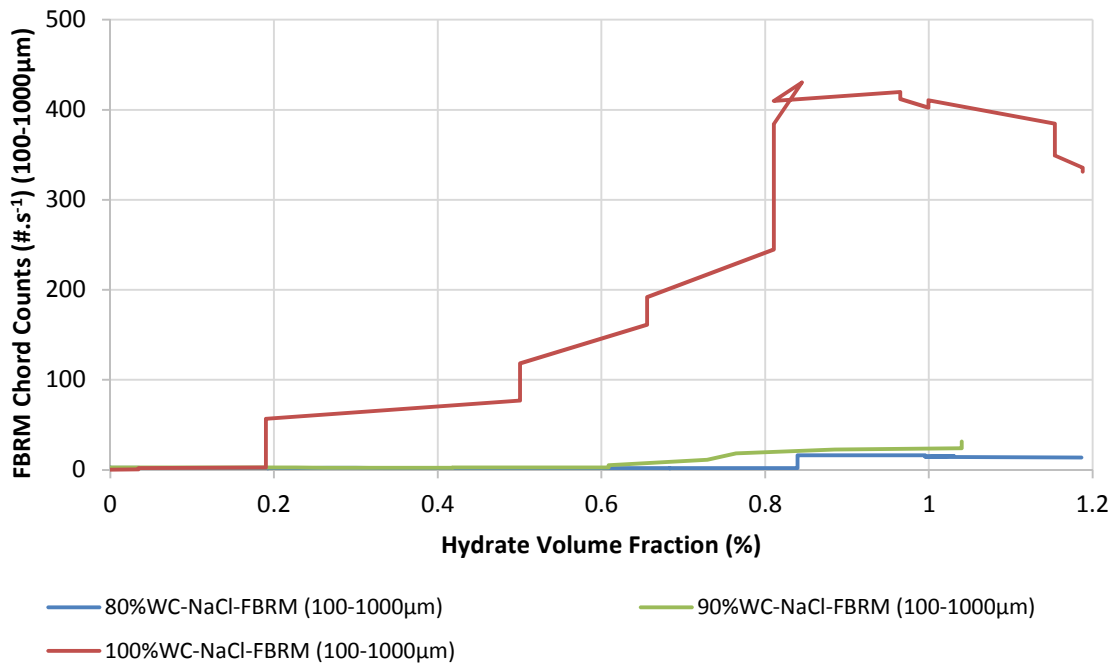
In high water cut systems, a significant increase in pressure drop in the separator was observed possibly due to the accumulation of hydrate (Figure 3. 9 a). This caused plugging rapidly in the separator. The pressure drop in the horizontal line experienced a small decrease in the experiments with 80-90%WC (due to a decrease and fluctuation in flowrate, see Appendix G). Additionally, a small increase in pressure drop for the experiment with 100%WC was observed due to the presence of hydrate particles in the horizontal line. Interestingly, at 30%WC in the presence of salt (Table 3. 1 and Figure 3. 14), it is noticed longer flowing time and higher hydrate volume transported compared to those in high water cut systems. This can be explained by the role of oil (in the presence of salt) to prevent plugging. The increase in pressure drop in the separator was also observed at 30%WC (Figure 3. 14). The increase in FBRM chord counts of the experiments with 30-80-90-100%WC-NaCl can be attributed to hydrate detached from the separator to the horizontal line (Figure 3. 9 b and c, and Figure 3. 15).



a)



b)

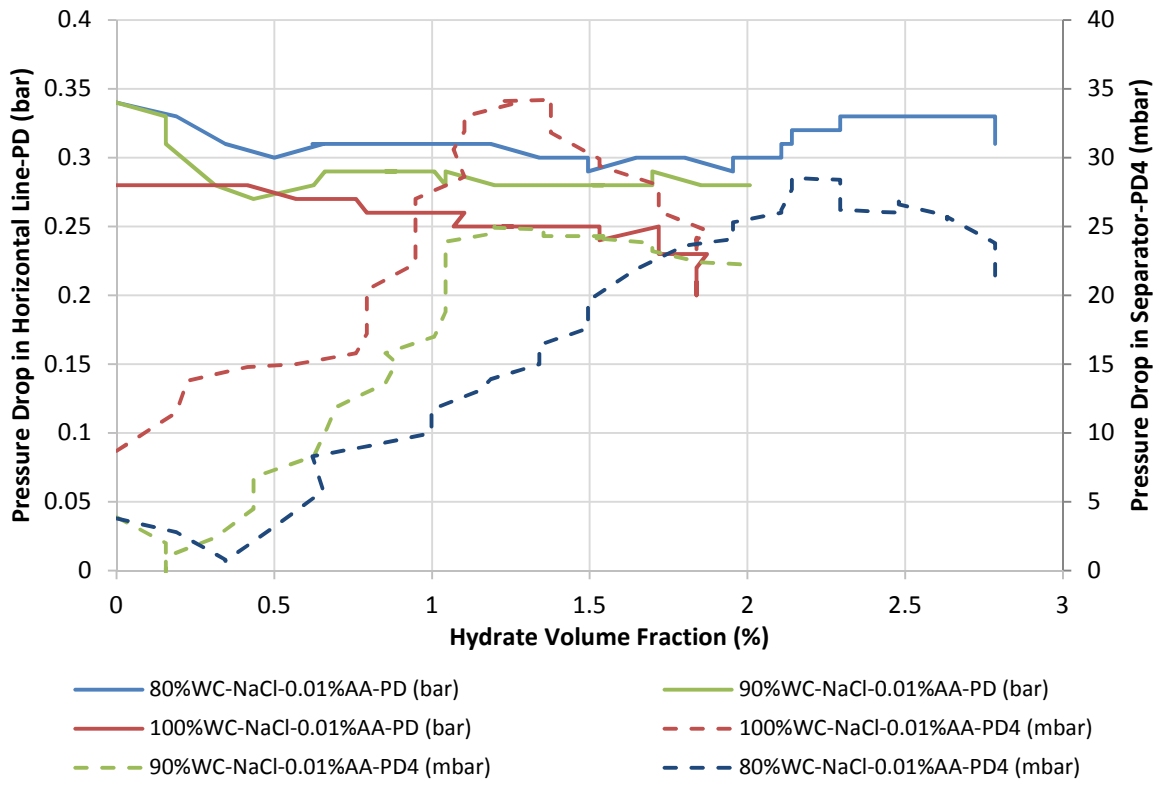


c)

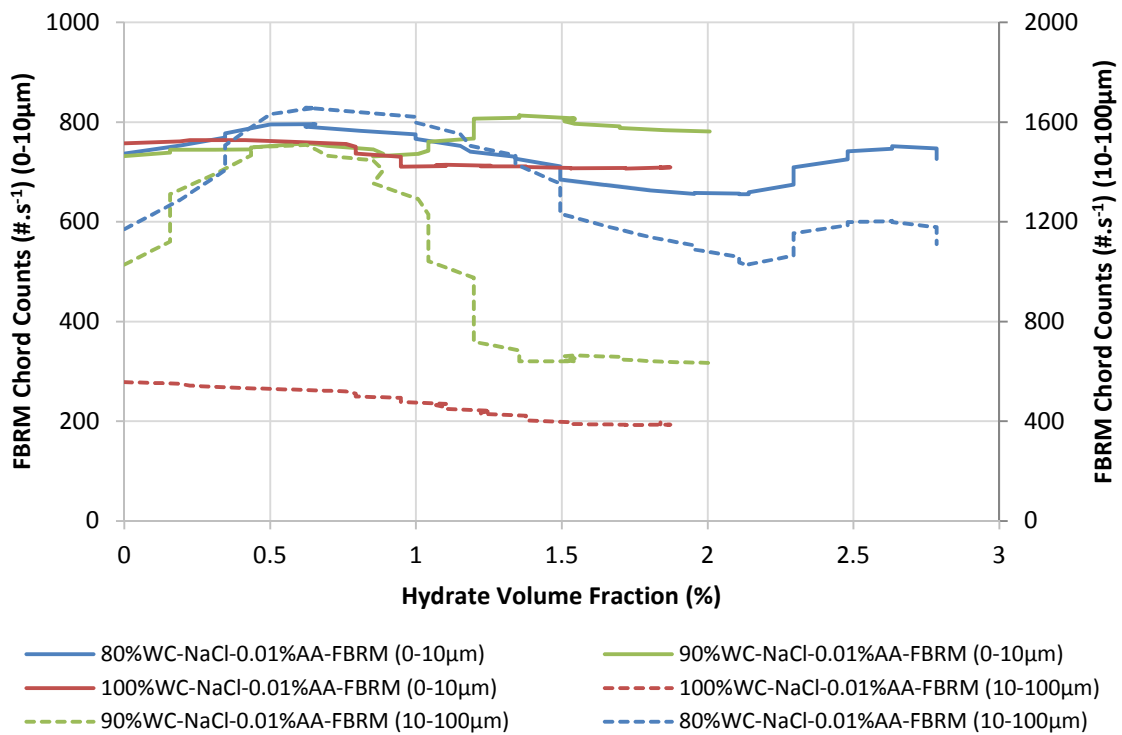
**Figure 3. 9: Experimental results with salt: (a) PD and PD4; (b) FBRM chord counts (0-100µm); and (c) FBRM chord counts (100-1000µm) as a function of hydrate volume fraction at 100-90-80%WC.**

#### 3.4.1.4. Experiments with additive and salt

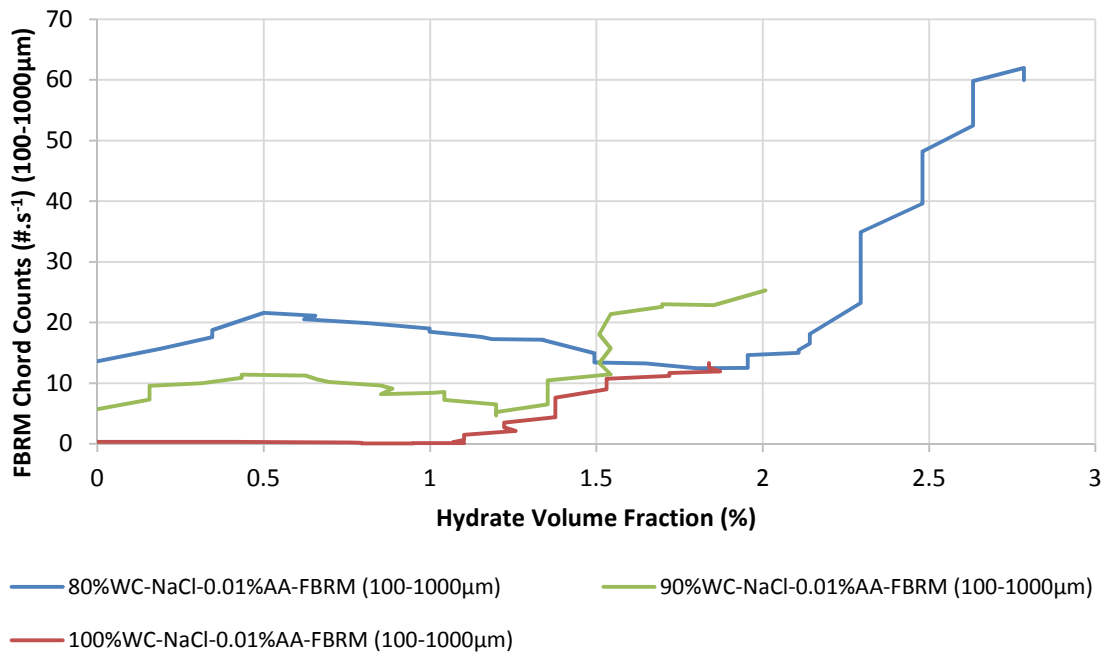
There was not much difference between the experiments in high water cut systems (80-90-100%WC) with both salt and AA-LDHI in terms of hydrate volume transported and plugging time (Figure 3. 10 and Table 3. 1). However, at 30%WC (Figure 3. 14 and Table 3. 1), longer flowing time and a higher hydrate volume transported were observed. This again confirmed the role of oil in maintaining flow in the presence of salt and additives. The increase in FBRM chord counts showed that hydrate particles appeared in the horizontal line (Figure 3. 10).



a)



b)



c)

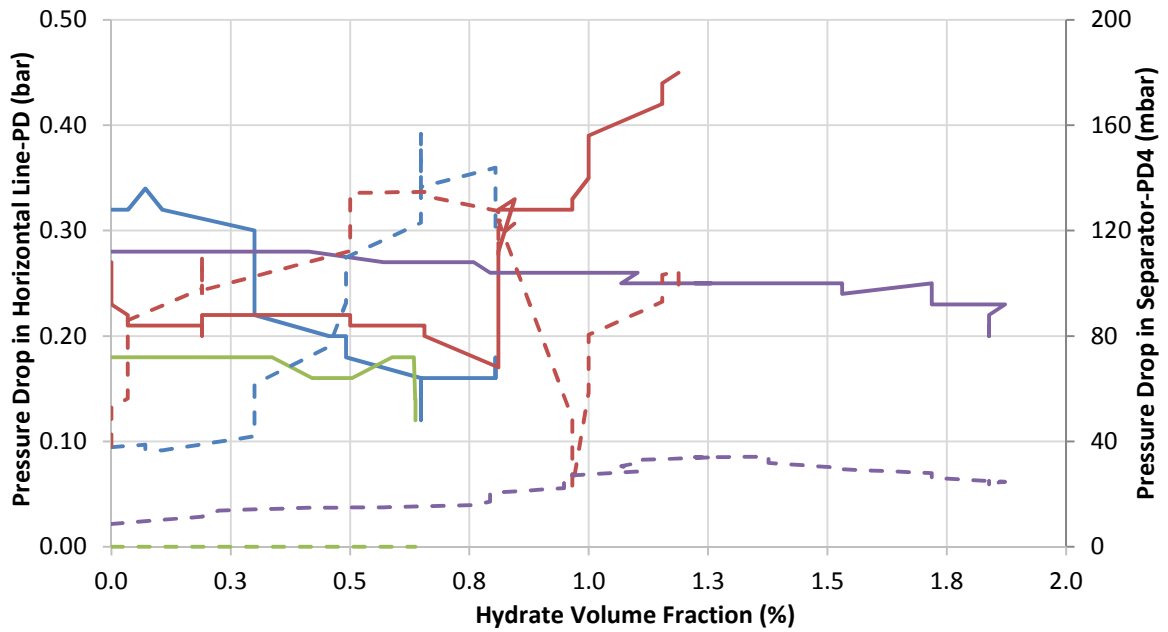
**Figure 3. 10: Experimental results with both salt and additive: (a) PD and PD4; (b) FBRM chord counts (0-100µm); and (c) FBRM chord counts (100-1000µm) as a function of hydrate volume fraction at 100-90-80%WC.**

### 3.4.2. Effect of additive and salt

Effects of additive and salt on hydrate formation and transport in high water cut systems are different from those in low water cuts systems. These experimental results are shown in section 3.4.2.1 and 3.4.2.2.

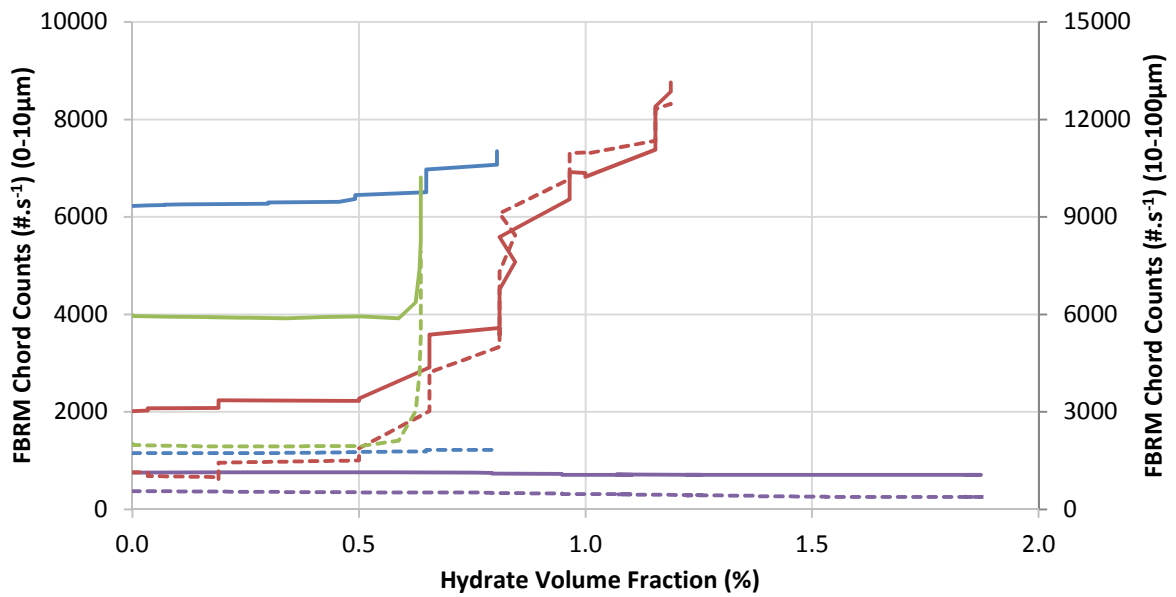
#### 3.4.2.1. In high water cut systems

The experimental results (Table 3. 1, Figure 3. 11, Figure 3. 12, and Figure 3. 13) demonstrated that in high water cut systems, the addition of a low quantity of 0.01%AA-LDHI was not sufficient to prevent agglomeration and plugging. There was not much difference between the experiments with 90 and 100%WC without AA-LDHI and those with AA-LDHI in terms of hydrate volume transported and plugging time (Table 3. 1, Figure 3. 11, and Figure 3. 12).



a)

- 100%WC-PD (bar)
- 100%WC-0.01%AA-PD (bar)
- - 100%WC-PD4 (mbar)
- - 100%WC-NaCl-PD4 (mbar)
- - 100%WC-0.01%AA-PD4 (mbar)-No purge
- - 100%WC-NaCl-0.01%AA-PD4 (mbar)
- 100%WC-NaCl-PD (bar)
- 100%WC-NaCl-0.01%AA-PD (bar)



b)

- 100%WC-FBRM (0-10µm)
- 100%WC-0.01%AA-FBRM (0-10µm)
- - 100%WC-FBRM (10-100µm)
- - 100%WC-NaCl-FBRM (10-100µm)
- - 100%WC-0.01%AA-FBRM (10-100µm)
- 100%WC-NaCl-FBRM (0-10µm)
- 100%WC-NaCl-0.01%AA-FBRM (0-10µm)

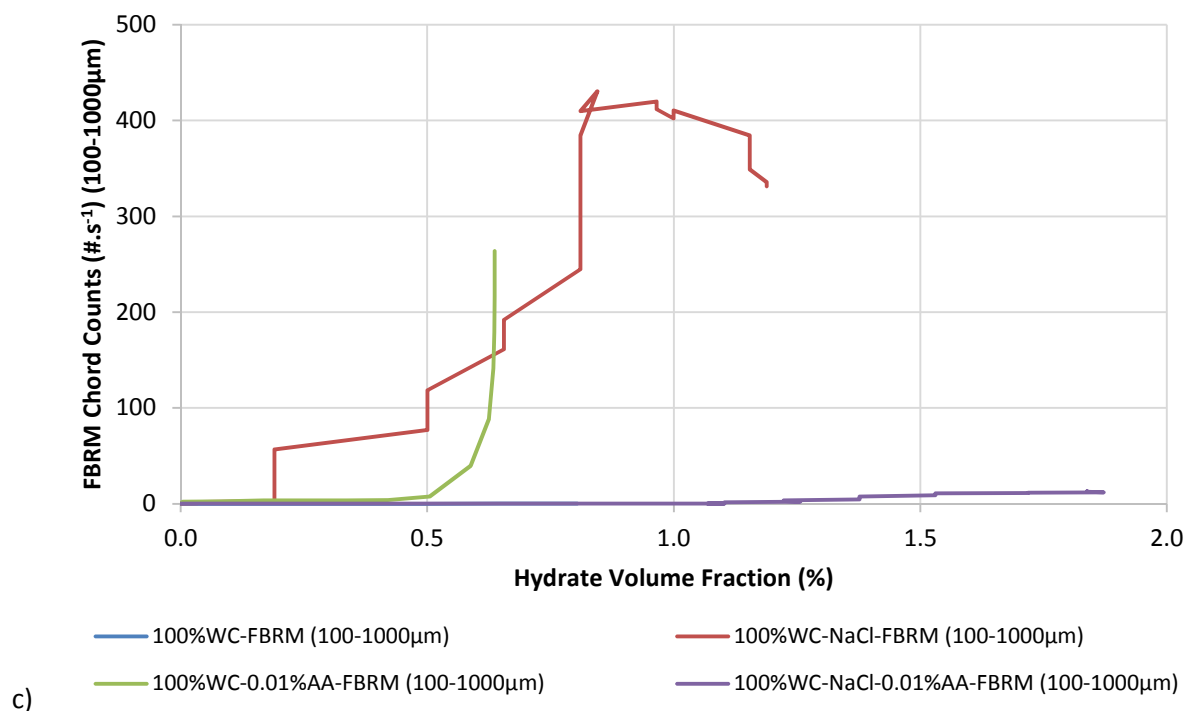
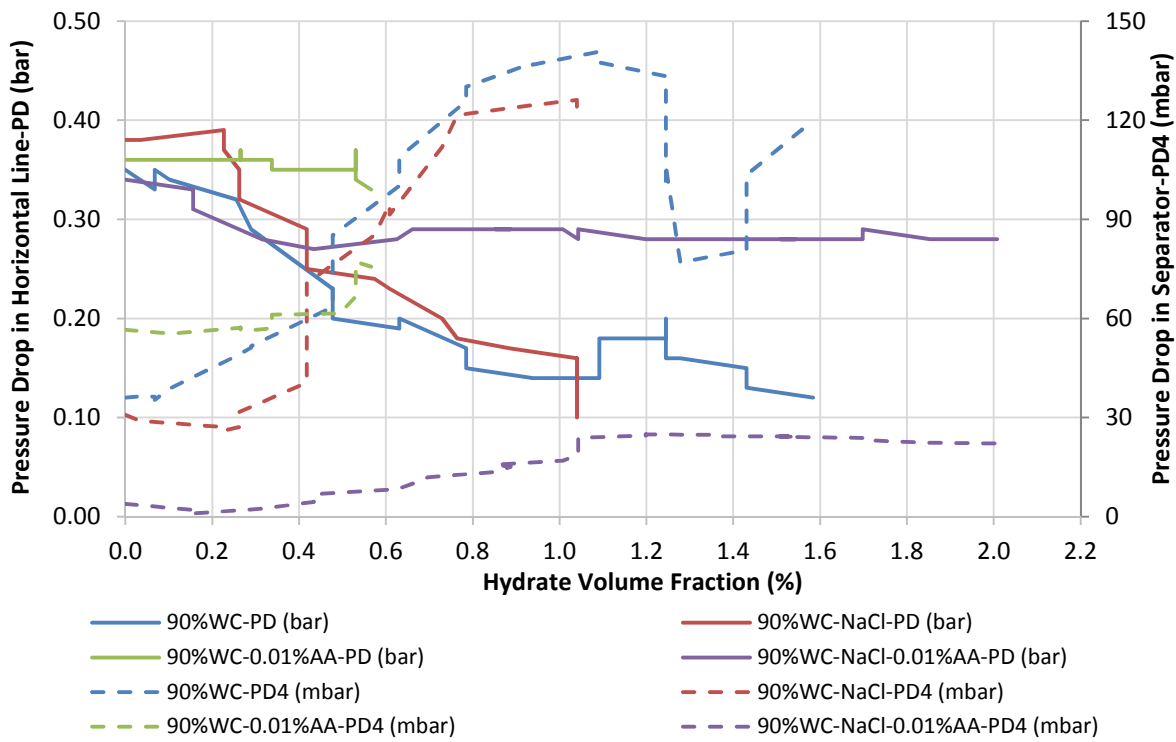
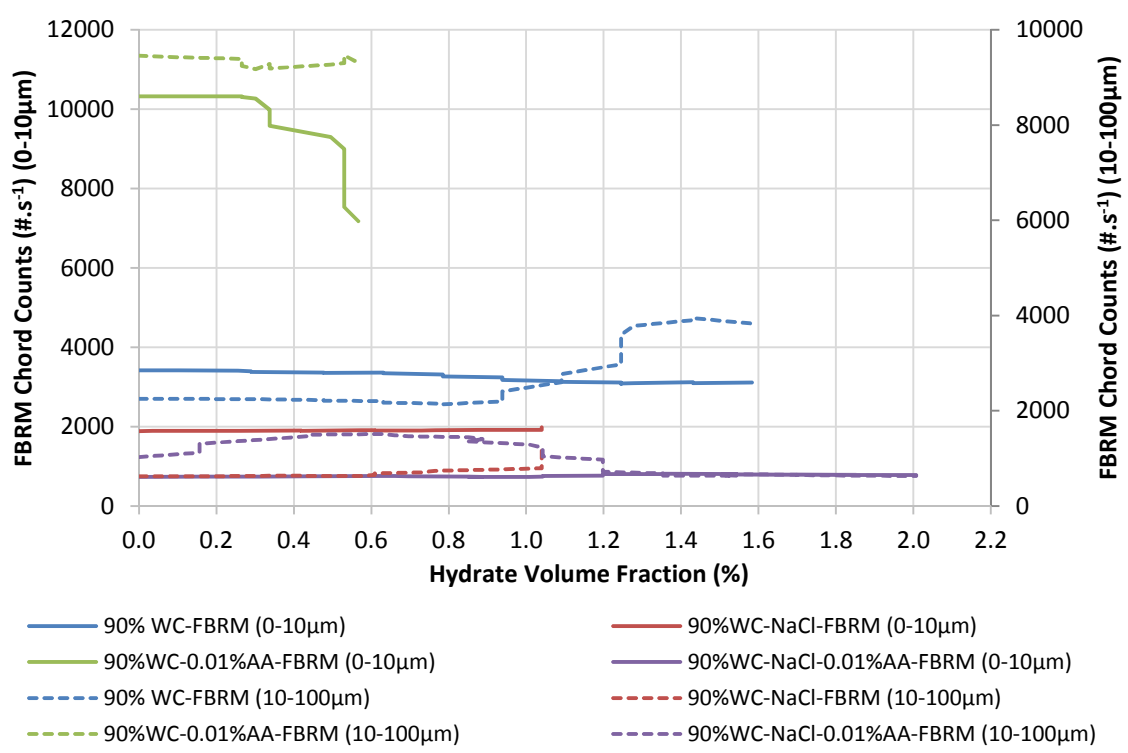


**Figure 3. 11: Experimental results at 100%WC: (a) PD and PD4; (b) FBRM chord counts (0-100µm); and (c) FBRM chord counts (100-1000µm) as a function of hydrate volume fraction.**

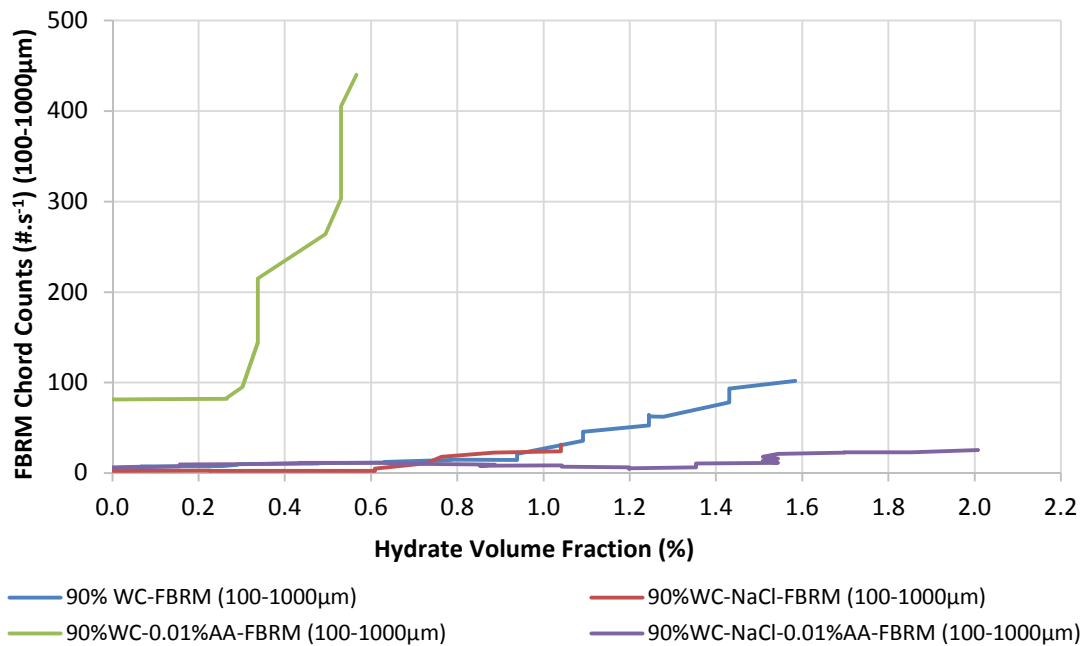
Interestingly, the experiment with 80%WC-0.01%AA-LDHI showed very short nucleation time compared to the experiment with 80%WC without AA-LDHI (Figure 3. 13). This can be attributed to the foam formed at 80%WC-0.01%AA-LDHI which promoted hydrate formation. Furthermore, the flowing time in the experiment with 80%WC-0.01%AA-LDHI was longer (higher hydrate volume transported) comparing with that without AA-LDHI. This indicated that AA-LDHI enhanced the hydrate slurry transport. Moreover, the addition of AA-LDHI (in the presence of salt) improved capability of preventing plug. Addition of salt increased the performance of AA-LDHI at 90-100%WC in term of hydrate volume transported (Table 3. 1, Figure 3. 11, and Figure 3. 12). This showed the role of AA-LDHI in preventing plug in the presence of salt in high water cut systems. There could be an interaction between AA-LDH and salt which enhanced the capability of AA-LDHI. The increase in FBRM chord counts showed the presence of hydrate particles in the horizontal line.



a)



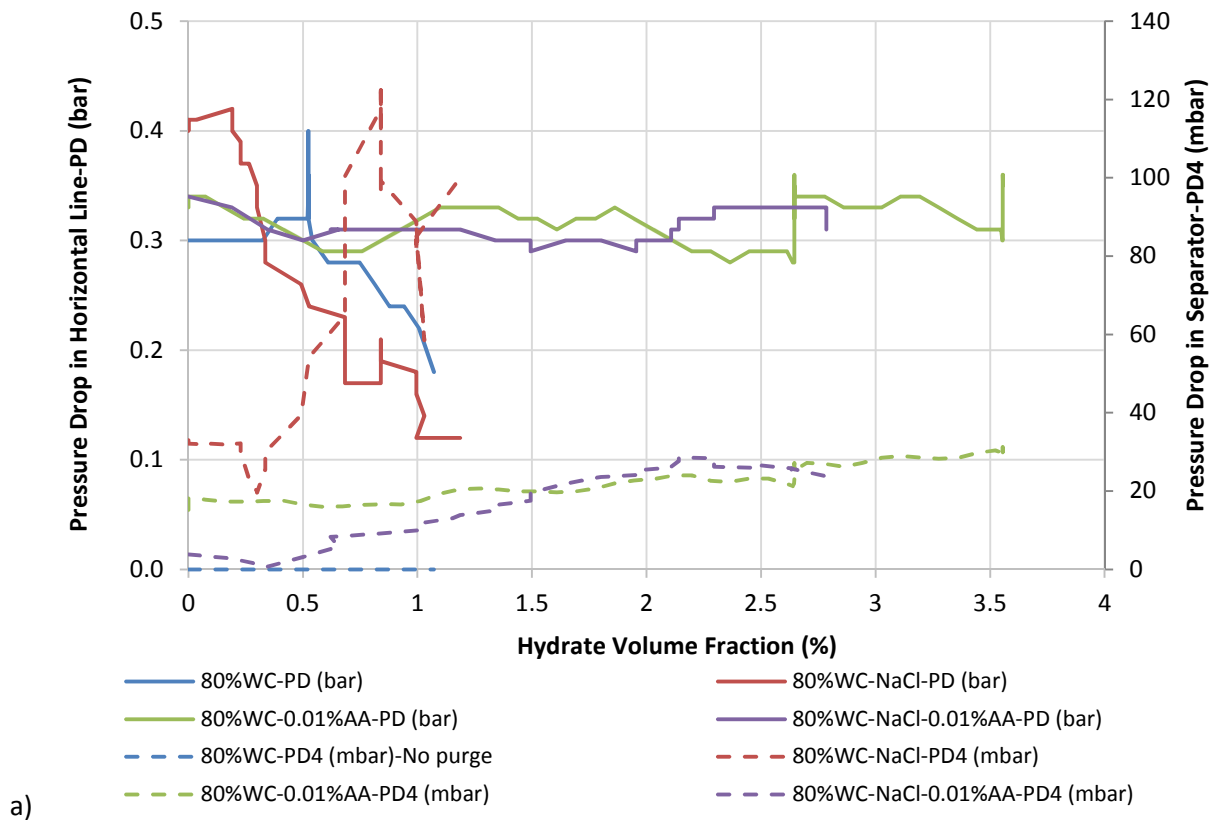
b)



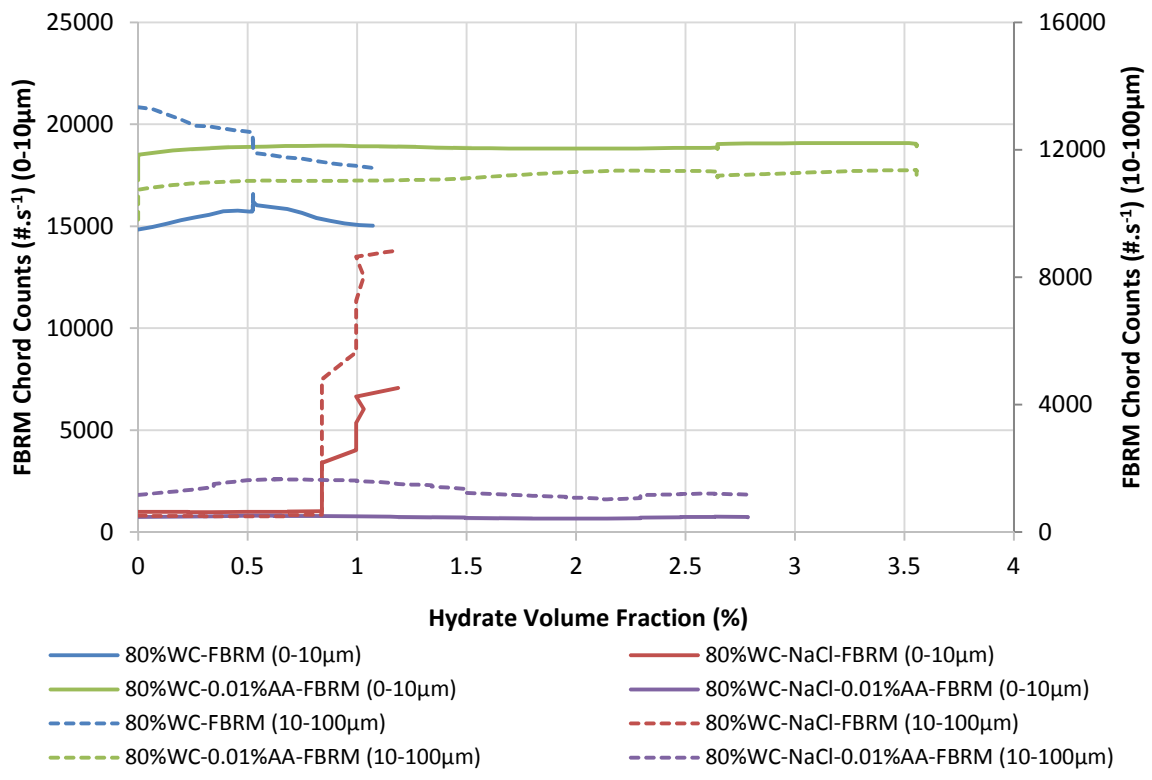
c)

**Figure 3. 12: Experimental results at 90%WC: (a) PD and PD4; (b) FBRM chord counts (0-100μm); and (c) FBRM chord counts (100-1000μm) as a function of hydrate volume fraction.**

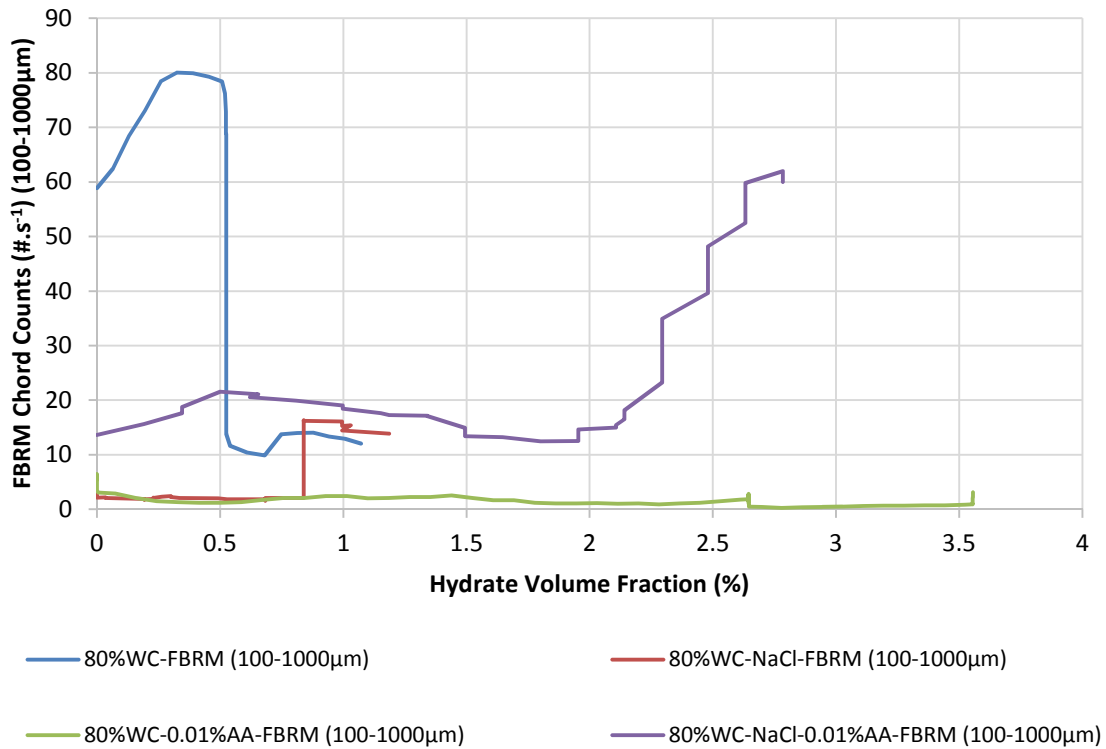
For the experiments with both salt and AA-LDHI in high water cut systems (Figure 3. 11, Figure 3. 12, and Figure 3. 13), an increase in the flowrate at the plugging time was observed. This is possibly due to viscosity decreased and/or pipe wall surface property changed from water-wet to oil-wet. The presence of foam (more foam with both salt and AA-LDHI compared to that with only AA-LDHI) increased the gas/liquid contact surface leading to sooner hydrate formation (Guo et al., 2017). Indeed, in the separator, there were liquid and gas phases. Once the gas-lift system started, this induced foam formation on the interface of gas and liquid in the separator. Foam is gas bubbles covered by a very thin film of liquid layer in the gas phase (very large surface areas with little liquid mass). It is supposed that hydrates formed more easily on the surface of foam compared to gas bubble in the liquid phase. This was due to the two sides of gas contact with a very thin liquid layer between them (huge volume of gas). This contributed to shorter induction time for experiments with both salt and AA-LDHI.



a)



b)

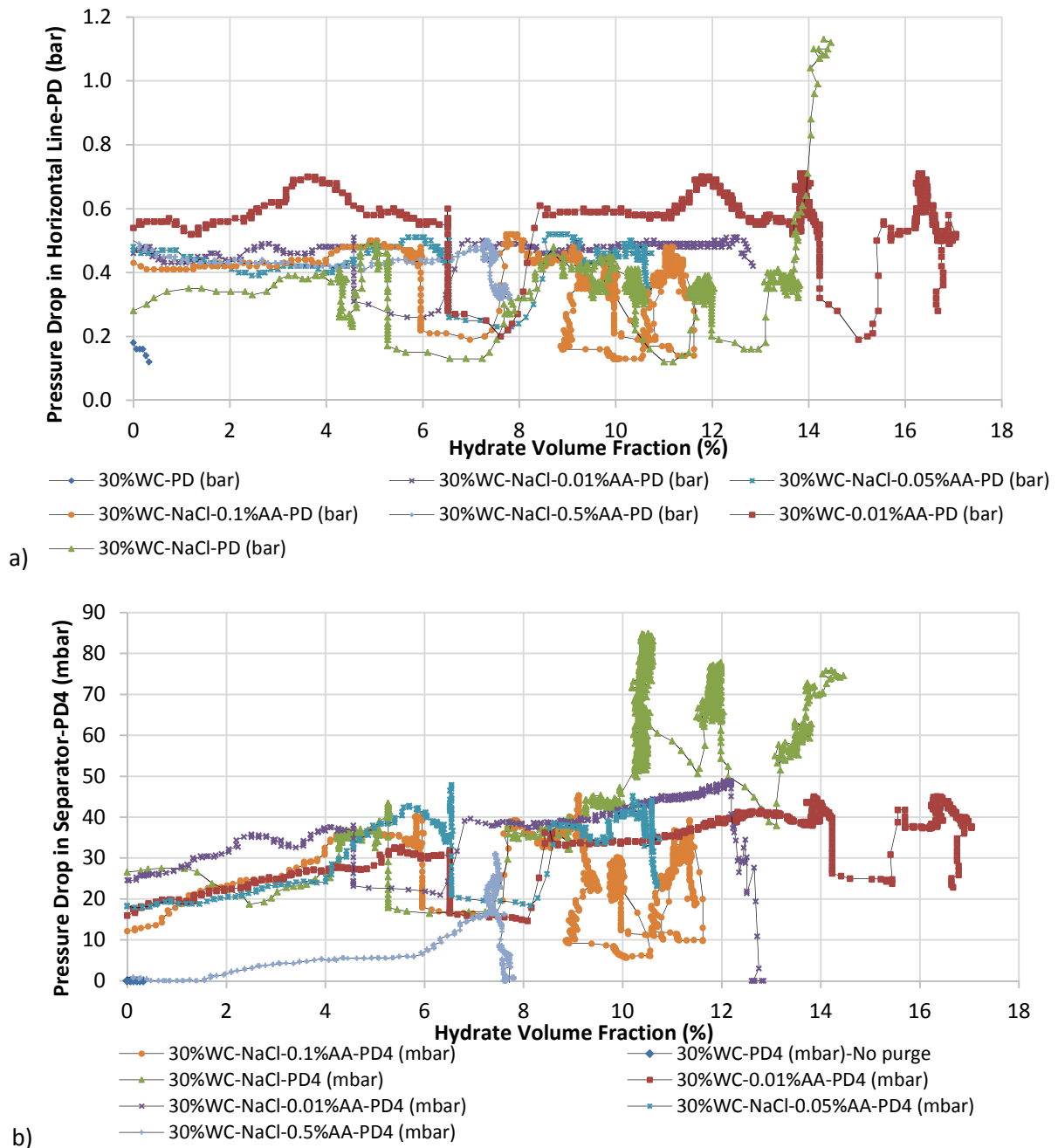


c)

**Figure 3. 13: Experimental results with 80%WC: (a) PD and PD4; (b) FBRM chord counts (0-100μm); and (c) FBRM chord counts (100-1000μm) as a function of hydrate volume fraction.**

### 3.4.2.2. In low water cut systems

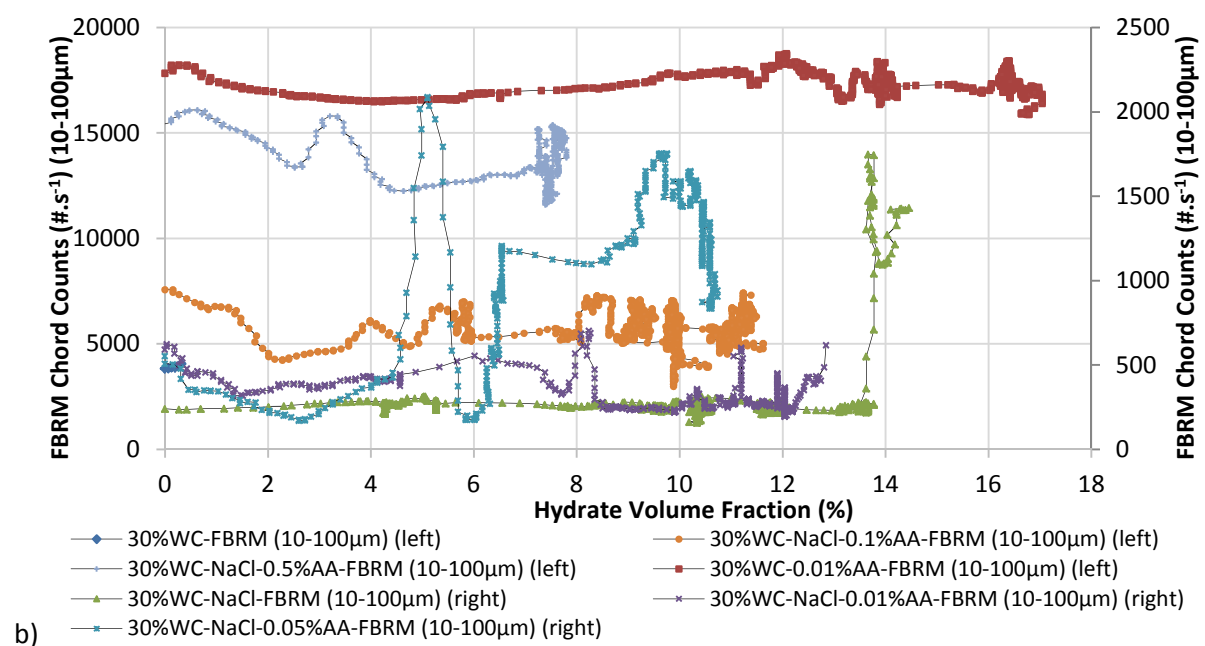
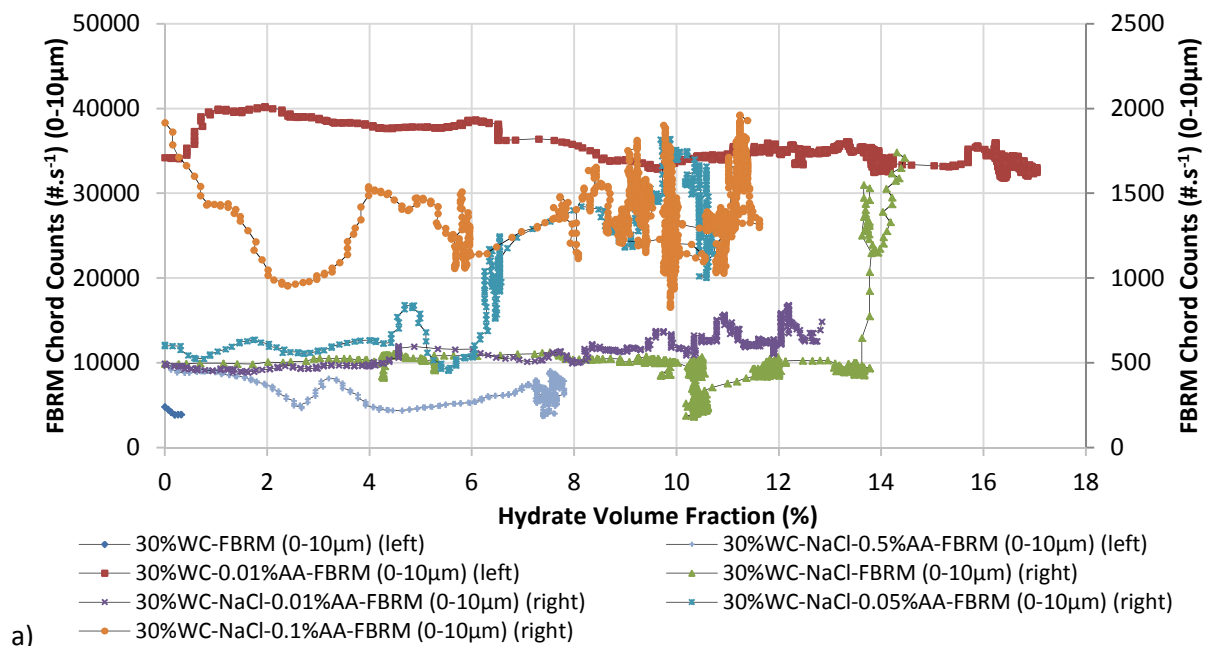
AA-LDHI facilitated hydrate particles dispersed in the oil phase once hydrate formed from dispersed water droplets in low water cut systems (Table 3. 1, Figure 3. 14, and Figure 3. 15). In fact, the amount of 0.01%AA-LDHI was sufficient to prevent plug for the experiment without salt. Besides, the addition of AA-LDHI (in the presence of salt) lowered performance in preventing plug compared to that with only salt. This could be that once hydrate formed, phase inversion occurred. The oil continuous phase (oil-wet pipe surface) shifted to the water continuous phase (water-wet pipe surface). This caused a higher risk of plug for experiments with both salt and AA-LDHI compared to that with salt. This is in agreement with the explanation in section 3.2.1.



**Figure 3. 14: Experimental results with 30%WC: (a) PD and (b) PD4 as a function of hydrate volume fraction. A sudden decrease or increase in PD and/or PD4 is because of stop and restart the ballast system (to increase pressure in the flowloop).**

In low water cut systems, the experiment with salt showed longer flowing time (higher hydrate volume transported) (Table 3. 1, Figure 3. 14, and Figure 3. 15) than that without salt. This can be explained by the salt lowered rate of crystallization (thermodynamic inhibition and less oil-water dispersion) leading to a slowdown in agglomeration. Moreover, addition of salt lowered the performance of AA-LDHI. This was due to the presence of salt (in presence of AA-LDHI) caused less

dispersion of water droplets in oil continuous phase compared to that with AA-LDHI. As a result, less dispersion of hydrate particles (higher risk of the plug) was observed once they formed. In FBRM chord counts, the stability and high intensity of chord counts in the range of 0-100 $\mu\text{m}$  (detected chord length) for the experiment with 30%WC-0.01%AA-LDHI compared to the other experiments in low water cut systems (Figure 3. 15 a and b) were observed. This can be explained by the role of AA-LDHI to disperse hydrate particles once hydrate formed preventing agglomeration and plugging. This also confirmed that hydrate formed on the surface of dispersed water droplets and their size did not change during crystallization (the mechanism is shown in section 3.6).



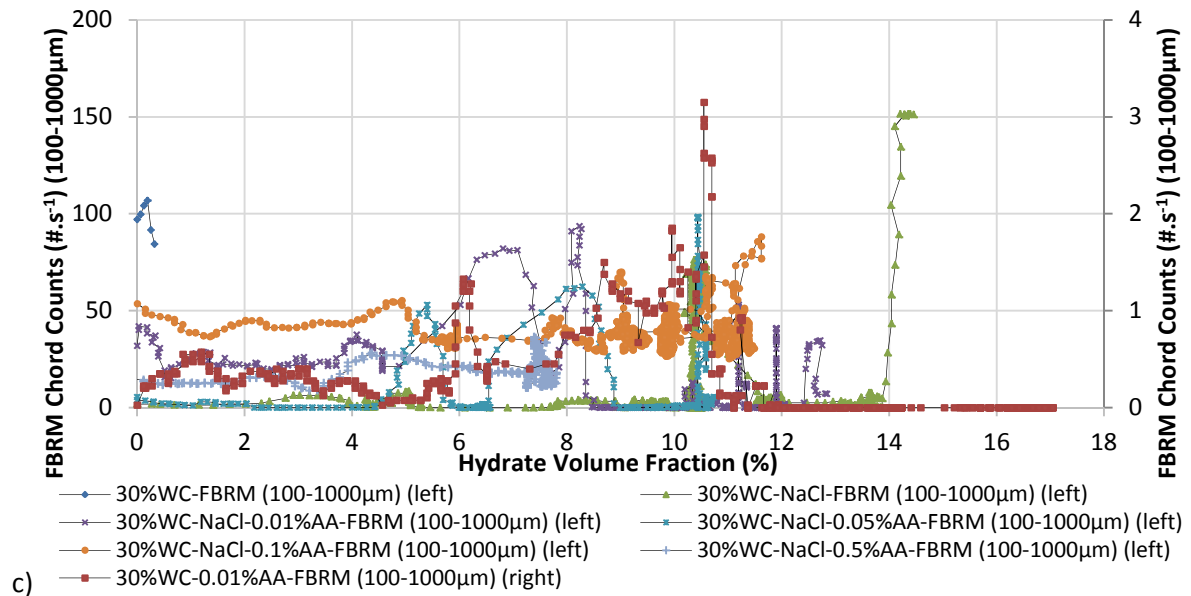


**Figure 3. 15: Experimental results with 30%WC: FBRM chord counts (a: 0-10µm; b: 10-100µm; and c: 100-1000µm) as a function of hydrate volume fraction.**

### 3.5. Role of gas bubbles in water and oil continuous phase

In high water cut systems, the experimental tests showed a quick increase in pressure drop in the separator, also a significant decline in the overall pressure in the flowloop, and quick plug once hydrate formation started. In low water cut systems, generally, the quick plug after gas hydrate formation was not observed. This difference between low and high water cut systems can be explained by the role of gas bubbles in the riser in different continuous phases. For the water continuous phase (high water cut systems), hydrates formed on the surface of gas bubbles which was in direct contact with water. These hydrates flowed in the water continuous phase and deposited probably on the water-wet wall surface of the riser and/or separator. For the oil continuous phase (low water cut systems), gas bubbles flowed into the oil and helped gas transfer better into the oil. This might cause a faster hydrate formation on the surface of water droplets dispersed in oil continuous phase (short induction time, see Table 3. 1). Once hydrates formed, they possibly agglomerated but less deposited due to the oil-wet surface of the pipe wall.

Several suggestions could be proposed to interpret the high rate of gas hydrate formation and quick plug in high water cut systems, as follows:

Firstly, it can be attributed to gas hydrate formation at the surface of gas bubbles which has been previously observed by (H.Tajima, 2010) and (Luo et al., 2007). Moreover, this must consider an unexpected formation of foam. Both gas bubbles and foam could be attributed to the high contact surface area between oil, water, and gas. Moreover, once hydrates formed, they could be broken

into smaller particles and this enhanced hydrate formation by liberating contact surface between gas and water.

Secondly, hydrate bridges between hydrate particles also contribute as one of the principal reasons for a rapid agglomeration in the riser and deposition in the separator. Here, hydrate film formed on the gas bubbles and/or foam surfaces perhaps favored links between hydrate particles. In this explanation, it is assumed that thanks to a lot of bubbles in the riser, hydrates can readily form on the surface of bubbles, and gas bubbles surrounded by water may play a role as the water-gas bubble bridges which later are easily transformed into hydrate-gas bubble bridges. This may create a higher rate of agglomeration in the riser resulting in a blockage on the separator.

Thirdly, in high water cut systems, water is the continuous phase and in contact with the pipeline surface. As a result, when hydrates formed, in the presence of water film between the pipe surface and hydrate particles, hydrates could stick into the pipe wall. It is a different case when oil is the continuous phase. The previous work (Aspenes et al., 2010) considered that the adhesion force of hydrate particles and pipe surface with water droplets is much higher than hydrate-hydrate cohesion force or hydrate-pipe wall interaction without water layer. This can explain hydrates deposited easily on the pipe wall once they formed leading to plugging quickly.

Finally, because of lower velocity of bubbles at higher height in the riser due to flow resistance, hydrate-covered bubbles caught up at the top of riser and they agglomerated and accumulated below the bulk gas-liquid interface in separator which led to a sudden increase in pressure drop in separator and caused plug, (Luo et al., 2007). Besides, bubbles in the riser not only enhanced gas transfer to the dispersion to reach a faster gas saturation accelerating hydrate formation but also promoted gas transfer once hydrate formed causing a higher rate of gas hydrate formation.

### **3.6. Proposed mechanisms**

According to (Fidel-Dufour et al., 2006), the flow in the riser of Archimède flowloop shows a slug flow pattern which is encountered in small diameter riser (<0.05 m). In high water cut systems, the mechanisms were proposed in Figure 3. 16 a and b. As discussed in section 3.5, it is considered that once hydrate formed on the gas bubble surface in the riser, hydrate-covered bubbles can be easily broken into free hydrate particles and free gas bubbles which can be recovered by a new hydrate film. These hydrate-covered bubbles can agglomerate thanks to the adherent forces between hydrate particles, (H.Tajima, 2010); (Yang et al., 2004b); (Luo et al., 2007). It is recalled that from experimental results, a very high rate of crystallization (gas consumption) was witnessed in the different high water cut (80-90-100%WC) experiments. This can be explained by the dominance of

gas bubbles in the riser over oil droplets. Furthermore, the oil droplets may contain some dissolved gases which lead to the formation of a hydrate layer covering their surface but perhaps fewer and smaller than hydrate-covered bubbles. The main reason explaining the quick plugs after hydrate formation could be the high rate of gas hydrate shell formation around the gas bubbles. This might be cracked easily from the hydrate shell in water continuous phase (this also helped to promote mass transfer). The rapid hydrate agglomeration was due to the water-gas bubble bridge between hydrate particles and hydrate deposition as described above (section 3.5). In low water cut systems, hydrate formed on the surface of water droplets dispersing in oil continuous phase. It is supposed that there was no hydrate broken from hydrate shell-covered water droplets in oil continuous phase. In this case, hydrates can agglomerate and deposit on the pipe wall. The gas transfer was enhanced by gas bubbles in the oil continuous phase, as shown in Figure 3. 16 c and d.

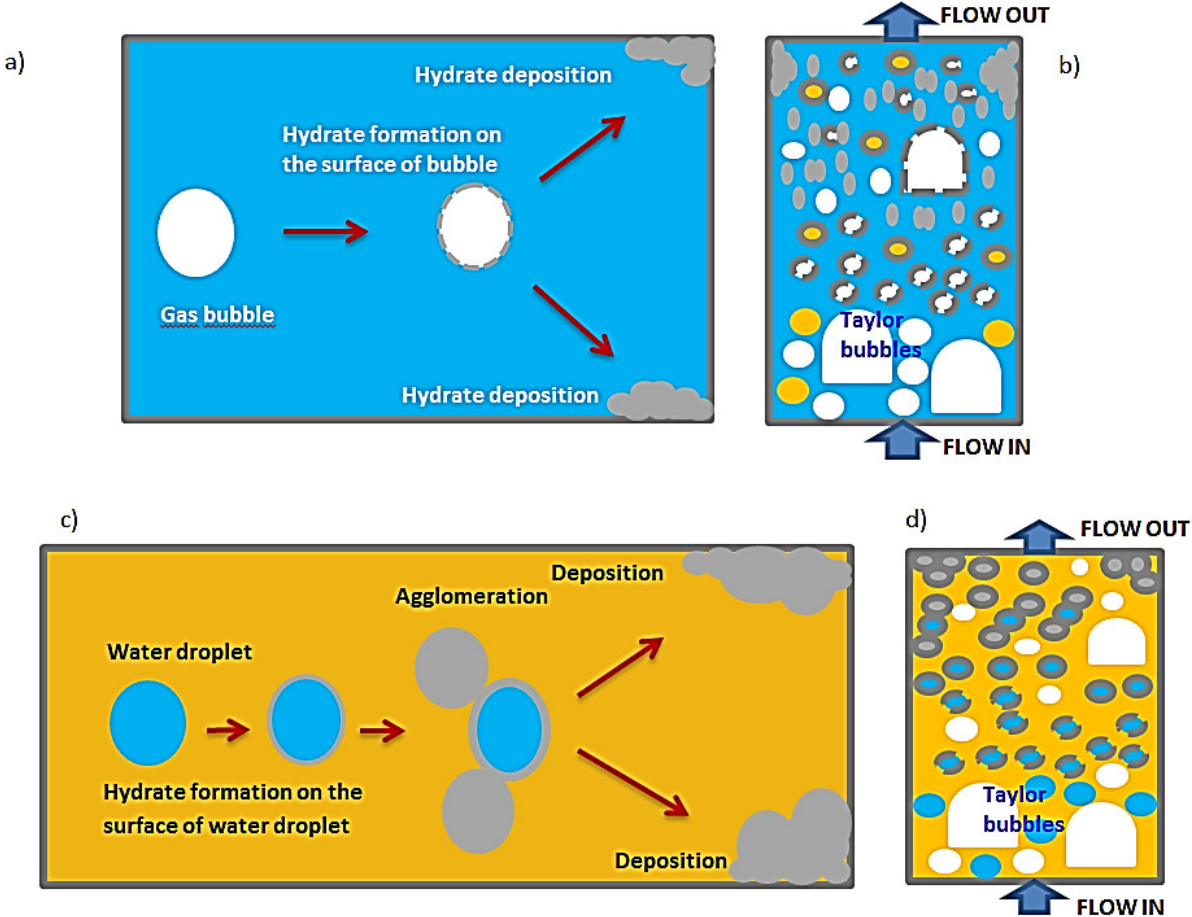


**Figure 3. 16: Conceptual models for hydrate formation and plugging in the gas-lift riser and separator without AA-LDHI: (a, b) in high water cut systems and (c, d) in low water cut systems.**

In low and high water cut systems, it is supposed that the size of gas bubbles decreased from bottom to the top of the riser. In high water cut systems, hydrates formed on the surface of gas

bubbles. Possibly, these hydrate-covered bubbles were not stable. They were also broken easily into hydrate particles and created new smaller gas bubbles. This is due to a certain amount of gas consumed to hydrate formation leading to smaller gas bubbles. In low water cut systems, gas bubbles improved gas transfer into liquid. Moreover, gas bubbles size decreased gradually as gas dissolved into the oil continuous phase.

In addition, a mechanism was proposed for low water cut systems with AA-LDHI which helped to prevent agglomeration and plugging (Figure 3. 17). It is assumed that thanks to AA-LDHI, water droplets are dispersed better in the oil continuous phase. And once hydrate formed, AA-LDHI adsorbed readily on the surface of hydrate particles forming the oil-wet surface of hydrate particles. This prevented hydrate agglomeration and plugging by dispersing hydrate particles, as discussed in section 3.4.2.

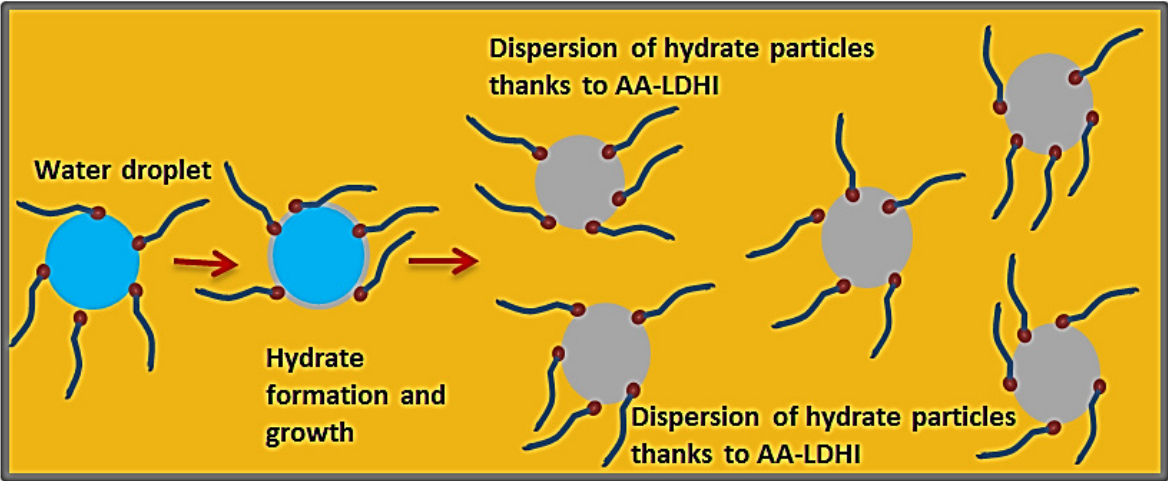


Figure 3. 17: Conceptual models for hydrate formation and plugging in the experiment with 30%WC-0.01%AA-LDHI.

### 3.7. Highlights and Conclusions

From experimental results with gas-lift protocol, several important findings can be drawn as follows:

Dispersion of oil and water in low and high water cut systems with/without salt and AA-LDHI were studied. The results showed that the addition of AA-LDHI increased the total chord counts of dispersion and stabilized dispersion but decreased mean droplet size of dispersion. Besides, the presence of salt decreased the total chord counts of dispersion and destabilized dispersion. Addition of AA-LDHI (in the presence of salt) stabilized dispersion in low water cut systems and destabilized dispersion in high water cut systems. The total numbers of chord length decreased with the increase in water fraction (in the presence of AA-LDHI) and decreased with the decrease in water fraction (in the presence of salt). Generally, the sizes of water droplets in oil continuous phase were smaller than those of oil droplets in water continuous phase.

In high water cut systems, quick hydrate blockage was observed because of the high rate of hydrate formation. This was proportional to the high gas/water (transfer rate) interface which was generated by bubbles. The low dosage of 0.01%AA-LDHI was not enough to prevent hydrate plug. In addition, a specific plug risk was identified in the separator where hydrates can accumulate. Enough dosage of oil partially contributed to hydrate dispersion in the presence of AA-LDHI. Combination of AA-LDHI and salt caused hydrate formation sooner. Furthermore, plug occurred at higher hydrate volume in almost experiments with both salt and AA-LDHI compared to those using salt and AA-LDHI separately.

In low water cut systems, for the experiments with salt, or AA-LDHI, or salt with AA-LDHI, a higher hydrate volume was transported than the one in high water cut systems. Plugging could be prevented by using only 0.01%AA-LDHI (without salt). Moreover, salt appeared to facilitate hydrate slurry transport. Combination of AA-LDHI and salt caused plug at a lower hydrate volume compared to using salt and AA-LDHI separately.

Mechanisms for gas hydrate formation, agglomeration, deposition and plugging in low and high water cut systems with gas-lift are proposed as follows:

- In high water cut systems, there were many bubbles in the water continuous phase, and hydrates formed on the surface of the gas bubble dispersion in the riser. It is assumed hydrate breaking from gas bubble shell and an accumulation and deposition of hydrate particles, particularly in the separator. This resulted in a quick plugging even at low hydrate fraction.

- In low water cut systems, the gas bubbles were mainly dispersed in the oil where they did not contact directly with water. However, gas bubbles enhanced the transfer of gas into the oil phase. The hydrates formed on the surface of the water droplets dispersed in the oil phase, agglomerated and deposited on the pipe wall. AA-LDHs prevented plugging (the experiment with 30%WC-0.01%AA-LDHI) thanks to well-dispersing water droplets in oil continuous phase with very small size. Once hydrate formed, hydrate particles dispersed better by absorption of AA-LDHs on the surface of hydrate particles.

### 3.8. Remarques et Conclusions (in French)

Plusieurs conclusions importantes peuvent être tirées des résultats expérimentaux avec protocole de gaz-lift :

La dispersion de l'huile et de l'eau pour des systèmes de basse à haute fraction d'eau avec/sans sel et AA-LDHI a été étudiée. Les résultats ont montré que l'addition d'AA-LDHI augmente le nombre total de longueurs de corde et stabilise la dispersion, mais elle diminue possiblement la taille moyenne des gouttelettes de la dispersion. En outre, la présence de sel diminue le nombre total de longueurs de corde et la déstabilise. L'addition d'AA-LDHI (en présence de sel) stabilise la dispersion pour des systèmes à faible fraction d'eau et déstabilise la dispersion pour des systèmes à haute fraction d'eau. Le nombre total de longueurs de corde diminue avec l'augmentation de la fraction d'eau (en présence d'AA-LDHI) et diminue avec la réduction de la fraction d'eau (en présence de sel). Généralement, les tailles des gouttelettes d'eau dans la phase continue de l'huile étaient plus petites que celles des gouttelettes d'huile dans la phase continue de l'eau.

Dans les systèmes à haute fraction d'eau, le risque élevé de blocage rapide des hydrates a été observé en raison du taux élevé de formation d'hydrates, proportionnel à l'interface gaz/eau (taux de transfert) élevé généré par les bulles. La faible dose de 0.01% d'AA-LDHI n'était pas suffisante pour empêcher le bouchage. De plus, nous avons identifié un risque spécifique dans le séparateur où les hydrates peuvent s'accumuler. Un dosage suffisant d'huile a partiellement contribué à la dispersion des hydrates en présence d'AA-LDHI. La combinaison d'AA-LDHI et de sel a provoqué la formation d'hydrates plus tôt et le bouchage est survenu à un volume d'hydrate plus élevé dans presque toutes expériences par rapport à celles qui utilisent de sel et d'AA-LDHI séparément.

Dans les systèmes à faible fraction d'eau, pour les expériences utilisant du sel et de l'AA-LDHI séparément ou tous les deux à la fois, un volume d'hydrate plus élevé a été maintenu en écoulement par rapport à celui des systèmes à haute fraction d'eau. Le colmatage pourrait être évité en utilisant seulement 0.01% d'AA-LDHI (sans sel). En outre, le sel est apparu pour aider à mieux hydrater le transport de la suspension. La combinaison d'AA-LDHI et de sel a causé un bouchage à un volume d'hydrate inférieur par rapport à l'utilisation de sel et d'AA-LDHI séparément.

Des mécanismes pour la formation, l'agglomération, le dépôt et le colmatage des hydrates de gaz dans les systèmes de basse et à haute fraction d'eau avec gaz-lift ont été proposés :

- Dans les systèmes à haute fraction d'eau, nous avons beaucoup de bulles dans la phase continue de l'eau, et des hydrates se formaient à la surface des bulles de gaz dans le gaz-lift. Nous suspectons que la coquille d'hydrate autour de la bulle de gaz s'est rompue et

qu'il y a eu une accumulation et un dépôt de particules d'hydrate en particulier dans le séparateur. Cela s'est traduit par un colmatage rapide, même avec une faible fraction d'hydrate.

- Dans les systèmes à faible fraction d'eau, les bulles de gaz étaient principalement dispersées dans l'huile où elles n'étaient pas en contact direct avec l'eau, mais les bulles de gaz agissaient en améliorant le transfert du gaz dans la phase huileuse. Les hydrates formés à la surface des gouttelettes d'eau se dispersent dans la phase huileuse, s'agglomèrent et se déposent sur la paroi de conduite. Les AA-LDHI ont permis d'éviter le colmatage (expérience de 30%WC-0.01%AA-LDHI) grâce à des gouttelettes d'eau de très petite taille bien dispersées en phase continue huileuse et aussi grâce aux particules d'hydrates bien dispersées une fois hydratées par absorption des AA-LDHI sur la surface des particules d'hydrate.

## CHAPTER 4. EXPERIMENTAL RESULTS WITH A MOINEAU PUMP WITH AND WITHOUT GAS-LIFT IN THE RISER

*Science is organized knowledge. Wisdom is organized life.*

*Immanuel Kant*

This chapter will focus on the results and discussion of the experiments with the Moineau pump with/without the gas-lift system. As described in Chapter 3, in the gas-lift system, the flow is induced through a “gas-lift” system without a volumetric pump. The aim of this chapter is to understand deeper hydrate crystallization and slurry transportability in the flowloop with and without AA-LDHIs and/or salt in high water cut systems with a Moineau pump. Moreover, the experimental results obtained in this chapter will clarify and confirm some interesting hydrate transport phenomena discussed in Chapter 3. As discussed in Chapter 3, the quick plug was encountered once hydrate formed in high water cut systems when using only the gas-lift system. Conversely, using only a Moineau pump with 100 vol.% liquid volume (LV), little hydrate formed due to less gas-liquid contact surface in the separator. Therefore, to increase the amount of hydrate formed to better understand hydrate transport phenomena and the role of AA-LDHI in preventing plug in pipelines, the liquid volume was decreased from 100 to 85 vol.%. Occasionally, both the gas-lift system and Moineau pump were employed.

The experiments with this present protocol were performed in the “Archimède” 80 bar - flowloop equipped with FBRM (Focused Beam Reflectance Measurement) and PVM (Particle Video Microscope) probes and sensors of temperature, pressure, pressure drop, flowrate, and density, etc. In this work, before crystallization study, rheology of water-oil dispersion (with and without AA-LDHI and/or salt) and gas transfer (into liquid) rate have been studied. Afterwards, effects of various parameters on methane hydrate formation and transport in a dispersion mixture of oil (Kerdane®) and water have been investigated, including velocity, water cut, amount of commercial anti-agglomerant low dosage hydrate inhibitor (AA-LDHI), water salinity, and pressure. The stability of hydrate slurry has been also studied by using SDR tests in the presence of AA-LDHI.

### 4.1. Experimental tests

A total of 45 experiments (including repeated ones) were performed in this study with a Moineau pump with and without gas-lift (ballasts) system with different water volume fractions with and without AA-LDHI and/or salt from low ( $150\text{L}\cdot\text{h}^{-1}$ ) to high flowrate ( $400\text{L}\cdot\text{h}^{-1}$ ). All experiments were carried out at a pressure of 75 bar (only several experiments were performed at 50-60-66-70-80 bar,

as remarked in Table 4. 1), and temperature of  $4.5\pm 0.5^{\circ}\text{C}$ . All experimental tests are summarized below in Table 4. 1.

**Table 4. 1: Experimental conditions and results with the Moineau pump (with and without gas-lift system).**

WC	Flowrate	Liquid Volume	Pressure	AA-LDHI	NaCl	Water Conversion	HV	Induction Time	PLUG
(%)	( $\text{L}\cdot\text{h}^{-1}$ )	(%)	(bar)	(wt.% of water)	( $\text{g}\cdot\text{L}^{-1}(\text{H}_2\text{O})$ )	(%)	(%)	(min)	-
100	150	100	50-75	0	0 GL(0.5')**	2.49	3.11	0.50	NO
	150-400	100	60	0	0 GL(14.4')**	2.99	3.72	29.00	NO
	150	85	66	0	0 GL(3.5'; 168')**	7.00	8.65	10.70	YES
	150	85	75	0	0 GL(16.5')**	11.38	14.03	20.80	YES
	150	85	75	0.01	0	1.24	1.55	9.90	YES
	150	85	75	0.05	0	2.03	2.54	2.90	YES
	150	90	75	0.05	0 GL(83.8')**	13.02	15.83	5.30	YES
	150	100	75	0.05	0 GL(50.7')**	1.39	1.74	9.50	NO
	150	85	75	0.5	0	12.78	15.62	4.40	YES
	400	85	75	0.5	0	22.60	26.78	0.30	YES
	150	85	75	1	0	20.10	24.02	0.08	YES
	400	85	75	1	0	18.94	22.53	1.00	NO
	150	85	75	2	0	10.50	12.79	2.90	YES
	400	85	70	2	0	22.75	26.90	0.60	NO
	400	85	75	2	0	19.48	23.33	2.10	NO
	150	85	75	0	30 GL(28.4'; 95.4')**	4.82	6.10	34.50	NO
	150rp(1)*	85	75	0	30	6.22	7.69	25.10	NO
	400	85	75	0	30	19.55	24.12	2.30	YES
	150	85	75	0.5	30	24.95	29.27	4.50	NO
	400	85	75	0.5	30	38.08	43.58	1.00	NO
150	85	75	1	30	18.19	21.89	35.20	NO	
150rp(1)*	85	75	1	30 GL (306')**	45.00	50.82	12.00	NO	
400	85	75	1	30	29.80	34.41	11.00	NO	
80	150	85	75	0	0	0.80	0.80	28.70	YES
	400	85	75	0	0 GL(262.7')**	29.00	28.26	12.60	YES

WC	Flowrate	Liquid Volume	Pressure	AA-LDHI	NaCl	Water Conversion	HV	Induction Time	PLUG
(%)	(L.h <sup>-1</sup> )	(%)	(bar)	(wt.% of water)	(g.L <sup>-1</sup> (H <sub>2</sub> O))	(%)	(%)	(min)	-
80	150	85	75	1	0	18.43	17.49	1.20	YES
	400	85	75	1	0	25.50	24.62	3.40	NO
	150	85	75	0	30	9.57	9.12	14.10	YES
	400	85	75	0	30	14.22	13.58	19.00	YES
	150	85	75	1	30 GL(355)**	36.17	33.57	2.70	NO
	400	85	75	1	30	42.05	38.20	18.00	NO
	200rp(2)*	100	80	0	0	-	-	-	-
	400rp(2)*	100	80	0	0	-	-	-	-
70	200 rp(3)*	100	80	0	0	-	-	-	-
	400 rp(7)*	100	80	0	0	6.00	5.23	28.20	NO

\*rp(x): the repeated experiments, x: number of repeats; \*\*GL(t<sub>1</sub>'; t<sub>2</sub>') : Gas-Lift, t<sub>1</sub>' and t<sub>2</sub>' are the starting time of the gas-lift system (from the beginning of the experiment: P=75 bar and flowrate=150 or 400L.h<sup>-1</sup>). It is noted that the gas-lift system can only work in several minutes together with Moineau pump (except for the experiment with 80%WC-NaCl-1%AA-LDHI-85%LV-150L.h<sup>-1</sup>, with more than 27 minutes). The gas-lift system was isolated immediately once it stopped working. Induction time is the starting time of hydrate formation from the beginning of the experiment (at P=75 or 80 bar and at flowrate=150 or 400L.h<sup>-1</sup>).

## 4.2. Dispersion and rheological study

This section will show experimental results and discuss the oil-water dispersion and rheological study before hydrate crystallization. These will help to understand better the hydrate formation and transport phenomena in pipelines.

### 4.2.1. Water-oil dispersion

This is noticed that the dispersion of oil and water with this protocol was induced by circulation with Moineau pump. The system was cooled down to 4.5±0.5°C at 1 bar. The flowrate and pressure drop were stabilized before methane injection for crystallization. The main focus of this part is to comprehend the liquid-liquid dispersion properties (homogeneity, stability, etc.) in terms of pressure drop, average chord length of dispersion droplets and the total chord counts of dispersion. It is highlighted that the preliminary understanding of liquid-liquid dispersion before crystallization is

crucial to a deeper insight into gas hydrate formation, agglomeration/deposition, and plugging in flowlines. The average chord lengths of dispersion systems (at 70-80%WC) are shown below in Table 4. 2. The results showed that in the presence of AA-LDHI, the average chord length decreased significantly because of lowering IFT between oil and water (Al-Sahhaf et al., 2005) and (Appendix E). Moreover, the addition of salt increased the average chord length of dispersion. For the experiments with 70-80%WC at 100%LV, the addition of oil lowered the average chord length of dispersion. Generally, the increase in flowrate lowered the average chord length of dispersion.

**Table 4. 2: Characteristics of dispersion systems at 4.5±0.5°C and 1 bar (before methane injection).**

WC	Flowrate	Liquid Volume	AA-LDHI	NaCl	Average Chord Length
(%)	(L.h <sup>-1</sup> )	(%)	(wt.% of water)	(g.L <sup>-1</sup> (H <sub>2</sub> O))	(µm)
80	150	85	0	0	19.60
	400	85	0	0	16.30
	150	85	1	0	10.00
	400	85	1	0	8.60
	150	85	0	30	24.80
	400	85	0	30	24.80
	150	85	1	30	13.40
	400	85	1	30	9.40
	200rp(2)*	100	0	0	17.50
	400rp(2)*	100	0	0	12.50
70	200rp(3)*	100	0	0	15.50
	400 rp(7)*	100	0	0	12.20

\*rp(x): the repeated experiments, x: number of repeats.

In agreement with Chapter 3, the experimental results (Figure 4. 1) confirmed that at low flowrate (150L.h<sup>-1</sup>), the mixture with AA-LDHI showed the highest total chord counts of dispersion due to lowering the interfacial tension between oil and water (Appendix E). On the contrary, the addition of salt caused less dispersed because of higher IFT (Cai et al., 1996).

At higher flowrate (400L.h<sup>-1</sup>) (Figure 4. 2), higher total chord counts of dispersion were observed compared to that at low flowrate. Interestingly, contrary to what happened at low flowrate, dispersion intensity of the mixture with 80%WC-NaCl-1%AA-LDHI at high flowrate (400L.h<sup>-1</sup>)

was higher than that of 80%WC with pure water. This all showed that high shear enhanced performance (distribution) of AA-LDHI by breaking dispersion into smaller droplets where AA-LDHI can adsorb better on.

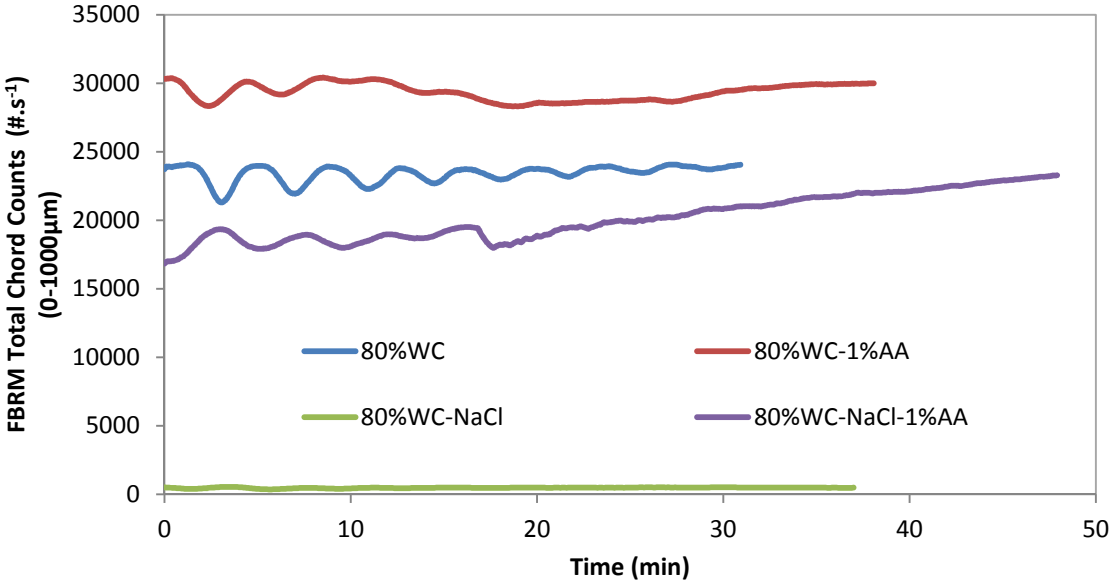


Figure 4. 1: FBRM total chord counts during the dispersion process of the experiments with 80%WC; 80%WC-1%AA-LDHI; 80%WC-NaCl; and 80%WC-NaCl-1%AA-LDHI (at 85%LV and 150L.h<sup>-1</sup>).

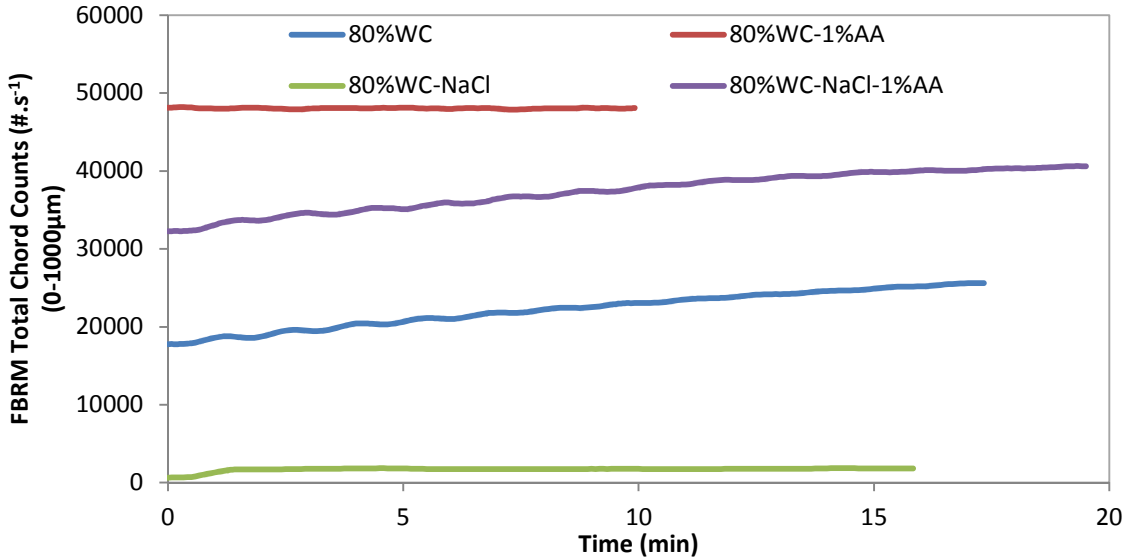


Figure 4. 2: FBRM total chord counts during the dispersion process of the experiments with 80%WC; 80%WC-1%AA-LDHI; 80%WC-NaCl; and 80%WC-NaCl-1%AA-LDHI (at 85%LV and 400L.h<sup>-1</sup>).

At 100%LV (Figure 4. 3), in agreement with 85%LV, the rise in flowrate augmented the distribution intensity. Additionally, the addition of oil increased the dispersion intensity.

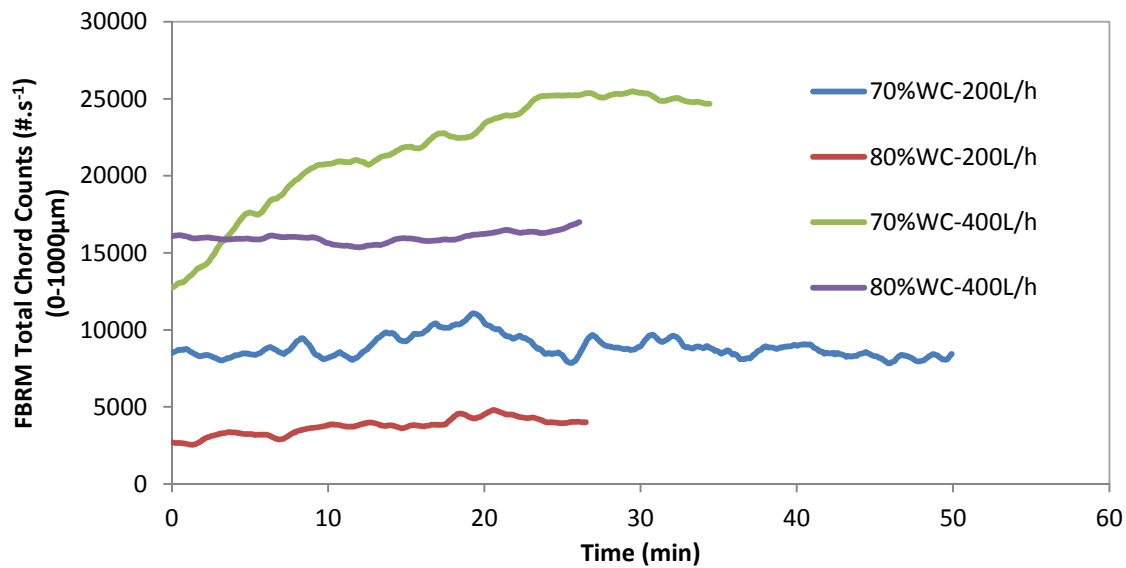


Figure 4. 3: FBRM total chord counts during the dispersion process of the experiments with 70-80%WC at 100%LV: 70%WC-200L.h<sup>-1</sup>; 80%WC-200L.h<sup>-1</sup>; 70%WC-400L.h<sup>-1</sup>; and 80%WC-400L.h<sup>-1</sup>.

#### 4.2.2. Rheological study of dispersion

The rheological study was performed at ambient temperature and 1 bar for the mixtures with 70-80%WC to study the behavior of dispersion with different flowrates (from 120L.h<sup>-1</sup> to 400L.h<sup>-1</sup>). In this section, the droplets distribution and mean droplet sizes of dispersion (average chord length) were investigated with varying fluid velocity with Moineau pump. Average chord length of dispersion droplets decreased once AA-LDHI was employed (more details in Appendix H).

#### 4.3. Hydrate formation and transport in flowlines

A typical experiment with 100%WC-0.5%AA-LDHI-85%LV-75bar-400L.h<sup>-1</sup> was depicted in Figure 4. 4, Figure 4. 5, Figure 4. 6, and Figure 4. 7. The beginning of hydrate formation can be identified by the increase in temperature, in pressure drop in the horizontal line, and in FBRM chord counts. This is also accompanied by the decrease in pressure, slight decrease in density, sharp increase in pressure drop in the separator, and PVM images. Plugging is defined as a phenomenon when flowrate falls down to zero and a considerable increase in pressure drop (in horizontal line or separator) was observed simultaneously. Gradually, hydrate flow became heterogeneous from homogeneous. Heterogeneous state of hydrate slurry was supposed to occur at 20 minutes (10%HV) after hydrate formation when the fluctuation of pressure drop was firstly observed. It is supposed that once hydrate volume reached a critical value (10%HV), hydrate particles start agglomerating and

depositing on the pipe wall. In this study, the critical value is defined as a limited value at which the state of systems is changed significantly and new phenomena occur. Additionally, when hydrates agglomerated and deposited, the pressure drop in the horizontal lines increased significantly (Figure 4. 5).

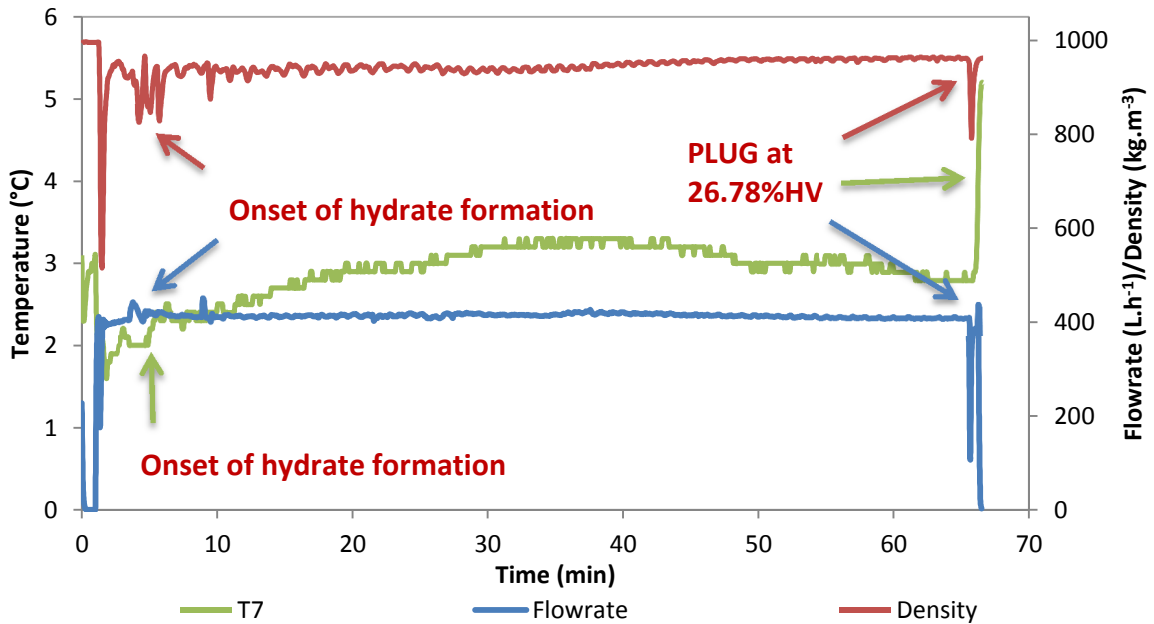


Figure 4. 4: Typical temperature (T7: temperature in the horizontal line); flowrate; and density during a crystallization experiment [100%WC-0.5%AA-LDHI-85%LV-75bar] at 400L.h<sup>-1</sup>.

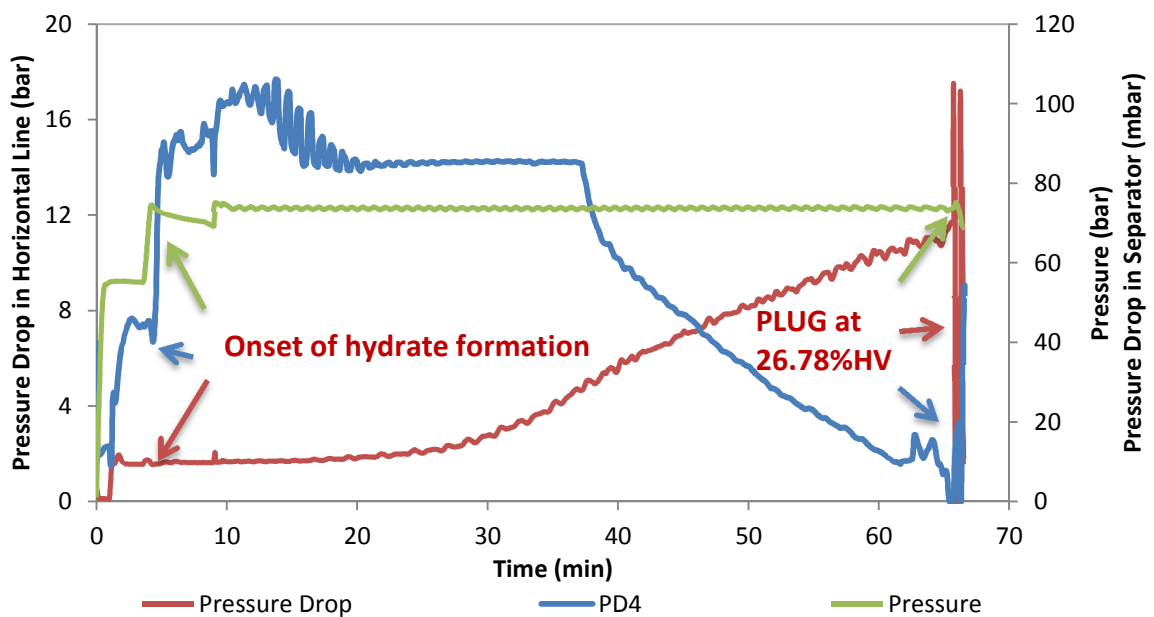


Figure 4. 5: Typical pressure drop (in the horizontal line); pressure drop in the separator (PD4); and pressure during a crystallization experiment [100%WC-0.5%AA-LDHI-85%LV-75bar] at 400L.h<sup>-1</sup>.

The increase in pressure drop in the separator can be attributed to a small amount of hydrates accumulated, deposited on the separator. At the later step of crystallization, the pressure drop in the separator decreased. This can suggest that hydrate particles which deposited in the separator possibly detached from the separator and flowed down into the horizontal line.

The small deposition could be seen at 35 minutes (17%HV). At this moment, there was a slight decrease in FBRM chord counts (Figure 4. 6) as well as an increase in density (Figure 4. 4). This will be discussed further in section Figure 4. 6. This seems that once hydrate deposited on the pipe wall in the horizontal lines, there was less hydrate coming to separator and pressure drop in the separator decreased gradually.

At the onset of plugging, a remarkable decrease in pressure (crystallization rate increased) in the flowloop was observed and a significant increase in pressure drop in the horizontal line and in FBRM chord counts along with pressure drop in the separator felt down to zero (Figure 4. 5 and Figure 4. 6). This occurred because hydrates deposited heavily on the pipe wall. Consequently, less hydrate accumulated in the separator or more free water phase presented. Additionally, the hydrate layer accumulated in the separator possibly detached and fell down to the horizontal line (PD4 decreased suddenly) which liberated again liquid-gas surface in the separator. This could improve gas transfer into the free water phase led to more hydrates formed. FBRM chord counts were increased by more hydrate formation and possibly by hydrates falling down from the separator and passing in front of FBRM probe.

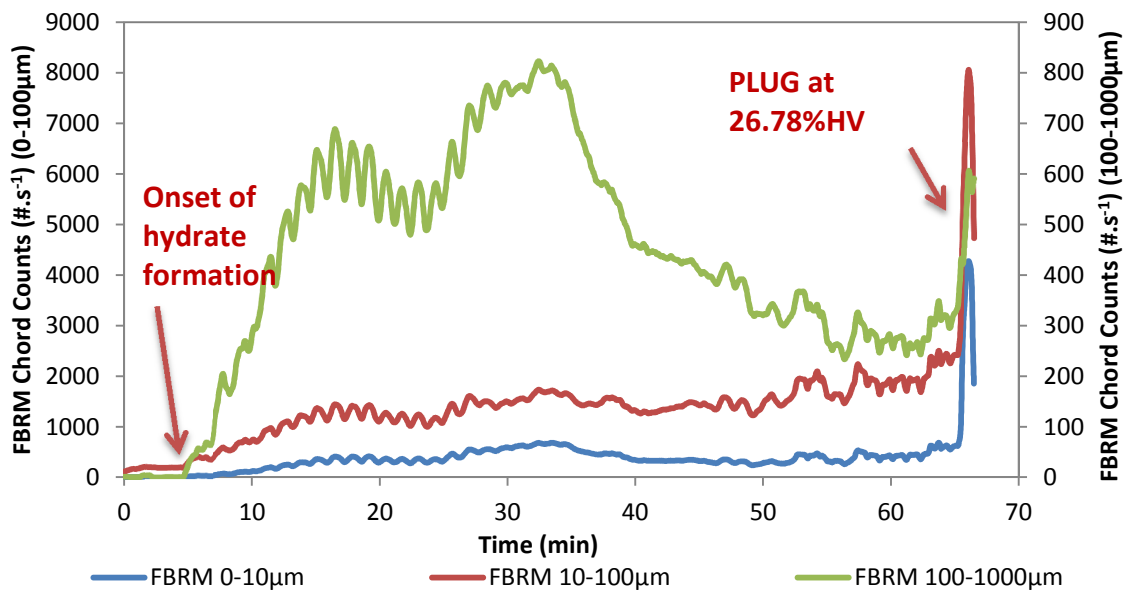
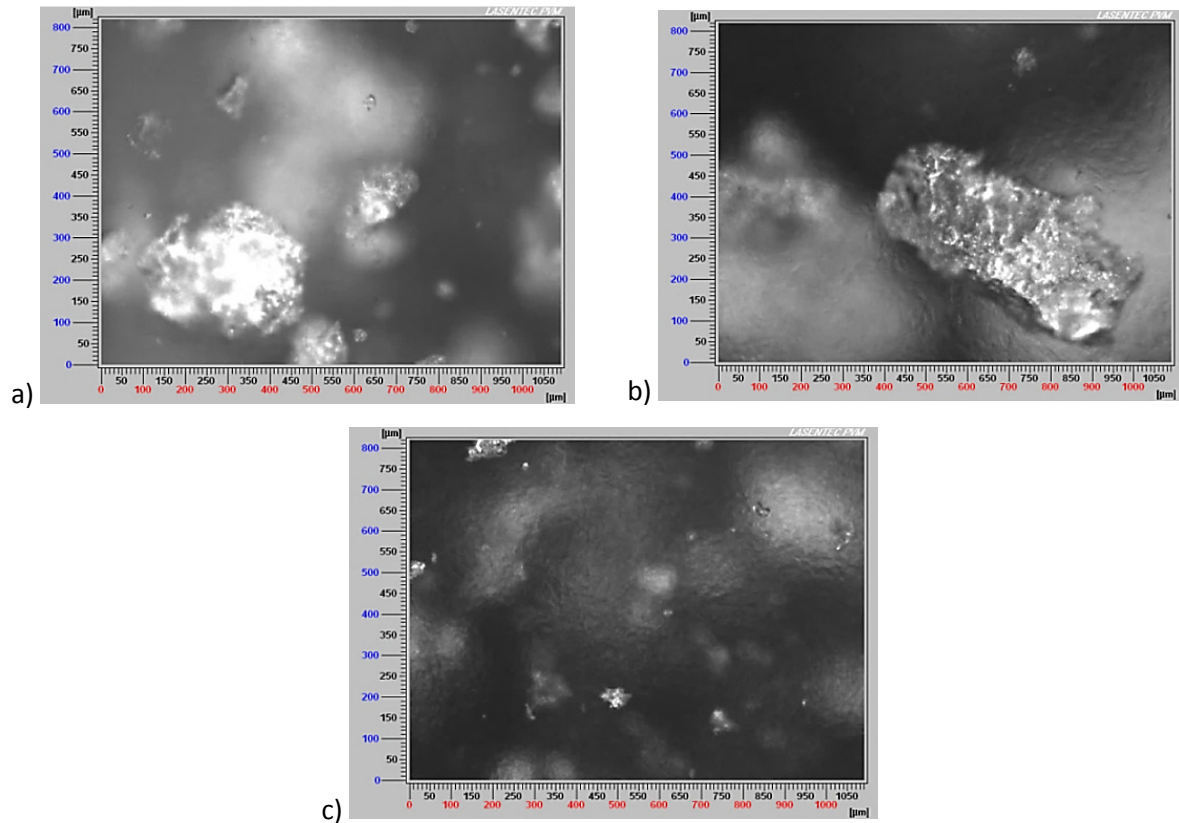


Figure 4. 6: Typical FBRM chord counts during a crystallization experiment [100%WC-0.5%AA-LDHI-85%LV-75bar] at 400L.h<sup>-1</sup>.

At the beginning of hydrate formation, there were many hydrate particles detected by PVM probe once hydrate formed (Figure 4. 7). However, at the onset of plugging, few hydrate particles in PVM images were observed. This confirmed that hydrates deposited at the end of the experiment leading to plugging.



**Figure 4. 7: PVM images of gas hydrate formation and plugging for the experiment with 100%WC-0.5% AA-LDHI at  $400\text{L}\cdot\text{h}^{-1}$  and 85%LV[(a): beginning of hydrate formation, 5.4 min; (b): during crystallization, 26.4 min; and (c): plugging, 65.4 min].**

#### 4.4. Overview of hydrate slurry transport phenomena in high water cut systems

In this study, three main types of hydrate transport phenomena were classified as follows: (1) high pressure drop in the horizontal line and stop flowing, (2) high pressure drop in the horizontal line and flowing, and (3) low pressure drop and flowing, as shown in Table 4. 3.

The induction time, driving force, and some kinetic parameters for all tests with and without additive and/or salt are shown in Table 4. 1, Table 4. 4, and Table 4. 5. Experimental results showed a low rate of crystallization at low flowrate or at high liquid volume (100 vol.%) or in presence of salt (Table 4. 5). Experiments without plug were due to a quite low hydrate volume fraction in flowlines or enough dosage of additive used (Table 4. 1). For several experiments, plug occurred quickly, even at a low hydrate volume or a low pressure drop in the horizontal line (Table 4. 1). This could be

explained by hydrate particles accumulated and deposited in the separator leading to plugging immediately. This result matched well with the experimental tests in Chapter 3 where plug occurred quickly in high water cut systems.

**Table 4. 3: Summary of hydrate slurry transport phenomena in high water cut systems.**

Pressure Drop and Flowing	Experiments	Phenomena in Hydrate Transport	Average Crystallization Rate - $\bar{R}(t)$ (%HV.min <sup>-1</sup> )	HV (%)
-	-	-	(%HV.min <sup>-1</sup> )	(%)
High pressure drop in horizontal line and stop flowing	≤0.5%AA-LDHI at 150-400L.h <sup>-1</sup> at 85-90%LV	Agglomeration and Deposition	Low-Intermediate	8.65-26.78
	1%AA-LDHI at 150L.h <sup>-1</sup>	Agglomeration and Deposition	Intermediate	17.49-24.02
	NaCl-400L.h <sup>-1</sup> and 80%WC-NaCl-150L.h <sup>-1</sup>	Agglomeration and Deposition	Low- Intermediate	9.12-24.12
High pressure drop in horizontal line and flowing	≥1%AA-LDHI at 400L.h <sup>-1</sup>	Agglomeration and Deposition	Intermediate -High	22.53-26.90
	NaCl and ≥0.5AA-LDHI at 400L.h <sup>-1</sup>	Less Agglomeration and Less Deposition	Intermediate	34.41-43.58
Low pressure drop and flowing	100%LV and ≤0.05%AA-LDHI	Agglomeration	Low	1.74-5.23
	100%WC with NaCl at 150L.h <sup>-1</sup>	Agglomeration and Deposition	Low	6.10-7.69
	NaCl and ≥0.5AA-LDHI at 150L.h <sup>-1</sup>	Less Agglomeration and Less Deposition	Intermediate	29.27-50.82

In this work (Table 4. 1), a dosage of 1% AA-LDHI was sufficient to prevent plugging at 400L.h<sup>-1</sup> without salt. However, only a dosage of 0.5% AA-LDHI was used to avoid plugging in the presence of salt at 100%WC (at both 150 and 400L.h<sup>-1</sup>). In fact, salt improved the performance of additive in preventing plug. The plug cannot be prevented at 150L.h<sup>-1</sup> up to 2%AA-LDHI without salt. It is supposed plugging occurred at low flowrate because of the low shear force to maintain flow. This conclusion agreed well with the experimental results in Chapter 3. Otherwise, the additive cannot avoid deposition. Commonly, the addition of additive increased the average crystallization rate (Table 4. 5) and shortened induction time (Table 4. 1). Indeed, the increase in crystallization rate may lead to an increase in agglomeration rate. As a result, heterogeneous hydrate slurry might occur quickly. Hence, more fluctuated signals were observed in pressure drop and FBRM chord counts.

**Table 4. 4: Driving force of the experiments with and without salt at an experimental temperature of 5°C.**

WC	Pressure	NaCl	$\Delta T = T_{eq} - T_{exp}^*$	$\Delta P = P_{exp} - P_{eq}^*$
(%)	(bar)	(g.L <sup>-1</sup> (H <sub>2</sub> O))	(°C)	(bar)
100	60	0	2.80	18
	66	0	3.70	24
	70	0	4.50	28
	75	0	4.90	33
	75	30	4.00	26
80	75	0	4.90	33
	75	30	4.00	26
	80	0	5.50	38
70	80	0	5.50	38

\*  $\Delta T$  and  $\Delta P$ : driving force;  $T_{eq}$  and  $T_{exp}$ : equilibrium and experimental temperatures;  $P_{eq}$  and  $P_{exp}$ : equilibrium and experimental pressures.

**Table 4. 5: Kinetics parameters of the experimental tests with Moineau pump and gas-lift system.**

WC	Flowrate	Liquid Volume	Pressure	AA-LDHI	NaCl	$\bar{R}(t)$	$R(t)^{MAX}$	DEPO.	PLUG
(%)	(L.h <sup>-1</sup> )	(%)	(bar)	(wt.% of water)	(g.L <sup>-1</sup> (H <sub>2</sub> O))	(%HV.min <sup>-1</sup> )	(%HV.min <sup>-1</sup> )	-	-
100	150	100	50-75	0	0	0.02	0.71	NO	NO
	150-400	100	60	0	0	0.03	0.40	NO	NO
	150	85	66	0	0	0.05	0.22	NO	YES
	150	85	75	0	0	0.18	0.70	NO	YES
	150	85	75	0.01	0	0.12	0.22	YES	YES
	150	85	75	0.05	0	0.07	0.20	YES	YES
	150	90	75	0.05	0	0.05	0.45	YES	YES
	150	100	75	0.05	0	0.03	0.25	YES	NO
	150	85	75	0.50	0	0.27	0.75	YES	YES
	400	85	75	0.50	0	0.43	1.38	YES	YES
	150	85	75	1	0	0.47	1.50	YES	YES
	400	85	75	1	0	0.81	1.15	YES	NO
	150	85	75	2	0	0.44	0.72	YES	YES
	400	85	70	2	0	0.35	1.48	YES	NO
	400	85	75	2	0	0.53	1.10	YES	NO

WC	Flowrate	Liquid Volume	Pressure	AA-LDHI	NaCl	$\bar{R}(t)$	$R(t)^{MAX}$	DEPO.	PLUG
(%)	(L.h <sup>-1</sup> )	(%)	(bar)	(wt.% of water)	(g.L <sup>-1</sup> (H <sub>2</sub> O))	(%HV.min <sup>-1</sup> )	(%HV.min <sup>-1</sup> )	-	-
100	150	85	75	0	30	0.04	0.33	YES	NO
	150rp(1)*	85	75	0	30	0.03	0.15	YES	NO
	400	85	75	0	30	0.08	0.39	YES	YES
	150	85	75	0.50	30	0.20	0.54	YES	NO
	400	85	75	0.50	30	0.35	0.71	NO	NO
	150	85	75	1	30	0.16	0.31	YES	NO
	150rp(1)*	85	75	1	30	0.16	0.37	YES	NO
	400	85	75	1	30	0.35	0.71	NO	NO
80	150	85	75	0	0	-	-	YES	YES
	400	85	75	0	0	0.11	0.90	NO	YES
	150	85	75	1	0	0.55	1.17	YES	YES
	400	85	75	1	0	0.72	0.89	YES	NO
	150	85	75	0	30	0.15	0.37	NO	YES
	400	85	75	0	30	0.32	0.71	NO	YES
	150	85	75	1	30	0.10	0.79	YES	NO
	400	85	75	1	30	0.18	0.45	YES	NO
	200rp(2)*	100	80	0	0	-	-	-	-
	400rp(2)*	100	80	0	0	-	-	-	-
70	200rp(3)*	100	80	0	0	-	-	-	-
	400rp(7)*	100	80	0	0	0.02	0.09	NO	NO

\*rp(x): the repeated experiments, x: number of repeats.

#### 4.5. Quick and slow (agglomeration and deposition) heterogeneity of hydrate slurry flow

The experimental results revealed that AA-LDHI prevented plugging at a dosage of 1 wt.% at 400L.h<sup>-1</sup>. However, AA-LDHI did not prevent hydrate deposition. It is supposed that once hydrates formed, hydrate slurry could become immediately heterogeneous (this is named as “quick heterogeneity of hydrate slurry”) and they might deposit on the pipe wall. This phenomenon was proved by the evidence from the following measurements: FBRM chord counts, pressure drop (in the horizontal lines of the flowloop), density and temperature. All data supported this phenomenon are shown in Figure 4. 8, Figure 4. 9, and Figure 4. 10. At the beginning of hydrate formation, hydrate slurry flow became quickly heterogeneous (fluctuation of all parameters was observed: FBRM chord counts, pressure drops, flowrate, density, and temperature). Besides, it is observed that FBRM chord counts increased after hydrate formation and this was the reason for both hydrate growth process and newly formed hydrate particles (Figure 4. 8). After a certain period of time (at 15%HV), FBRM chord counts started decreasing. This proved that hydrates started agglomerating and depositing on

the pipe wall. This was also verified by an increase in pressure drop and density measurements (density of hydrate is less than that of pure water) (Figure 4. 9 and Figure 4. 10). All parameters at this moment were less fluctuated due to less heterogeneous hydrate slurry in multiphase-flow by means of deposition.

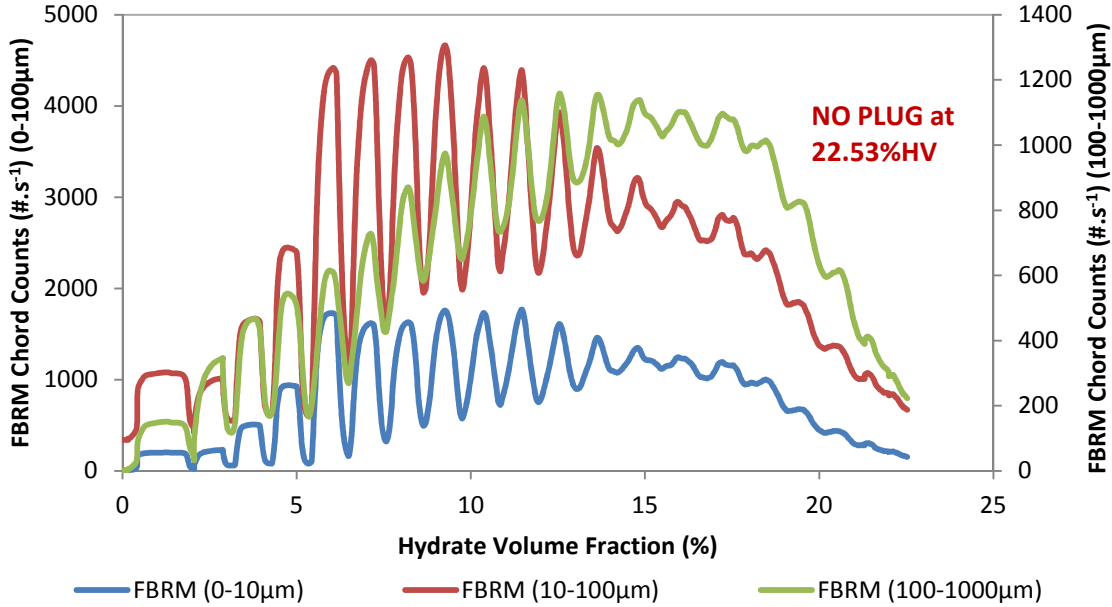


Figure 4. 8: FBRM chord counts as a function of hydrate volume in the experiment with 100%WC-1%AA-LDHI-85%LV-400L.h<sup>-1</sup>-75bar.

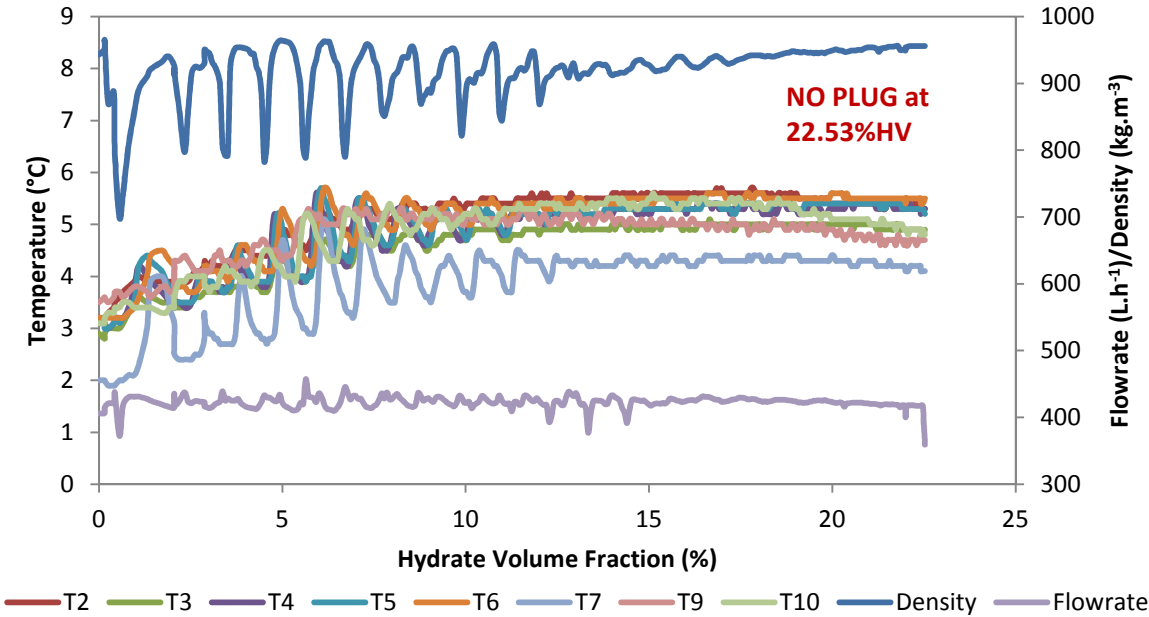
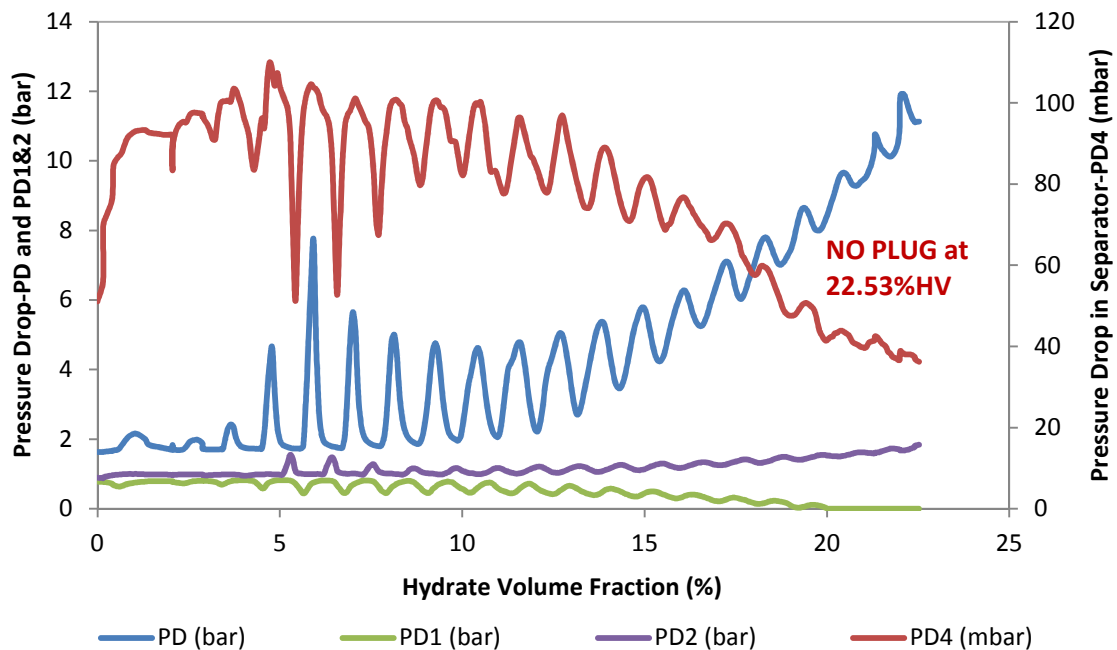


Figure 4. 9: Temperature; flowrate; and density as a function of hydrate volume in the experiment with 100%WC-1%AA-LDHI-85%LV-400L.h<sup>-1</sup>-75bar.

The fluctuations were observed in many signals (temperature, pressure drops, flowrate, density, FBRM chord counts, etc.). This could be an evidence of a heterogeneous flow: a flow with a section with a high concentration of agglomerates as well as a section with a low concentration of hydrate particles. In this case, the heterogeneity appeared immediately. This phenomenon is named as “quick heterogeneity of hydrate slurry flow”.



**Figure 4. 10: Pressure drops in the flowloop as a function of hydrate volume in the experiment with 100%WC-1%AA-LDHI-85%LV-400L.h<sup>-1</sup>-75bar.**

The other experimental results confirmed again that hydrates formed, grew, agglomerated and deposited during crystallization but in a different way (less and slower heterogeneous hydrate slurry flow formed) from the quick heterogeneity of hydrate slurry flow (Figure 4. 11). When hydrates formed and grew, an increase in FBRM chord counts, pressure drop and a decrease in density (density of hydrate is lower than that of pure water) were observed. Once hydrate volume reached a critical value (approximately, 12%HV in this case), hydrate flow became heterogeneous due to agglomeration and hydrate particles started to deposit on the pipe wall. Agglomeration, heterogeneity of hydrate slurry flow, and hydrate deposition occurred almost simultaneously. This is due to the fluctuation and decrease in FBRM chord counts, also the fluctuation and increase in pressure drop in horizontal lines and arise of density (fewer hydrate particles in the fluid phase) occurred at the nearly same time. In addition, once hydrates deposited, less fluctuated pressure drop was observed during a certain time (up to 18%HV). However, at the end (closed to plugging time), the pressure drop in horizontal line was more fluctuated and sharply increased and also FBRM chord

counts increased (more hydrate formed possibly by liberating separator from hydrate particles accumulated). It is supposed that hydrate slurry flow was more heterogeneous because some large agglomerates formed in liquid flow or detached from the pipe wall. In this case study, the heterogeneity required longer time, as well as a higher hydrate volume (10%HV) compared to the quick heterogeneity (less than 5%HV). This is named as “slow heterogeneity of hydrate slurry flow”. It is supposed that in all cases, hydrates may accumulate and deposit somewhere in the flowloop as separator (partially), pipelines (mainly), purges, dead space, etc.

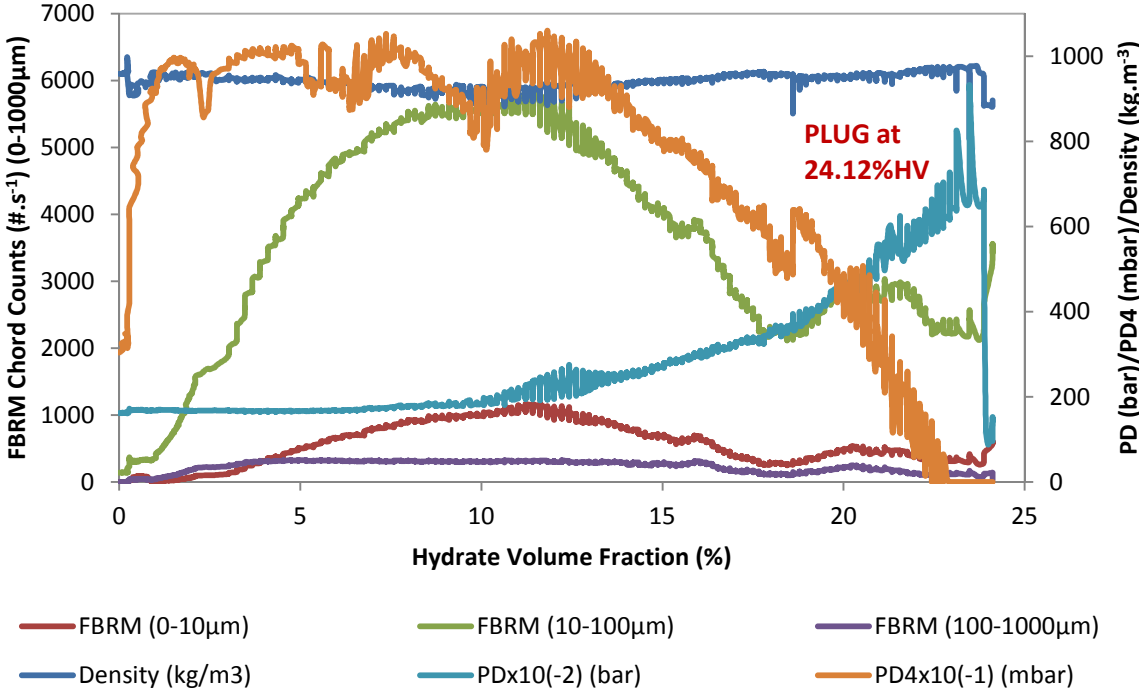


Figure 4. 11: FBRM chord counts; pressure drops; and density as a function of hydrate volume in the experiment with 100%WC-NaCl-85%LV-400L.h<sup>-1</sup>-75bar.

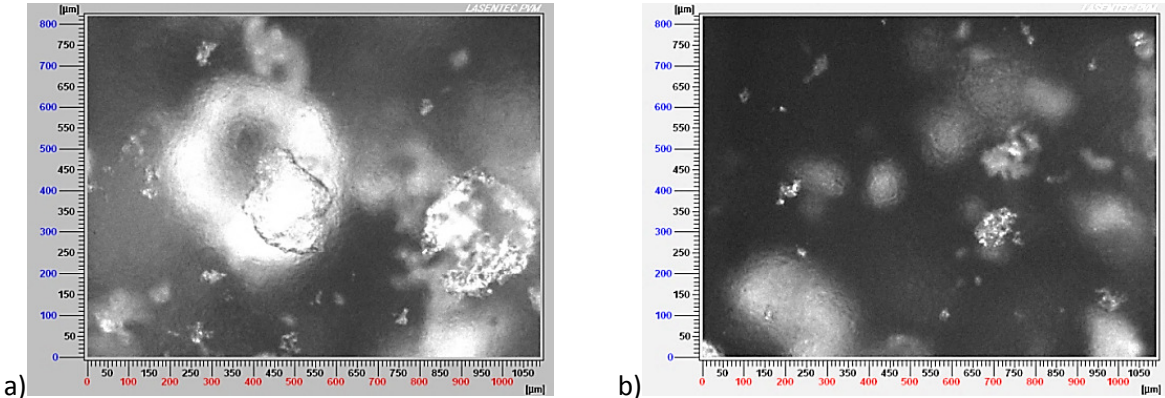


Figure 4. 12: PVM images of gas hydrate formation (before and after deposition) for the experiment with 100%WC-1% AA-LDHI at 400L.h<sup>-1</sup> and 85%LV[(a): before hydrate deposition and (b): after hydrate deposition].

From PVM images (Figure 4. 12 and Figure 4. 13), fewer hydrate particles were detected by PVM probe when hydrates deposited on the pipe wall. Normally, when hydrates formed, the color of fluid became brighter and the morphology of hydrate particles can be obviously observed. Once hydrate particles started to deposit, the environment color gradually became darker like the environment before gas hydrate formation. This was in agreement with FBRM chord counts.

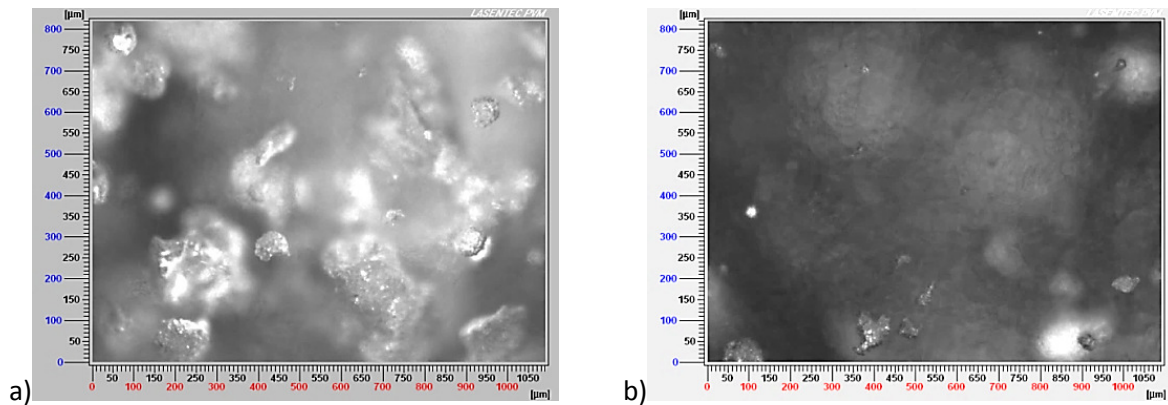


Figure 4. 13: PVM images of gas hydrate formation (before and after deposition) for the experiment with 100%WC-NaCl at  $400\text{L}\cdot\text{h}^{-1}$  and 85%LV [(a): before hydrate deposition and (b): after hydrate deposition].

#### 4.6. Effect of gas hydrate formation on flowing

Once hydrate formed (in the experiment with 80%WC-NaCl), flowing became less stable and was much fluctuated. Herein, it is supposed that hydrate slurry flow became heterogeneous quickly once hydrate formed based on the fluctuation in pressure drop and flowrate (Figure 4. 14).

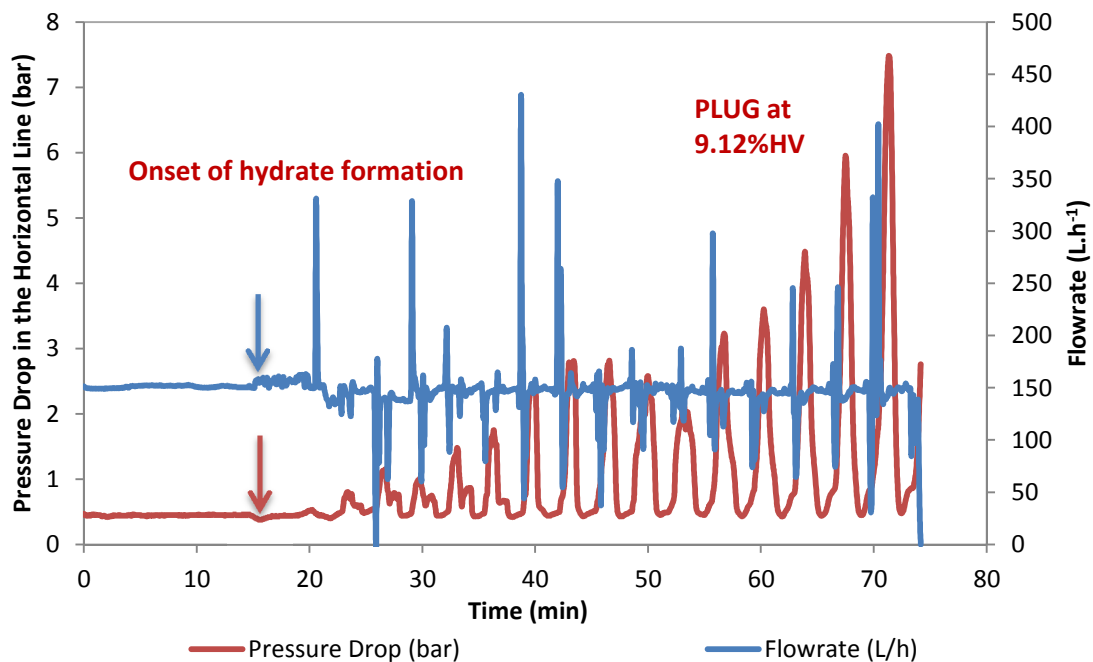


Figure 4. 14: Flowrate and pressure drop of the experiment with 80%WC-NaCl-85%LV- $150\text{L}\cdot\text{h}^{-1}$ -75bar.

The role of commercial additives was investigated once a dosage of 1%AA-LDHI was added into the experiment with 80%WC-NaCl. In Figure 4. 15, the stability of flowrate and pressure drop was observed after approximately one hour when hydrate formed.

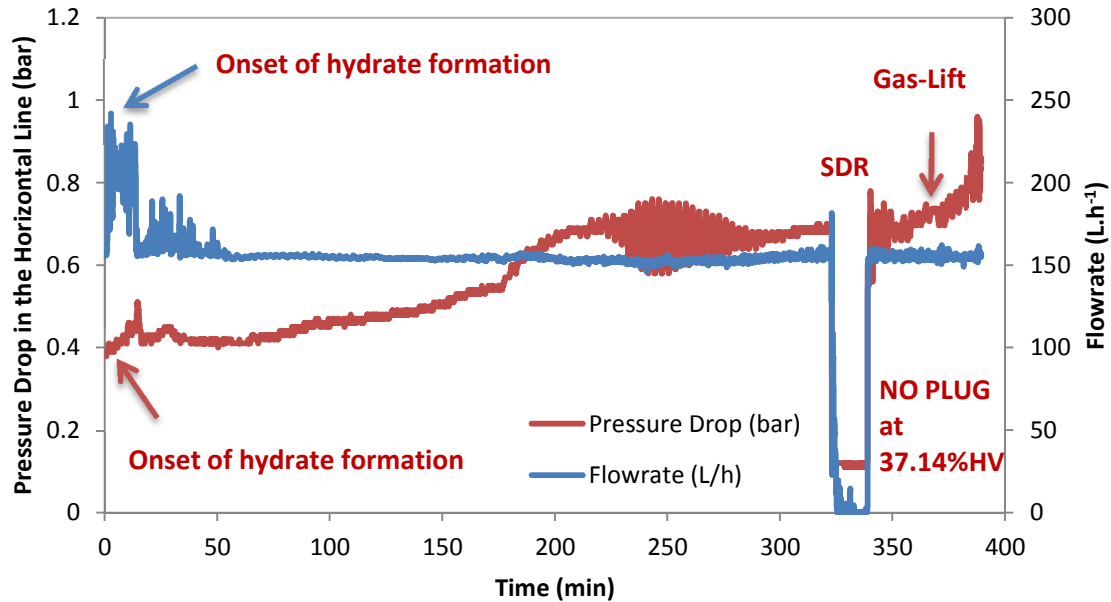


Figure 4. 15: Flowrate and pressure drop of the experiment with 80%WC-NaCl-1%AA-LDHI-85%LV-150L.h<sup>-1</sup>-75bar.

#### 4.7. Effect of hydrate formation on the stability of liquid-liquid dispersion

Figure 4. 16 shows that once hydrate formed, the density and pressure drop increased but FBRM chord counts decreased and increased immediately. The increase in pressure drop was interpreted by an increase in hydrate slurry viscosity. Hydrate formation also decreased dispersion creating less number of the chord length. As a result, a decrease in FBRM chord counts was observed. Afterwards, FBRM chord counts increased immediately because of gas hydrate particles continued to form. Surprisingly, the density of the slurry increased immediately. This was explained by the breaking of oil-water dispersion into oil-water stratified flow which impacted on density measurement (the explanation is shown in section 4.2). However, it is interesting to note that the pressure drop and FBRM chord counts decreased only several minutes after hydrate formation. It is supposed that hydrate formation caused liquid-liquid dispersion breaking (less dispersed) and hydrate deposition led to decreasing viscosity of the suspension. This was confirmed by the decrease in pressure drop and FBRM chord counts for a long period of time (up to 130 mins). Moreover, it is supposed that the decrease in pressure drop might be due to a smooth hydrate layer deposited on the pipe wall. This led to the change of roughness and properties of pipe surface (probably from the hydrophilic to hydrophobic surface or from water-wet to oil-wet hydrate layer on the pipe wall

thanks to AA-LDHI). At the end of the experiment, an increase and fluctuation of pressure drop, an increase in FBRM chord counts and the decrease in density were observed. This was because of hydrate particles detaching from the pipe wall, agglomerating, flowing and/or due to hydrate volume reached the critical value. The destabilization of water-oil dispersion was also mentioned by previous studies as Erlend O. Straume et al., (2016), A. A. Majid et al., (2016), Vijayamohan, (2015), (Yan et al., 2014) and (Peng et al., 2012).

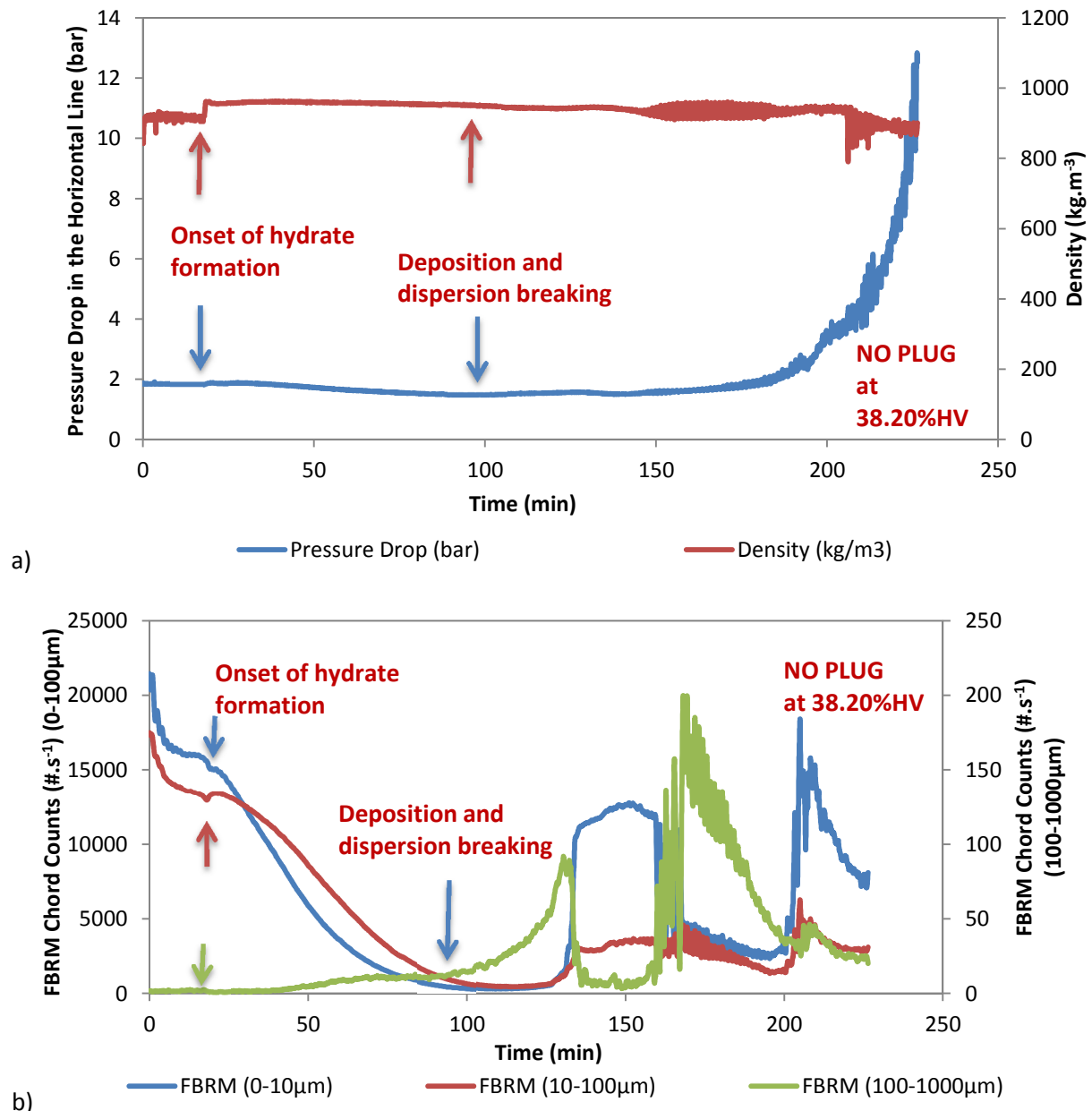


Figure 4. 16: Density-pressure drop (a) and FBRM chord counts (b) of the experiment with 80%WC-NaCl-1%AA-LDHI-85%LV-400L.h<sup>-1</sup>-75bar.

#### 4.8. Effect of velocity

The hydrate formation, agglomeration, and deposition at high flowrate were different from those at low flowrate. Figure 4. 17 clarifies that the higher flowrate, the higher average rate of hydrate formation. This was explained by better gas-liquid contact and faster gas transfer into the liquid phase at higher flowrate. Interestingly, at high flowrate, the pressure drop curve in the horizontal line was different from the one at low flowrate. Particularly, pressure drop at high flowrate increased significantly than the one at low flowrate up to plugging. It is assumed that higher shear force at higher flowrate enhanced hydrate particles dispersion. Hydrate agglomerates might be broken (or disrupted) into smaller ones in the liquid phase at higher flowrate (Mills, 1985). The gradual increase in pressure drop up to plugging at high flowrate was attributed to an increase in hydrate slurry viscosity. At low flowrate, it is hypothesized that plugging was not only because of increase in hydrate slurry (volume) viscosity but also it was due to bigger agglomerates formed and deposited. Indeed, low shearing caused more chance for hydrate particles to build up agglomerates (Mills, 1985) and/or deposit on the pipe wall. In fact, the pressure drop in the horizontal line fluctuated (heterogeneous state of hydrate flow) at 10%HV at high flowrate while it was 6%HV at low flowrate. This was also confirmed by FBRM chord counts (in Figure 4. 18) where the number of chord counts increased significantly (no or less deposition) at high flowrate and decreased (much deposition) at low flowrate after hydrate formation.

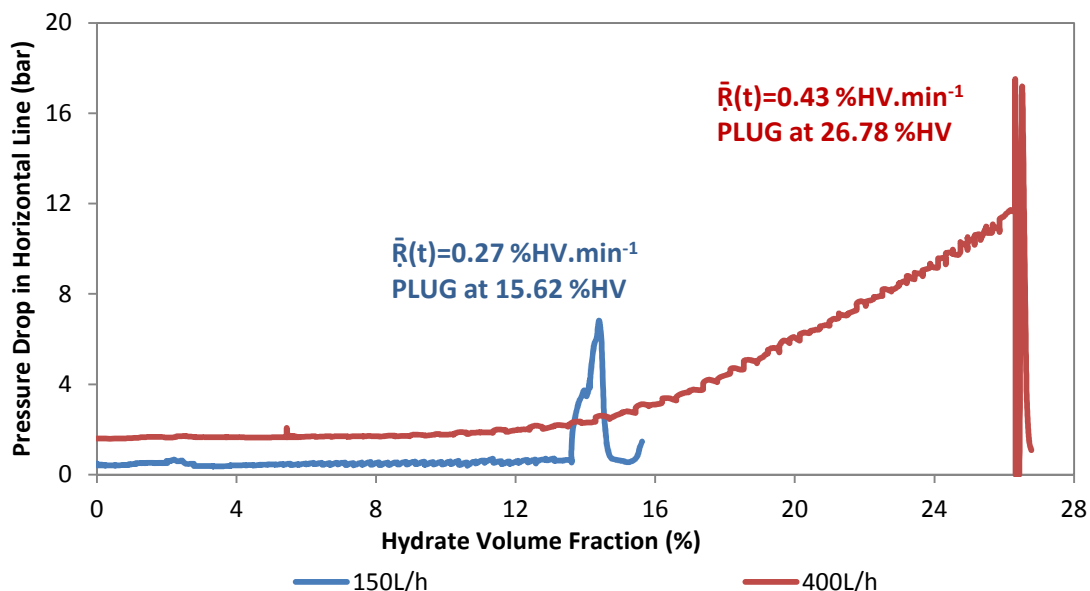


Figure 4. 17: Effect of velocity on pressure drop and average rate of crystallization [the experiments with 100%WC-0.5%AA-LDHI-85%LV-75bar at 150 and 400L.h<sup>-1</sup>].

Higher velocity transported better the hydrate slurry with higher shear force and/ or this dispersed better hydrate particles where AA-LDHI can better adsorb on (better performance of AA-LDHI at higher flowrate, as shown in section 4.2.1). In fact, the plug occurred at 26.78%HV at high flowrate compared to 15.62%HV at low flowrate.

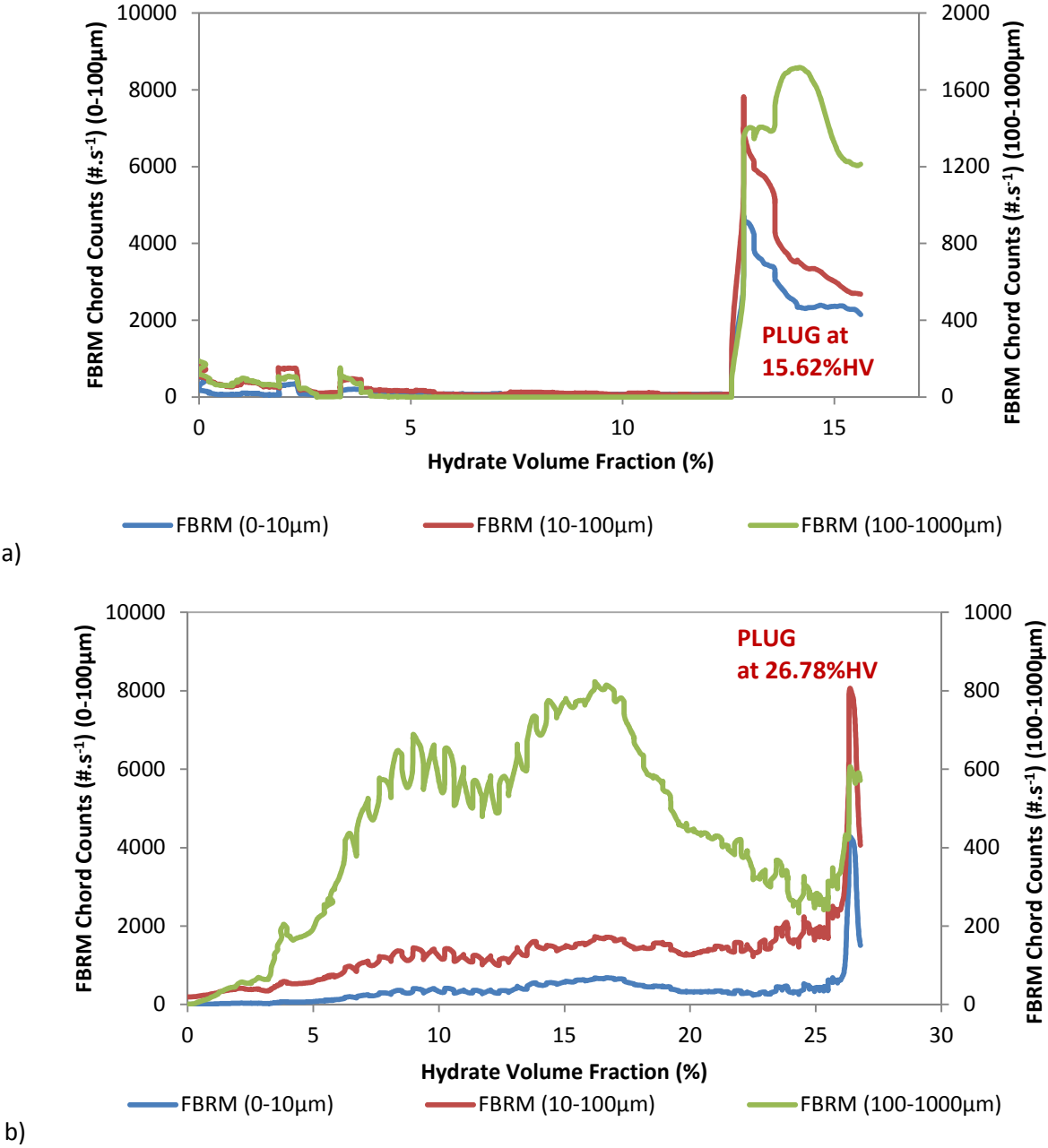


Figure 4. 18: Effect of velocity on FBRM chord counts [the experiments with 100%WC-0.5%AA-LDHI-85%LV-75bar at 150 (a) and 400 (b) L.h<sup>-1</sup>].

#### 4.9. Effect of water cut

Average crystallization rate of the experiment with 100%WC-NaCl was much lower than that at 80%WC-NaCl (Figure 4. 19). This was explained by the gas transfer rate to oil was higher than that to water. In details, in the presence of oil, gas can transfer into the water to form hydrate in two ways: by contact surface between water and oil and by gas contacts directly with water in the separator. In the opposite way, at 100%WC, gas and water contact directly in the separator.

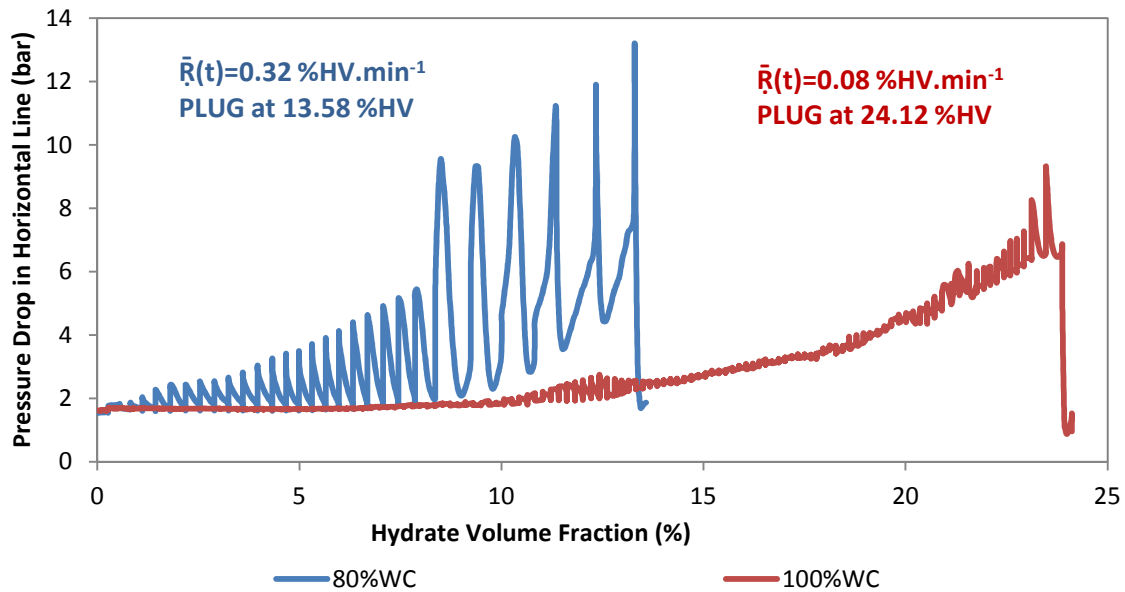


Figure 4. 19: Effect of water cut on pressure drop and average rate of crystallization [the experiments with 80 and 100%WC-NaCl-85%LV-400L.h<sup>-1</sup>-75bar].

Higher average rate of crystallization at 80%WC might lead to higher rate of agglomeration compared to that at 100%WC. As a result, bigger agglomerates formed at 80%WC compared to those at 100%WC (Figure 4. 19 and Figure 4. 20). As a result, the hydrate slurry flow at 80%WC became heterogeneous faster than that at 100%WC. Moreover, a complicated hydrate slurry flow (oil, water, and hydrate phase) might cause a higher and more fluctuated pressure drop at 80%WC than that at 100%WC. This is proven by pressure drops of experiments with 80 and 100%WC as seen in Figure 4. 19. Indeed, at the same hydrate volume, pressure drop at 80%WC was higher than that at 100%WC. This was probably due to the heterogeneous state of hydrate slurry flow at 80%WC causing a higher pressure drop. This was also confirmed by PVM images (section 4.15). This should be noted that the pressure drop not only depended on the hydrate volume but also strongly depended on the dispersion (the homogeneity, heterogeneity, and structure of hydrate agglomerates) of hydrate

particles in the flowlines. As a result, at 100%WC, hydrate can be transported with a larger hydrate volume (24.12%HV) than that at 80%WC (13.58%HV).

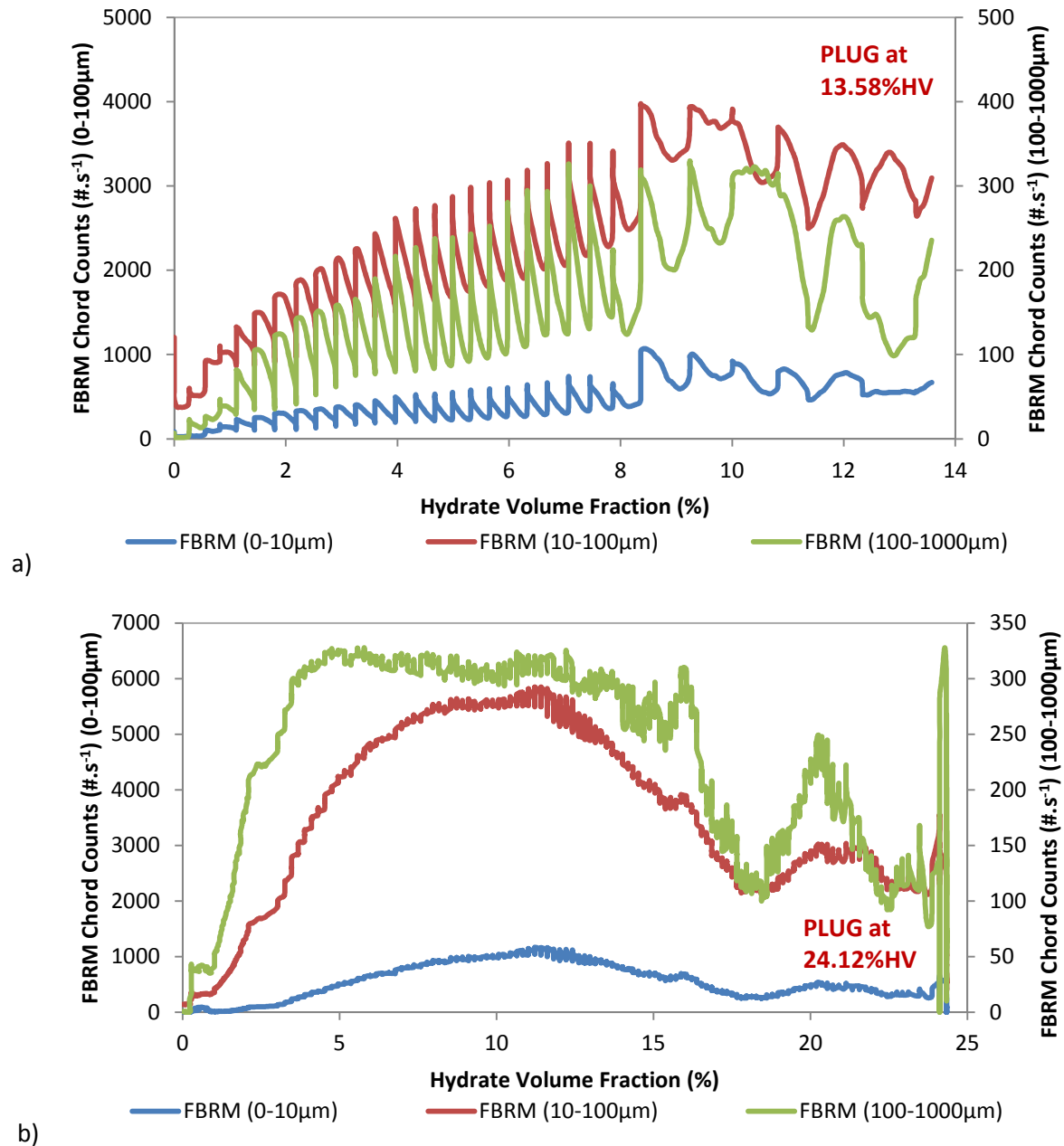


Figure 4. 20: Effect of water cut on FBRM chord counts [the experiments with 80%WC (a) and 100%WC (b)- NaCl-85%LV-400L.h<sup>-1</sup>-75bar].

#### 4.10. Effect of additive

This is obvious that addition of AA-LDHI increased average rate of crystallization (Figure 4. 21). The role of AA-LDHI to nucleate and promote hydrate formation was witnessed by reducing induction time (Table 4. 1) (Kumar et al., 2015). Herein, this is supposed that AA-LDHI could lower the

interfacial tension between gas and liquid phases leading to faster gas transfer into the liquid phase. The higher amount of AA-LDHI caused the higher average rate of crystallization (Karaaslan & Parlaktuna, 2002). However, the average crystallization rate at 2%AA-LDHI was lower than that at 2%AA-LDHI (Table 4. 5). This is possibly because the dosage of 1 wt.% was below the CMC of AA-LDHI in water but the dosage of 2%AA-LDHI exceeded the CMC value (Karaaslan & Parlaktuna, 2000); (Watanabe et al., 2005) and (J. Lee et al., 2010). This led to less AA-LDHI participated in promoting hydrate formation and/or gas transferring into liquid phase or in preventing plug (the experiment with 2%AA-LDHI was plugged at lower hydrate volume than that at 1%AA-LDHI).

The rise in the amount of AA-LDHI (up to 1%AA-LDHI) enhanced the hydrate volume transported. In addition, the presence of AA-LDHI reduced pressure drop at the same hydrate volume. It is supposed that AA-LDHI changed the hydrate agglomeration and deposition structure leading to prevent plugging.

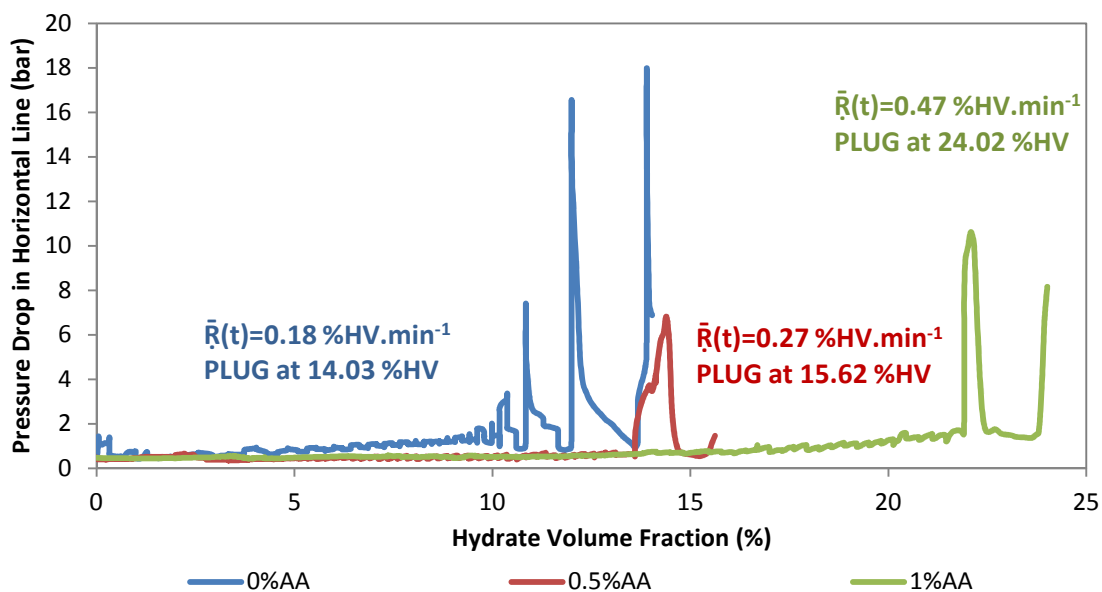
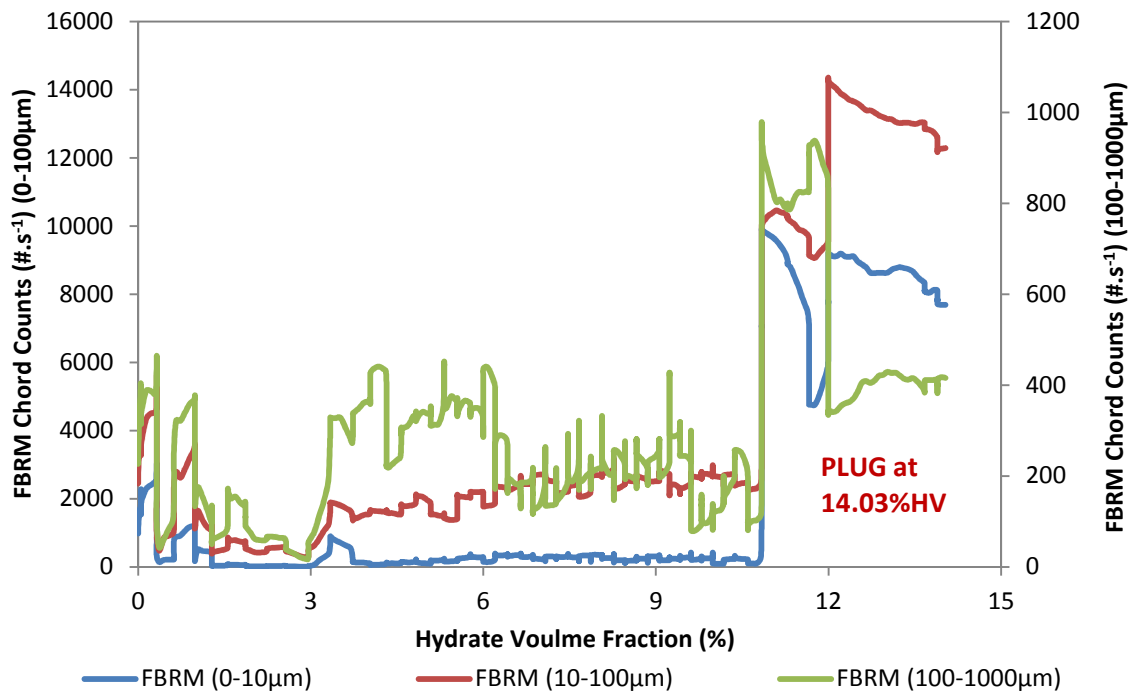
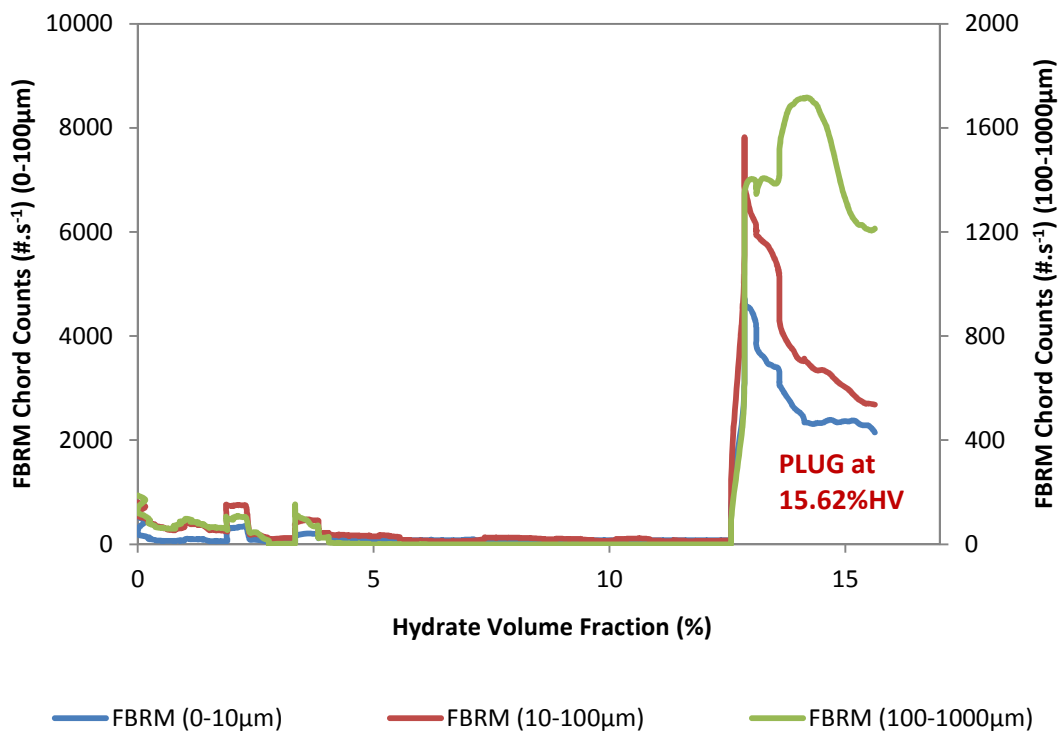


**Figure 4. 21: Effect of additive on pressure drop and average rate of crystallization [the experiments with 100%WC-0-0.5-1%AA-LDHI-85%LV-150L.h<sup>-1</sup>-75bar].**

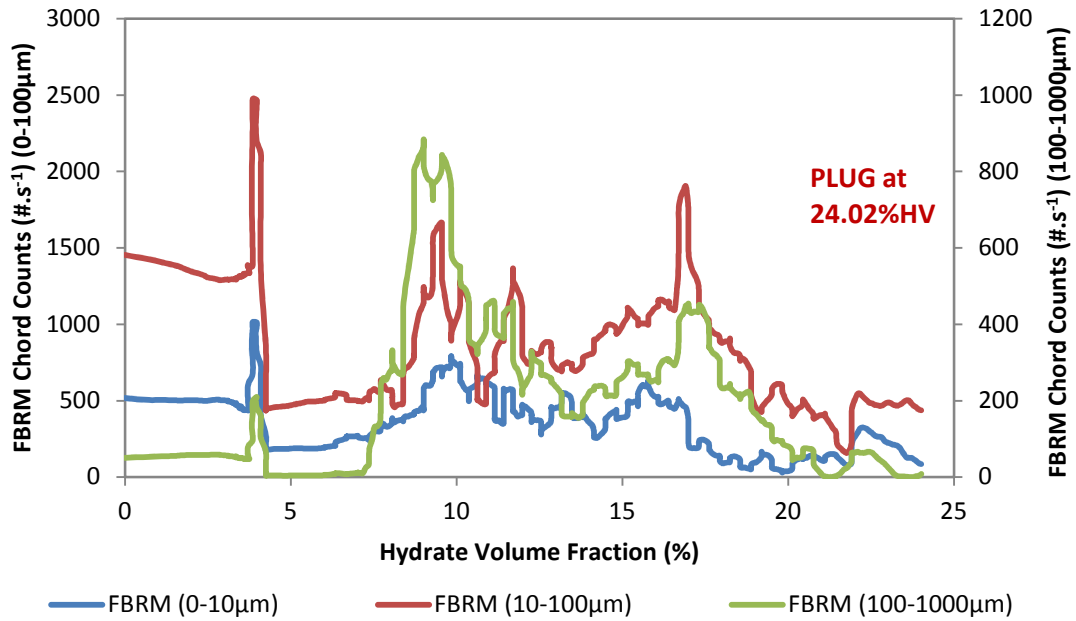
Generally, there was a deposition once AA-LDHI was added due to a decrease in FBRM chord counts (Figure 4. 22). The experiment with 100%WC-1%AA-LDHI-150L.h<sup>-1</sup> showed agglomeration and deposition while the experiment with 0.5%AA-LDHI showed only deposition (the number of chords was very few compared to the experiment with 1%AA-LDHI).



a)



b)



c)

**Figure 4. 22: Effect of additive on FBRM chord counts [the experiments with 100%WC-0 (a)-0.5 (b)-1 (c) %AA-LDHI-85%LV-150L.h<sup>-1</sup>-75bar].**

#### 4.11. Effect of salt

At 100%WC, salt inhibited gas hydrate formation with the lower average rate of crystallization (Figure 4. 23). Less hydrate formed at the experiment with 100%WC-NaCl-150L.h<sup>-1</sup> compared to that of 100%WC-150L.h<sup>-1</sup> (Figure 4. 23). This was explained by the lower driving force of the experiments with salt (Table 4. 4) and less dispersion of oil in water leading (section 4.2.2) to less contact surface between oil and water. The experiment with salt did not show plug because there was not enough hydrate volume (7.69%HV). At the same hydrate volume, the pressure drop in the experiment without salt was higher and more fluctuated than that in the experiment with salt. This is again explained by a higher average rate of hydrate formation caused a higher agglomeration rate. Consequently, more heterogeneous hydrate flow formed with bigger agglomerates.

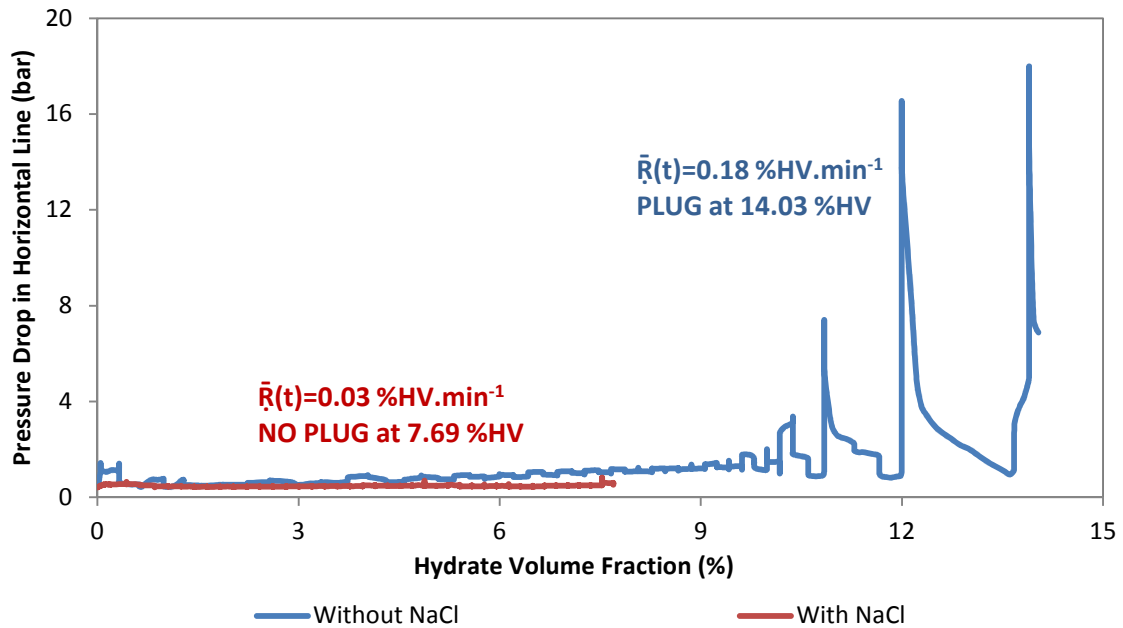
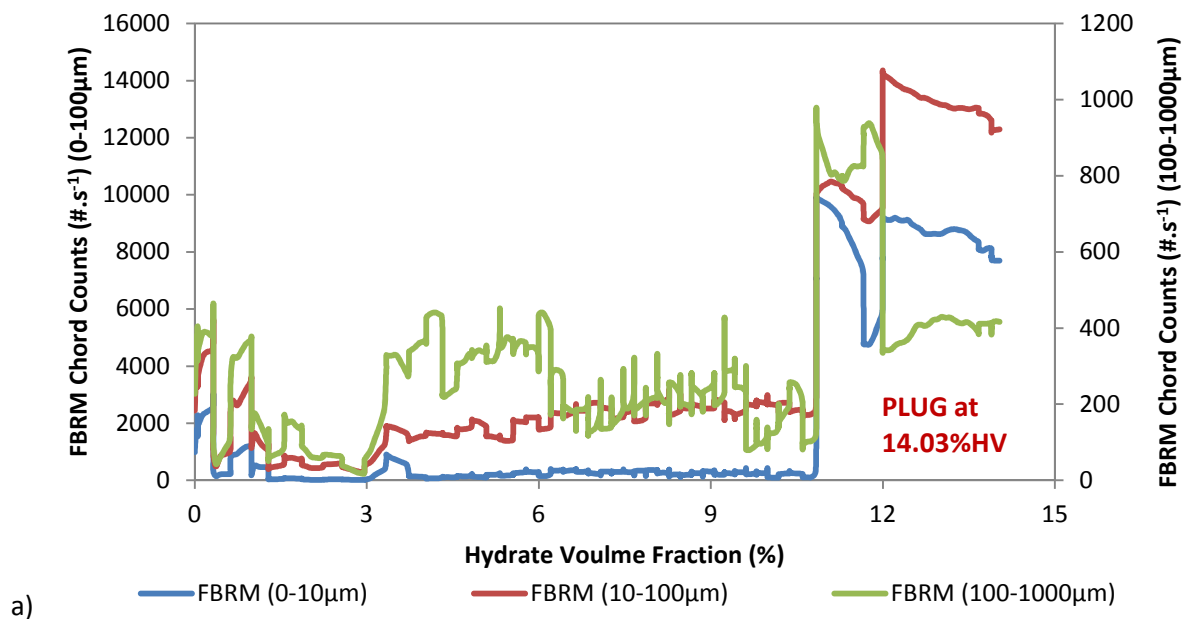
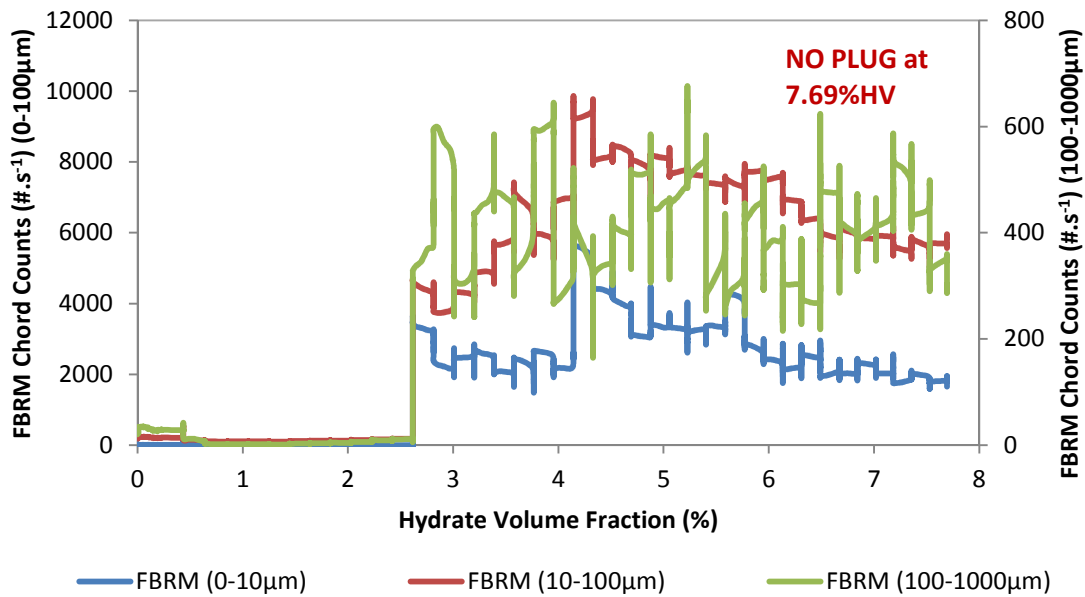


**Figure 4. 23: Effect of salt on pressure drop and average rate of crystallization [the experiments with 100%WC-85%LV-150L.h<sup>-1</sup>-75bar without and with NaCl].**

A small deposition of hydrate particles was observed for both experiments without and with salt. At hydrate volume of 11% and 2.6% for the experiment without and with salt, respectively, FBRM chord counts increased sharply (Figure 4. 24). It is supposed that hydrate which deposited on the pipe wall flowed and dispersed continuously in the flowlines.



a)



b)

**Figure 4. 24: Effect of salt on FBRM chord counts [the experiments with 100%WC-85%LV-150L.h<sup>-1</sup>-75bar without (a) and with (b) NaCl].**

#### 4.12. Effect of combination of additive and salt on hydrate transportability

The result revealed that using additive and salt separately did not prevent effectively plugging. However, in the presence of salt, a better performance of AA-LDHI was observed as mentioned in the previous studies of Moradpour (2011); A. A. Majid et al., (2014); and Dong et al., (2017). The mechanism of this positive effect of salt on the performance of AA-LDHI at 80 and 100%WC will be discussed in section 5.1.3.

##### 4.12.1. Experiments with 80%WC

A combination of salt and AA-LDHI decreased the average rate of crystallization compared to the experiments with only salt and only AA-LDHI (Figure 4. 25). This led to less heterogeneous hydrate slurry flow than that in the experiments with only salt and only AA-LDHI in terms of pressure drop and FBRM chord counts (Figure 4. 25 and Figure 4. 26). This means that heterogeneous hydrate flow occurred in these experiments (with salt and AA-LDHI separately) after hydrate formation at a quite low hydrate volume. In addition, the pressure drop in the experiment with both salt and AA-LDHI showed a lower value than that in the experiments with only AA-LDHI and only salt at the same hydrate volume. This was attributed to the lower average rate of crystallization leading to less and slower agglomeration. Moreover, a positive effect of salt on the performance of AA-LDHI was observed.

The presence of salt decreased the average crystallization rate in the presence of AA-LDHI was noticed. This is possibly due to the addition of salt decreased the oil-water dispersion (section 4.2.1) leading to the less oil-water contact surface. Furthermore, the presence of salt lowered driving force of crystallization process and/or decreased the CMC of AA-LDHIs (Noll, 1991) (led to fewer AA-LDHIs contributed to hydrate formation). Addition of AA-LDHI in the presence of salt lowered average rate of hydrate formation probably due to the interaction between salt and AA-LDHI led to phase inversion (from water to oil continuous phase, as discussed in section 5.1.3). This limited gas transfer into the water phase. While without salt, the addition of AA-LDHI promoted average crystallization rate at 80%WC (Table 4. 5).

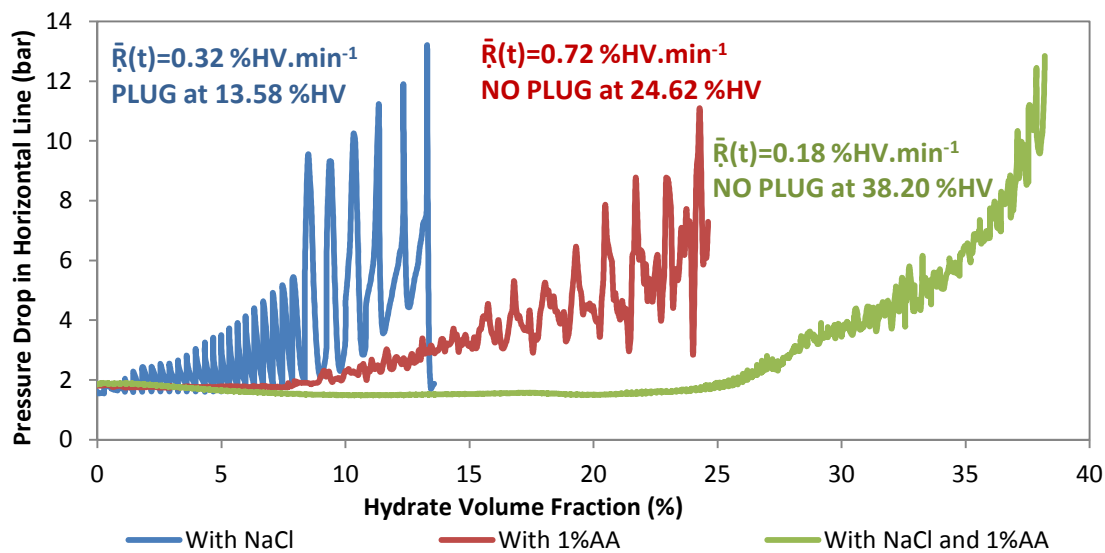
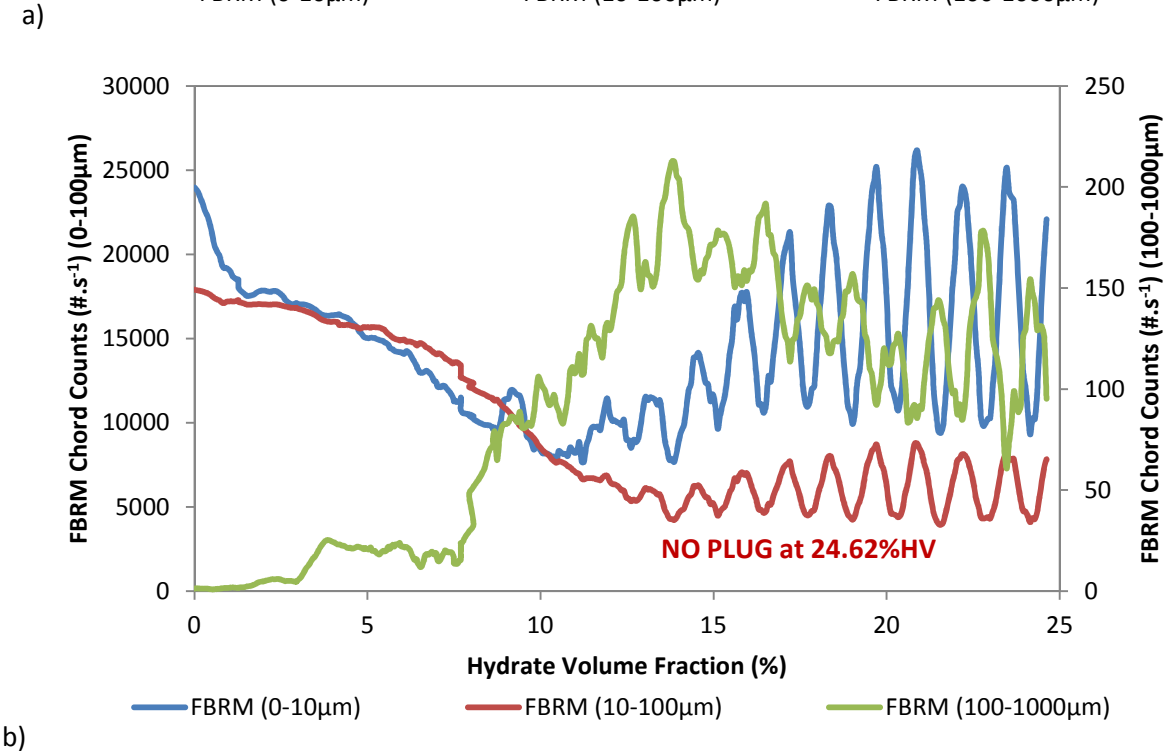
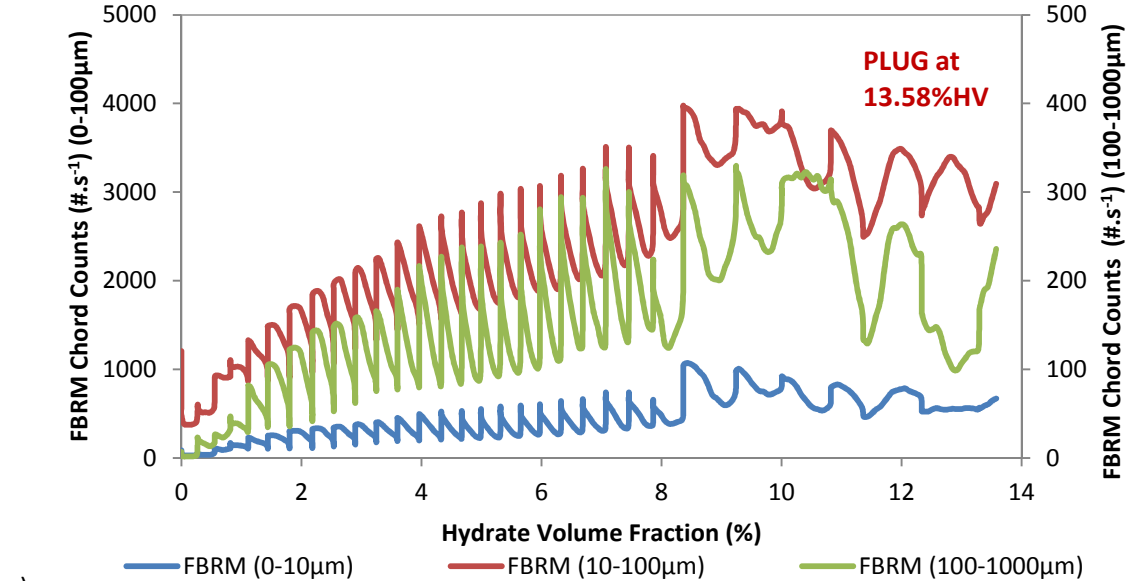


**Figure 4. 25: Effect of a combination of salt and additive on pressure drop and average rate of crystallization [the experiments with 80%WC-85%LV-75bar-400L.h<sup>-1</sup> with NaCl - with 1%AA-LDHI - with NaCl and 1%AA-LDHI].**

This should be highlighted that the experiment with both salt and AA-LDHI showed no plug up to 38.20%HV whereas plug occurred at 13.58%HV for the experiment with salt. The experiment with 1%AA-LDHI did not show plug but pressure drop showed too much oscillation at 24.62%HV. This confirmed again that AA-LDHI functioned better in the presence of salt. Remarkably, a decrease in pressure drop was observed for the experiment with 80%WC-NaCl-1%AA-LDHI. This was already interpreted in section 4.7.

In the presence of both salt and AA-LDHI, the average crystallization rate of the experiment with 80%WC was lower than that of the experiment with 100%WC (Figure 4. 25 and Figure 4. 27). This was probably because AA-LDHI enhanced gas transfer into the water at the gas-water surface at 100%WC more than that at 80%WC. At 80%WC, AA-LDHI may adsorb on the contact surface of oil

droplets dispersed in water bulk leading to less AA-LDHI on the contact surface of the water-gas phase. This slowed down gas transfer rate into the water at 80%WC. Generally, hydrate slurry flow at 80%WC was more heterogeneous (more fluctuated pressure drop) than that at 100%WC, especially at the end of crystallization process (see pressure drops in Figure 4. 25 and Figure 4. 27). This was explained by the different suspension of liquid (water-oil)-hydrate at 80%WC from that of liquid (water)-hydrate at 100%WC. This could be that larger agglomerates at 80%WC than those at 100%WC. This explanation was based on the fluctuation of FBRM chord counts during the final stage of the crystallization (see FBRM chord counts in Figure 4. 26 and Figure 4. 28).



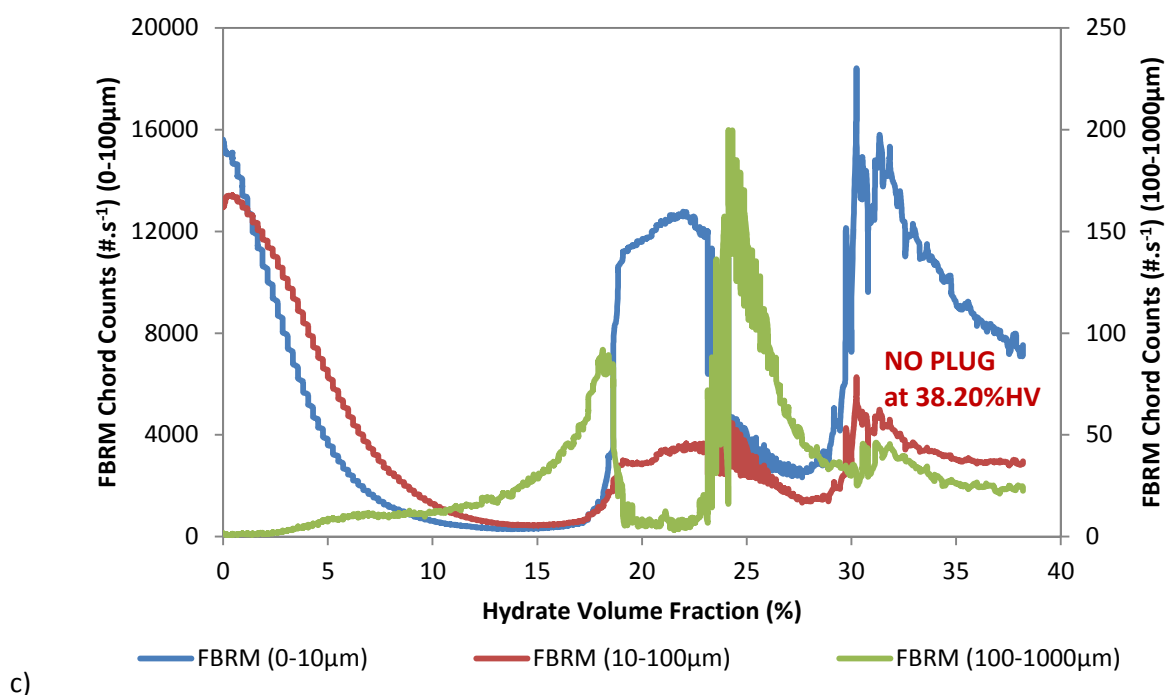
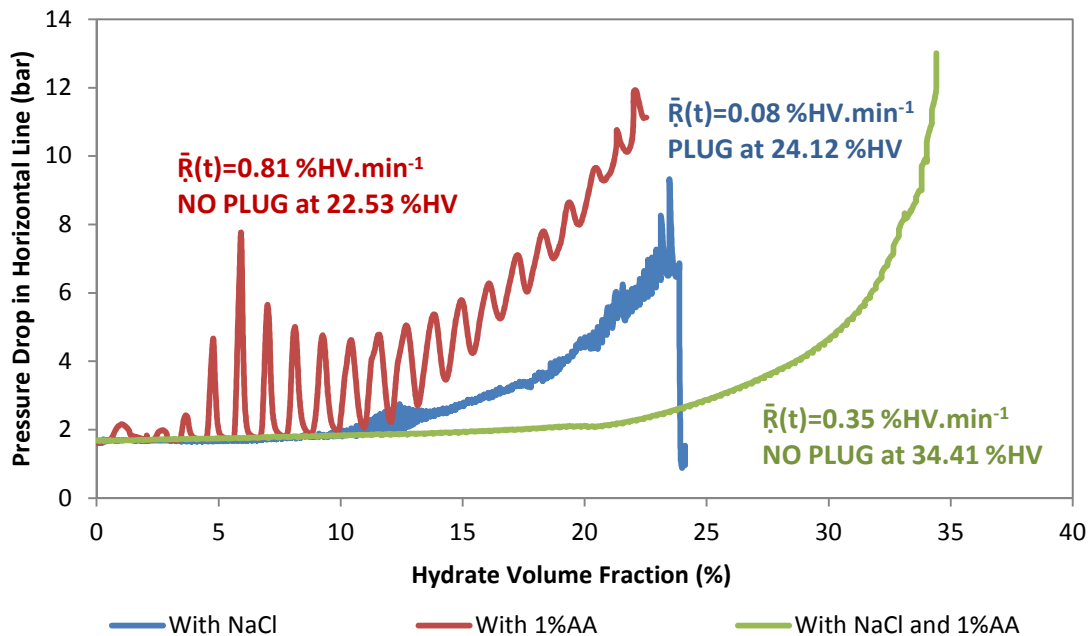


Figure 4. 26: Effect of a combination of salt and additive on FBRM chord counts [the experiments with 80%WC-85%LV-75bar-400L.h<sup>-1</sup> with NaCl (a) - with 1%AA-LDHI (b) - with NaCl and 1%AA-LDHI (c)].

#### 4.12.2. Experiments with 100%WC

This is clear from Figure 4. 27 that a combination of salt and AA-LDHI decreased the average crystallization rate compared to the experiment with AA-LDHI. This was due to the lower driving force and the lower CMC of AA-LDHI (led to fewer AA-LDHIs contributed to hydrate crystallization) in addition of salt. However, this combination increased average hydrate formation rate, shortened induction time and decreased pressure drop compared to the experiment with only salt. Additionally, the pressure drop became smoother (more homogeneous) than that in the absence of AA-LDHI. This agreed with the case without salt that AA-LDHI promoted the average rate of crystallization. This was explained by the role of AA-LDHI in nucleating and promoting hydrate formation and also improving gas transfer into the liquid phase. This is because AA-LDHI lowered the interfacial tension between gas and water. This result was different from the one at 80%WC that AA-LDHI inhibited hydrate formation in the presence of salt (section 4.12.1). This was explained that at 100%WC, AA-LDHI improved gas transfer into liquid. However, at 80%WC, the addition of AA-LDHI was less important as oil played a vital role to enhance gas transfer into liquid.



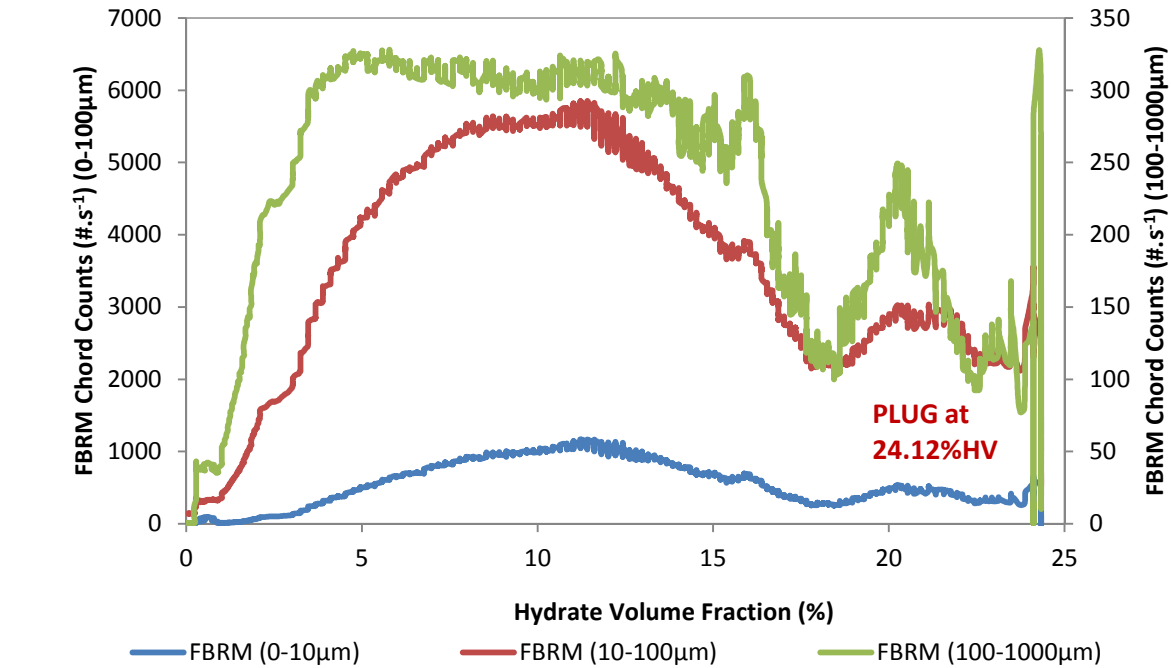
**Figure 4. 27: Effect of a combination of salt and additive on pressure drop and average rate of crystallization [the experiments with 100%WC-85%LV-75bar-400L.h<sup>-1</sup> with NaCl - with 1%AA-LDHI - with NaCl and 1%AA-LDHI].**

However, the experiment with 1%AA-LDHI did not show a higher average crystallization rate than the one of 0.5%AA-LDHI (even lower average crystallization rate at 1%AA-LDHI than the one at 0.5%AA-LDHI with salt at 150L.h<sup>-1</sup> as seen in Table 4. 5). This could be explained by the CMC of AA-LDHI. It is supposed that the 0.5%AA-LDHI in the presence of salt probably reached the CMC value at 100%WC compared to the 2%AA-LDHI in the absence of salt (Noll, 1991), see section 4.10. As a result, further addition of AA-LDHI did not promote gas transfer into liquid phase or even lowered performance of AA-LDHI (pressure drop at 0.5%AA-LDHI was lower than at 1%AA-LDHI, at the same hydrate volume in the presence of salt).

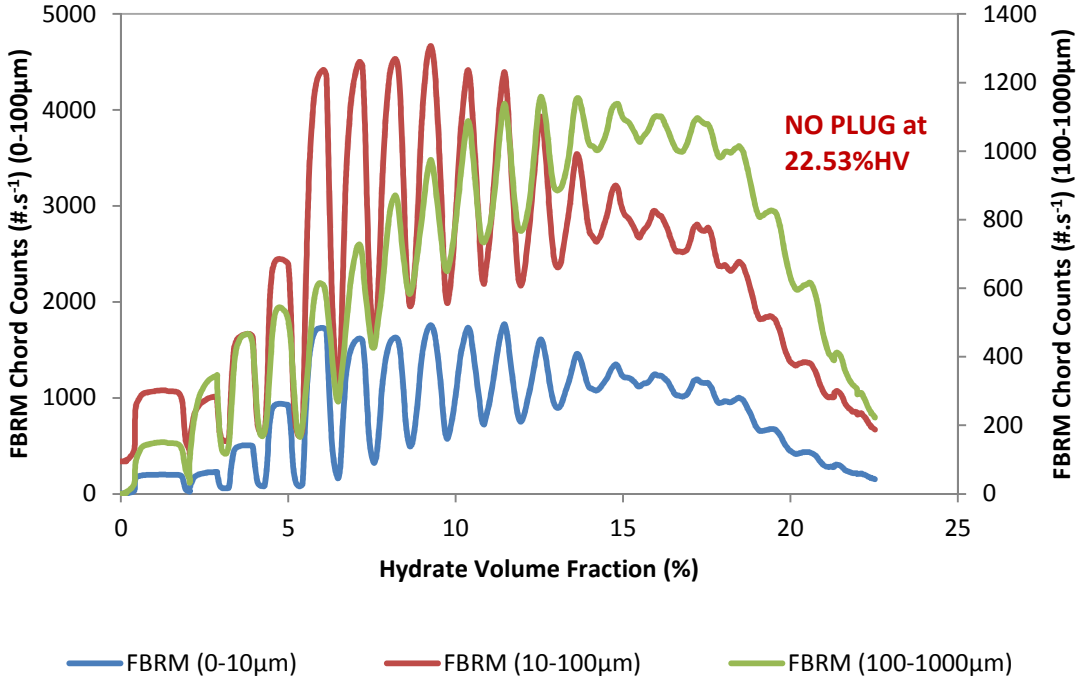
In fact, combining salt and AA-LDHI improved hydrate slurry transport with less heterogeneous flow compared to those with only salt and only AA-LDHI as seen in the pressure drop and FBRM chord counts (Figure 4. 27 and Figure 4. 28). In the presence of salt, AA-LDHI became more effective to prevent plugging (Gao, 2009). In details, there was no plug at hydrate volume of 34.41 and 43.58%HV for the experiment with both salt and AA-LDHI.

Indeed, the pressure drop of the experiment with both salt and AA-LDHI was smaller than that in the experiments with only AA-LDHI or only salt at same hydrate volume. In details, for the experiment with both salt and AA-LDHI, pressure drop reached 12 bar at 34%HV and there was no plug at this hydrate volume. In contrast, the experiment with salt plugged at 24.12%HV at a pressure

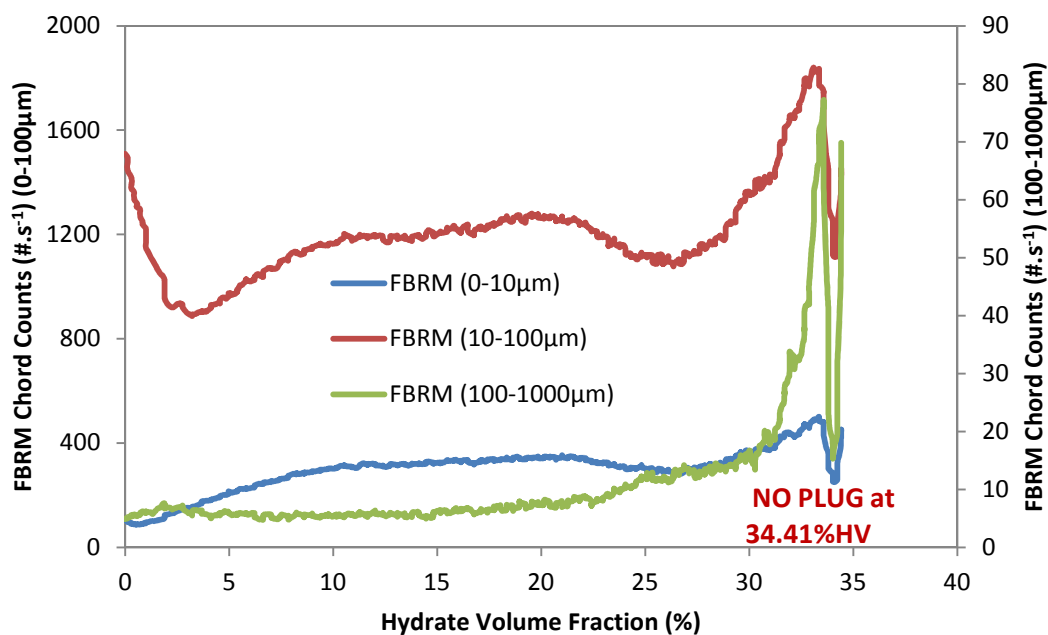
drop of 10 bar; and the experiment with 1%AA-LDHI reached 12 bar at hydrate volume of 22.53%. In the experiments with salt or AA-LDHI, hydrate deposition was observed when FBRM chord counts decreased. The combination of salt and AA-LDHI decreased the hydrate deposition as seen in FBRM chord counts (Figure 4. 28).



a)



b)



c)

**Figure 4. 28: Effect of a combination of salt and additive on FBRM chord counts [the experiments with 100%WC-85%LV-75bar-400L.h<sup>-1</sup> with NaCl (a) - with 1%AA-LDHI (b) - with NaCl and 1%AA-LDHI (c)].**

#### 4.13. Effect of pressure

The experimental result showed that the higher pressure, the higher average hydrate formation rate. This was interpreted by the lower driving force of the experiment with lower pressure (Table 4. 4). Interestingly, the results indicated the same trend of pressure drops and FBRM chord counts at different pressures (Figure 4. 29 and Figure 4. 30). However, the intensities of FBRM chord counts and pressure drop in the two experiments (at 70 and 75 bar) were not the same. The rise in experimental pressure increased the intensity of these values at the same hydrate volume. This means that more hydrate particles formed at high pressure than that at low pressure. This was also explained by higher average crystallization rate at higher pressure.

In term of homogeneity of hydrate slurry, the increase in pressure enhanced the fluctuation of the experimental signals. This can be explained by the higher average rate of crystallization leading to higher agglomeration rate and quicker heterogeneity of hydrate slurry formed. As a result, the pressure drop in the experiment at higher pressure was higher than that at lower pressure at the same hydrate volume. Both cases showed deposition at the end of the experiment confirmed by a decrease in FBRM chord counts (Figure 4. 30). However, hydrate particles at higher pressure showed quicker deposition (deposit at lower hydrate volume) than that at lower pressure. This could be attributed to the higher average crystallization rate (at higher pressure) which led to quicker

agglomeration with larger hydrate agglomerates. As a consequence, the bigger agglomerates might lead to faster deposition.

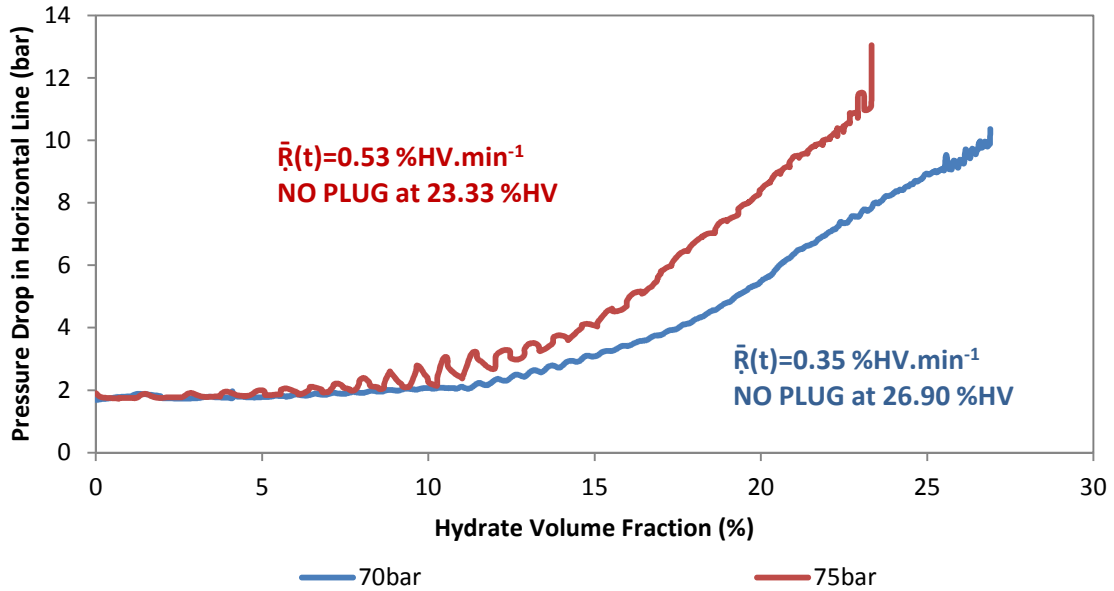
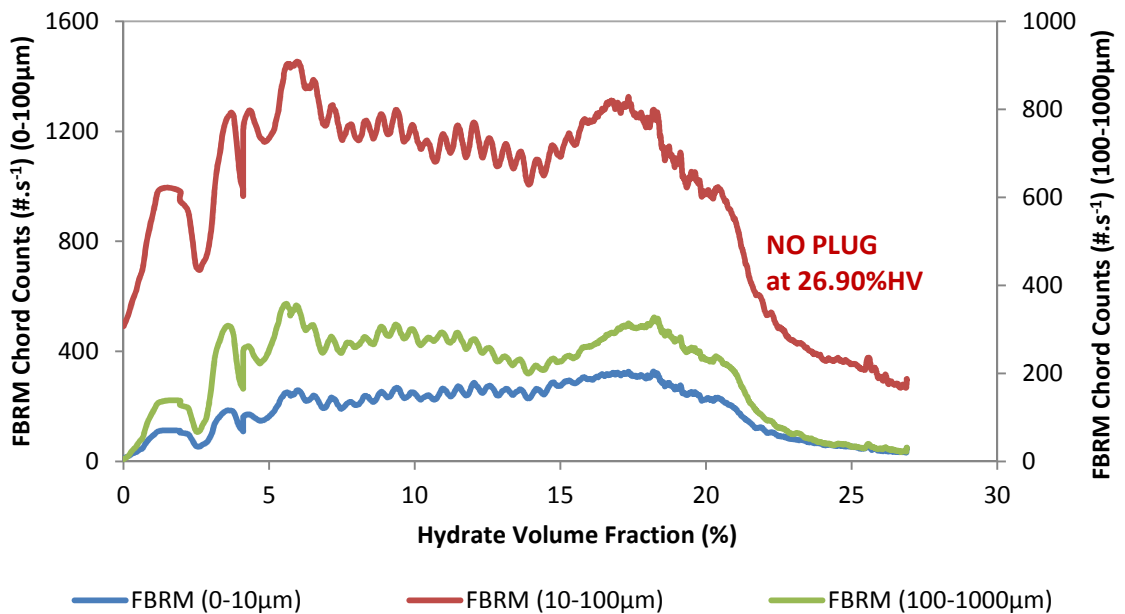
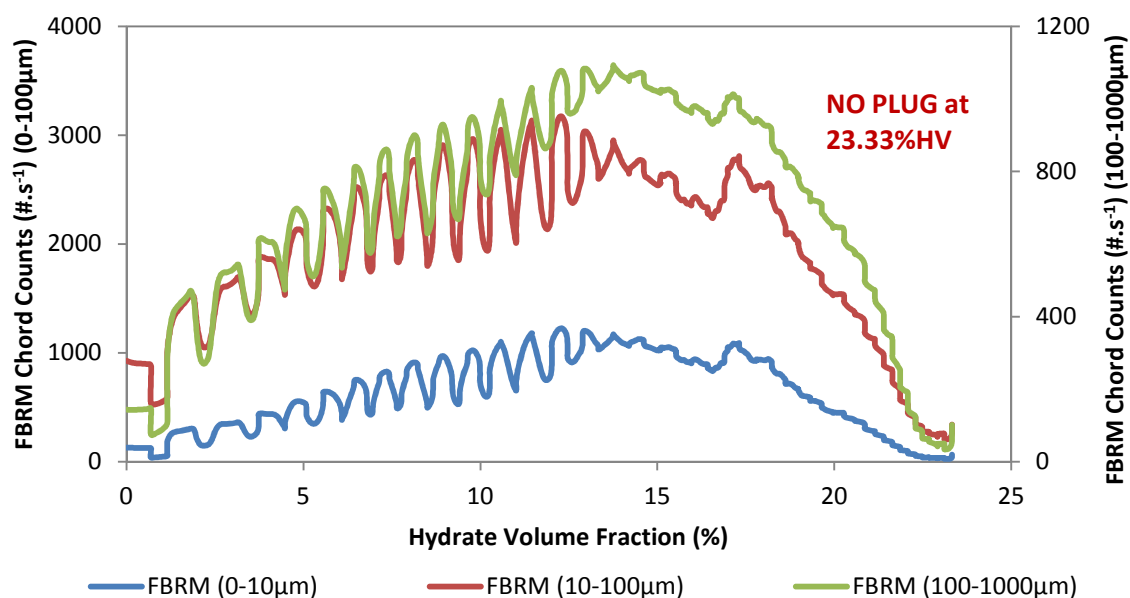


Figure 4. 29: Effect of pressure on pressure drop and average rate of crystallization [the experiments with 100%WC-2%AA-LDHI-85%LV-400L.h<sup>-1</sup> at 70bar and 75bar].



a)



b)

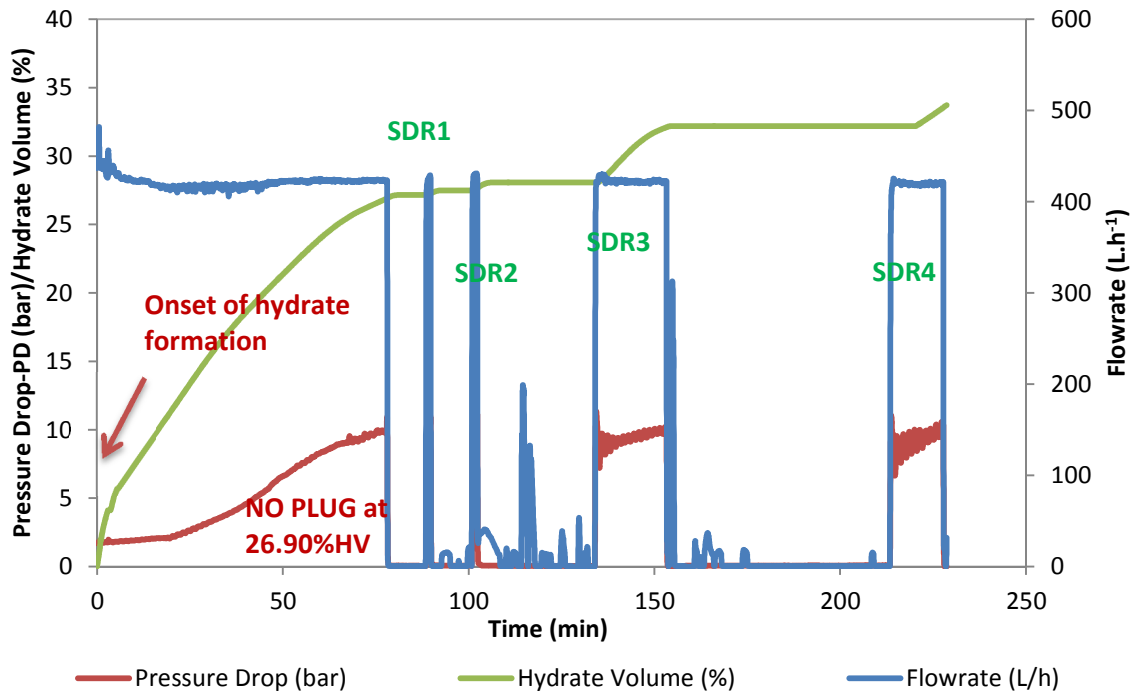
**Figure 4. 30: Effect of pressure on FBRM chord counts [the experiments with 100%WC-2%AA-LDHI-85%LV-400L.h<sup>-1</sup> at 70bar (a) and 75bar (b)].**

#### 4.14. Stability of hydrate slurry (SDR Tests)

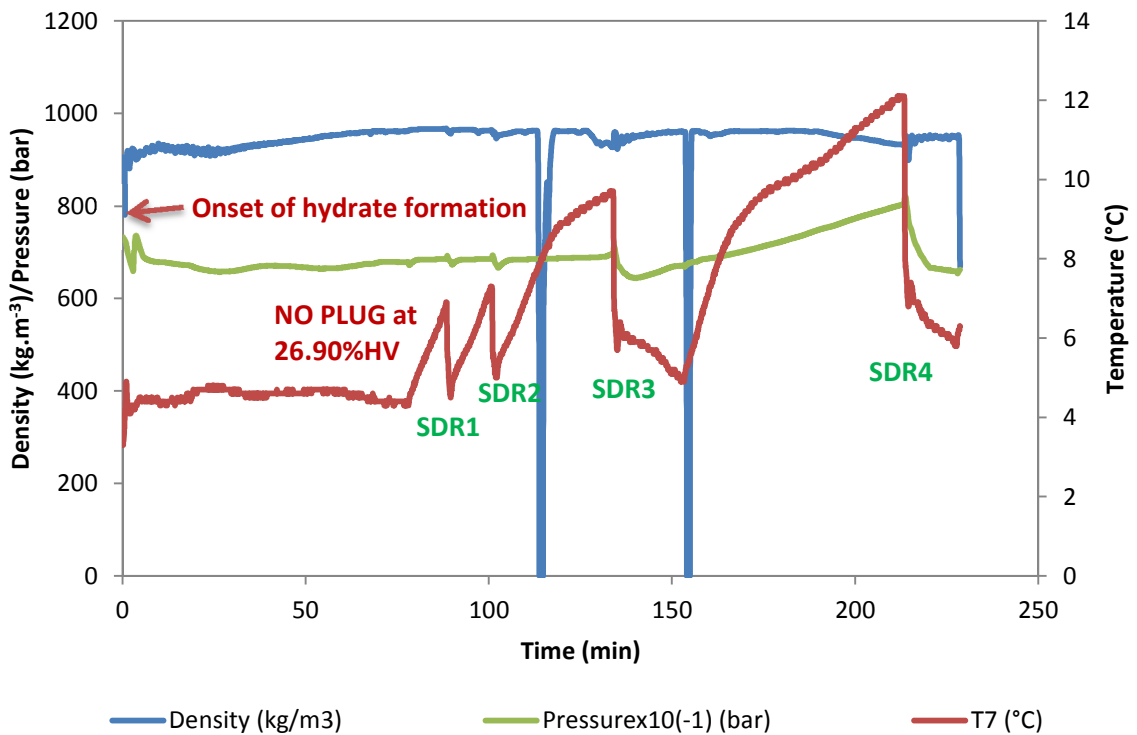
The shutdown and restart (SDR) tests were conducted four times (10-10-30-60 minutes) for the experiment with 100%WC-2%AA-LDHI-85%LV-400L.h<sup>-1</sup>-70bar (Figure 4. 31). The results showed that after shut down for a certain period of time (up to 60 minutes), the system can be restored safely. The fact that the pressure drop, density, and flowrate were almost stable and the same as before shutdown even at higher hydrate volume in the flowloop (hydrate continued to form during SDR tests). This stability was maybe because AA-LDHI prevented hydrate agglomeration and avoided plug during the shutdown period and after restarting the flowloop system. From FBRM chord counts (Figure 4. 31), after restarting the system, the number of chord length increased and decreased just after several minutes. This was explained by recirculation and afterwards deposition of hydrate particles in the flowloop.

The SDR 3&4 showed continuous hydrate formation after restarting the system (Figure 4. 31). In addition, for SDR4, the temperature of the system before restarting system was higher than equilibrium dissociation temperature (9.5°C and 70 bar). It is supposed that in this SDR4, some hydrates dissociated and then continued to form after restarting the system. Deposition was still observed before and after SDR. The higher increase in a number of FBRM chord counts in SDR4 than that in SDR3 could be due to hydrate reformation. The hydrate volume just before shutdown system was 26.90%HV. Interestingly, after several SDR tests, although hydrate volume increased, the

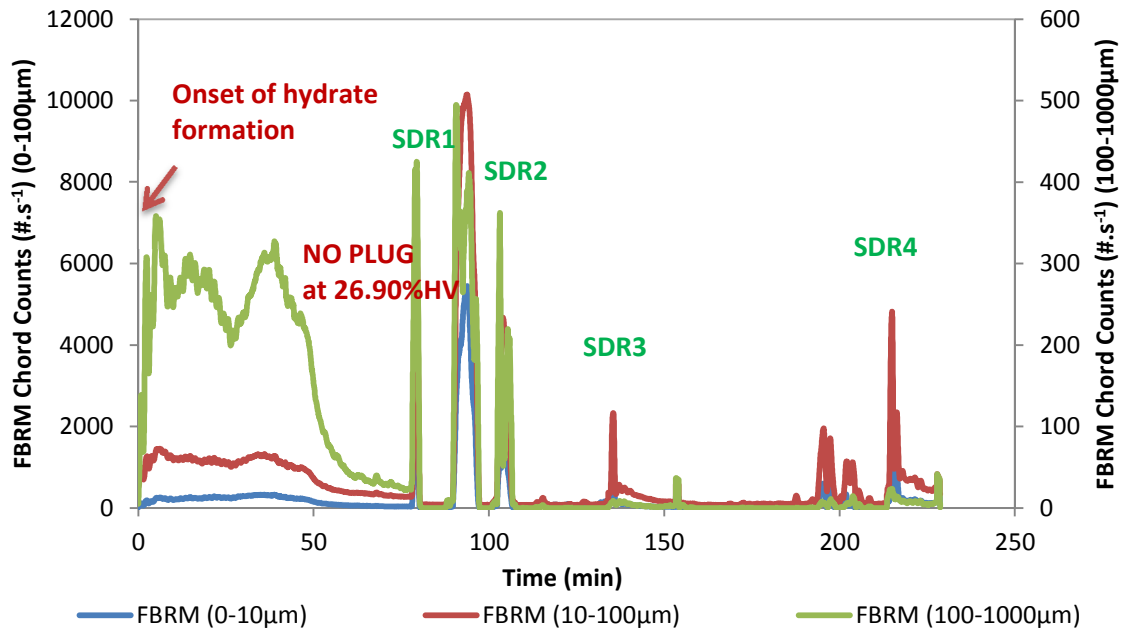
pressure drop was almost constant but more fluctuated due to hydrate slurry flow became more heterogeneous during SDR tests. This confirmed again the role of AA-LDHI to disperse hydrate particles in pipelines.



a)



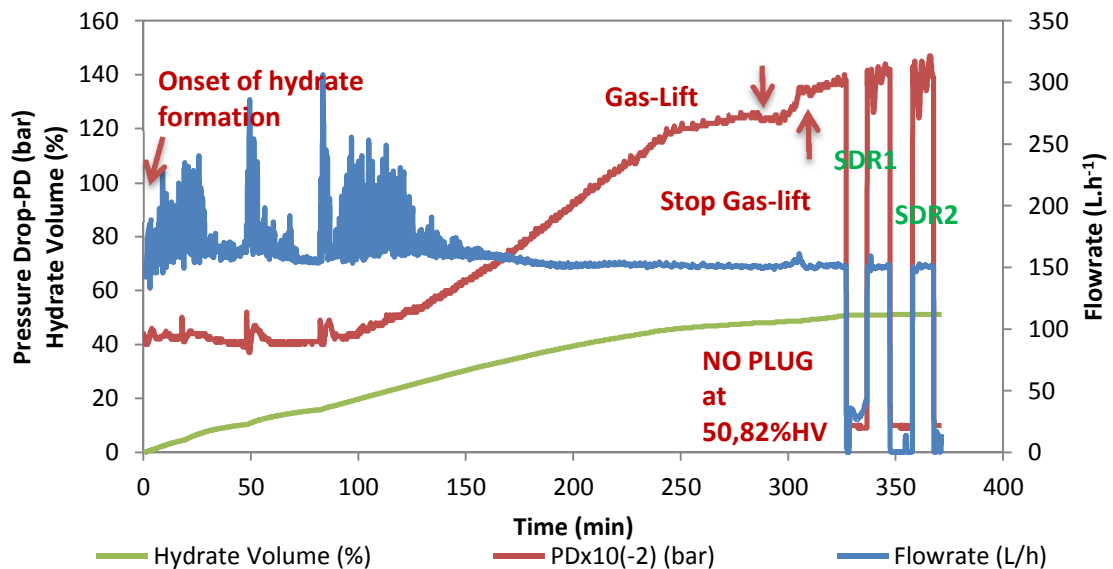
b)



c)

Figure 4. 31: Shutdown and restart tests for the experiment with 100%WC-2%AA-LDHI-85%LV-400L.h<sup>-1</sup>-70bar: (a) pressure drop, hydrate volume, and flowrate; (b) density, pressure, and temperature; and (c) FBRM chord counts.

At the end of the experiment with 100%WC-NaCl-1%AA-LDHI-85%LV-150L.h<sup>-1</sup>-75bar, two SDR tests were performed, 10 minutes each (Figure 4. 32).



a)

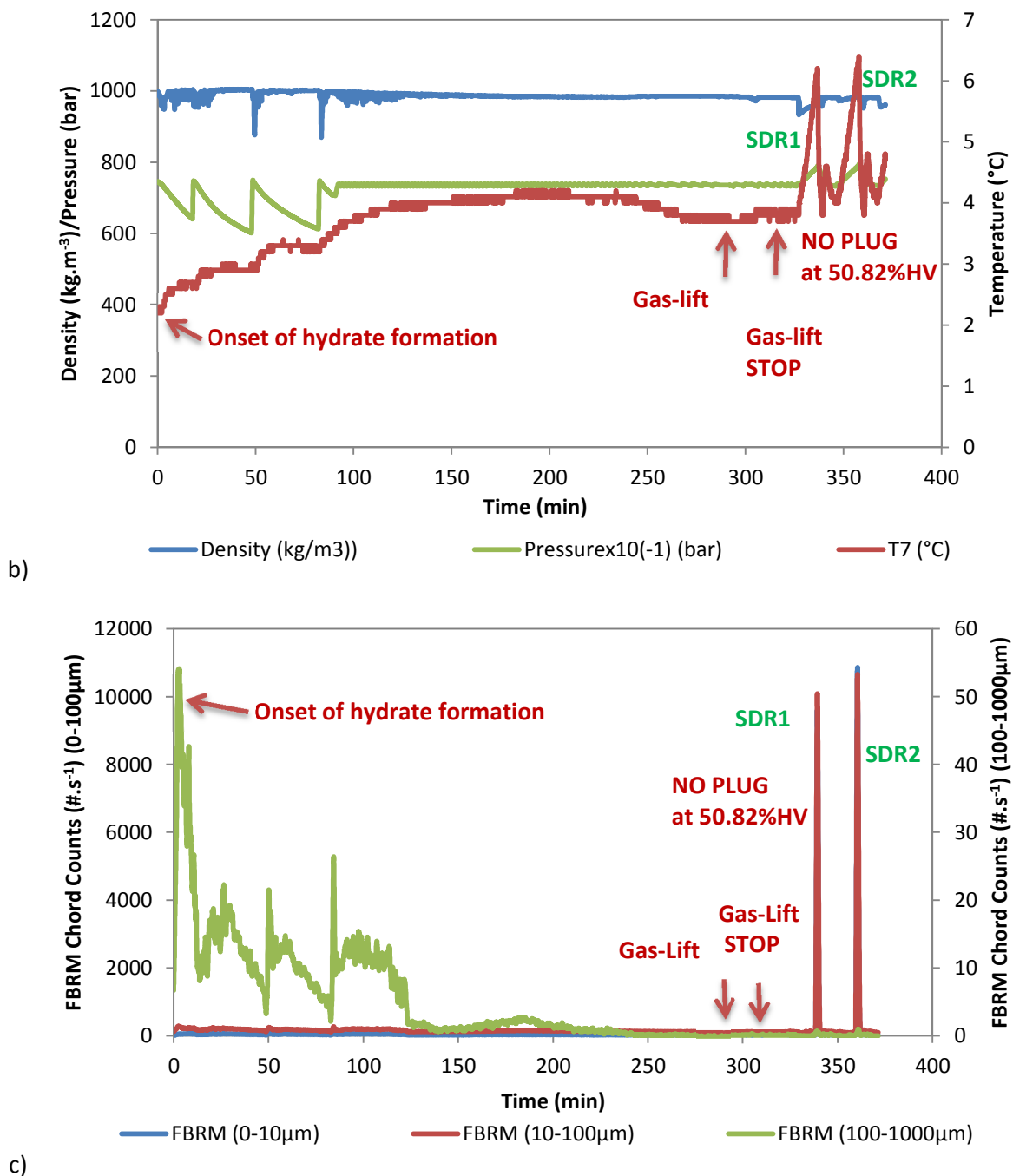


Figure 4. 32: Shutdown and restart tests for the experiment with 100%WC-NaCl-1%AA-LDHI-85%LV-150L.h<sup>-1</sup>-75bar: (a) pressure drop, hydrate volume, and flowrate; (b) density, pressure, and temperature; and (c) FBRM chord counts.

No plug was observed during SDR tests (Figure 4. 32). The significant increase in a number of chord length after restarting system could be due to recirculation of hydrate particles and they deposited immediately afterwards. The hydrate volume just before SDR was 50.82%HV. No hydrate

dissociation was observed at SDR tests (6.5°C and 74 bar). Deposition still occurred after two times of SDR tests.

#### 4.15. Morphology of hydrate particles

In this present work, stunning and clear pictures of hydrate particles were obtained from PVM measurements in which the morphology of hydrate particles formed in the pipelines was better understood. In fact, the experiments with different amount of AA-LDHI and salt showed different morphologies of hydrate particles at different water fraction of 70, 80 and 100%WC.

##### 4.15.1. Hydrate morphology at 70 and 80%WC

Morphology of hydrate particles at 70-80%WC was identified by PVM images. It is obvious that there was a predominance of sphere shape along with the non-sphere shape of hydrate particles. It is supposed that spherical shape was created once hydrate formed on the surface of oil droplets. Besides, the non-sphere shape can be attributed to hydrate formed in the liquid water bulk and/or to hydrate detached from hydrate shell-covered oil droplet. The different composition of mixtures showed the different morphology of hydrate particles as shown in Figure 4. 33, Figure 4. 34, Figure 4. 35, Figure 4. 36, Figure 4. 37, Figure 4. 38, and Figure 4. 39.

PVM images from the experiment with 70%WC at  $400\text{L}\cdot\text{h}^{-1}$  and 100%LV in Figure 4. 33 showed the round-shapes of hydrate particles. This was hypothesized that hydrates formed mainly from oil droplets which oriented spherical morphology of hydrate particles. Hydrate formation in the water bulk phase was also observed. This might be due to hydrate layer detached from hydrate shell-covered oil droplets and/or hydrate formed freely in the water bulk phase.

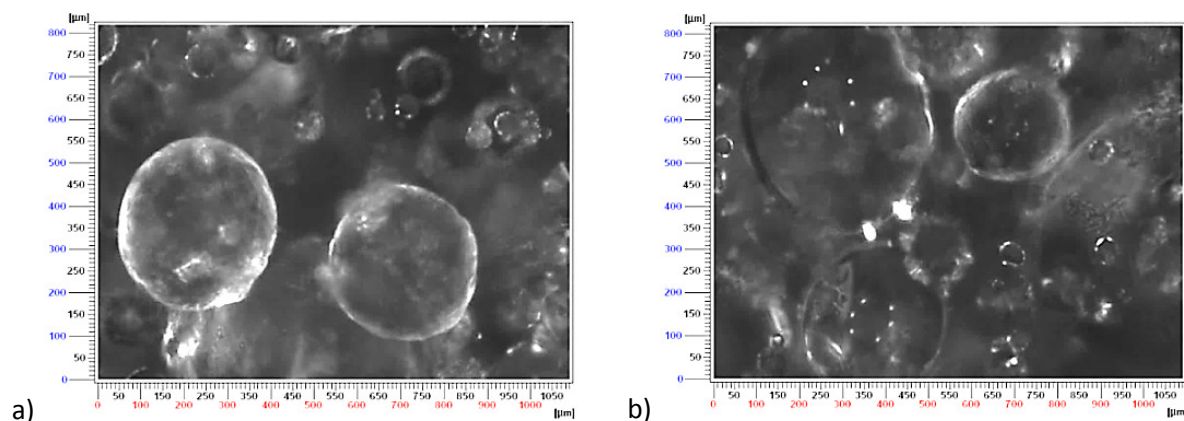


**Figure 4. 33: PVM images of gas hydrate formation and plugging for the experiment with 70%WC at  $400\text{L}\cdot\text{h}^{-1}$  and 100%LV [(a) 3 min and (b) 8 min after gas hydrate formation].**

Commonly, the experiment with 80%WC without AA-LDHI and salt showed bigger hydrate particles and quicker agglomeration than the experiments with AA-LDHI and salt. This was explained

by the absence of AA-LDHI. For the experiment with 80%WC at  $150\text{L}\cdot\text{h}^{-1}$ , the hydrate nucleation and agglomeration occurred only in a few minutes (Figure 4. 34). At the beginning of hydrate formation, very small hydrate particles were probably formed in the free water phase and on the surface of oil droplets. After 2 minutes, hydrate slurry occurred with the spherical and random shapes of hydrate particles.

At higher flowrate ( $400\text{L}\cdot\text{h}^{-1}$ ), for the experiment with 80%WC (Figure 4. 35), it is clear that hydrate formed on the surface of oil droplets (spherical shape) and in the water bulk phase. Besides, bigger agglomerates formed in the absence of AA-LDHI.

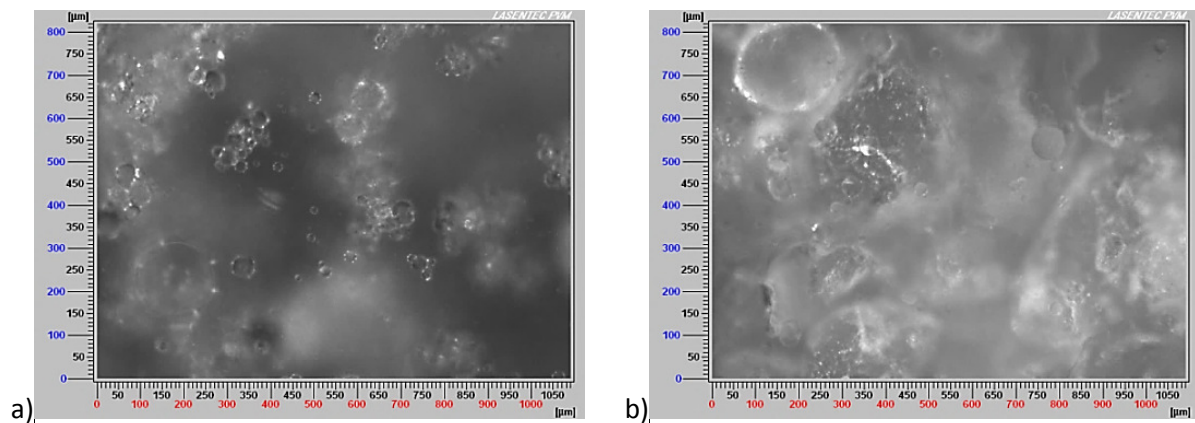


**Figure 4. 34: PVM images of gas hydrate formation and plugging for the experiment with 80%WC at  $150\text{L}\cdot\text{h}^{-1}$  and 85%LV [(a) 0.5 min and (b) 2 min after gas hydrate formation].**

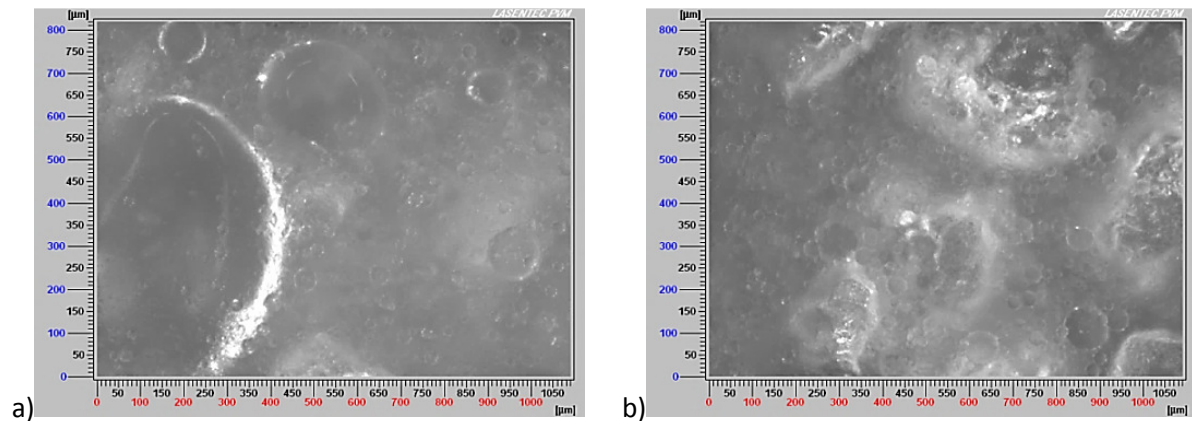


**Figure 4. 35: PVM images of gas hydrate formation and plugging for the experiment with 80%WC at  $400\text{L}\cdot\text{h}^{-1}$  and 85%LV [(a) 118.4 min and (b) 257.4 min after gas hydrate formation].**

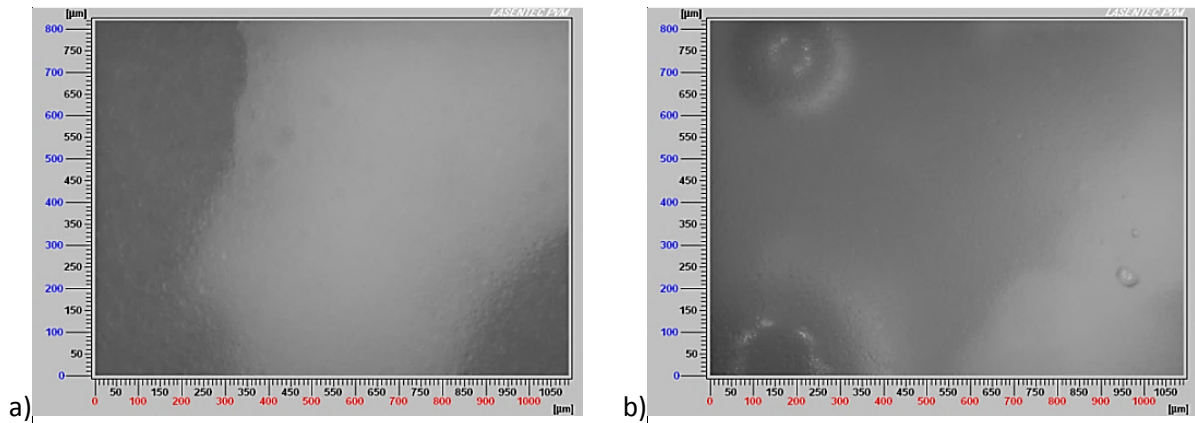


**Figure 4. 36: PVM images of gas hydrate formation and plugging for the experiment with 80%WC-1%AA-LDHI at 400L.h<sup>-1</sup> and 85%LV [(a) 5.7 min and (b) 25.7 min after gas hydrate formation].**

In the presence of additives (80%WC-1% AA-LDHI), hydrate particles were smaller and very fine (Figure 4. 36) compared to those without AA-LDHI. This was interpreted by the role of commercial additive to disperse oil droplets with a smaller size before hydrate formation and also a better dispersion of hydrate particles in the fluid once they formed.

At low flowrate (150L.h<sup>-1</sup>), in the presence of salt, the experiment with 80%WC showed sticky agglomerates (rough hydrate surface) once hydrate formed (Figure 4. 37). In fact, the spherical and individual shapes of hydrate particles were not observed.

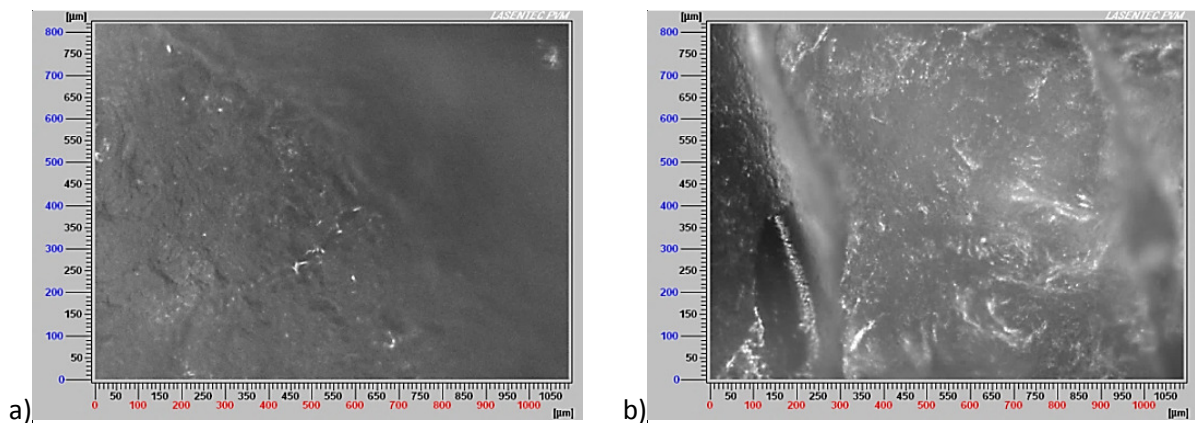


**Figure 4. 37: PVM images of gas hydrate formation and plugging for the experiment with 80%WC-NaCl at 150L.h<sup>-1</sup> and 85%LV [(a) 7.1 min and (b) 10.1 min after gas hydrate formation].**

In the experiment with 80%WC-NaCl at higher flowrate (400L.h<sup>-1</sup>), it is obvious that hydrates formed on the surface of oil droplets and also in the water continuous phase (Figure 4. 38).

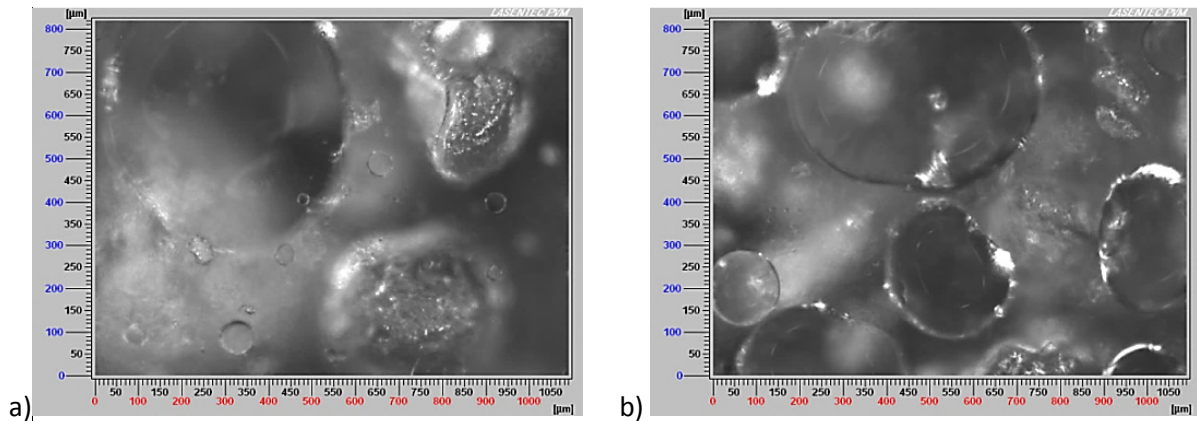


**Figure 4.38: PVM images of gas hydrate formation and plugging for the experiment with 80%WC-NaCl at  $400\text{L}\cdot\text{h}^{-1}$  and 85%LV [(a) 29.4 min and (b) 40.3 min after gas hydrate formation].**

The combination of salt and AA-LDHI demonstrated that smaller and very fine hydrate particles formed on the surface of oil droplets (Figure 4.39).

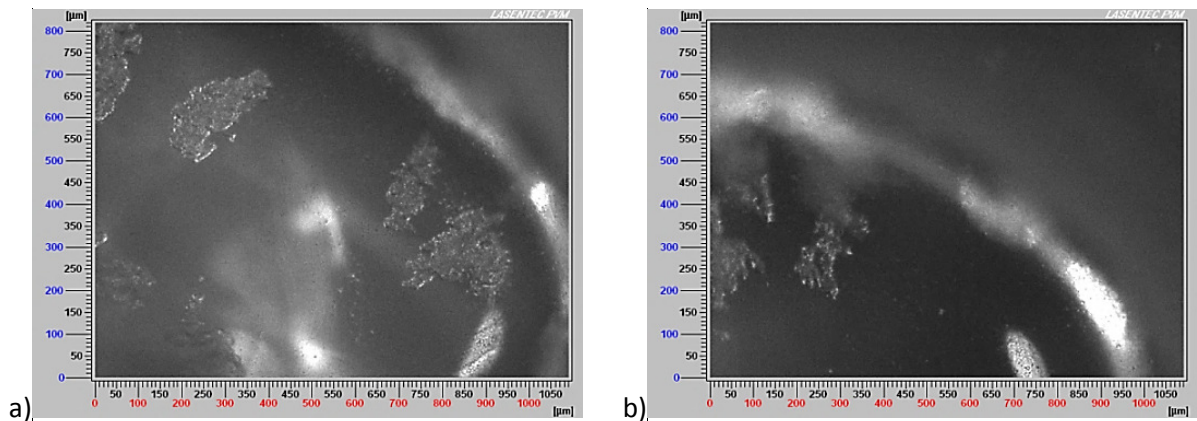


**Figure 4.39: PVM images of gas hydrate formation and plugging for the experiment with 80%WC-NaCl-1%AA-LDHI at  $400\text{L}\cdot\text{h}^{-1}$  and 85%LV [(a) 138.8 min and (b) 163.8 min after gas hydrate formation].**

#### 4.15.2. Hydrate morphology at 100%WC

Contrary to hydrate particles morphology of 70-80%WC, hydrate morphology at 100%WC was totally non-sphere due to non-shape-orientation of oil. At 100%WC, the effects of salt and AA-LDHIs on the morphology of hydrate particles are shown in Figure 4.40, Figure 4.41, Figure 4.42, Figure 4.43, Figure 4.44, Figure 4.45, and Figure 4.46.

PVM images of the experiment with pure water (Figure 4.40) showed the non-spherical shape of hydrate particles. Moreover, the complicated network of hydrate particles like porous structure was observed. Addition of 0.05%AA-LDHI changed the morphology of hydrate particles. They were smaller in the presence of AA-LDHI (Figure 4.41).

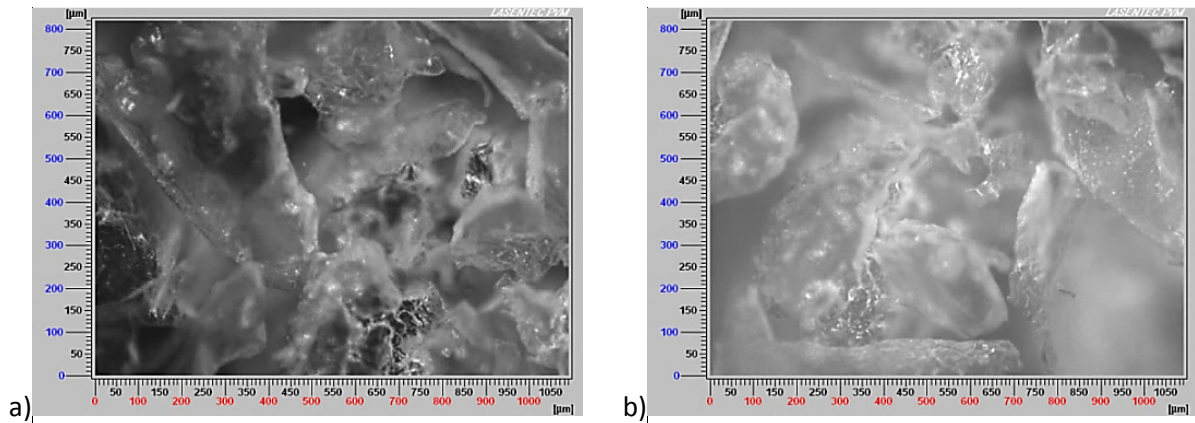


**Figure 4. 40: PVM images of gas hydrate formation and plugging for the experiment with 100%WC at 150L.h<sup>-1</sup>, 75bar and 85%LV [(a) 0.7 min and (b) 1.7 min after gas hydrate formation].**

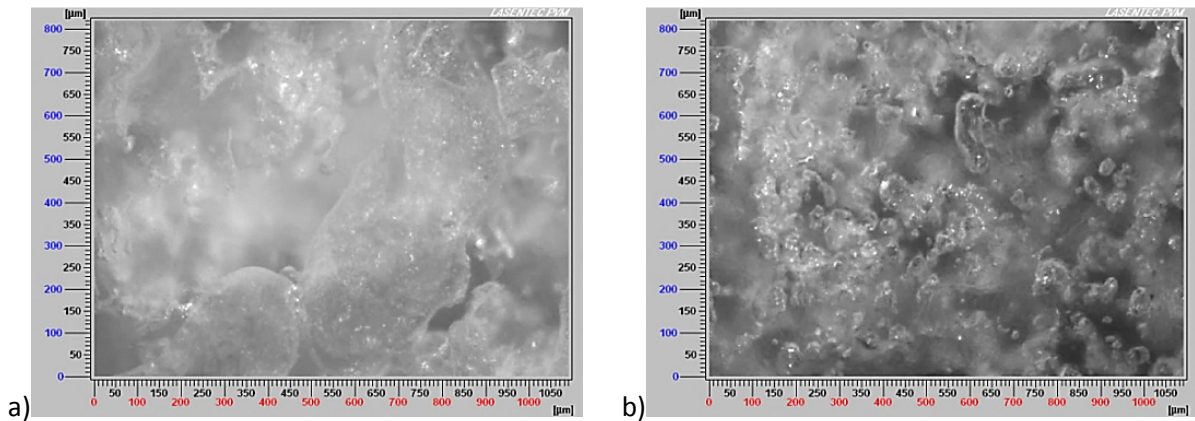


**Figure 4. 41: PVM images of gas hydrate formation and plugging for the experiment with 100%WC-0.05%AA-LDHI at 150L.h<sup>-1</sup> and 90%LV [(a) 288.4 min and (b) 320.4 min after gas hydrate formation].**

When the dosage of AA-LDHI was added up to 1 wt.%, several bigger hydrate particles co-exist with much smaller ones were observed by the PVM images (Figure 4. 42).

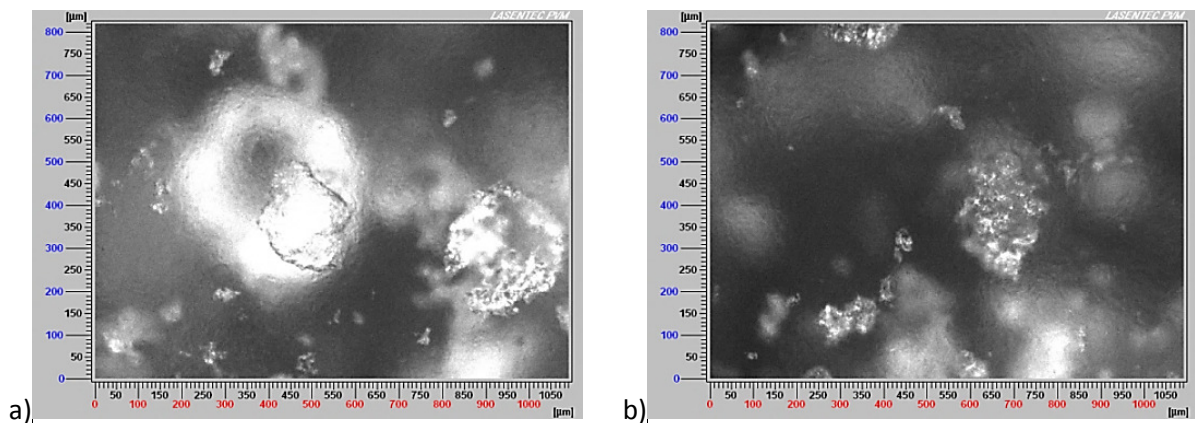


**Figure 4. 42: PVM images of gas hydrate formation and plugging for the experiment with 100%WC-1%AA-LDHI at 400L.h<sup>-1</sup> and 85%LV [(a) 22.8 min and (b) 24.8 min after gas hydrate formation].**

In the presence of salt, hydrate particles were bigger with the rougher surface (Figure 4. 43). They existed quite separately with varied shapes and sizes. A complicated network as a porous structure between hydrate particles was not observed at 100%WC without salt and AA-LDHI.

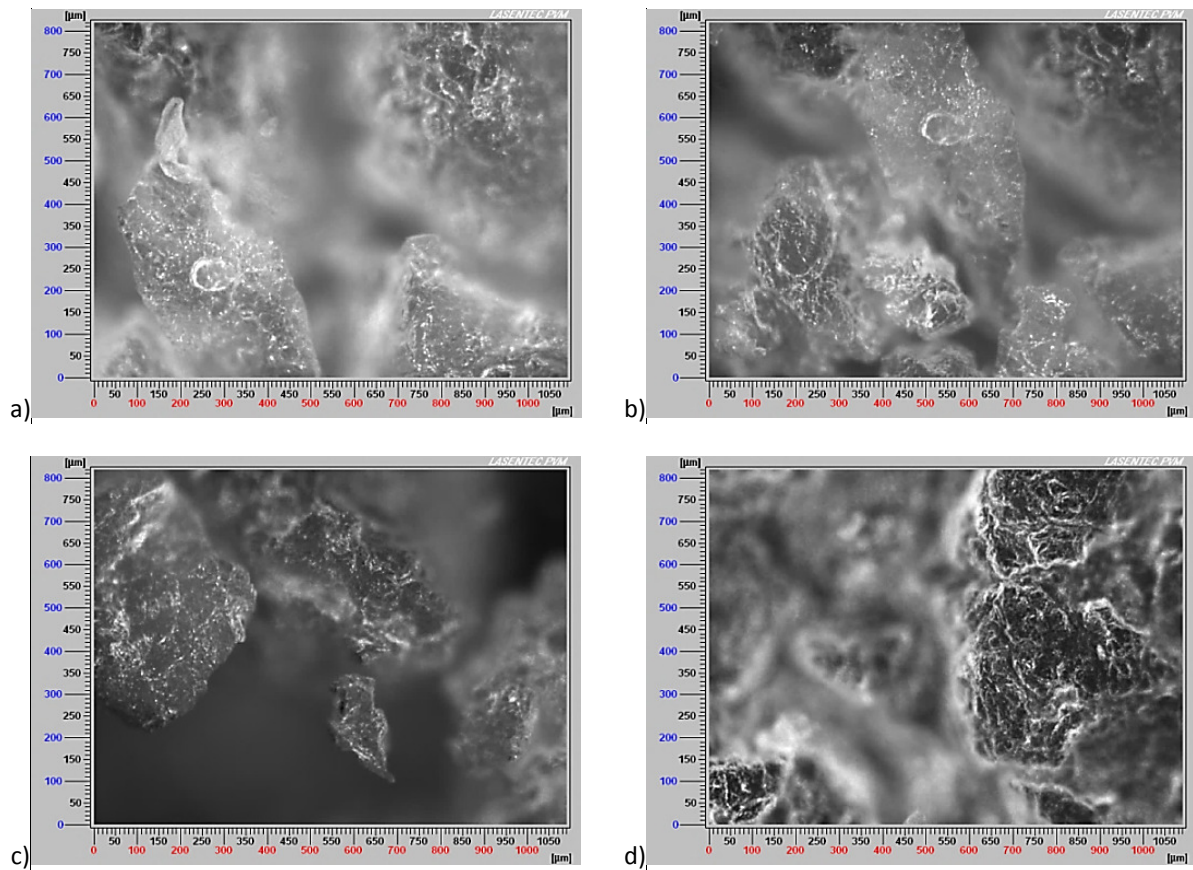


**Figure 4. 43: PVM images of gas hydrate formation and plugging for the experiment with 100%WC-NaCl at  $150\text{L}\cdot\text{h}^{-1}$  and 85%LV [(a) 2.5 min; (b) 3.5 min; (c) 4.5 min; and (d) 5.5 min after gas hydrate formation].**

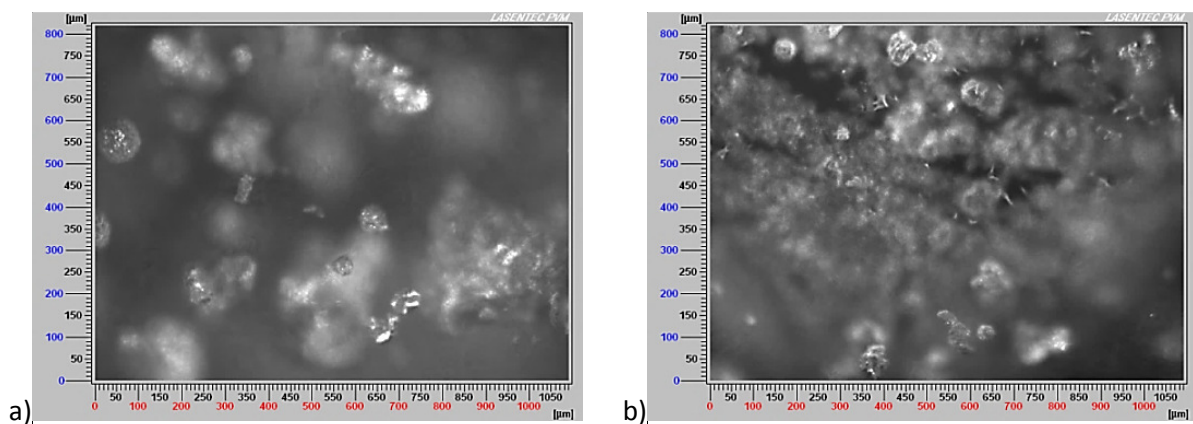


**Figure 4. 44: PVM images of gas hydrate formation and plugging for the experiment with 100%WC-NaCl at  $400\text{L}\cdot\text{h}^{-1}$  and 85%LV [(a) 52 min and (b) 157 min after gas hydrate formation].**

For the experiment with 100%WC at higher flowrate ( $400\text{L}\cdot\text{h}^{-1}$ ) and with salt, smaller hydrate particles than those in low flowrate ( $150\text{L}\cdot\text{h}^{-1}$ ) were observed. This could be explained by the higher shear at the higher flowrate which helped better disperse and/or to crack/break hydrate particles (Figure 4. 44). The presence of both salt and AA-LDHI controlled the hydrate particles towards round-shape and rougher surface (Figure 4. 45 and Figure 4. 46).

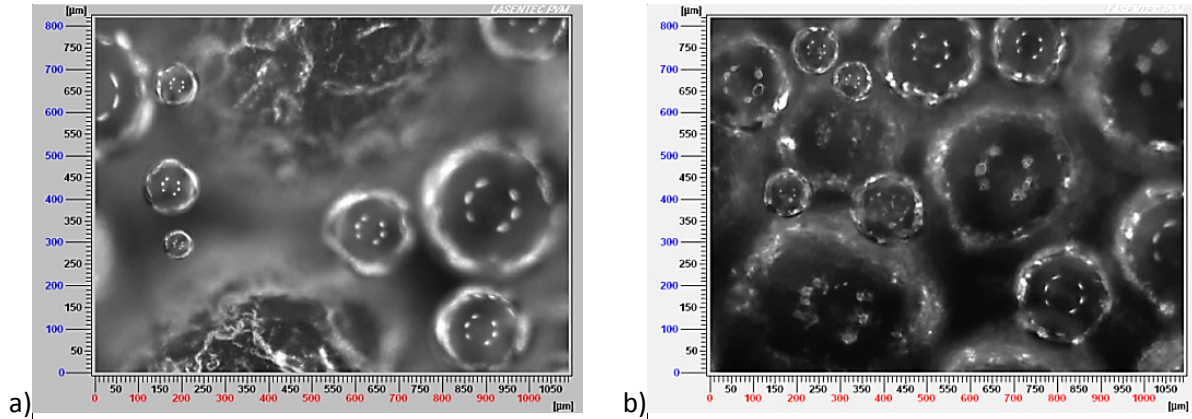


**Figure 4. 45: PVM images of gas hydrate formation and plugging for the experiment with 100%WC-NaCl-1%AA-LDHI at  $150\text{L}\cdot\text{h}^{-1}$  and 85%LV [(a) 1.5 min and (b) 269 min after gas hydrate formation].**

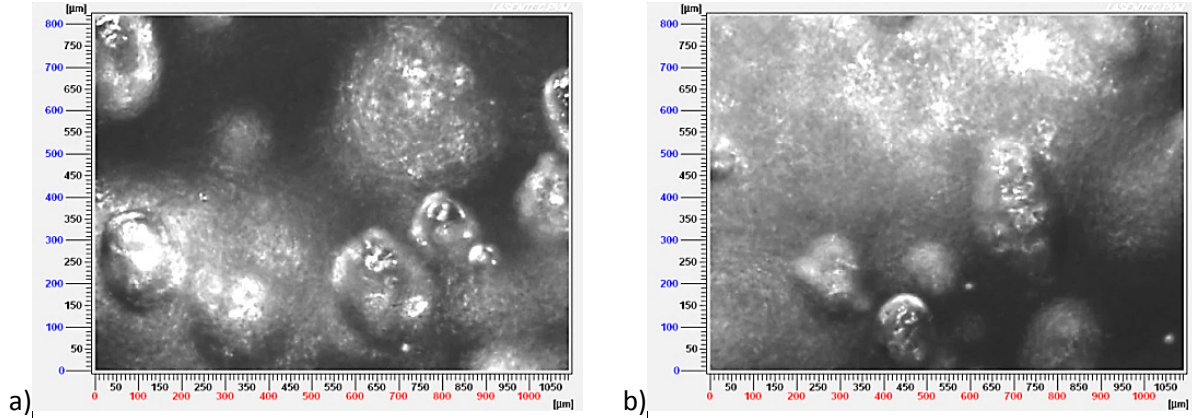


**Figure 4. 46: PVM images of gas hydrate formation and plugging for the experiment with 100%WC-NaCl-1%AA-LDHI at  $400\text{L}\cdot\text{h}^{-1}$  and 85%LV [(a) 53 min and (b) 93.5 min after gas hydrate formation].**

#### 4.16. Highlights and Conclusions

From the experimental results with Moineau pump protocol with and without gas-lift system, several important points can be drawn as follows:

Dispersion of oil and water and its rheology in high water cut systems (70-80%WC) with/without salt and AA-LDHI were investigated. The results showed that the addition of AA-LDHI increased the total chord counts of dispersion but decreased mean droplet size of dispersion. Besides, the presence of salt decreased the total chord counts of dispersion and increased mean droplet size of dispersion. The addition of oil declined the average chord length and increased the total chord counts of dispersion. The increase in flowrate lowered the mean droplet size of dispersion and augmented the total chord counts of dispersion. Higher shear improved performance of AA-LDHI (dispersion of oil in water) in the presence of salt.

Gas transfer rate into liquid phase with/without salt and AA-LDHI was investigated. In details, the rise in flowrate increased the  $k_{La}$ . Generally, the addition of AA-LDHI promoted the gas transfer into liquid. It was observed that a higher amount of oil corresponds to a higher value of  $k_{La}$ .

Effects of hydrate formation on the stability of water-oil dispersion and flowing were observed. Hydrate formation destabilized water-oil dispersion. Addition of AA-LDHI stabilized hydrate slurry flow and prevented plugging. Hydrate growth, agglomeration, heterogeneous hydrate flow and deposition on the pipe wall were observed by FBRM chord counts, hydrate morphology, density, pressure drop, and crystallization rate.

Effects of velocity, water cut, and pressure on gas hydrate formation, growth, and transportability in pipelines were also clarified. The increase in velocity increased the average rate of crystallization and improved hydrate slurry transport. Generally, the rise in water cut lowered the average rate of crystallization. In the presence of both AA-LDHI and salt, the increase in water cut enhanced the average rate of crystallization. The increase in pressure augmented the average rate of crystallization. Mostly, the rise in the average rate of crystallization led to quicker agglomeration rate.

Generally, the addition of adequate dosage of AA-LDHI prevent plug but AA-LDHIs increased the average crystallization rate and shortened the induction time. At 80%WC, interestingly, the addition of AA-LDHI (in the presence of salt) caused a lower average rate of hydrate formation. Otherwise, the effect of AA-LDHI on preventing deposition was negligible. Normally, the AA-LDHIs

lowered pressure drop, helped hydrate slurry flow more homogeneous, and prevented plugging. The AA-LDHs changed probably the hydrate particle size, structure of agglomeration and deposition.

Commonly, the addition of salt lowered significantly the average rate of crystallization and impacted positively on the performance of AA-LDHI (better performance of AA-LDHI in the presence of salt) such as lower pressure drop, less heterogeneous hydrate slurry flow, reducing hydrate deposition (in some cases) and avoiding plug.

The stability of hydrate slurry was investigated by SDR tests: the hydrate slurry flowing system was safely recovered after 10 minutes up to one hour of shutdown in the presence of 1-2%AA-LDHI.

Morphology of hydrate particles at 70-80-100%WC with/without AA-LDHI and/or salt was clearly observed by PVM images. The morphologies of hydrate particles depended on the initial composition of the experiments. There was a predominance of sphere shape along with the non-sphere shape of hydrate particles in the presence of oil phase. Hydrate morphology at 100%WC was totally non-sphere. Smaller hydrate particles were observed in the presence of AA-LDHI. In the presence of salt, sticky hydrate agglomerates were observed with a bigger and rougher surface. The presence of both salt and AA-LDHI led to a round-shape and rougher surface of hydrate particles.

#### 4.17. Remarques et Conclusions (in French)

A partir des résultats expérimentaux avec protocole de pompe Moineau avec et sans système de gaz-lift, plusieurs points importants peuvent être tirés :

Nous avons étudié la dispersion et la rhéologie de l'huile et de l'eau dans des systèmes à haute fraction d'eau (70-80% WC) avec/sans sel et AA-LDHI. Les résultats ont montré que l'addition d'AA-LDHI augmentait le nombre total de longueurs de corde mais diminuait la taille moyenne des gouttelettes en dispersion. En outre, la présence de sel diminuait le nombre total de longueurs de corde et augmentait la taille moyenne des gouttelettes de la dispersion. L'ajout d'huile a diminué la longueur de corde moyenne et augmenté le nombre total de longueurs de corde. Plus le débit était élevé, plus faible était la taille moyenne des gouttelettes et plus élevée était le nombre total de longueurs de corde. Un cisaillement plus élevé a amélioré les performances d'AA-LDHI (dispersion de l'huile dans l'eau) en présence de sel.

Le taux de transfert de gaz dans la phase liquide avec/sans sel et AA-LDHI a été étudié. En particulier, plus le débit est élevé, plus le  $k_L a$  est élevé. Généralement, l'addition d'AA-LDHI a favorisé le transfert de gaz dans le liquide. Plus la quantité d'huile était élevée, plus le  $k_L a$  était élevé.

Les effets de la formation d'hydrates sur la stabilité de la dispersion eau-huile et sur l'écoulement ont été observés. La formation d'hydrates déstabilise la dispersion eau-huile. L'ajout d'AA-LDHI peut aider à stabiliser l'écoulement d'hydrates et à empêcher le colmatage. La croissance, l'agglomération, le dépôt de particules d'hydrate, l'écoulement d'hydrates hétérogène et le dépôt d'hydrates sur la paroi de conduite ont été observés par sondes FBRM, PVM, par mesure de perte de charge et de densité ainsi que par calcul du taux de cristallisation.

Les effets de la vitesse, de la fraction d'eau et de la pression sur la formation, la croissance et le transport des hydrates de gaz dans les pipelines ont été mis en avant en détail. Plus le débit était élevé, plus la vitesse de cristallisation était élevée et meilleur était le transport de la suspension d'hydrates. En général, plus la fraction d'eau était haute, plus la vitesse de cristallisation était faible. En présence à la fois d'AA-LDHI et de sel, plus la fraction d'eau était haute, plus le taux de cristallisation était élevé. Plus la pression était élevée, plus la vitesse de cristallisation était élevée. Généralement, plus le taux de cristallisation était élevé, plus le taux d'agglomération était rapide.

Généralement, l'ajout d'une dose adéquate d'AA-LDHI a aidé à prévenir le bouchage, mais les AA-LDHIs ont principalement aidé à augmenter le taux moyen de cristallisation et à raccourcir le temps d'induction. À 80% WC, il est intéressant de noter que l'ajout d'AA-LDHI (en présence de sel) a

entraîné une diminution du taux de formation des hydrates. L'AA-LDHI n'a pas semblé aider à éviter les dépôts. Normalement, les AA-LDHI ont abaissé la perte de charge et aidé à avoir un écoulement d'hydrates plus homogène, ce qui a empêché le colmatage en changeant la taille des particules d'hydrate, la structure de l'agglomération et le dépôt.

Généralement, l'addition de sel abaissait significativement le taux de cristallisation et améliorait la performance d'AA-LDHI (meilleure performance d'AA-LDHI en présence de sel) avec une perte de charge plus faible, un écoulement d'hydrate moins hétérogène, en réduisant les dépôts d'hydrates (dans certains cas) et en évitant le bouchage.

La stabilité de l'écoulement d'hydrate a été étudiée par des tests de SDR : après une heure d'arrêt maximum en présence de 1 à 2% d'AA-LDHI, le système a été remis en écoulement en retrouvant ses conditions de fonctionnement initiales.

La morphologie des particules d'hydrates à 70-80-100%WC avec/sans AA-LDHI et/ou sel a été clairement observée par les images PVM. Les morphologies des particules d'hydrate dépendaient de la composition initiale des expériences. Il y avait majoritairement des hydrates sous la forme de sphères et sous la forme de petites particules non sphériques en présence de la phase huileuse. La morphologie des hydrates à 100%WC était totalement non sphérique. De plus petites particules d'hydrate ont été observées en présence d'AA-LDHI. En présence de sel, les particules d'hydrate semblaient être plus grandes avec une surface rugueuse et des agglomérats collants ont été observés. La présence de sel et d'AA-LDHI semble orienter les particules d'hydrate vers une forme ronde et une surface plus rugueuse.

## **CHAPTER 5. PROPOSED MECHANISMS AND RELATIVE PRESSURE DROP MODEL IN HIGH WATER CUT SYSTEMS**

*Go as far as you can see; when you get there, you'll be able to see further.*

*Thomas Carlyle*

This chapter will show the proposed mechanisms for hydrate formation, agglomeration, deposition and plugging in high water cut systems with Moineau pump protocol. A relative pressure drop model is also developed based on the Mills model (1985). This developed model uses  $K_v$  factor (hydrate agglomerate structure which is a function of pressure, dosage of salt and AA-LDHI, water cut and velocity) and describes the relative pressure drop in flowlines once hydrate formed.

### **5.1. Proposed mechanisms at 100%WC**

In this study, two important phenomena during crystallization were observed: (1) quick and slow heterogeneity of hydrate slurry (details in section 4.4) and (2) low and high flowrate plugging mechanism (sections 4.3 and 4.8). In addition, a positive effect of salt on the performance of AA-LDHI to prevent plug was revealed. All these mechanisms are proposed in the following sections: 5.1.1, 5.1.2, and 5.1.3.

#### **5.1.1. Quick and slow heterogeneity of hydrate slurry**

From the previous common findings, it was believed that hydrate slurry becomes gradually heterogeneous from the homogeneous state. However, in this work (section 4.4), heterogeneous hydrate slurry at the beginning of hydrate formation was witnessed. This was explained by the high rate of crystallization and quick agglomeration of hydrate particles. Based on these observations and explanations, two mechanisms were proposed for a quick (a) and slow (b) heterogeneity of hydrate slurry (Figure 5. 1). In the mechanism of quick heterogeneity of hydrate slurry (Figure 5. 1 a), once hydrates formed, they can attach quickly forming large agglomerates. This caused rapidly a heterogeneous hydrate flow. Afterwards, these large agglomerates might deposit on the pipe wall. When hydrates deposited, hydrate slurry flow was more homogeneous. In the mechanism of slow heterogeneity of hydrate slurry (Figure 5. 1 b), once hydrates formed, they can be dispersed in the flow. Progressively, hydrates agglomerate leading to heterogeneous flow. This could cause hydrate deposition on the pipe wall and/or the presence of hydrate moving beds in the flow.

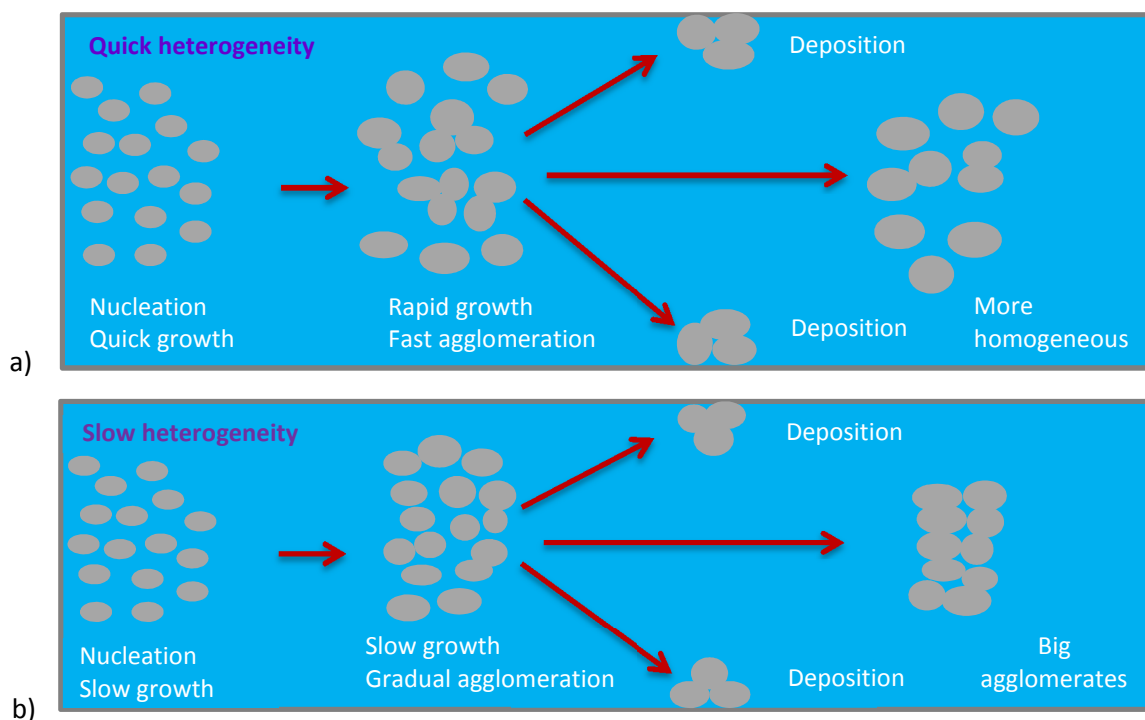
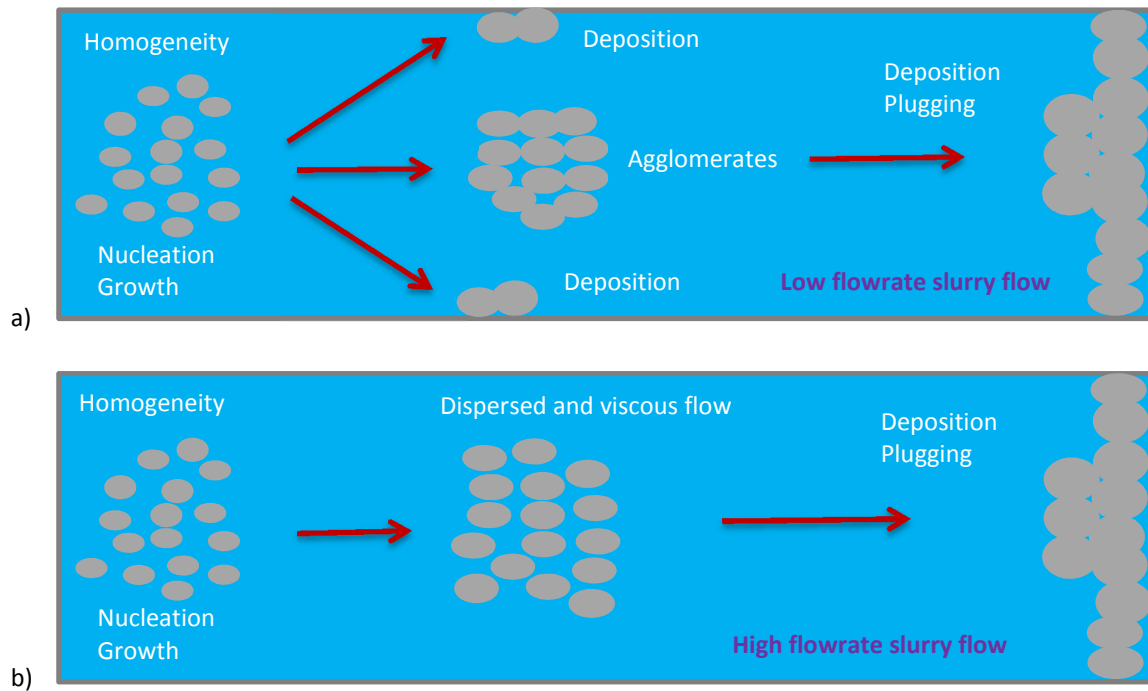


Figure 5. 1: Mechanism of quick (a) and slow (b) heterogeneity of hydrate slurry.

### 5.1.2. Low and high flowrate plugging mechanisms

As aforementioned (sections 4.3 and 4.8), low and high flowrate had different effects on plugging mechanisms. In fact, higher flowrate enhanced hydrate slurry transport compared to the low flowrate. In details, the high shear improved the dispersion of hydrate particles in flowlines. In all experiments at high flowrate, pressure drop increased gradually up to 8-12 bar and plugging occurred once pressure drop reached the limit value (for experiments without or with a dosage of AA-LDHI less than 0.5 wt.%). On the contrary, at low flowrate, hydrate particles was less dispersed or more deposited in the flowloop (in the separator and/or wall of pipe). Consequently, plugging occurred suddenly although pressure drop was quite low (~2 bar) compared to pressure drop in high flowrate (8-12 bar). In both low and high flowrate, once plugging occurred, flowrate fell down to zero and pressure drop increased suddenly to the highest value (12-15 bar). Based on these observations and explanations, two mechanisms were proposed for plugging at low (a) and high (b) flowrate as shown in Figure 5. 2. In the low flowrate plugging mechanism (Figure 5. 2 a), in the onset of hydrate formation, hydrate flow can be in the homogeneous state. However, hydrate might deposit and/or agglomerate to form a plug. These phenomena are because of low shear at low flowrate. In the high flowrate plugging mechanism (Figure 5. 2 b), once hydrates formed, hydrate flow can be in the homogeneous state during a long period of time. This is due to high shear at high flowrate enhanced

hydrates dispersion in pipelines. Finally, hydrate particles can agglomerate (causing heterogeneous hydrate flow) and/or deposit, forming a plug.



**Figure 5. 2: Mechanism of hydrate slurry plugging at low (a) and high (b) flowrate.**

### 5.1.3. Role of salt to enhance the performance of additive

In fact, the nature of hydrate is a combination of water and gas molecules building hydrate structure. Because water is a polar molecule, it means that on the surface of hydrate particles there are a partial negative charge of oxygen and a partial positive charge of hydrogen. These are created by the interaction between an atom of oxygen and two hydrogen atoms in the water molecule. As a result, hydrates attract polar molecules and ions. Indeed, the addition of salt (NaCl) caused more ions in the mixture. Therefore, cation ( $\text{Na}^+$ ) and anion ( $\text{Cl}^-$ ) dissolved (from NaCl molecule) in water will adsorb on the surface of hydrate particles. As a result, this will help AA-LDHI adsorb easily in many different ways on the surface of hydrate particles (much better than the absence of NaCl). As a result, this will prevent agglomeration and plug by decreasing the cohesion forces between hydrate particles. Thanks to the absorption of AA-LDHI on the surface of hydrate particles, the size of hydrate particles would be smaller and finer (see Figure 4. 39 and Figure 4. 46 in section 4.15). This mechanism is described in Figure 5. 3.

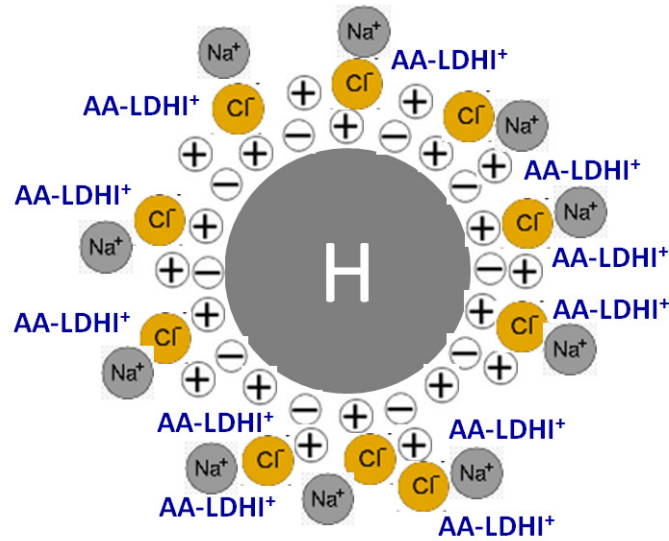


**Figure 5. 3: Proposed mechanism of hydrate particle-AA-LDHI-salt interaction in preventing plug.**

In addition, at 80%WC, (Zerpa, 2013) suggested that the presence of salt could decrease the interaction energy of surfactant and water phase. Once hydrate formed, the amount of water decreased. Consequently, the amount of salt in liquid water increased gradually. These phenomena led to a change from water continuous phase to oil continuous phase. As a result, hydrate particles were transported in the oil continuous phase better than that in the water continuous phase in the presence of AA-LDHI by lowering adhesion forces between hydrate particles and pipe surface (agreed with the conclusion in Chapter 3). Nagappayya et al., (2015) also indicated that higher salinity increased the solubility of surfactants in oil forming W/O emulsion which impacts positively on the performance of AA-LDHIs.

## 5.2. Relative pressure drop model developed

Pressure drop depends significantly on the viscosity of fluids (and the presence of solids) in the pipelines. The increase in pressure drop is attributed to the increase in viscosity caused by hydrate particles and agglomerate structures. In this study, the correlation of relative pressure drop ( $RPD$  or  $\Delta P_r$ ) as a function of hydrate volume ( $\phi$ ) and agglomerate structure ( $K_v$ ) was performed by modifying the model of Mills (1985) and replacing  $\mu_r$  (relative viscosity) by  $\Delta P_r$  with a correction (structural) or effective volume fraction factor ( $K_v$ ) and additional exponent coefficient ( $n$ ). The relative pressure drop was calculated as the ratio of the instantaneous pressure drop (after hydrate crystallization) to the pressure drop measured prior to hydrate formation. This developed model (as shown in equation 5.1 and 5.2) is to predict relative pressure drop in oil and gas production and transportation in offshore pipelines in high water cut systems. It is based on the flowloop

experimental results with Moineau pump protocol. The term of  $K_v$  is defined as the ratio of total volume fraction ( $\phi_{\text{eff}}$ ) of hydrate agglomerates and liquid (oil and/or water) trapped in hydrate agglomerates and inside the hydrate shell (Douglas J. Turner et al., 2009) to the volume fraction of hydrate agglomerates ( $\phi$ ), as shown in Figure 5. 4. In details, a total (effective) hydrate volume fraction ( $\phi_{\text{eff}}$ ) is defined as the sum of the real volume of hydrate particles (agglomerates) plus the volume of trapped liquids between particles (agglomerates) and/or plus the volume of liquids (oil and/or water) in the hydrate shell. The  $K_v$  is also a so-called structural agglomerate factor. The fact that the  $K_v$  can be significantly higher than 1, depending on the experimental conditions (Figure 5. 4 a-f). The  $K_v$  also depends principally on the size of hydrate particles and the way they attach to form hydrate agglomerate structure. In addition, unconverted water and/or oil in hydrate shell contribute to the increase in  $K_v$ . Several previous studies proved that once hydrate formed, hydrate particles tend to attach forming porous hydrate agglomerates with liquid trapped inside (Camargo, 2002), (Colombel et al., 2009), (Fidel-Dufour et al., 2006), (Palermo et al., 2005), (Leba et al., 2010b), (Pauchard et al., 2005), and (Austvik et al., 2000). It is supposed that the size of hydrate agglomerates depends on the balance between the rate of hydrate particles agglomeration and breakage or between hydrodynamic (shear) and adhesive force (Colombel et al., 2009). The role of AA-LDHI in this present study is to reduce the size of hydrate agglomerates but not prevent agglomeration completely.

From the experimental results, it is observed that at dilute disperse system (0-0.1 of hydrate volume fraction), there is a very small increase in relative pressure drop. It is assumed that there is not enough hydrate volume to increase considerably the relative pressure drop and almost no liquid trapped inside individual hydrate particles. However, at more concentrated disperse system (from a range of 0.1-0.2 of hydrate volume fraction), a considerable increase in relative pressure drop is observed. This is possibly due to the higher viscosity of suspension with higher hydrate volume and the significant liquid trapped between hydrate particles and agglomerates. This hydrate volume range (0.1-0.2 of HV) could be an agglomeration transition threshold. As described in section 1.3.4.2, it is necessary to add an extra coefficient in the model of Mills (1985) to convert the relative viscosity model to the relative pressure drop model. In this study, an exponent coefficient ( $n$ ) was added for the variable of  $(\phi_{\text{eff}}/\phi_{\text{max}})$  into the model of Mills to fit better the experimental data with a developed model which also applies to highly concentrated disperse systems. The developed model is as follows:

$$\Delta P_r = \frac{\Delta P(t)}{\Delta P(t_0)} = \frac{1 - \Phi_{eff}}{\left[1 - \left(\frac{\Phi_{eff}}{\Phi_{max}}\right)^n\right]^2} \text{ and } \Phi_{max} = 0.74 \quad (5.1)$$

$$\Phi_{eff} = K_v \Phi \quad (5.2)$$

Where  $\Delta P(t)$  is the instantaneous pressure drop at the time ( $t$ ) of the crystallization process;  $\Delta P(t_0)$  is the initial pressure drop at the time ( $t_0$ ) just before hydrate formation;  $n$  is a new degree of freedom to convert the relative viscosity model of Mills (1985) to the relative pressure drop model ( $n=1$  for laminar regime and  $n>1$  for turbulent regime). In this present work, it is supposed that the flow regime is always turbulent in the presence of hydrate particles and the optimized  $n$  is equal to 1.26;  $\phi_{eff}$  is an effective particle hydrate volume fraction (-);  $\phi$  is the real hydrate volume fraction (-);  $K_v$  is correction (structural) agglomerate factor;  $\phi_{max}$  is the maximum volume fraction of randomly packed hydrate particles. The  $\phi_{max}$  is equal to 0.74 which represents highly poly-dispersed systems, (Quemada, 1977) and (Krieger, 1972).

In this work, it is supposed that the agglomerate structure factor ( $K_v$ ) was influenced by the presence of additive and/or salt. This factor also depends on the velocity, water cut, and pressure. It is important to note that generally, the higher crystallization rate, the larger and faster hydrate agglomerates formed. This also caused the more heterogeneous hydrate flow (Hoekstra et al., 1992). The higher value of  $K_v$  corresponds to the larger hydrate agglomerates and the larger liquid trapped in a specific volume of hydrate agglomerates. The bigger hydrate agglomerates, the higher pressure drop was observed. In the presence of both salt and AA-LDHI, a small increase in pressure drop in flowlines was witnessed even at a relative high hydrate volume, probably due to very little fluid trapped between very small hydrate particles. As mentioned above and in section 4.12, at 80%WC, there was not only liquid water but also oil droplets trapped inside the hydrate agglomerates. Consequently, more complex hydrate agglomerates and heterogeneous multiphase flow are formed at 80%WC than those at 100%WC.

In the present work, the coefficient of multiple determinations ( $R^2$  is in the range of 0 to 1) is used to determine the fit between the experimental data and developed model. If the coefficient of multiple determinations approaches 1 then this is supposed to attain a good agreement between the experimental and regressed data.  $\bar{R}(t)$  is the average crystallization rate which was described in section 2.6.4 and details in Appendix D.

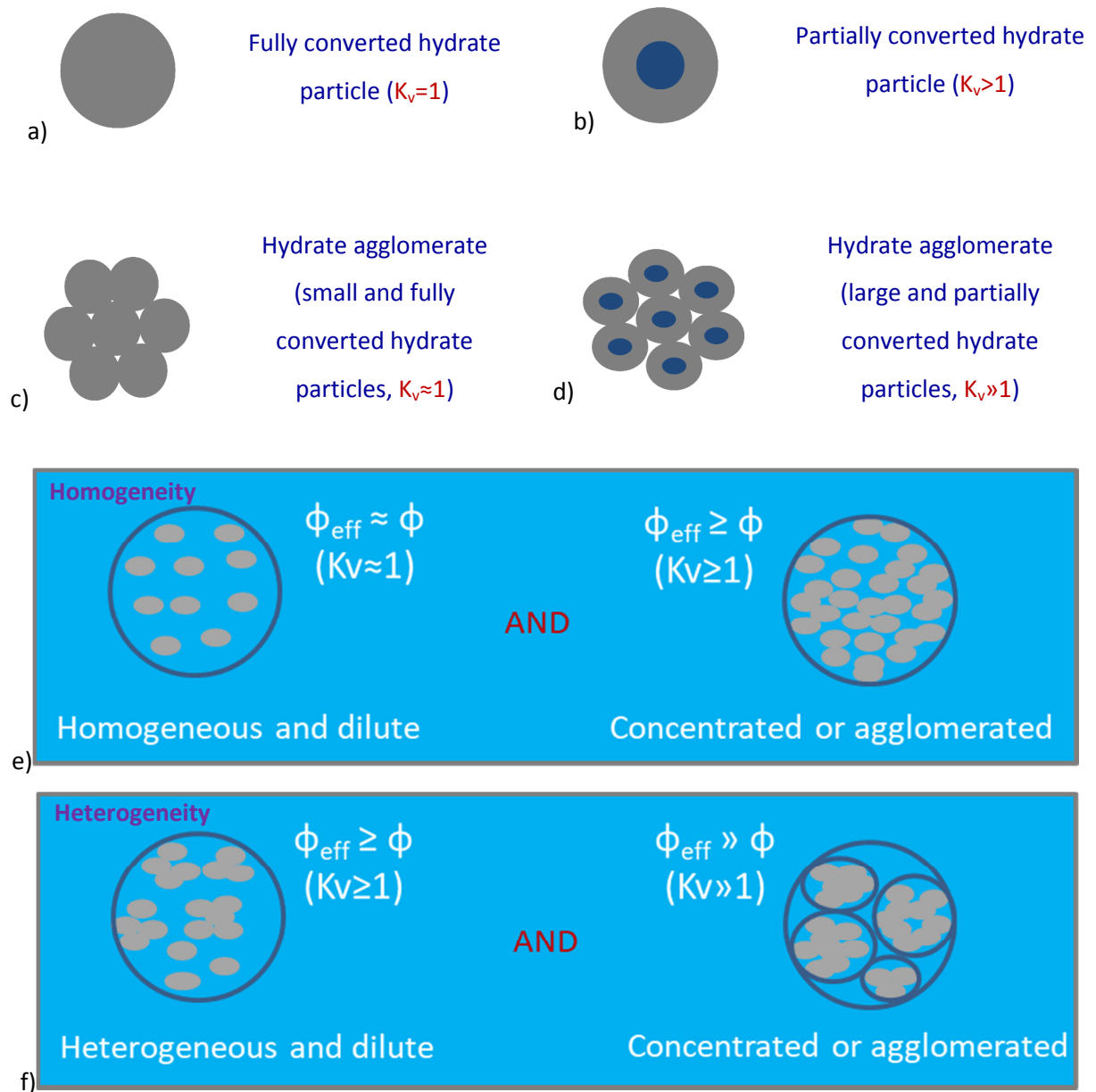


Figure 5. 4: Fully (a) and partially (b) converted hydrate particle; different hydrate agglomerate structures (c-d); homogeneous (e) and heterogeneous (f) hydrate suspension flow.

### 5.2.1. Effect of velocity

At a higher velocity, a higher average crystallization rate was observed. This may lead to a higher rate of agglomeration and also larger hydrate agglomerates or higher  $K_v$ , or higher relative pressure drop (Figure 5. 5).

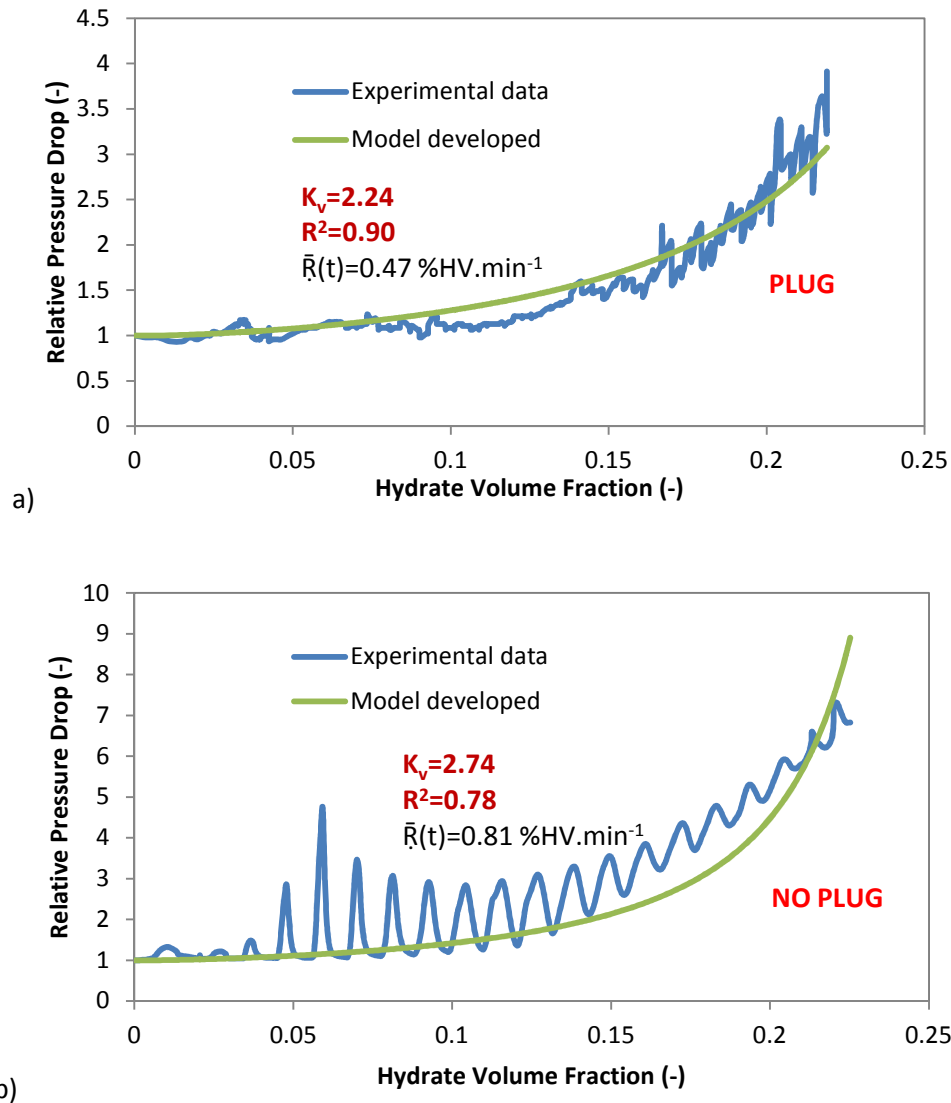


Figure 5. 5: Effect of velocity on relative pressure drop [the experiments with 100%WC-1%AA-LDHI-85%LV-75bar: 150L.h<sup>-1</sup> (a) and 400L.h<sup>-1</sup> (b)].

### 5.2.2. Effect of water cut

The presence of oil increased the value of  $K_v$  in the presence of AA-LDHI and salt (Figure 5. 6). It is supposed that after hydrate formation, hydrate flow at 80%WC contained hydrate agglomerates with larger sizes than those at 100%WC. As a result, more heterogeneous (more fluctuated relative pressure drop) hydrate flow was observed at 80%WC than the one at 100%WC.

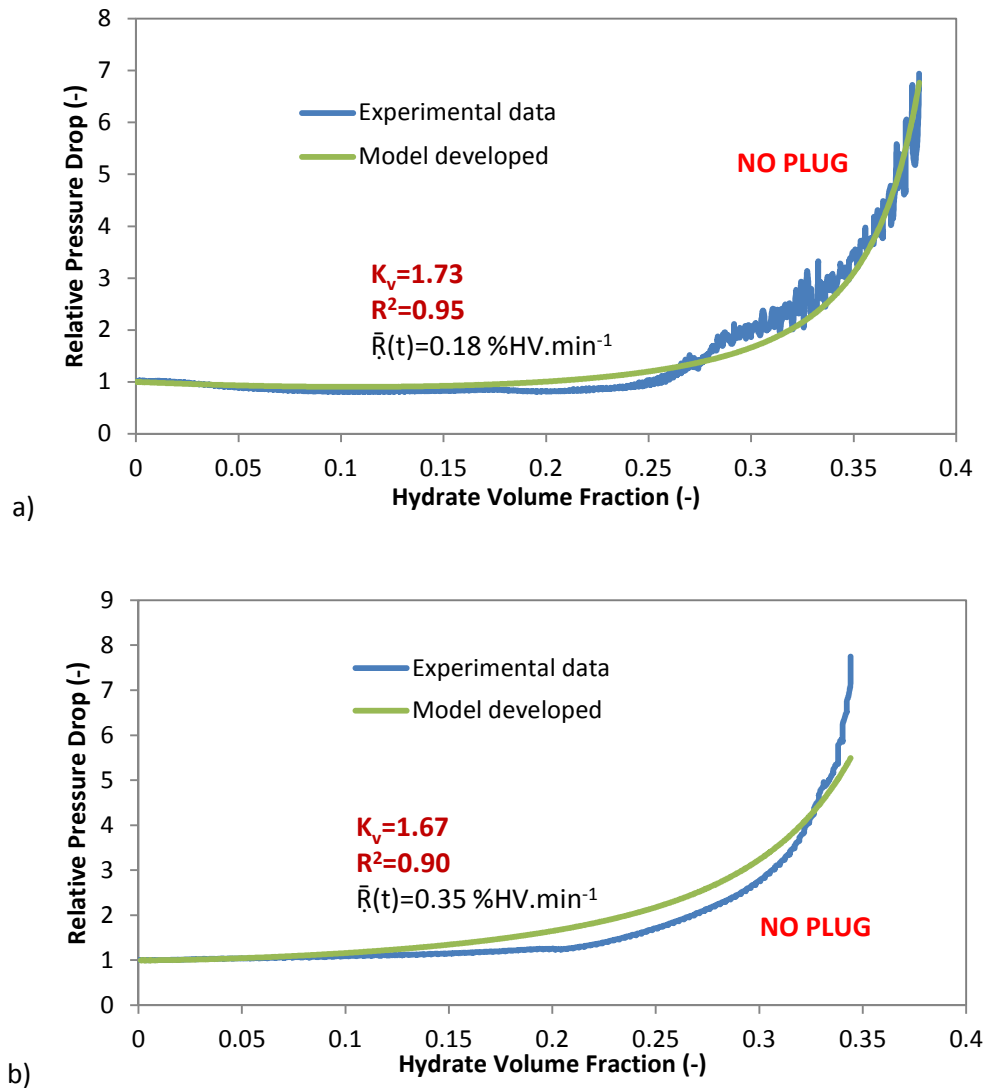
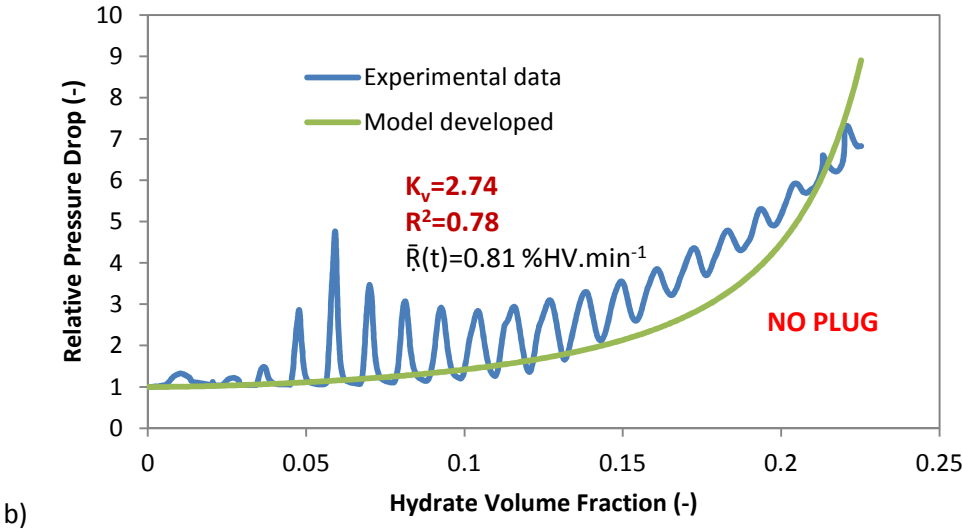
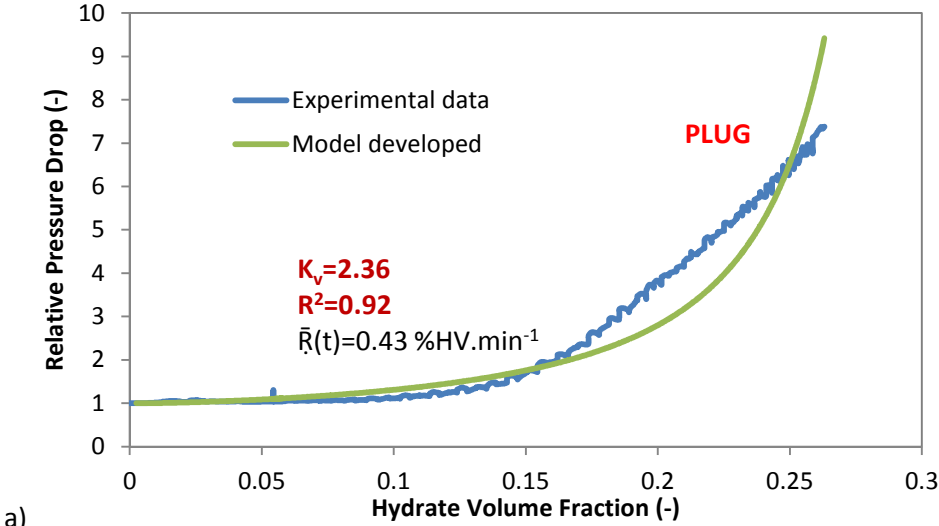


Figure 5. 6: Effect of water cut on relative pressure drop [the experiments with NaCl-1%AA-LDHI-85%LV-400L.h<sup>-1</sup>-75bar: 80%WC (a) and 100%WC (b)].

### 5.2.3. Effect of additive

As aforementioned,  $K_v$  represents the agglomerate structure and the liquid trapped in a volume of hydrate slurry. Different relative pressure drops with different dosage of AA-LDHI were observed (Figure 5. 7). This was assumed that the more fluctuation of relative pressure drop, the more heterogeneity hydrate slurry flow. This variation of relative pressure drops observed was due to the difference in the rate of crystallization. The increase in the rate of hydrate formation augmented the rate of agglomeration leading to more heterogeneous hydrate flow. Indeed, it was found that the heterogeneity of hydrate flow was proportional to structural factor ( $K_v$ ). It is assumed that the higher rate of agglomeration led to the larger size of agglomerates. Consequently, more

liquid trapped in a hydrate volume or  $\Phi_{eff}$  was much larger than  $\phi$ . Moreover, the higher value of  $K_v$ , the more fluctuated relative pressure drop was observed at the same hydrate volume. The experiments with a dosage of AA-LDHI starting from 1 wt.% of water did not show plug while the experiment with 0.5%AA-LDHI showed plug at the same RPD=7.3. This can be attributed to the role of commercial AA-LDHI in dispersing hydrate particles and preventing plug.



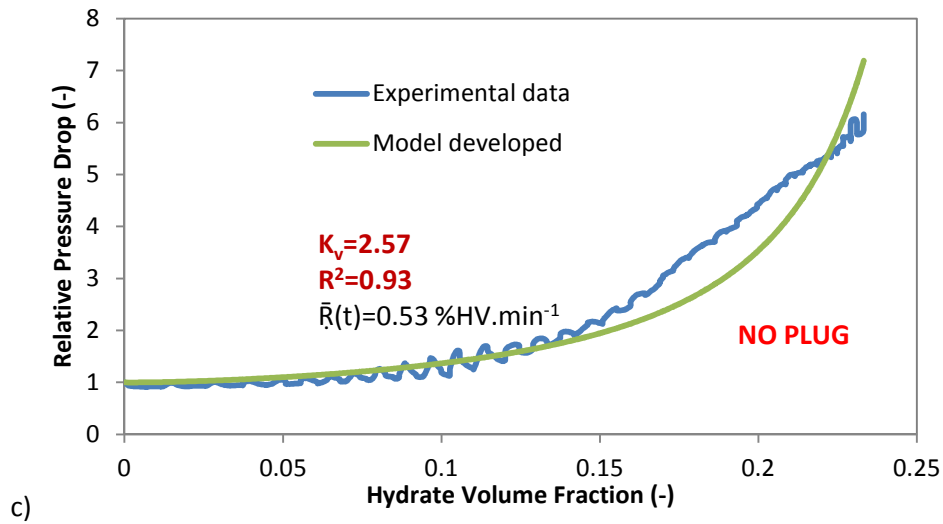
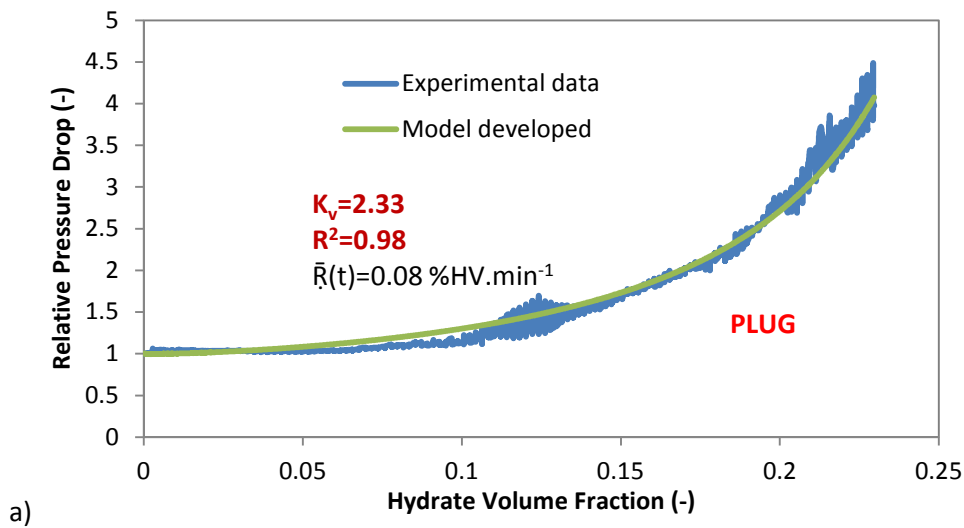


Figure 5. 7: Effect of additive on relative pressure drop [the experiments with 100%WC-85%LV-400L.h<sup>-1</sup>-75bar: 0.5% (a) - 1% (b) - 2% (c) AA-LDHI].

The effect of AA-LDHI (in the presence of salt) on the RPD is also shown in Figure 5. 8. The AA-LDHI increased the rate of crystallization. However, more homogeneity of hydrate slurry flow was noticed. This was attributed to the role of AA-LDHI (in the presence of salt) in dispersing hydrate particles and decreasing RPD. The value of  $K_v$  in the experiment with AA-LDHI was lower than the one in the experiment without AA-LDHI. It is supposed that larger hydrate agglomerates formed in the absence of AA-LDHI even at low average crystallization rate. These large hydrate agglomerates caused more heterogeneity of hydrate flow and also more liquid trapped in the aggregated hydrate volume which led to higher RPD (higher  $K_v$ ).



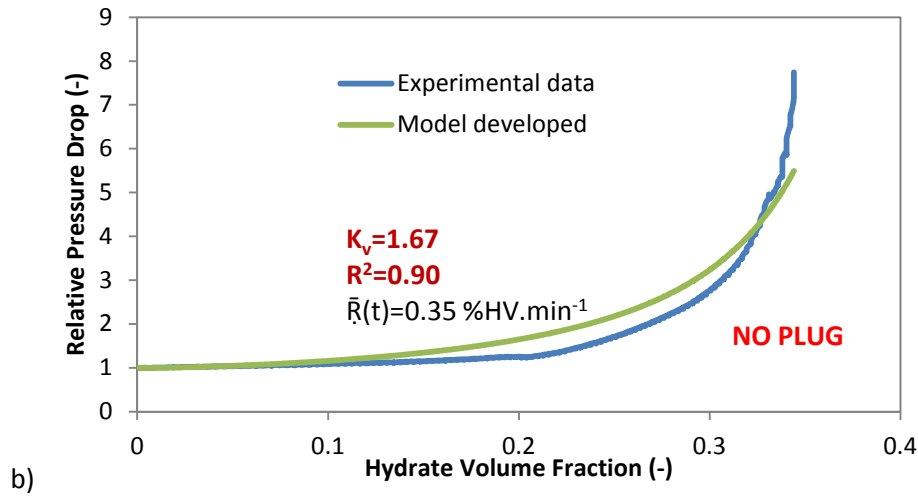


Figure 5. 8: Effect of additive on relative pressure drop [the experiments with 100%WC-NaCl-85%LV-400L.h<sup>-1</sup>-75bar: 0% (a) - 1% (b) AA-LDHI].

#### 5.2.4. Effect of salt

Combination of salt and AA-LDHI increased the performance of AA-LDHI. A smoother curve of pressure drop for the experiment with both salt and AA-LDHI compared to the one with only AA-LDHI was observed (Figure 5. 9). Furthermore, at the same hydrate volume, RPD of the experiment with only AA-LDHI was higher than that of the experiment with both salt and AA-LDHI. This can be explained as follows: firstly, the addition of salt decreased the average crystallization rate leading to a decrease in the rate of agglomeration. As a result, hydrate slurry flow was more homogeneous at a lower rate of hydrate formation. Secondly, as stated in section 5.1.3, salt helped to attract more AA-LDHI on the surface of hydrate particles. Therefore, this prevented agglomeration and also decreasing hydrate particle size. This means that there was less liquid trapped between hydrate particles in contact due to the decrease in their free spaces. This was also explained by the more oil-wet surface of hydrate particles formed.

This is obvious that the structural factor value of the experiment with both salt and AA-LDHI ( $K_v= 1.00$  with both AA-LDHI and salt) was lower than that of the experiment with only AA-LDHI ( $K_v= 2.24$  with only AA-LDHI) (Figure 5. 9). This evidence confirmed the different agglomerate structures between two hydrate slurries. The lower value of  $K_v$  corresponds to the more homogeneity of hydrate slurry flow.

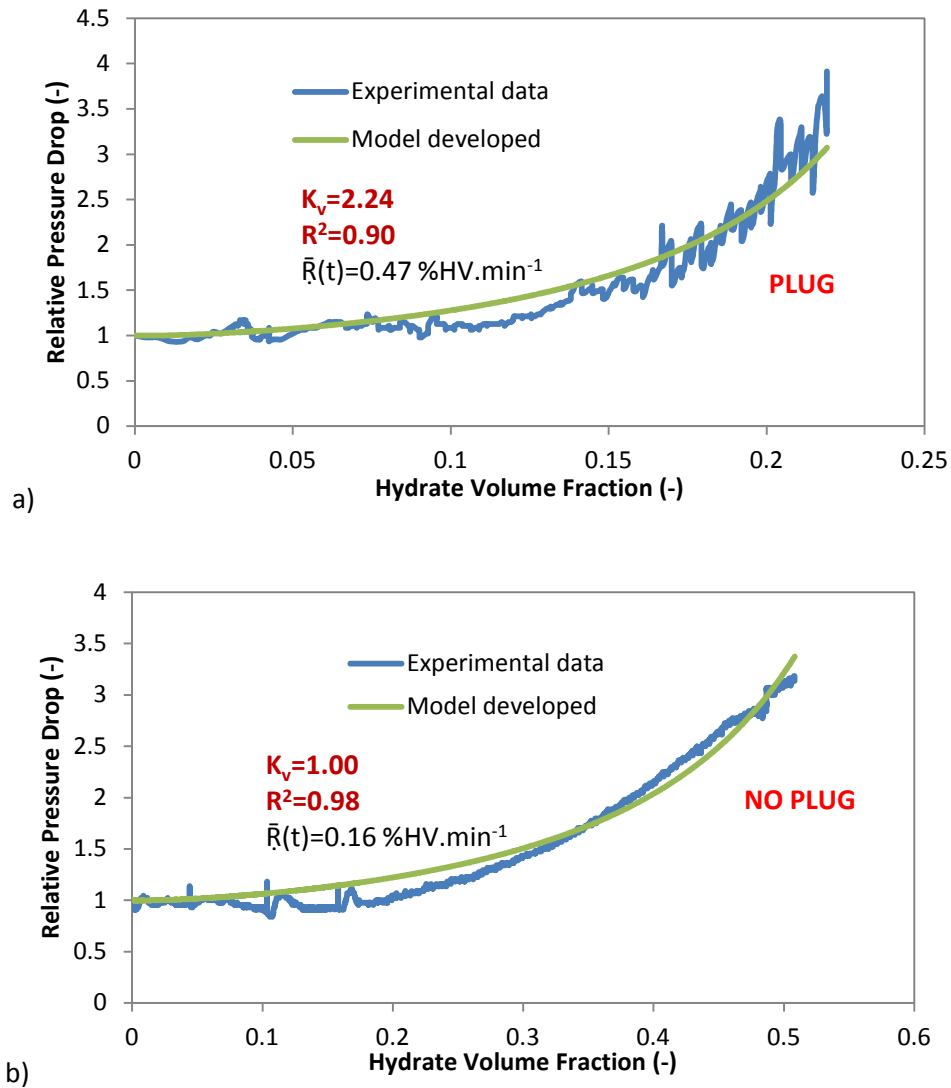


Figure 5. 9: Effect of salt on relative pressure drop [the experiments with 100%WC-1%AA-LDHI-85%LV-150L.h<sup>-1</sup>-75bar: without (a) and with salt (b)].

### 5.2.5. Effect of pressure

The relative pressure drop in the experiment at higher pressure was more fluctuated than the one at lower pressure (Figure 5. 10). This was again explained by the higher rate of crystallization at higher pressure leading to higher rate of agglomeration. As a consequence, the higher pressure led to the more heterogeneous hydrate flow. This caused higher RPD at higher pressure (at the same hydrate volume) as seen in Figure 5. 10. It is obvious that the value of  $K_v$  at higher pressure was higher than that at lower pressure. This was explained that the higher pressure caused the larger hydrate agglomerates with more liquid trapped inside.

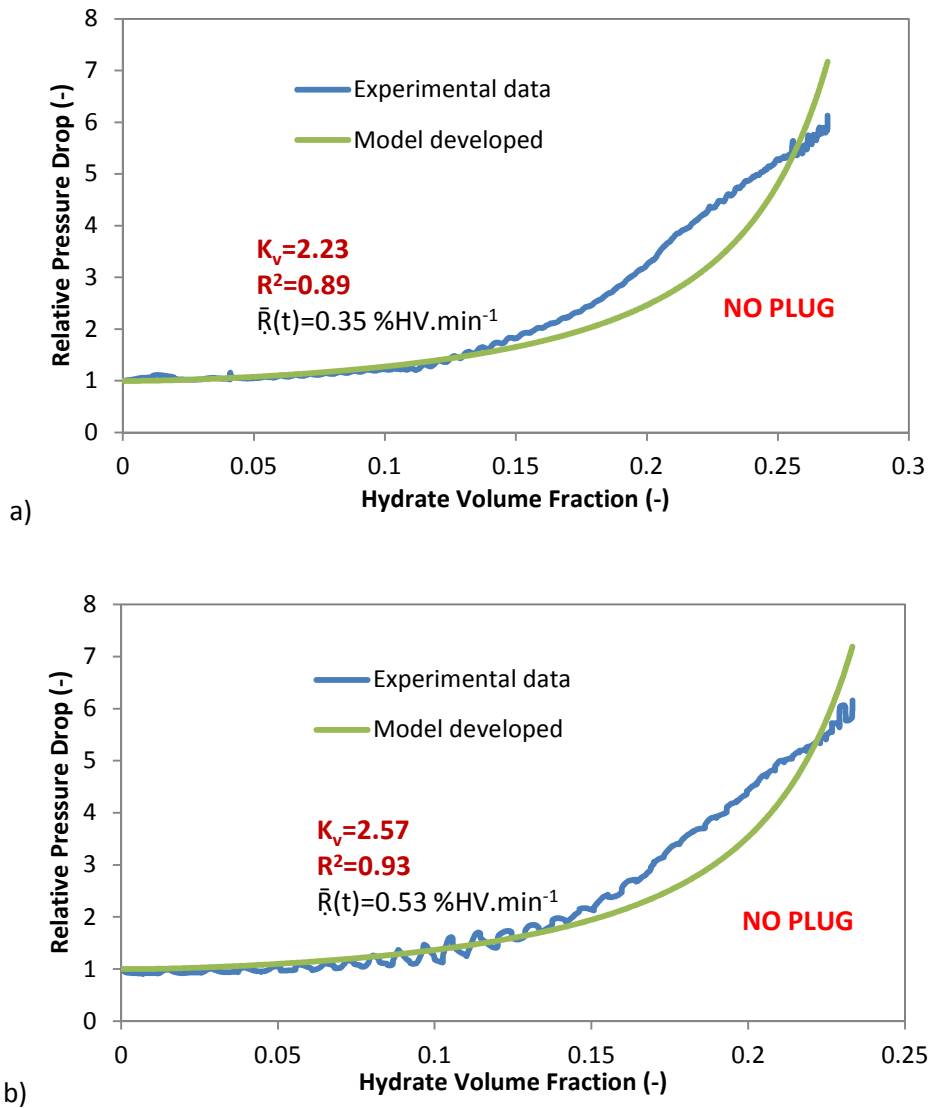


Figure 5. 10: Effect of pressure on relative pressure drop [the experiments with 100%WC-2%AA-LDHI-85%LV-400L.h<sup>-1</sup>: 70bar (a) and 75bar (b)].

### 5.2.6. Effect of hydrate formation on the stability of suspension

As aforementioned in section 4.7, hydrate formation can impact on the oil-water-hydrate suspension. Indeed, a decrease in pressure drop from the beginning of hydrate formation up to 25%HV was observed. This was attributed to the breaking of oil-water dispersion (decrease in viscosity) after hydrate formation. This might also because a very smooth hydrate layer on the pipe wall modified the roughness and behavior of pipe wall surface. After a certain period of time, hydrate particles detached from the pipe wall and then agglomerated forming large hydrate moving beds. This led to a sharp increase and fluctuation in pressure drop. This phenomenon (decrease in pressure

drop) was different from those mentioned above. In this case, it is supposed that the coefficient  $n$  was equal to 2.15.  $K_v$  calculated was of 1.73 (Figure 5. 11).

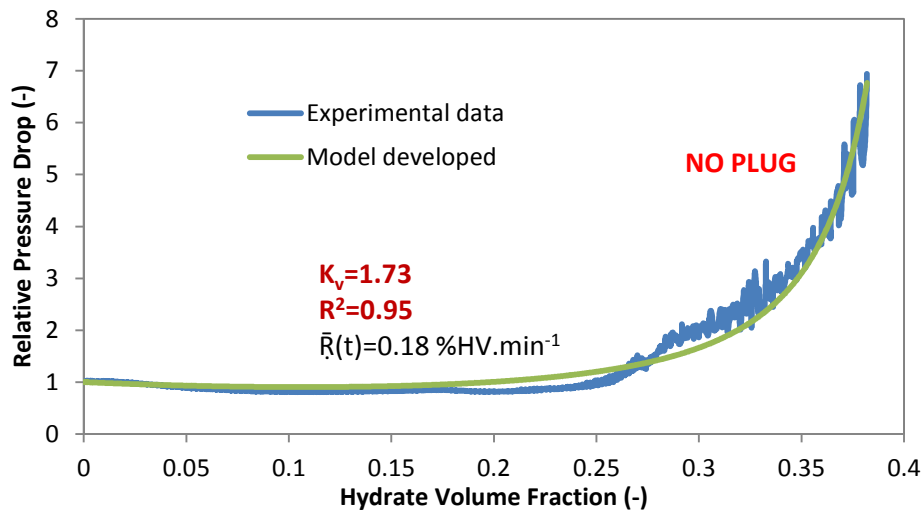


Figure 5. 11: Effect of hydrate formation on the stability of suspension (relative pressure drop) at 80%WC-NaCl-1%AA-LDHI-85%LV-400L.h<sup>-1</sup>-75bar.

### 5.2.7. Evaluation of model developed

Comparing the model developed with experimental results, it agreed well with the experimental data, especially with homogeneous hydrate flow. The coefficient of multiple determinations ( $R^2$ ) is in the range of 0.76 to 0.98. It is recalled that this proposed model describes well the hydrate agglomerate structures ( $K_v$ ) and is to predict the relative pressure drop in pipelines. The  $K_v$  is between 1.00 and 2.74. A list of crucial parameters in order to develop the presented model is given in Table 5. 1. The deviations might be explained by several assumptions as follows:

- (1) It is supposed that  $\phi_{max}$  is constant (0.74) regardless of flowrate, salt, and AA-LDHI. The fact that the  $\phi_{max}$  might be a function of shear (Quemada, 1977) and/or depend on the presence of salt and/or AA-LDHI.
- (2) In this study, it is supposed that  $K_v$  is constant. In fact, the  $K_v$  can change until hydrate particles reaching a maximum packing volume fraction,  $\phi_{max}$  (Quemada, 1977).  $K_v$  might be dependent on crowding and shearing effects on the formation of agglomerates.
- (3) In this model, the hydrate deposition phenomenon was not taken completely into account yet.

**Table 5. 1: Important parameters ( $K_v$ ,  $R^2$ , and  $\bar{R}(t)$ ) of the experimental tests to develop relative pressure drop model.**

WC	Flowrate	Liquid Volume	Pressure	AA-LDHI	NaCl	$\bar{R}(t)$	Structural agglomerate factor	Coefficient of multiple determination	PLUG
(%)	(L.h <sup>-1</sup> )	(%)	(bar)	(wt.% of water)	(g.L <sup>-1</sup> (H <sub>2</sub> O))	(%HV.min <sup>-1</sup> )	( $K_v$ )	( $R^2$ )	-
100	400	85	75	0.50	0	0.43	2.36	0.92	YES
	150	85	75	1	0	0.47	2.24	0.90	YES
	400	85	75	1	0	0.81	2.74	0.78	NO
	400	85	70	2	0	0.35	2.23	0.89	NO
	400	85	75	2	0	0.53	2.57	0.93	NO
	400	85	75	0	30	0.08	2.33	0.98	YES
	400	85	75	0.50	30	0.35	1.33	0.95	NO
	150	85	75	1	30	0.16	1.00	0.98	NO
	400	85	75	1	30	0.35	1.67	0.90	NO
80	400	85	75	1	0	0.72	2.22	0.83	NO
	150	85	75	1	30	0.10	1.12	0.76	NO
	400	85	75	1	30	0.18	1.73	0.95	NO

### 5.3. Highlights and Conclusions

Several conclusions in this chapter are provided as follows:

The new hydrate transport phenomena obtained from the flowloop experimental results helped to understand and propose new conceptual mechanisms of gas hydrate formation/agglomeration/deposition and plugging in flowlines in high water cut systems. Different flowrates led to different agglomeration/deposition and plugging mechanisms. The higher rate of crystallization led to the faster rate of hydrate slurry agglomeration and heterogeneity.

The role of salt to enhance the effectiveness of additive was attributed to (1) the more additives adsorbed on the surface of hydrate particles and (2) the phase inversion from water to oil continuous phase.

A relative pressure drop model was proposed by developing the model of Mills (1985). Our model used relative pressure drop instead of relative hydrate slurry viscosity. A good agreement between the experimental and model data was obtained.  $K_v$  in our model represented the structure of hydrate agglomerates. The higher value of  $K_v$ , the larger hydrate agglomerates were observed. This led to more liquid trapped inside of aggregated hydrate particles. The larger hydrate agglomerates led to the higher relative pressure drop and the more heterogeneous flow which may cause a higher risk of hydrate plug.

AA-LDHI, salt, velocity, water cut, and pressure impacted on the hydrate agglomerate structure factor ( $K_v$ ) which was proportional to RPD. In fact, AA-LDHI decreased the size of hydrate particles and agglomerates which led to lower RPD (decrease in  $K_v$ ), preventing plug. However, the higher amount of AA-LDHI might cause bigger hydrate agglomerates because of a higher rate of crystallization (AA-LDHIs promoted hydrate formation). The higher velocity and pressure caused a higher rate of hydrate crystallization leading to larger hydrate agglomerate size and more heterogeneous hydrate flow. Generally, the presence of oil augmented the value of  $K_v$ . The combination of AA-LDHI and salt decreased RPD or  $K_v$ . In other words, this decreased the size of hydrate agglomerates and led to the better dispersion of hydrate particles. Effect of hydrate formation on the stability of suspension (relative pressure drop) was also mentioned.

#### 5.4. Remarques et Conclusions (in French)

Plusieurs conclusions peuvent être tirées dans ce chapitre :

Les nouveaux phénomènes de transport d'hydrates observés lors des expériences ont aidé à proposer de nouveaux mécanismes conceptuels de formation/agglomération/dépôt et bouchage d'hydrates de gaz dans les conduites d'écoulement à haute fraction d'eau. Différents débits ont conduit à différents mécanismes d'agglomération/dépôt et de blocage. Un taux plus élevé de cristallisation conduit à une vitesse plus rapide d'agglomération de la suspension d'hydrates et de son hétérogénéité.

Le rôle du sel pour améliorer l'efficacité de l'additif a été interprété par (1) l'amélioration des additifs adsorbés sur la surface des particules d'hydrate et (2) l'inversion de la phase continue en eau à une phase continue en huile.

Un modèle de perte de charge relative a été proposé à partir du modèle de Mills (1985), en utilisant la perte de charge relative au lieu de la viscosité relative de la suspension d'hydrate. Il y a une bonne cohérence entre les données expérimentales et les données développées par le modèle. Le terme de  $K_v$  dans le modèle de perte de charge relative représente la structure des agglomérats d'hydrates. Plus grande est la valeur de  $K_v$ , plus gros sont les agglomérats d'hydrates et plus la quantité de liquide piégé à l'intérieur du volume d'hydrate aggloméré est importante. Plus gros sont les agglomérats d'hydrates, plus la perte de charge relative est importante et l'écoulement hétérogène, ce qui peut causer un risque plus élevé de formation de bouchons d'hydrates.

L'AA-LDHI, le sel, la vitesse, la fraction d'eau et la pression ont influé sur le facteur de structure des agglomérats d'hydrates ( $K_v$ ) qui est proportionnel à la RPD. En fait, l'AA-LDHI favorise la réduction de la taille des particules d'hydrates et des agglomérats, ce qui conduit à une diminution de la RPD (diminution de  $K_v$ ) empêchant la formation de bouchons. Cependant, la quantité plus élevée d'AA-LDHI peut provoquer des agglomérats d'hydrates plus importants en raison d'un taux de cristallisation plus élevé (l'AA-LDHI favorise la formation d'hydrates). La vitesse et la pression plus élevées ont provoqué un taux plus élevé de cristallisation des hydrates conduisant à une plus grande taille des agglomérats d'hydrates et à un écoulement des hydrates plus hétérogène. Généralement, la présence d'huile a augmenté la valeur de  $K_v$ . La combinaison d'AA-LDHI et de sel a diminué le RPD ou le  $K_v$ . En d'autres termes, la taille des agglomérats d'hydrates a été diminuée et les particules d'hydrate ont été mieux dispersées. L'effet de la formation d'hydrates sur la stabilité de la suspension (perte de charge relative) a également été mentionné.

## CONCLUSIONS AND PERSPECTIVES

### 1. Conclusions

From the experimental and model results in this work, the most important conclusions are provided hereby:

Concerning the oil-water dispersion, the addition of AA-LDHI stabilized the dispersion and the presence of salt destabilized the dispersion. The increasing of shear helped to have a better performance of AA-LDHI (dispersion of oil in water) in the presence of salt. Generally, the sizes of water droplets in oil continuous phase were smaller than those of oil droplets in water continuous phase. The increase in the flowrate increased the  $k_{La}$  and the addition of AA-LDHI promoted gas transferring into liquid. The higher amount of oil led to a higher value of  $k_{La}$ .

The experimental results with gas-lift protocol showed that at high water cut, a quick blockage of flowlines corresponds to a high rate of hydrate formation, proportional to the high gas/water (transfer rate) interface from bubbles. Also, a specific risk was identified in the separator where hydrates can accumulate. Enough dosage of oil partially contributed to hydrate dispersion in the presence of AA-LDHI. Furthermore, plug occurred at higher hydrate volume in almost experiments with both salt and AA-LDHI compared to those using salt and AA-LDHI separately. At low water cut, for the experiments with salt and AA-LDHI separately or both salt and AA-LDHI, a higher hydrate volume was transported than the one in high water cut systems. Finally, plugging could be prevented by using only 0.01%AA-LDHI (without salt) and salt appeared to improve the hydrate slurry transport. Mechanisms for gas hydrate formation, agglomeration, deposition and plugging in low and high water cut systems were proposed.

The experimental results with Moineau pump protocol showed that hydrate formation destabilized water-oil dispersion. The addition of AA-LDHI stabilized the hydrate slurry flow and prevented plugging. The increase in velocity increased the average rate of crystallization and improved hydrate slurry transport. On the contrary, the rise in water cut lowered the average rate of crystallization. In the presence of both AA-LDHI and salt, the increase in water cut enhanced the average rate of crystallization. Mostly, the increase in average rate of crystallization led to quicker agglomeration rate.

Generally, the addition of adequate dosage of AA-LDHI lowered pressure drop and helped hydrate slurry to flow more homogeneously and prevented plugging. The use of AA-LDHIs probably changed the hydrate particle size, structure of agglomeration and deposition. Commonly, the

addition of salt lowered significantly the average rate of crystallization and impacted positively on the performance of AA-LDHI such as lower pressure drop, less heterogeneous hydrate slurry flow, less hydrate deposition (in some cases) and avoided plugging.

The morphologies of hydrate particles depended on the water cuts and the presence of salt and AA-LDHI. There was a predominance of sphere shape along with the non-sphere shape of hydrate particles in the presence of oil phase. Hydrate morphology at 100%WC was totally non-spherical. Smaller hydrate particles were observed in the presence of AA-LDHI. In the presence of salt, sticky hydrate agglomerates were observed with a bigger and rougher surface. The presence of both salt and AA-LDHI governed hydrate particles towards round-shape and rougher surface.

The use of different flowrates led to different agglomeration/deposition and plugging mechanisms. The higher rate of crystallization led to a faster rate of hydrate slurry agglomeration and heterogeneity. The role of salt to enhance the effectiveness of additive was interpreted by enhancement of additives adsorbed on the surface of hydrate particles and probably by phase inversion.

A relative pressure drop model was proposed by modifying the model of Mills (1985), using relative pressure drop instead of relative hydrate viscosity. There was a good agreement between the experimental and model results. The term  $K_v$  in the relative pressure drop model represented the structure of hydrate agglomerates. The higher value of  $K_v$  corresponds to the larger hydrate agglomerates, higher relative pressure drop and the more heterogeneous hydrate slurry flow.

Generally, the presence of AA-LDHI decreased the size of hydrate particles and agglomerates but in some cases, the higher amount of AA-LDHI might cause bigger hydrate agglomerates because of a higher rate of crystallization (AA-LDHIs promoted hydrate formation). The higher velocity and pressure caused a higher rate of hydrate crystallization leading to larger hydrate agglomerate size and more heterogeneous hydrate flow. Generally, the presence of oil augmented the value of  $K_v$ . The combination of AA-LDHI and salt decreased RPD or  $K_v$ . In other words, this decreased the size of hydrate agglomerates and led to a better dispersion of hydrate particles.

## **2. Perspectives**

Further work could be carried out as experiments with a specific probe should be done in order to determine the phase inversion during crystallization.

In addition, a comprehensive model for kinetics of hydrate formation, agglomeration, deposition and plugging in multiphase flow coupled with flow patterns in the presence of additives

should be performed and developed (based on the experimental results obtained from the flowloop experiments) to predict hydrate formation and plugging in different oil/water/gas systems.

For a better visual comprehension of the flow regime as well as the effects of hydrate formation, agglomeration, deposition and plugging on the flow regimes, several windows along with a video camera should be installed in some sections of the flowloop to confirm the previous and present experimental results obtained from PVM, FBRM, pressure drop and density measurements.

Furthermore, several new commercial additives could be tested with different concentrations of salt to understand the behavior of different additives at different conditions from oil and gas subsea pipelines transportation.

To better simulate the real conditions in oil and gas transportation in deep sea pipelines, this current study could go further by using natural gas (hydrate former of structure II) instead of methane (hydrate former of structure I). Investigations of hydrate formation in multiphase (gas-water-oil-hydrate) flow with different flow regimes should be performed in the horizontal lines of the flowloop to completely understand the hydrate problems occurring in oil and gas industry.



## CONCLUSIONS ET PERSPECTIVES (IN FRENCH)

### 1. Conclusions

Les résultats expérimentaux et de modélisation obtenus dans ce travail ont permis d'en tirer des conclusions importantes :

Les dispersions de l'huile et de l'eau avec l'addition d'AA-LDHI se stabilisent et en présence de sel se déstabilisent. L'augmentation du cisaillement a montré une amélioration des performances d'AA-LDHI (dispersion de l'huile dans l'eau) en présence de sel. D'une manière générale, les tailles des gouttelettes d'eau dans la phase continue de l'huile sont plus petites que celles des gouttelettes d'huile dans la phase continue de l'eau. Quand le débit est plus élevé, le  $k_L a$  augmente. L'addition d'AA-LDHI favorise le transfert de gaz dans le liquide. Ainsi que, l'augmentation de la quantité d'huile était élevée, le  $k_L a$  est plus élevé.

Les résultats expérimentaux obtenus avec le gaz-lift, les systèmes à haute fraction d'eau ont montré un risque plus élevé de blocage en raison du taux élevé de formation d'hydrates, proportionnel à l'interface gaz/eau (taux de transfert) élevé généré par les bulles. De plus, nous avons identifié un risque spécifique de blocage dans le séparateur où les hydrates peuvent s'accumuler. Un dosage suffisant d'huile contribue partiellement à la dispersion des hydrates en présence d'AA-LDHI. En outre, le bouchage survient à un volume d'hydrate plus élevé dans presque toutes les expériences avec l'AA-LDHI et sel, par rapport à celles qui utilisent que du sel et que d'AA-LDHI séparément. Dans les systèmes à faible fraction d'eau, pour les expériences utilisant du sel et de l'AA-LDHI séparément ou tous les deux à la fois, un volume d'hydrate plus élevé a été maintenu en écoulement par rapport à celui des systèmes à haute fraction d'eau. Le colmatage a pu être évité en utilisant seulement 0.01% d'AA-LDHI (sans sel). En outre, le sel semble aider à mieux hydrater le transport de la suspension. Des mécanismes pour la formation, l'agglomération, le dépôt et le colmatage des hydrates de gaz dans les systèmes de basse et à haute fraction d'eau avec gaz-lift ont été proposés.

Les résultats expérimentaux avec la pompe Moineau montrent que la formation d'hydrates déstabilise la dispersion eau-huile. L'ajout d'AA-LDHI aide à stabiliser l'écoulement d'hydrates et à empêcher le colmatage. Quand le débit est élevé, la vitesse de cristallisation augmente améliorant le transport de la suspension d'hydrates. Au contraire, plus la fraction d'eau est haute, plus la vitesse de cristallisation est faible. En présence à la fois d'AA-LDHI et de sel, quand la fraction d'eau augmente, le taux de cristallisation est plus élevé. Généralement, plus le taux de cristallisation est élevé, l'agglomération est plus rapide. L'ajout d'une dose adéquate d'AA-LDHI permet abaisser la perte de

charge et maintenir l'écoulement d'hydrates plus homogène, par conséquent, le colmatage est évité. Ceci est dû au changement de la taille des particules d'hydrate, de la structure de l'agglomération et du dépôt. L'addition de sel abaisse significativement le taux de cristallisation et améliore la performance d'AA-LDHI (meilleure performance d'AA-LDHI en présence de sel), en conséquence, une perte de charge plus faible, un écoulement d'hydrate moins hétérogène, moins de dépôts d'hydrates (dans certains cas) et en évitant le bouchage.

Les morphologies des particules d'hydrate dépendent de la fraction d'eau et de la présence de sel et d'AA-LDHI. Il y a majoritairement des hydrates sous la forme de sphères et sous la forme de petites particules non sphériques en présence de la phase huileuse. La morphologie des hydrates à 100%WC est totalement non sphérique. Ainsi, de plus petites particules d'hydrate ont été observées en présence d'AA-LDHI. En présence de sel, les particules d'hydrate semblent être plus grosses avec une surface rugueuse et des agglomérats collants entre eux. La présence de sel et d'AA-LDHI à la fois semble orienter les particules d'hydrate vers une forme ronde et une surface plus rugueuse.

L'utilisation de différents débits a conduit à l'obtention de différents mécanismes d'agglomération/dépôt et de blocage : un taux plus élevé de cristallisation conduit à une vitesse plus rapide d'agglomération de la suspension d'hydrates et de son hétérogénéité. Le sel semble améliorer l'efficacité de l'additif par en induisant l'amélioration de l'adsorption des additifs sur la surface des particules d'hydrate et l'inversion de phase continue en eau en phase continue huile.

A partir du modèle de Mills (1985), un modèle de perte de charge relative a été proposé, en utilisant la perte de charge relative au lieu de la viscosité relative de la suspension d'hydrate. Il y a une bonne cohérence entre les données expérimentales et les données développées par le modèle. Le terme de  $K_v$  dans le modèle de perte de charge relative représente la structure des agglomérats d'hydrates : plus grande est la valeur de  $K_v$ , plus gros sont les agglomérats d'hydrates, plus la perte de charge relative est importante et l'écoulement sera hétérogène.

D'une manière générale, la présence d'AA-LDHI favorise la réduction de la taille des particules d'hydrates et des agglomérats, cependant, en certains cas de système, la quantité plus élevée d'AA-LDHI peut provoquer des agglomérats d'hydrates plus importants en raison d'un taux de cristallisation plus élevé (AA-LDHI favorise la formation d'hydrates). A vitesse et pression plus élevées, le taux de cristallisation des hydrates est plus élevé conduisant à une plus grande taille des agglomérats d'hydrates et à un écoulement hétérogène des hydrates. La présence d'huile en générale augmente la valeur de  $K_v$  ; la combinaison d'AA-LDHI et de sel diminue le RPD ou le  $K_v$ . En

d'autres termes, la taille des agglomérats d'hydrates diminue et les particules d'hydrate sont mieux dispersées.

## **2. Perspectives**

Quelques pistes pour des futurs travaux peuvent concerner expérimentations utilisant une sonde spécifique pour déterminer l'inversion de phase pendant la cristallisation.

Un modèle complet de cinétique de formation, d'agglomération, de dépôt et de colmatage des hydrates dans un écoulement poly-phasique couplé à des régimes d'écoulement en présence d'additifs pourra être réalisé et développé (sur la base des résultats expérimentaux obtenus à partir des expériences sur la boucle). Ceci pour prédire la formation d'hydrates et le bouchage de différents systèmes huile/eau/gaz.

Afin de mieux comprendre le régime d'écoulement et de mieux observer les effets de la formation, de l'agglomération, du dépôt et du bouchage des hydrates sur les régimes d'écoulement, plusieurs fenêtres d'observation (hublots) ainsi qu'une caméra vidéo pourra être installées dans certaines sections de la boucle pour confirmer les résultats expérimentaux des autres mesures (PVM, FBRM, perte de charge et mesures de densité).

De plus, plusieurs additifs commerciaux peuvent être testés à différentes concentrations de sel afin de comprendre l'action de ces additifs dans différentes conditions de transport de gaz et de pétrole sous-marins.

Pour mieux reproduire les conditions réelles du transport de pétrole et de gaz dans les pipelines, cette étude pourrait aller plus loin en utilisant du gaz naturel (hydrate de structure II) au lieu du méthane (hydrate de structure I). Des études sur la formation d'hydrates dans un écoulement multiphasique (gaz-liquide-liquide-hydrate) avec différents régimes d'écoulement devront être effectuées dans les lignes horizontales de la boucle pour comprendre complètement les problèmes liés à l'apparition d'hydrates dans l'industrie pétrolière et gazière.

## LIST OF PUBLICATIONS

1. **Trung-Kien PHAM**, Ana CAMEIRAO, Jean-Michel HERRI, Philippe GLENAT, "*Crystallization of methane hydrates from an emulsion in a flowloop: experiments in a gas-liquid-liquid system using gas-lift riser*", 16th Conference SFGP 2107, Nancy, France, July, (2017) page 170
2. **Trung-Kien PHAM**, Ana CAMEIRAO, Jean-Michel HERRI, Philippe GLENAT, "*Experimental study on methane hydrate formation and transport from emulsions in a gas lift riser in a flowloop*" 9<sup>th</sup> International Conference on Gas Hydrates (ICGH9), Denver, Colorado, USA, June (2017) page 13
3. **Trung-Kien PHAM**, Ana CAMEIRAO, Jean-Michel HERRI, "*Experimental flowloop study on methane hydrate formation and agglomeration in high water cut emulsion systems*" Integrated Petroleum Engineering, ESASGD International Conference, Hanoi, Vietnam, November, (2016) pages 187-198
4. Jean-Michel HERRI, **Trung-Kien PHAM**, Amadeu K. SUM, Ana CAMEIRAO, Baptiste BOUILLOT, "*Prevention of crystallization of gas hydrates. Management of the risk with solids: modelling the flow pattern*" Integrated Petroleum Engineering, ESASGD International Conference, Hanoi, Vietnam, November, (2016) pages 158-177
5. **Trung-Kien PHAM**, Aline MENDES-MELCHUNA, Ana CAMEIRAO, Jean-Michel HERRI, Pierre Duchet-SUCHAUX, Philippe GLENAT, "*Kinetic modelling of methane hydrate formation and agglomeration with and without anti-agglomerants from the emulsion in pipelines*", Annual Conference CODEGEPRA on Chemical Engineering, Clermont-Ferrand, France, November (2015) page 30
6. **Trung-Kien PHAM**, Ana CAMEIRAO, Jean-Michel HERRI, Philippe GLENAT, "*Hydrate formation and transport in low and high water cut systems in a gas - bubble (lift) flowloop*" (in preparation to be submitted)
7. **Trung-Kien PHAM**, Ana CAMEIRAO, Jean-Michel HERRI, Philippe GLENAT, "*Hydrate formation and transport in a flowloop at high water cut in the presence of salt and anti-agglomerants*" (in preparation to be submitted)
8. **Trung-Kien PHAM**, Ana CAMEIRAO, Jean-Michel HERRI, Philippe GLENAT, "*Relative pressure drop model for hydrate formation and transportability in flowlines in high water cut systems*" (in preparation to be submitted)

## REFERENCES

- Akhfash, M., Aman, Z. M., Du, J., Pickering, P. F., Johns, M. L., Koh, C. A., & May, E. F. (2017). Microscale Detection of Hydrate Blockage Onset in High-Pressure Gas-Water Systems. *Energy and Fuels*, 31(5), 4875–4885.
- Al-Sahhaf, T., Elkamel, A., Suttar Ahmed, A., & Khan, a. R. (2005). The Influence of Temperature, Pressure, Salinity, and Surfactant Concentration on the Interfacial Tension of the N-Octane-Water System. *Chemical Engineering Communications*, 192(5), 667–684.
- Alapati, R., Lee, J., & Beard, D. (2008). Two Field Studies Demonstrate That New AA-LDHI Chemistry is Effective at High Water Cuts Without Impacting Oil/Water Quality. *Offshore Technology Conference*, 1–14.
- Albal. (1983). Mass transfer in multiphase agitated contactors. *The Chemical Engineering Journal*, 27, 61–80.
- Aman, Z. M., Joshi, S. E., Sloan, E. D., Sum, A. K., & Koh, C. A. (2012). Micromechanical cohesion force measurements to determine cyclopentane hydrate interfacial properties. *Journal of Colloid and Interface Science*, 376(1), 283–288.
- Andersson, V. (2000). Flow Properties of Hydrate-in-Water Slurries. *Annals of the New York Academy of Sciences*, 912(1), 322–329.
- Anklam. (2008). Effects of Antiagglomerants on the Interactions between Hydrate Particles. *AIChE Journal*, 54(2), 565–574.
- Aspenes, G., Dieker, L. E., Aman, Z. M., Høiland, S., Sum, A. K., Koh, C. A., & Sloan, E. D. (2010). Adhesion force between cyclopentane hydrates and solid surface materials. *Journal of Colloid and Interface Science*, 343(2), 529–536.
- Austvik, T., Li, X., & Gjertsen, L. H. (2000). Hydrate Plug Properties: Formation and Removal of Plugs. *Annals of the New York Academy of Sciences*, 912(1), 294–303.
- Azarinezhad, R., Chapoy, A., Anderson, R., & Tohidi, B. (2008). HYDRAFLOW : A Multiphase Cold Flow Technology for Offshore Flow Assurance Challenges. *Offshore Technology Conference*, (19485), 1–8.
- Bailey, B. (2000). Water Control. *Schlumberger*, 30–51.
- Balakin, B. V., Lo, S., Kosinski, P., & Hoffmann, A. C. (2016). Modelling agglomeration and deposition of gas hydrates in industrial pipelines with combined CFD-PBM technique. *Chemical Engineering Science*, 153, 45–57.
- Barnea, E., & Mizrahi, J. (1973). A generalized approach to the fluid dynamics of particulate systems. *The Chemical Engineering Journal*, 5(2), 171–189.
- Behar. (1991). Advances in hydrate control. In *Proceedings of the 70th gas processors association conference*. San Antonio, March 11–12.
- Boxall, J., Greaves, D., Mulligan, J., Koh, C., & Sloan, E. D. (2008). Gas Hydrate Formation and Dissociation From Water-in- Oil Emulsions Studied Using Pvm and Fbrm Particle Size Analysis. In *Proceedings of the 6th International Conference on Gas Hydrates (ICGH 2008)*.
- Brennen, C. (2005). *Fundamentals of Multiphase Flows*. Cambridge University Press.
- Brooks. (2010). Thermal Mass Flow Controllers and Thermal Mass Flow Meters; Standard Flow vs. Actual Flow. *Brooks Instrument Corporate Website*.
- Cai, B.-Y., Yang, J.-T., & Guo, T.-M. (1996). Interfacial Tension of Hydrocarbon + Water / Brine Systems under High Pressure. *J. Chem. Eng. Data*, 41, 493–496.
- Camargo, R. (2002). Rheological Properties of Hydrate Suspensions in an Asphaltenic Crude Oil. In *Proceedings of the 4th International Conference on Gas Hydrates* (pp. 880–885). Yokohama

- Symposia, Yokohama, Japan.
- Chaudhari. (2015). *Development of Hydrate Risk Quantification in Oil and Gas Production*. PhD Thesis, Colorado School of Mines.
- Chen, L., Sloan, E. D., Koh, C. A., & Sum, A. K. (2014). Methane Hydrate Formation and Dissociation on Suspended Gas Bubbles in Water. *J. Chem. Eng. Data*, 59(4), 1045–1051.
- Chua, P. C., & Kelland, M. A. (2013). Study of the Gas Hydrate Anti-agglomerant Performance of a Series of *n*-Alkyl-tri(*n*-butyl)ammonium Bromides. *Energy & Fuels*, 27(3), 1285–1292.
- Colombel, E., Gateau, P., Barré, L., Gruy, F., & Palermo, T. (2009). Discussion sur les mécanismes d'agglomération entre particules d'hydrate dans les émulsions eau dans huile. *Oil and Gas Science and Technology*, 64(5), 629–636.
- D. Lippmann, D. KESSEL, A. I. R. (1994). Gas Hydrate Equilibria and Kinetics of Gas / Oil / Water Mixtures. *Ann. N. Y. Acad. Sci*, 715, 525–527.
- Dalmazzone, D., Hamed, N., & Dalmazzone, C. (2009). DSC measurements and modelling of the kinetics of methane hydrate formation in water-in-oil emulsion. *Chemical Engineering Science*, 64(9), 2020–2026.
- DataPhysics Instruments GmbH. (2006). Operating manual DCAT. *Operating Manual Dataphysics DCAT 11 and DCAT 21*.
- Davies, S. R., Boxall, J. A., Dieker, L. E., Sum, A. K., Koh, C. A., Sloan, E. D., Creek, J. L., & Xu, Z. G. (2010). Predicting hydrate plug formation in oil-dominated flowlines. *Journal of Petroleum Science and Engineering*, 72(3–4), 302–309.
- Dong, S., Li, M., & Firoozabadi, A. (2017). Effect of salt and water cuts on hydrate anti-agglomeration in a gas condensate system at high pressure. *Fuel*, 210, 713–720.
- Einstein, A. (1906). Eine neue bestimmung der moleküldimensionen. *Ann. Phys.*, 324(2), 289–306.
- Einstein, A. (1911). Berichtigung zu meiner arbeit: eine neue bestimmung der moleküldimensionen. *Ann. Phys.*, 339(3), 591–592.
- Englezos, P., Kalogerakis, N., Dholabhai, P. D. D., & Bishnoi, P. R. R. (1987). Kinetics of formation of methane and ethane gas hydrates. *Chemical Engineering Science*, 42(11), 2647–2658.
- FBRM, M.-T. (2005). *FBRM Control Interface Users ' Manual v6.7.0*.
- Fidel-Dufour, A. (2004). *Influence d'additifs anti-agglomérants sur l'agrégation et les propriétés de transport des hydrates de méthane dans des émulsions eau/dodécane*. PhD Thesis, Ecole des Mines de Saint-Etienne.
- Fidel-Dufour, A., Gruy, F., & Herri, J. M. (2006). Rheology of methane hydrate slurries during their crystallization in a water in dodecane emulsion under flowing. *Chemical Engineering Science*, 61(2), 505–515.
- Fordedal, H. (1996). Crude oil emulsions in high electric fields as studied by dielectric spectroscopy. Influence of interaction between commercial and indigenous surfactants. *Colloids and Surfactants*, 106, 33–47.
- Gao, S. (2009). Hydrate risk management at high watercuts with anti-agglomerant hydrate inhibitors. *Energy and Fuels*, 23(4), 2118–2121.
- Gluyas, J. G. and H. M. H. (2003). United kingdom oil and gas fields: commemorative millennium volume.
- Grasso, G. A. (2015). *Investigation of hydrate formation and transportability in multiphase flow systems*. PhD Thesis, Colorado School of Mines.
- Greaves, D., Boxall, J., Mulligan, J., Sloan, E. D., & Koh, C. A. (2008). Hydrate formation from high water content-crude oil emulsions. *Chemical Engineering Science*, 63(18), 4570–4579.

- Gumerov, N., & Chahine, G. (1998). Dynamics of bubbles in conditions of gas hydrate formation. *Proceedings of the Eighth International Offshore and Polar Engineering Conference, Montreal, Canada*, 66–72.
- Guo, Y., Pu, W., Zhao, J., Guo, Y., Lian, P., Liu, Y., Wang, L., & Yu, Y. (2017). Effect of the foam of sodium dodecyl sulfate on the methane hydrate formation induction time. *International Journal of Hydrogen Energy*, 42(32), 20473–20479.
- H.Tajima. (2010). Direct observation of the effect of sodium dodecyl sulfate on the gas hydrate formation process in a static mixer. *Energy & Fuels*, (24), 432–438.
- Herri, J.-M. (1999). Methane Hydrate Crystallization Mechanism from In-Situ Particle Sizing. *AIChE Journal*, 45(3), 590–602.
- Herri, J. M. (1996). *Etude de la formation de l'hydrate de methane par turbidimétrie in situ*. PhD Thesis, Pierre et Marie Curie (Paris VI).
- Hester, C. G. and K. (2011). Physical Properties of Hydrates, Gas Hydrates, Green Energy and Technology. *Springer-Verlag London Limited 2011*, 1–12.
- Hoekstra, L. L., Vreeker, R., & Agterof, W. G. M. (1992). Aggregation of colloidal nickel hydroxycarbonate studied by light scattering. *Journal of Colloid And Interface Science*, 151(1), 17–25.
- Høiland, S., Askvik, K. M., Fotland, P., Alagic, E., Barth, T., & Fadnes, F. (2005). Wettability of Freon hydrates in crude oil/brine emulsions. *Journal of Colloid and Interface Science*, 287(1), 217–225.
- Huo, Z., Freer, E., Lamar, M., Sannigrahi, B., Knauss, D. M., & Sloan, E. D. (2001). Hydrate plug prevention by anti-agglomeration. *Chemical Engineering Science*, 56(17), 4979–4991.
- Israelachvili, J. N. (2011). *Intermolecular and Surface Forces*. Academic Press.
- Jassim, E., Abdi, M. A., & Muzychka, Y. (2010). A new approach to investigate hydrate deposition in gas-dominated flowlines. *Journal of Natural Gas Science and Engineering*, 2(4), 163–177.
- Jeffrey, G. A. (1984). Hydrate inclusion compounds. *Journal of Inclusion Phenomena*, 1(3), 211–222.
- Joshi, S. V., Grasso, G. A., Lafond, P. G., Rao, I., Webb, E., Zerpa, L. E., Sloan, E. D., Koh, C. A., & Sum, A. K. (2013). Experimental flowloop investigations of gas hydrate formation in high water cut systems. *Chemical Engineering Science*, 97, 198–209.
- Joshi, S. V. (2012). *Experimental investigation and modeling of gas hydrate formation in high water cut producing oil pipelines*. PhD Thesis, Colorado School of Mines.
- Jullien, R. (1990). The application of fractals to investigations of colloidal aggregation and random deposition. *New Journal of Chemistry*, 14(3).
- Karaaslan, U., & Parlaktuna, M. (2000). Surfactants as hydrate promoters? *Energy and Fuels*, 14(5), 1103–1107.
- Karaaslan, U., & Parlaktuna, M. (2002). Promotion effect of polymers and surfactants on hydrate formation rate. *Energy and Fuels*, 16(6), 1413–1416.
- Karanjkar, P. U., Lee, J. W., & Morris, J. F. (2012). Calorimetric investigation of cyclopentane hydrate formation in an emulsion. *Chemical Engineering Science*, 68(1), 481–491.
- Katz, D. L. . (1959). *Handbook of natural gas engineering*. McGraw-Hill.
- Kelland. (2009). *Production chemicals for the oil and gas industry*. Boca Raton, FL: CRC Press.
- Kelland, M. A. (2008). Feasibility Study for the Use of Kinetic Hydrate Inhibitors in Deep Water Drilling Fluids. *Energy & Fuels*, 22, 2405–2410.
- Kelland, M. A., Svartaas, T. M., Øvsthus, J., Tomita, T., & Chosa, J. ichi. (2006). Studies on some zwitterionic surfactant gas hydrate anti-agglomerants. *Chemical Engineering Science*, 61(12), 4048–4059.

- Kelland, M. A., Svartaas, T. M., Øvsthus, J., Tomita, T., & Mizuta, K. (2006). Studies on some alkylamide surfactant gas hydrate anti-agglomerants. *Chemical Engineering Science*, *61*(13), 4290–4298.
- Kelland, M. a. (2006). History of the Development of Low Dosage Hydrate Inhibitors. *Energy Fuels*, *20*(3), 825–847.
- Klomp. (1995). World Patent Application WO 95/17579.
- Klomp, U. . (1999). World Patent Application, WO 99/13197.
- Krieger, I. . (1972). Rheology of monodisperse latices. *Advances in Colloid and Interface Science*, *3*, 111–136.
- Kumar, A., Bhattacharjee, G., Kulkarni, B. D., & Kumar, R. (2015). Role of Surfactants in Promoting Gas Hydrate Formation. *Industrial and Engineering Chemistry Research*, *54*(49), 12217–12232.
- Lachance, J. W., Dendy Sloan, E., & Koh, C. A. (2008). Effect of hydrate formation/dissociation on emulsion stability using DSC and visual techniques. *Chemical Engineering Science*, *63*(15), 3942–3947.
- Larsen, R. (1997). *Clathrate Hydrate Single Crystals: Growth and Inhibition*. Thesis, Norwegian University of Science and Technology.
- Leba, H. (2009). *Formation et agglomération de particules d ' hydrate de gaz dans une émulsion eau dans huile : Etude expérimentale et modélisation*. PhD Thesis, Ecole des Mines de Saint-Etienne.
- Leba, H., Cameirao, A., Herri, J. M., Darbouret, M., Peytavy, J. L., & Glénat, P. (2010a). Chord length distributions measurements during crystallization and agglomeration of gas hydrate in a water-in-oil emulsion: Simulation and experimentation. *Chemical Engineering Science*, *65*(3), 1185–1200.
- Leba, H., Cameirao, A., Herri, J. M., Darbouret, M., Peytavy, J. L., & Glénat, P. (2010b). Chord length distributions measurements during crystallization and agglomeration of gas hydrate in a water-in-oil emulsion: Simulation and experimentation. *Chemical Engineering Science*, *65*(3), 1185–1200.
- Lee, J., Shin, C., & Lee, Y. (2010). Experimental investigation to improve the storage potentials of gas hydrate under the unstirring condition. *Energy and Fuels*, *24*(2), 1129–1134.
- Lee, S. Y., Kim, H. C., & Dong, J. (2014). Morphology study of methane – propane clathrate hydrates on the bubble surface in the presence of SDS or PVCap. *Journal of Crystal Growth*, *402*, 249–259.
- Leifer, I., & Patro, R. K. (2002). The bubble mechanism for methane transport from the shallow sea bed to the surface: A review and sensitivity study. *Continental Shelf Research*, *22*(16), 2409–2428.
- Li, C., & Huang, T. (2016). Simulation of gas bubbles with gas hydrates rising in deep water. *Ocean Engineering*, *112*, 16–24.
- Li, M., Wilkinson, D., & Patchigolla, K. (2005). Comparison of particle size distributions measured using different techniques. *Particulate Science and Technology*, *23*(3), 265–284.
- Li, S.-L., Sun, C.-Y., Liu, B., Li, Z.-Y., Chen, G.-J., & Sum, A. K. (2014). New observations and insights into the morphology and growth kinetics of hydrate films. *Scientific Reports*, *4*, 4129.
- Li, X., Chen, C., Chen, Y., Li, Y., & Li, H. (2015). Kinetics of methane clathrate hydrate formation in water-in-oil emulsion. *Energy and Fuels*, *29*(4), 2277–2288.
- Lorenzo, M. Di, Aman, Z. M., Kozielski, K., Norris, B. W. E., Johns, M. L., & May, E. F. (2018). Modelling hydrate deposition and sloughing in gas-dominant pipelines. *The Journal of Chemical Thermodynamics*, *117*, 81–90.
- Luo, Y. T., Zhu, J. H., Fan, S. S., & Chen, G. J. (2007). Study on the kinetics of hydrate formation in a

- bubble column. *Chemical Engineering Science*, 62(4), 1000–1009.
- Lv, X., Shi, B., Wang, Y., & Gong, J. (2013). Study on gas hydrate formation and hydrate slurry flow in a multiphase transportation system. *Energy and Fuels*, 27(12), 7294–7302.
- M. Elimelech, J. Gregory, X. J. & R. W. (1995). *Particle Deposition and Aggregation*. Butterworth & Heinemann Ltd., Oxford.
- Main, B. B., & Bishnoi, P. R. (1981). Experimental investigation of hydrate formation behaviour of a natural gas bubble in a simulated deep sea environment. *Chemical Engineering Science*, 36(1), 183–189.
- Majid, A. A. A., Braniff, M., Liu, C., Delgado-linares, J., Creek, J. L., Sloan, E. D., Sum, A. K., & Koh, C. A. (2014). Gas Hydrate Formation From High Water Content Systems Containing Anti-Agglomerant Surfactant and Salt. *Proceedings of the 8th International Conference on Gas Hydrates*, 1–7.
- Majid, A. A., Lee, W., Srivastava, V., Chen, L., Grasso, G., Vijayamohan, P., Chaudhari, P., Sloan, E. D., Koh, C. A., & Zerpa, L. (2016). The Study of Gas Hydrate Formation and Particle Transportability Using A High Pressure Flowloop. *Offshore Technology Conference*, (OTC-27276-MS), 1–14.
- Melchuna, A., Cameirao, A., Herri, J. M., & Glenat, P. (2016). Topological modeling of methane hydrate crystallization from low to high water cut emulsion systems. *Fluid Phase Equilibria*, 413, 158–169.
- Mendes-Melchuna. (2016). *Étude expérimentale et modélisation de la cristallisation d'hydrates de méthane en écoulement à partir d'une émulsion à pourcentages variables d'eau et d'anti-agglomérant*. PhD Thesis, Ecole des Mines de Saint-Etienne.
- Mettler-Toledo. (2007). *Lasentec FBRM D600 Hardware Manual*. Copyright 2006 by Mettler-Toledo AutoChem, Inc.
- Midoux, N. (1993). *Mécanique et Rhéologie des Fluides en Génie Chimique*. Edition Lavoisier.
- Mills, P. (1985). Non-Newtonian behaviour of flocculated suspensions. *Journal de Physique Lettres*, 46(7), 301–309.
- Monnier, O., Klein, J.-P., Ratsimba, B., & Hoff, C. (1996). Particle Size Determination by Laser Reflection: Methodology and problems. *Particle & Particle Systems Characterization*, 13(1), 10–17.
- Mooney. (1950). The viscosity of a concentrated suspension of spherical particles. *Journal of Colloid Sciences*, (113), 162–170.
- Moradpour, H. (2011). *An Experimental and Modelling Investigation of the Rheological Properties of Water/Oil/Gas Hydrate Mixtures*. PhD Thesis, Heriot-Watt University.
- Moradpour, H., Chapoy, A., & Tohidi, B. (2011). Bimodal model for predicting the emulsion-hydrate mixture viscosity in high water cut systems. *Fuel*, 90(11), 3343–3351.
- Morgado, A. O. (2016). Review on vertical gas-liquid slug flow. *International Journal of Multiphase Flow*, 85, 348–368.
- Mu, L., Li, S., Ma, Q.-L., Zhang, K., Sun, C.-Y., Chen, G.-J., Liu, B., & Yang, L.-Y. (2014). Experimental and modeling investigation of kinetics of methane gas hydrate formation in water-in-oil emulsion. *Fluid Phase Equilibria*, 362, 28–34.
- Nagappayya, S. K., Lucente-Schultz, R. M., Nace, V. M., & Ho, V. M. (2015). Antiagglomerant hydrate inhibitors: The link between hydrate-philic surfactant behavior and inhibition performance. *Journal of Chemical and Engineering Data*, 60(2), 351–355.
- Noll, L. A. (1991). The Effect of Temperature, Salinity, and Alcohol on the Critical Micelle Concentration of Surfactants. *SPE International Symposium on Oilfield Chemistry*, 337–343.
- Oilstates. (2017). <http://oilstates.com/offshore/subsea-pipeline-products/> (13/06/2017).

- Pal, R. (2000). Viscosity–Concentration Equation for Emulsions of Nearly Spherical Droplets. *Journal of Colloid and Interface Science*, 231(1), 168–175.
- Pal, R., & Rhodes, E. (1985). A novel viscosity correlation for non-newtonian concentrated emulsions. *Journal of Colloid And Interface Science*, 107(2), 301–307.
- Palermo, T., Arla, D., Borregales, M., & Dalmazzone, C. (2005). Study of the Agglomeration Between Hydrate Particles in Oil Using Differential Scanning Calorimetry (DSC). *Proceedings of the Fifth International Conference on Gas Hydrates, June 12-16, 2005. Trondheim, Norway*.
- Pauchard, V., Palermo, T., Peytavy, J. L. ., & Mussumeci, A. (2005). Transformation of a Concentrated Oil/Water Emulsion Into A Gel Due to Slight Hydrates Formation. *5th International Conference on Gas Hydrates*.
- Peng, B. Z., Chen, J., Sun, C. Y., Dandekar, A., Guo, S. H., Liu, B., Mu, L., Yang, L. Y., Li, W. Z., & Chen, G. J. (2012). Flow characteristics and morphology of hydrate slurry formed from (natural gas+diesel oil/condensate oil+water) system containing anti-agglomerant. *Chemical Engineering Science*, 84, 333–344.
- Potantin, A. A. (1991). On the mechanism of aggregation in the shear flow of suspensions. *Journal of Colloid and Interface Science*, 145(1), 140–157.
- Preston W.C. (1948). Some correlating principles of detergent action. *Journal of Physical Chemistry*, 52(1), 84–97.
- Pump, P. M. (2017). <http://edmond.peulot.pagesperso-orange.fr/POMPES.HTM>.
- PVM, M.-T. (2009). PVM® V819 System Manual Unparalleled Particulate Process Understanding.
- Quemada, D. (1977). Rheology of Concentrated Disperse Systems and Minimum Energy-Dissipation Principle .1. Viscosity-Concentration Relationship. *Rheologica Acta*, 16(1), 82–94.
- Rao, I. (2013). *Multiphase Flow Modeling and Deposition of Hydrates in Oil and Gas Pipelines*. PhD Thesis Colorado School of Mines.
- Richardson. (1933). Über die Viskosität von Emulsionen. *Kolloid Zeitschrift*, 32–37.
- Roscoe. (1952). The viscosity of suspensions of rigid spheres. *Br. J. Appl. Phys.* 3, 267- 269 (1952).
- Rosemount. (1997). Model 3051 Smart Pressure Transmitter Family. *Rosemount Inc*.
- Sato, J., Iida, T., Kiyono, F., & Sato, T. (2016). Cohesion Force Measurement of Methane Hydrate and Numerical Simulation of Rising Bubbles Covered with a Hydrate Membrane within a Contracting Pipe. *Energy & Fuels*, 30(9), 7100–7107.
- Sato, Y., Kiyono, F., Ogasawara, K., Yamamoto, Y., Sato, T., Hirabayashi, S., & Shimizu, Y. (2013). An Experimental Study on the Dynamics of a Rising Methane Bubble Covered with Hydrates. *Journal of MMIJ*, 129(4), 124–131.
- Schramm. (2005). *Emulsions , Foams , and Suspensions* (WILEY-VCH). WILEY-VCH Verlag GmbH & Co. KGaA, Weinheim.
- Shi, B. H., Gong, J., Sun, C. Y., Zhao, J. K., Ding, Y., & Chen, G. J. (2011). An inward and outward natural gas hydrates growth shell model considering intrinsic kinetics, mass and heat transfer. *Chemical Engineering Journal*, 171(3), 1308–1316.
- Sjöblom, J. (2006). *Emulsions and emulsion stability*. Taylor and Francis Group, LLC.
- Sjöblom, J., Aske, N., Harald, I., Brandal, Ø., Erik, T., & Sæther, Ø. (2003). Our current understanding of water-in-crude oil. Recent characterization techniques and high pressure performance. *Advances in Colloid and Interface Science*, 102, 399–473.
- Skovborg, P., & Rasmussen, P. (1994). A mass transport limited model for the growth of methane and ethane gas hydrates. *Chemical Engineering Science*, 49(8), 1131–1143.
- Sloan, & Koh, C. A. (2008). *Clathrate hydrates of natural gases* (Third). Taylor and Francis Group, LLC.

- Sloan, Koh, C., & Sum, A. (2010). *Natural gas hydrates in flow assurance*. Gulf Professional Publishing.
- Sohn, Y. hoon, Kim, J., Shin, K., Chang, D., Seo, Y., Aman, Z. M., & May, E. F. (2015). Hydrate plug formation risk with varying watercut and inhibitor concentrations. *Chemical Engineering Science*, *126*, 711–718.
- Straume, E. O., Kakitani, C., Merino-Garcia, D., Morales, R. E. M., & Sum, A. K. (2016). Experimental study of the formation and deposition of gas hydrates in non-emulsifying oil and condensate systems. *Chemical Engineering Science*, *155*, 111–126.
- Sun, C. Y., Chen, G. J., Ma, C. F., Huang, Q., Luo, H., & Li, Q. P. (2007). The growth kinetics of hydrate film on the surface of gas bubble suspended in water or aqueous surfactant solution. *Journal of Crystal Growth*, *306*(2), 491–499.
- Sun, C. Y., Chen, G. J., & Yang, L. Y. (2004). Interfacial tension of methane + water with surfactant near the hydrate formation conditions. *Journal of Chemical and Engineering Data*, *49*(4), 1023–1025.
- Sun, & Firoozabadi, A. (2015). Gas hydrate powder formation - Ultimate solution in natural gas flow assurance. *Fuel*, *146*, 1–5.
- Sun, M. (2015). Hydrate size measurements in anti-agglomeration at high watercut by new chemical formulation. *Energy and Fuels*, *29*(5), 2901–2905.
- Sun, M., & Firoozabadi, A. (2013). New surfactant for hydrate anti-agglomeration in hydrocarbon flowlines and seabed oil capture. *Journal of Colloid and Interface Science*, *402*, 312–319.
- Tajima, H., Nakajima, Y., Otomo, J., Nagamoto, H., Yamasaki, A., & Kiyono, F. (2010). Direct Observation of the Effect of Sodium Dodecyl Sulfate (SDS) on the Gas Hydrate Formation Process in a Static Mixer. *Energy & Fuels*, (24), 432–438.
- Talatori, S., & Barth, T. (2011). Rate of hydrate formation in crude oil/gas/water emulsions with different water cuts. *Journal of Petroleum Science and Engineering*, *80*(1), 32–40.
- Taylor. (1932). The Viscosity of a Fluid Containing Small Drops of Another Fluid. *Proceedings of the Royal Society of London. Series A, Containing Papers of a Mathematical and Physical Character*, 41–48.
- Taylor, C. J., Dieker, L. E., Miller, K. T., Koh, C. A., & Sloan, E. D. (2007). Micromechanical adhesion force measurements between tetrahydrofuran hydrate particles. *Journal of Colloid and Interface Science*, *306*(2), 255–261.
- Taylor, C. J., Miller, K. T., Koh, C. A., & Sloan, E. D. (2007). Macroscopic investigation of hydrate film growth at the hydrocarbon/water interface. *Chemical Engineering Science*, *62*(23), 6524–6533.
- Tom O'Banion. (2013). Coriolis: The Direct Approach to Mass Flow Measurement. *Chemical Engineering Progress (CEP), An AIChE Publication*, 41–46.
- Trallero, J. L., Intevap, S. a, Sarica, C., Brill, J. P., & Tulsa, U. (1997). A Study of Oil / Water Flow Patterns in Horizontal Pipes. *SPE Production & Facilities*, *13*, 165–172.
- Turner, D., Boxall, J., Yang, S., Kleehamer, D., Koh, C., Miller, K., Sloan, E. D., Xu, Z., Technology, S. P., Energy, C., Company, T., & Talley, L. (2005). Development of a Hydrate Kinetic Model and Its Incorporation Into the Olga2000<sup>®</sup> Transient Multi-Phase Flow Simulator. *Proceedings of the Fifth International Conference on Gas Hydrates, June 12-16, 2005. Trondheim, Norway*.
- Turner, D. J. (2006). *Clathrate Hydrate Formation in Water-in-Oil Dispersions*. PhD Thesis, Colorado School of Mines.
- Turner, D. J., Kleehammer, D. M., Miller, K. T., Koh, C. a, Sloan, E. D., & Talley, L. D. (2005). Formation of hydrate obstructions in pipelines: Hydrate particle development and slurry flow. *Proceedings of the Fifth International Conference on Gas Hydrates, June 12-16, 2005. Trondheim, Norway*.
- Turner, D. J., Miller, K. T., & Dendy Sloan, E. (2009). Methane hydrate formation and an inward

- growing shell model in water-in-oil dispersions. *Chemical Engineering Science*, 64(18), 3996–4004.
- Turner, D. J., Miller, K. T., & Sloan, E. D. (2009). Direct conversion of water droplets to methane hydrate in crude oil. *Chemical Engineering Science*, 64(23), 5066–5072.
- Vijayamohan, P. (2015). *Experimental investigation of gas hydrate formation, plugging and transportability in partially dispersed and water continuous systems*. PhD Thesis, Colorado School of Mines.
- Wang, W., Fan, S., Liang, D., & Li, Y. (2010). A model for estimating flow assurance of hydrate slurry in pipelines. *Journal of Natural Gas Chemistry*, 19(4), 380–384.
- Wang, Z., Zhang, J., Sun, B., Chen, L., Zhao, Y., & Fu, W. (2017). A new hydrate deposition prediction model for gas-dominated systems with free water. *Chemical Engineering Science*, 163, 145–154.
- Wang, Z., Zhao, Y., Sun, B., Chen, L., Zhang, J., & Wang, X. (2016). Modeling of Hydrate Blockage in Gas-Dominated Systems. *Energy and Fuels*, 30(6), 4653–4666.
- Warzinski, R. P. (2014). Dynamic morphology of gas hydrate on a methane bubble in water: Observations and new insights for hydrate film models. *Geophysical Research Letters*, 6841–6847.
- Watanabe, K., Imai, S., & Mori, Y. H. (2005). Surfactant effects on hydrate formation in an unstirred gas/liquid system: An experimental study using HFC-32 and sodium dodecyl sulfate. *Chemical Engineering Science*, 60, 4846–4857.
- Wilson, A. (1989). *Foams: Physics, Chemistry and Structure; Principles of Foam Formation and Stability*. Springer, London.
- Yan, K. Le, Sun, C. Y., Chen, J., Chen, L. T., Shen, D. J., Liu, B., Jia, M. L., Niu, M., Lv, Y. N., Li, N., Song, Z. Y., Niu, S. S., & Chen, G. J. (2014). Flow characteristics and rheological properties of natural gas hydrate slurry in the presence of anti-agglomerant in a flow loop apparatus. *Chemical Engineering Science*, 106, 99–108.
- Yang, S. O., Kleehammer, D. M., Huo, Z., Sloan, E. D., & Miller, K. T. (2004a). Temperature dependence of particle-particle adherence forces in ice and clathrate hydrates. *Journal of Colloid and Interface Science*, 277(2), 335–341.
- Yang, S. O., Kleehammer, D. M., Huo, Z., Sloan, E. D., & Miller, K. T. (2004b). Temperature dependence of particle-particle adherence forces in ice and clathrate hydrates. *Journal of Colloid and Interface Science*, 277(2), 335–341.
- York, J. D. (2008). Effect of Salinity on Hydrate Antiagglomeration. *Energy & Fuels*, 23(9), 2937–2946.
- York, J. D., & Firoozabadi, A. (2008). Alcohol cosurfactants in hydrate antiagglomeration. *Journal of Physical Chemistry B*, 112(34), 10455–10465.
- Zanota, M. L., Dicharry, C., & Graciaa, A. (2005). Hydrate plug prevention by quaternary ammonium salts. *Energy and Fuels*, 19(2), 584–590.
- Zerpa, L. E. (2013). *A Practical Model to Predict Gas Hydrate Formation, Dissociation and Transportability in Oil and Gas Flowlines*. PhD Thesis, Colorado School of Mines.
- Zhao, H., Sun, M., & Firoozabadi, A. (2016). Anti-agglomeration of natural gas hydrates in liquid condensate and crude oil at constant pressure conditions. *Fuel*, 180, 187–193.

## APPENDIX

### Appendix A – Composition of Kerdane® used

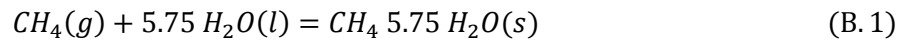
The composition of Kerdane® provided by TOTAL FLUIDES is shown in Table A. 1.

Table A. 1: Chemical composition and properties of Kerdane®.

Substances/Properties	Kerdane®
Chemical Composition	Hydrocarbons, C11-C14, n-alkanes, iso-alkanes, cyclic, < 2% aromatics
Appearance	Clear light yellow
Boiling Point/Interval	180-260°C
Flash Point	>64°C
Density	790-825 kg.m <sup>-3</sup> at 15°C
Kinematic Viscosity	2.1 mm <sup>2</sup> .s <sup>-1</sup> at 25°C

### Appendix B – Water conversion calculation

To calculate the water conversion, these following equations were used:



$$n_{crw} = n_{CH_4} * 5.75 \quad (B.2)$$

Where  $n_{crw}$  is the number of mol of water consumed for crystallization [mol] and  $n_{CH_4}$  is the number of mol of methane consumed [mol].

$$\eta = \frac{n_{crw}}{n_w^i} 100\% \quad (B.3)$$

Where  $n_w^i$  is initial mol of water [mol] and  $\eta$  is the water conversion (%).

$$n_w^i = \frac{m_w^i}{M_w} \quad (B.4)$$

Where  $m_w^i$  is initial mass of water [g] and  $M_w$  is molecular weight of water [g/mol].

## Appendix C – Hydrate volume fraction calculation

To calculate the hydrate volume, these following equations are applied:

$$N_{crw} = n_{crw} * N(Avogadro) \quad (C.1)$$

Where  $N_{crw}$  is the number of water molecules consumed;  $n_{crw}$  is the number of mol of water consumed [mol] and  $N(Avogadro)$  is the Avogadro number ( $6.022 \times 10^{23} \text{ mol}^{-1}$ ).

$$n_{cell} = \frac{N_{crw}}{46} \quad (C.2)$$

Where  $n_{cell}$  is the number of hydrate cells in the hydrate structure  $l$  and 46 is the number of water molecules of one unit cell for hydrate structure  $l$ .

$$V_H = n_{cell} * V_{cell} \quad (C.3)$$

Where  $V_H$  is the hydrate volume [ $\text{m}^3$ ] and  $V_{cell}$  is the volume of one unit cell of hydrate structure  $l = 1.728 \times 10^{-27} \text{ [m}^3/\text{cell}]$ .

$$HV = \frac{V_H}{V_{total}} 100\% \quad (C.4)$$

Where  $HV$  the hydrate volume fraction [%] and  $V_{total}$  is the total volume of hydrate and liquid [ $\text{m}^3$ ].

## Appendix D – Rate of crystallization

To calculate the rate of crystallization  $R(t)$  and average crystallization rate  $\bar{R}(t)$ , these following equations were used:

$$R_i(t) = \frac{\%HV(t(i+1)) - \%HV(t(i))}{(t(i+1) - t_i)} \text{ [%HV/min]}; [t_{i+1} - t_i = 2,5 \text{ min}] \quad (D.1)$$

$$\bar{R}(t) = \frac{\%HV(total)}{\Delta t(\text{time of crystallization})} = \sum_{i=1}^{n-1} \frac{R_i(t)}{n-1} \text{ [%HV/min]} \quad (D.2)$$

$$R(t)^{MAX} = MAX(R_i(t)) \text{ [%HV/min]} \quad (D.3)$$

## Appendix E – Interfacial tension measurement

The interfacial tension (IFT) of water and Kerdane<sup>®</sup> without and with 0.01%AA-LDHI is shown in Table E. 1.

**Table E. 1: The interfacial tension (IFT) of water and Kerdane<sup>®</sup> without and with 0.01%AA-LDHI.**

Temperature	AA-LDHI	IFT
(°C)	(wt.% of water)	(mN.m <sup>-1</sup> )
18	0	47.7
20	0.01	0.40



## Appendix F – Stability and average chord length of dispersion (Gas-lift protocol)

Figure F. 1 shows the pressure drop and average chord length during the dispersion process for the experiments without AA-LDHI at low and high water cut. It is obvious that the dispersion was quite homogeneous during the time. In fact, in high water cut systems, a constant pressure drop was observed. In low water cut system (30%WC), pressure drop and average chord length presented a significant fluctuation due to less homogeneous dispersion. The instability of liquid-liquid dispersion in low and high water cut systems was explained by the lack of emulsifiers. Indeed, this dispersion was only maintained mechanically due to shear. The average chord length of dispersion decreased with the decrease in water cut. This is also due to the higher amount of oil dispersed better in high water cut systems. This also means that the size of water droplets dispersed in the oil continuous phase was smaller than the size of oil droplets dispersed in the water continuous phase. This can be explained that higher viscosity of oil than that of water.

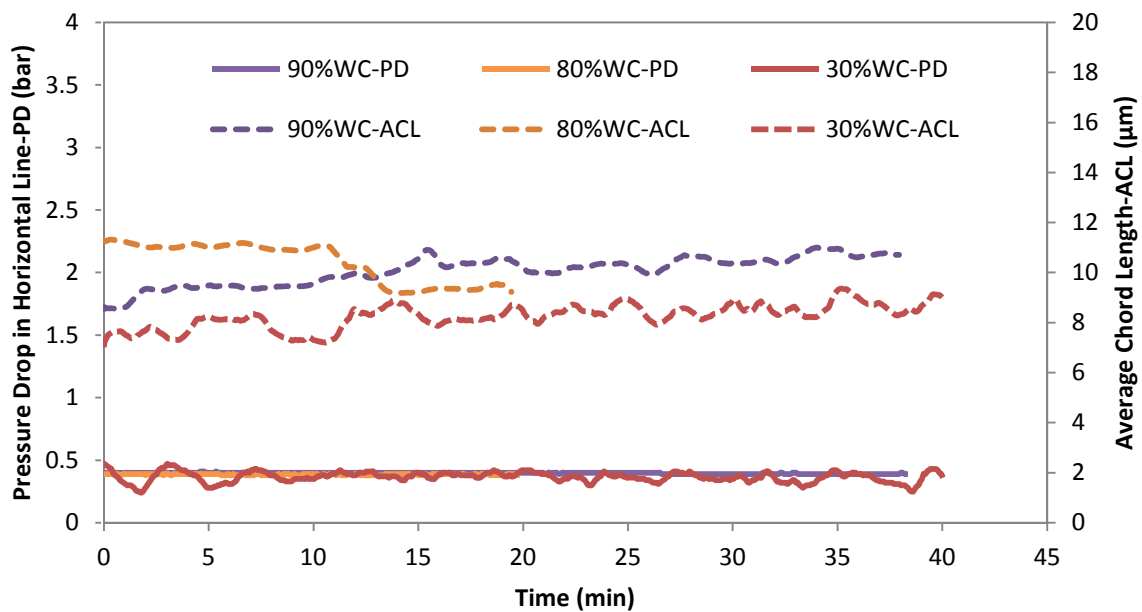


**Figure F. 1: Pressure drop (solid line) and average chord length (dashed line) during the dispersion of the experiments without additive and salt.**

In the presence of AA-LDHI (Figure F. 2), dispersions were more stable in terms of pressure drop and average chord length measurements compared to dispersions without AA-LDHI. However, the concentration of additives was not sufficient to stabilize the dispersion completely. A little of foam was also observed in the mixtures with AA-LDHI during dispersion process induced by compressed air. This was assumed that the addition of AA-LDHI lowered the interfacial tension between oil, water, and air (Appendix E) leading to easier and greater dispersion and foaming (Al-Sahhaf et al., 2005) and (Wilson, 1989). Generally, the average chord length of dispersions with AA-

LDHI was smaller compared to that without AA-LDHI in the low water cut system. Similar to experiments without AA-LDHI, the average chord length of dispersion with AA-LDHI declined with the reduction in water cut. The explanation for experiments without AA-LDHI can be applied to those without AA-LDHI.

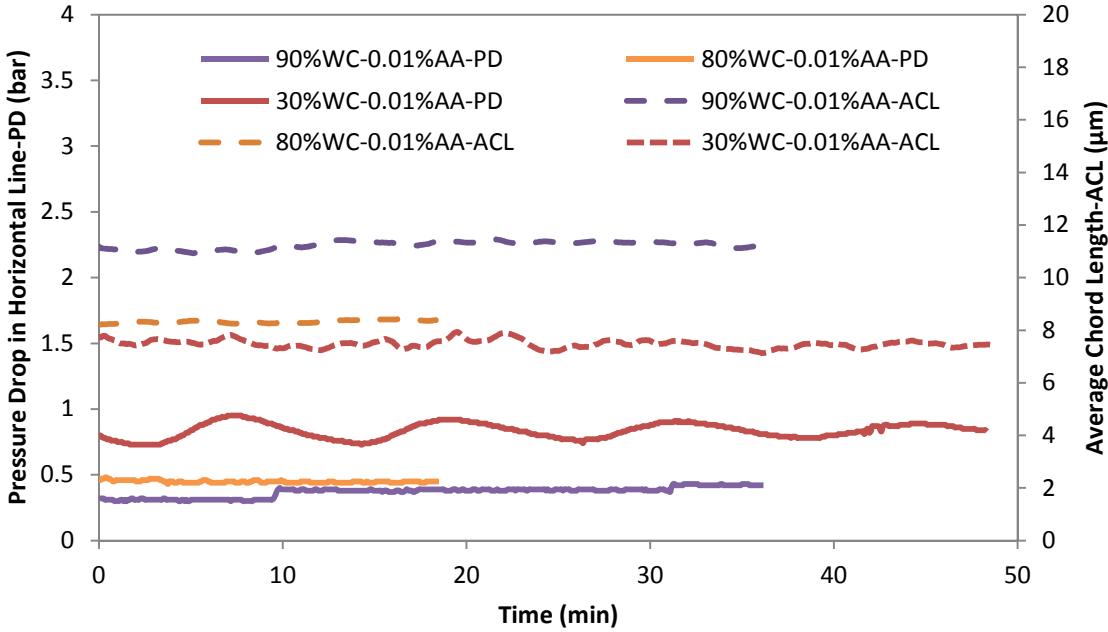


**Figure F. 2: Pressure drop (solid line) and average chord length (dashed line) during the dispersion of the experiments with additive.**

The experiments with salt exhibited less homogeneity than those without salt (Figure F. 3) in term of pressure drop. This showed some effects of salt on the stability of dispersions. Especially, in the low water cut system, there was a disturbing trend in pressure drop and average chord length signals. Given the fact that adding salt caused higher interfacial tension between salt water and oil (Cai et al., 1996). As a result, the dispersion became less dispersed and non-homogeneous. Interestingly, the average chord length of dispersion increased with the decline in water cut. This is probably because the presence of salt increased the IFT between oil and water. This cause more coalescence at a higher volume of the dispersed phase. As a result, the higher amount of oil lowered the dispersion leading to a higher average chord length of dispersion.

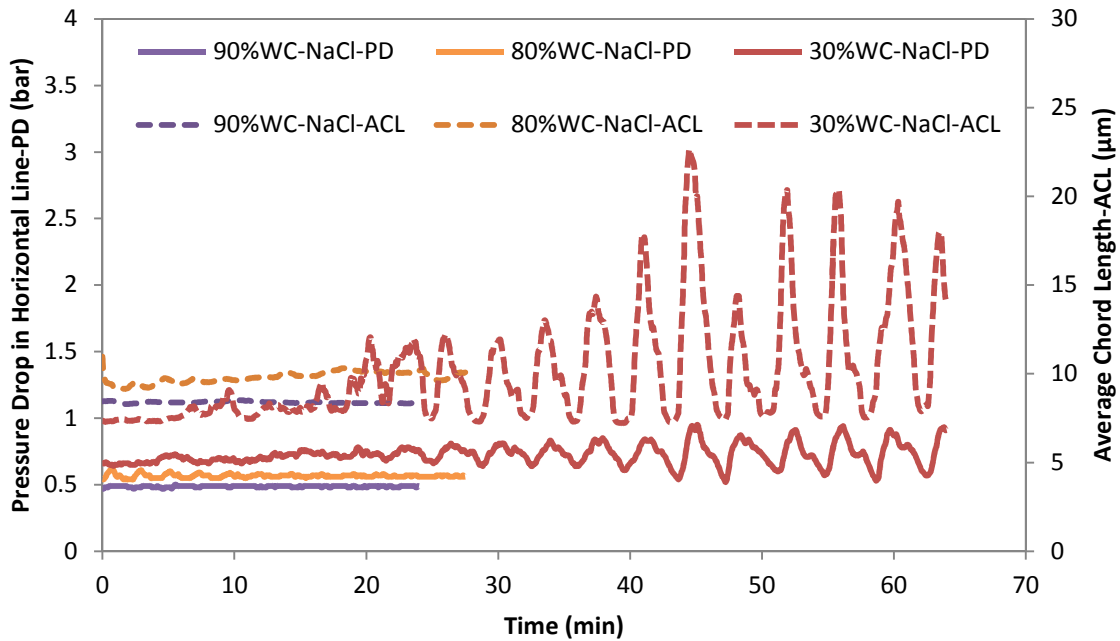


**Figure F. 3: Pressure drop (solid line) and average chord length (dashed line) during the dispersion of the experiments with salt.**

Dispersions of mixtures with both salt and AA-LDHI from low to high water cut systems are illustrated in Figure F. 4. In high water cut systems, average chord length and pressure drop measurements fluctuated during the course of the experiments. In the low water cut system, the average chord length experienced a more stability compared to those in high water cut systems. This can be explained that the oil continuous phase probably could stabilize the dispersion. Compared to the experiments with only salt (Figure F. 3), the addition of AA-LDHI stabilized dispersion in the low water cut system and destabilized dispersion in high water cut systems when salt was present. This also can be explained by various behaviors of AA-LDHI at different continuous phases. This can infer that AA-LDHI revealed a better performance oil continuous phase (in the presence of salt). Compared to the experiments with merely AA-LDHI (Figure F. 2), it was found that addition of salt (in the presence of AA-LDHI) caused the instability of dispersion in both low and high water cut systems. This can be again explained by higher IFT between water and oil in the presence of salt, caused less dispersion and less homogeneity. Similar to experiments with and without AA-LDHI, the average chord length of dispersion with both salt and AA-LDHI decreased with the decrease in water cut. The explanation for experiments with and without AA-LDHI can be applied to those with both salt and AA-LDHI.

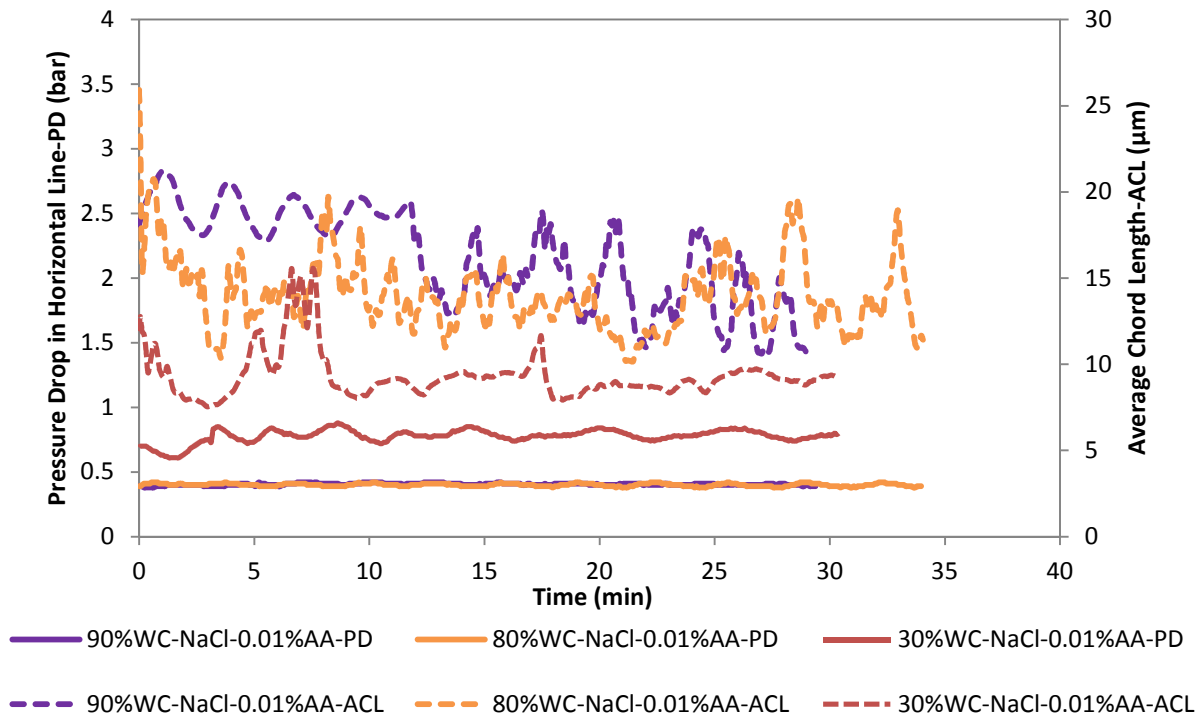


**Figure F. 4: Pressure drop (solid line) and average chord length (dashed line) during the dispersion of the experiments with both salt and additive.**

Dispersion with both salt and different amount of AA-LDHI in low water cut systems (30%WC) indicated an unsteady trend of pressure drop and average chord length (as shown in Figure F. 5) compared to the experiment with 30%WC-0.01%AA-LDHI (Figure F. 2). This can be interpreted as an interaction between salt and AA-LDHI, lowering the performance of AA-LDHI. This caused unstable dispersion and formation of foam. However, in comparison with the experiment with 30%WC-NaCl (Figure F. 3), the trends of pressure drop and average chord length of the experiments with both salt and AA-LDHI (Figure F. 5) were more steady. This means that AA-LDHI improved the stability of dispersion. The fact that almost constant pressure drop and average chord length were observed at the end of dispersion process of the experiment with salt and 0.5 wt.% dosage of AA-LDHI. Interestingly, it is observed that the average chord length of dispersion with 0.01%AA-LDHI was lower than those at 0.05, 0.1, and 0.5%AA-LDHI. This is explained that at 0.01%AA-LDHI, the water droplets dispersed in the oil continuous phase with quite small sizes. However, from 0.05%AA-LDHI, phase inversion may occur. Consequently, the oil droplets dispersed in the water continuous phase with bigger sizes compared to the water droplets in oil continuous phases. This is also in agreement with the conclusions as stated above. Additionally, from 0.05 wt.% dosage of AA-LDHI, the rise in the amount of AA-LDHI declined the average chord length of dispersion. This is due to the AA-LDHI lowered the IFT between oil and water.

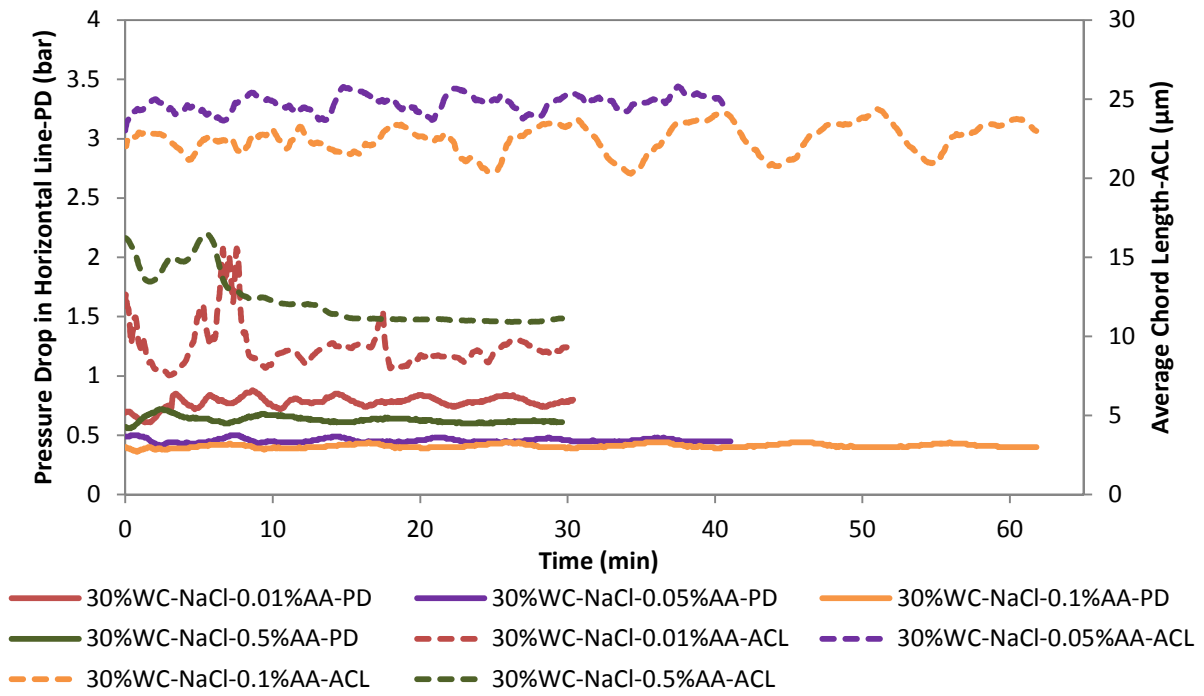
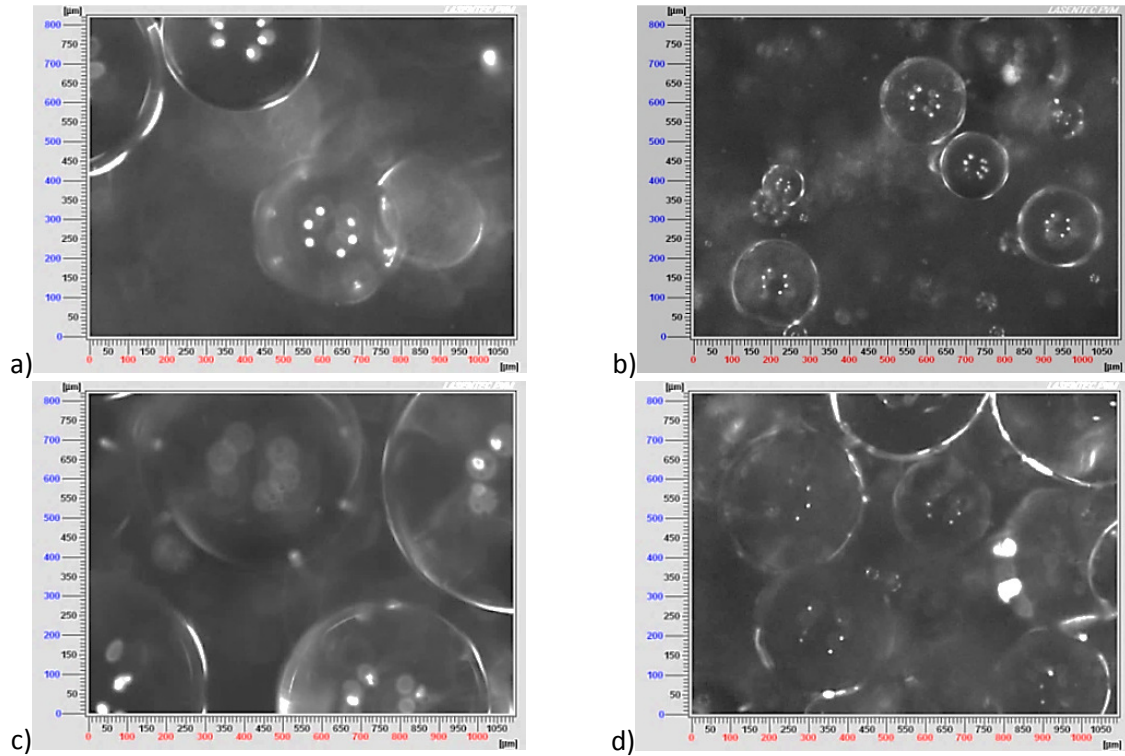
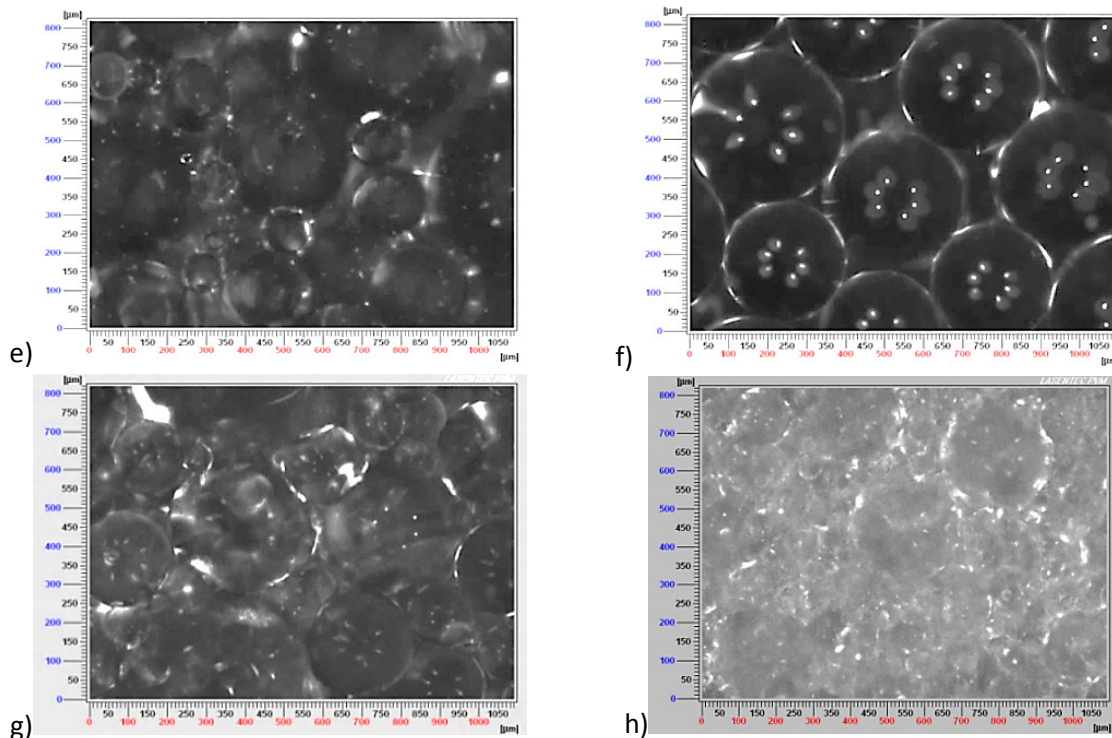


Figure F. 5: Pressure drop (solid line) and average chord length (dashed line) during the dispersion of the experiments with both salt and additive with 30%WC.





**Figure F. 6: PVM images of different mixtures during the dispersion process at  $4.5\pm 0.5^\circ\text{C}$  and 1 bar: (a) 90%WC-NaCl without AA-LDHI; (b) 90%WC-NaCl with 0.01% AA-LDHI; (c) 80%WC-NaCl without AA-LDHI; (d) 80%WC-NaCl with 0.01% AA-LDHI; (e) 30%WC without AA-LDHI and salt; (f) 30%WC-NaCl without AA-LDHI; (g) 30%WC-NaCl with 0.05%AA-LDHI; and (h) 30%WC-NaCl with 0.5% AA-LDHI.**

PVM images (Figure F. 6) show numerous droplets in the oil-water dispersion with and without salt and/or AA-LDHI. In this study, in high water cut dispersion systems (80-90%WC), it was supposed that oil droplets were dispersed in a water continuous phase. On the contrary, in low water cut systems (30%WC), it was assumed that water droplets were dispersed in the oil continuous phase. These PVM images supported the hypothesis that the droplets were poly-dispersed at all water cuts. Generally, in high water cut systems (Figure F. 6 a, b, c, d and e), addition of AA-LDHI decreased the size of droplets dispersed in the continuous phase. In low water cut systems, the addition of salt caused bigger droplets due to higher interfacial tension between oil and salty water (Figure F. 6 f, g, h, i, and j). Addition of AA-LDHI (in the presence of salt) created smaller droplets co-existing with bigger droplets.

## Appendix G – Experimental results (density & flowrate) with Gas-lift protocol

### G.1. Experiments with 100%WC

The experimental results (density & flowrate) at 100%WC with the gas-lift protocol are shown in Figure G. 1.

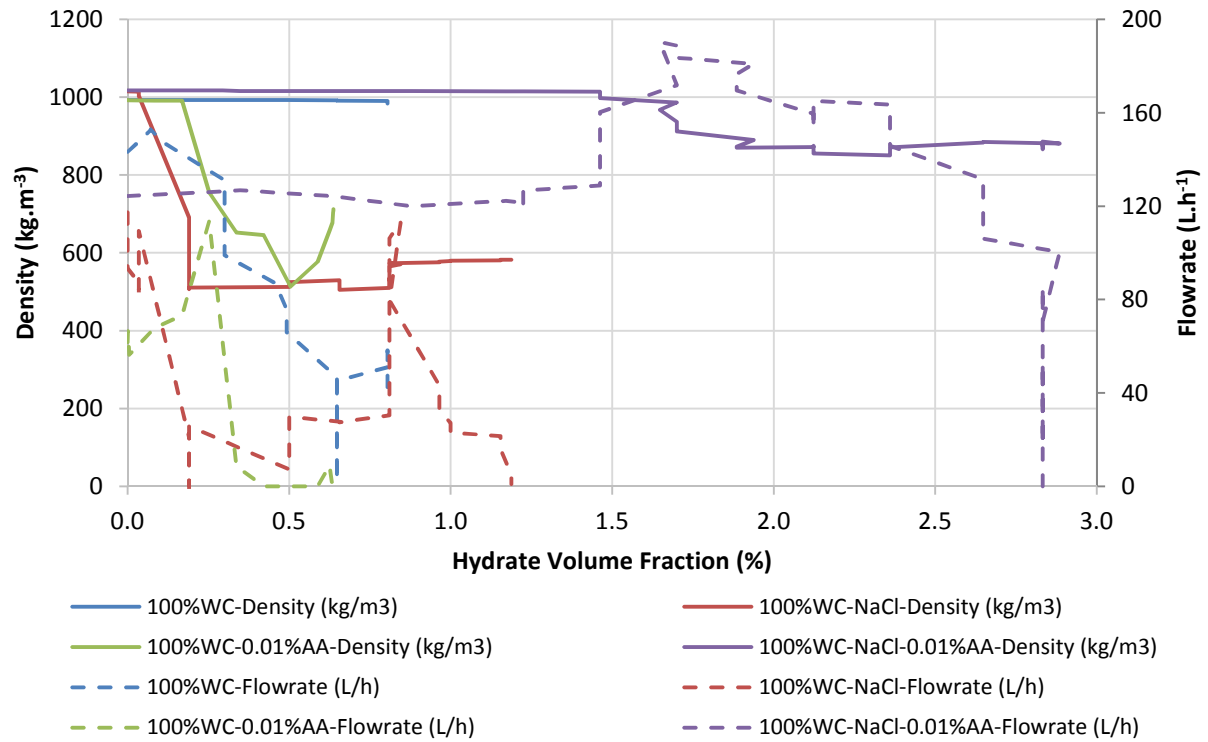
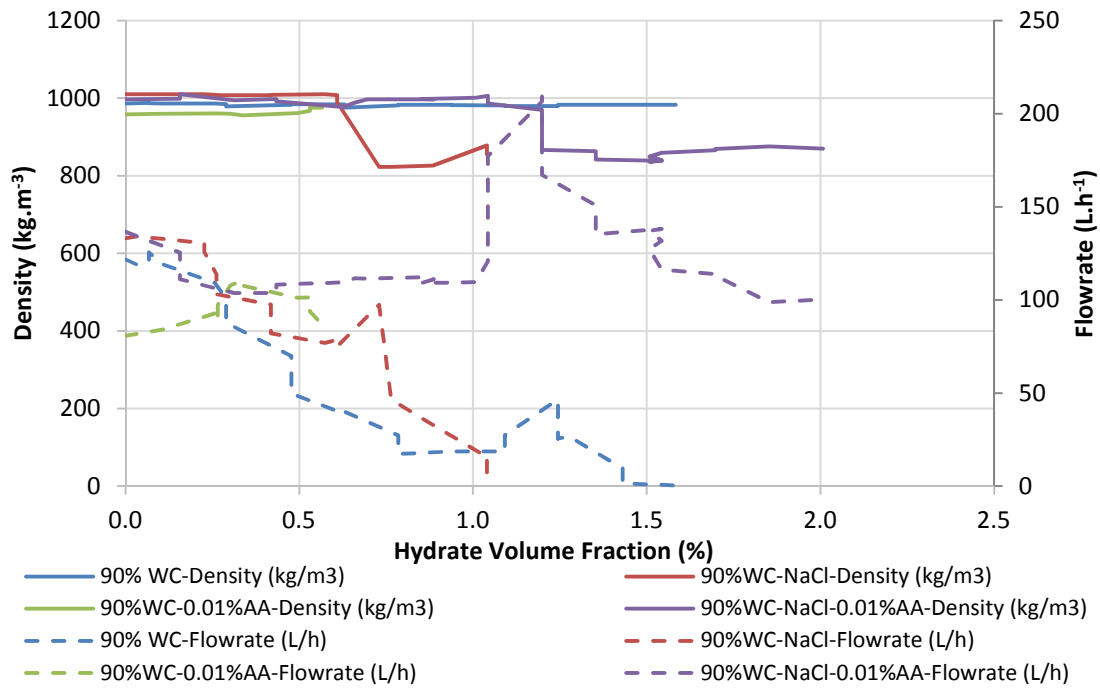


Figure G. 1: Experimental results with the gas-lift protocol (density and flowrate as a function of hydrate volume fraction) with 100%WC.

### G.2. Experiments with 90%WC

The experimental results (density & flowrate) at 90%WC with the gas-lift protocol are shown in Figure G. 2.



**Figure G. 2: Experimental results with the gas-lift protocol (density and flowrate as a function of hydrate volume fraction) with 90%WC.**

### G.3. Experiments with 80%WC

The experimental results (density & flowrate) at 80%WC with the gas-lift protocol are shown in Figure G. 3.

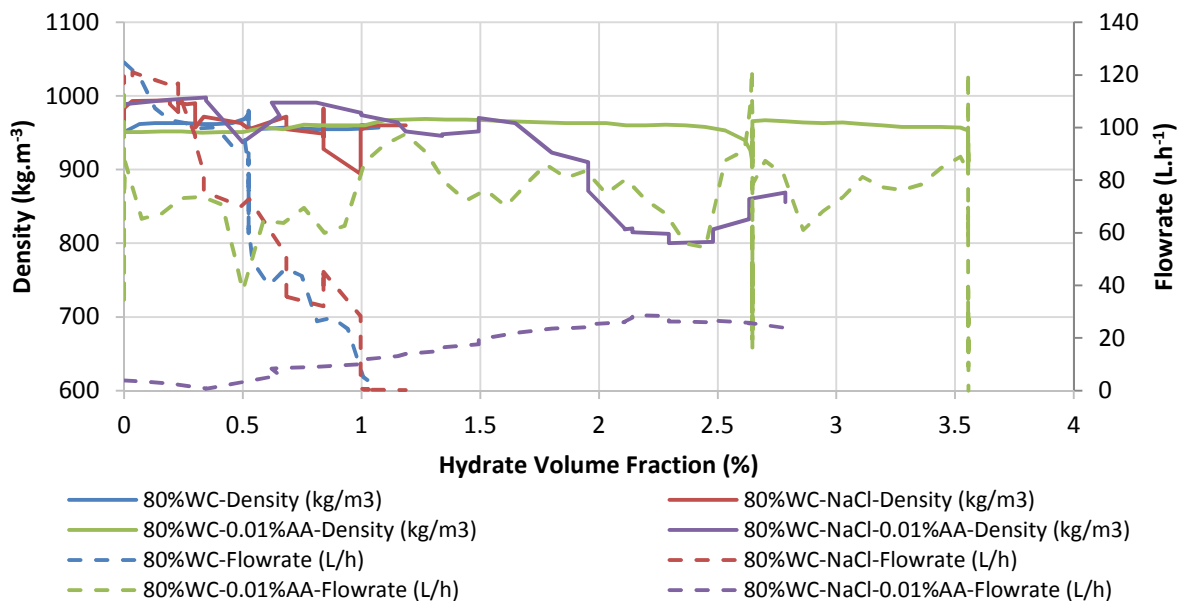


**Figure G. 3: Experimental results with the gas-lift protocol (density and flowrate as a function of hydrate volume fraction) with 80%WC.**

#### G.4. Experiments with 30%WC

In the series of the experiments (density & flowrate) at 30%WC (Figure G. 4), it is noted that sometimes gas injection into the flowloop was performed manually to enhance hydrate formation. For this, the ballasts system has to stop for several minutes to increase pressure and restart once pressure reached desire value (75 bar) because of system security. It is highly noted that a sudden decrease or increase in flowrate and/or density is because of stop and restart the ballast system (to increase pressure in the flowloop).

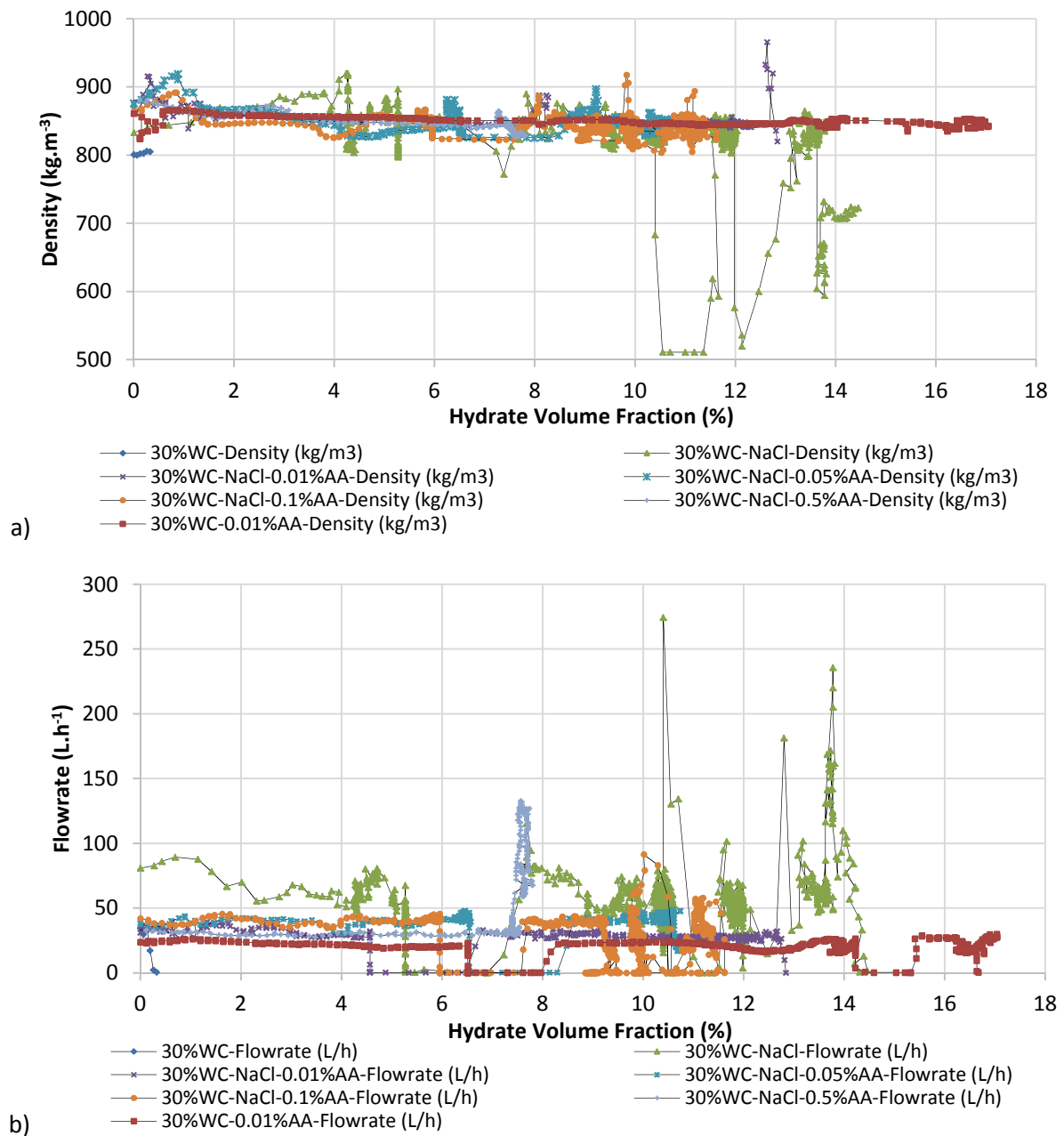
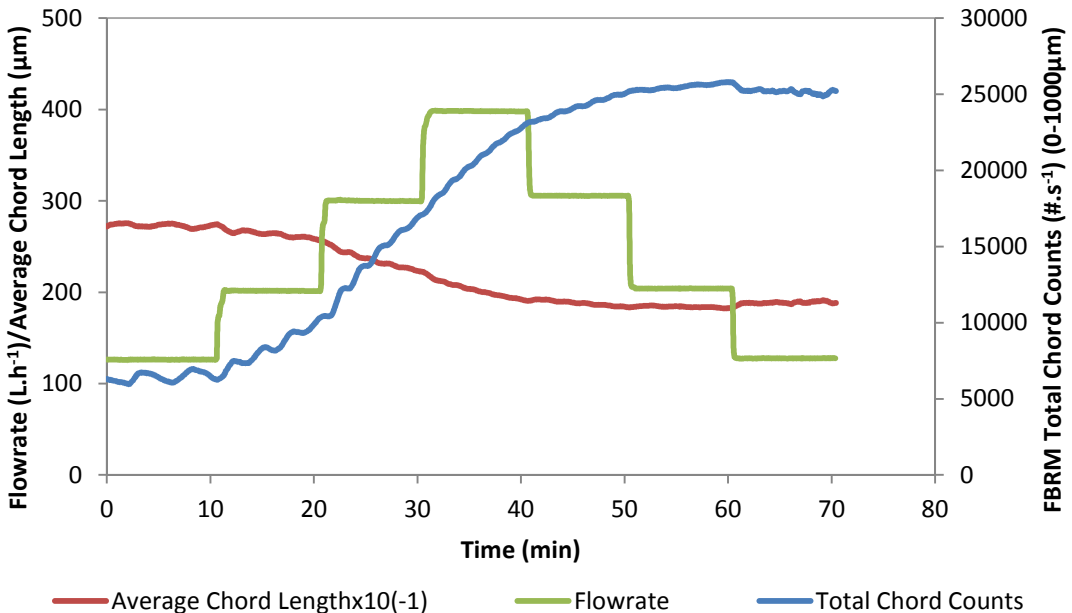


Figure G. 4: Experimental results with the gas-lift protocol: (a) density and (b) flowrate as a function of hydrate volume fraction) with 30%WC.

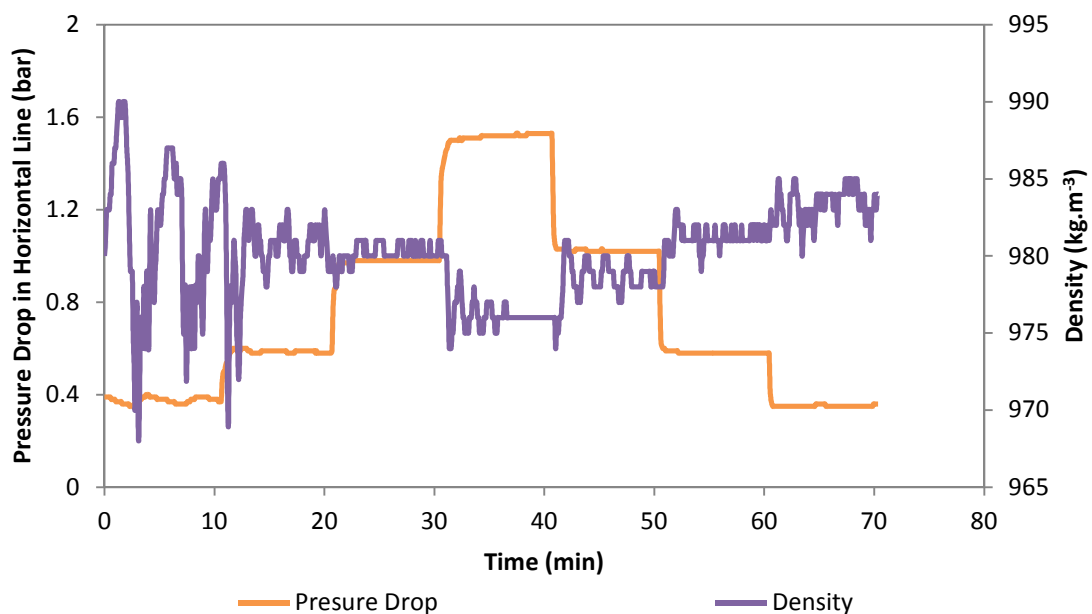
**Appendix H – Rheological study of dispersion with 80%WC (Moineau pump protocol)**

The higher flowrate increased the FBRM total chord counts of dispersion and lowered the mean droplets size of dispersion with 80%WC (Figure H. 1). The homogeneity of dispersion might be also identified through the FBRM total chord counts, average chord length, pressure drop, and density. At the beginning of dispersion (or low flowrate, from 125-200L.h<sup>-1</sup>), fluctuations of density, pressure drop, FBRM total chord counts, and average chord length were observed. At higher flowrate (300-400L.h<sup>-1</sup>), higher stability and better dispersion were observed. Interestingly, the increase in flowrate decreased the density. It is assumed that at low flowrate, oil and water are less dispersed because of lower shear force compared to that at high flowrate. A stratified flow pattern was hence probably occurred at low flowrate. As the viscosity of the oil is higher than the viscosity of water, water might flow faster than oil. In addition, oil can be trapped somewhere in the pipelines. As a result, densimeter Coriolis detected more water than oil in flow. Thus a higher density of dispersion measured at lower flowrate was obtained.

Once the flowrate reached the highest value (400L.h<sup>-1</sup>), flowrate was decreased step by step from 400 to 300, 200, and 125L.h<sup>-1</sup>. Indeed, a significant increase in average chord length and a considerable decrease in the FBRM total chord counts of dispersion were not observed as the theory. This is explained that when flowrate decreased, the dispersion cannot reach its initial state. This is due to less coalescence of droplets at lower flowrate.



a)



b)

**Figure H. 1: Rheological study of the experiment with 80%WC-85%LV: (a) flowrate, average chord length, and FBRM total chord counts and (b) pressure drop and density.**

PVM images in Figure H. 2 confirmed again the dispersion behavior as stated above with more and smaller droplets at higher flowrate for the mixture with 80%WC and 85%LV.

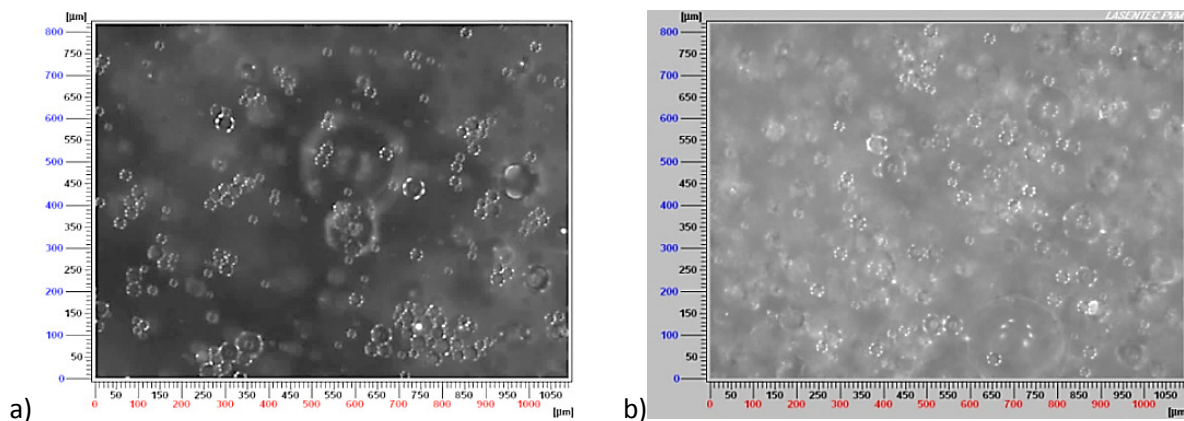


**Figure H. 2: PVM images of dispersion in the rheological study of the experiment with 80%WC-85%LV: (a) 120L.h<sup>-1</sup> and (b) 400L.h<sup>-1</sup>.**

The same trend was observed for the mixture with 80%WC-1%AA-LDHI compared to the mixture with 80%WC (Figure H. 3). In other words, the fluctuations of density, pressure drop, FBRM total chord counts, and average chord length at the beginning of dispersion process (low flowrate) were observed. Furthermore, the increase in the FBRM total chord counts and the decrease in the

average chord length of dispersion with the increase in flowrate were witnessed. However, the FBRM total chord counts of dispersion for the mixture with 80%WC-1%AA-LDHI was considerably higher than the one with 80%WC. Furthermore, mean droplets size of dispersion with 80%WC-1%AA-LDHI was smaller and experienced a bigger step of changing with the varying of flowrate. This is due to AA-LDHI which helped better dispersion of droplets by lowering the interfacial tension between water and oil (Al-Sahhaf et al., 2005); (Appendix E) and prevented coalescence of droplets under shear.

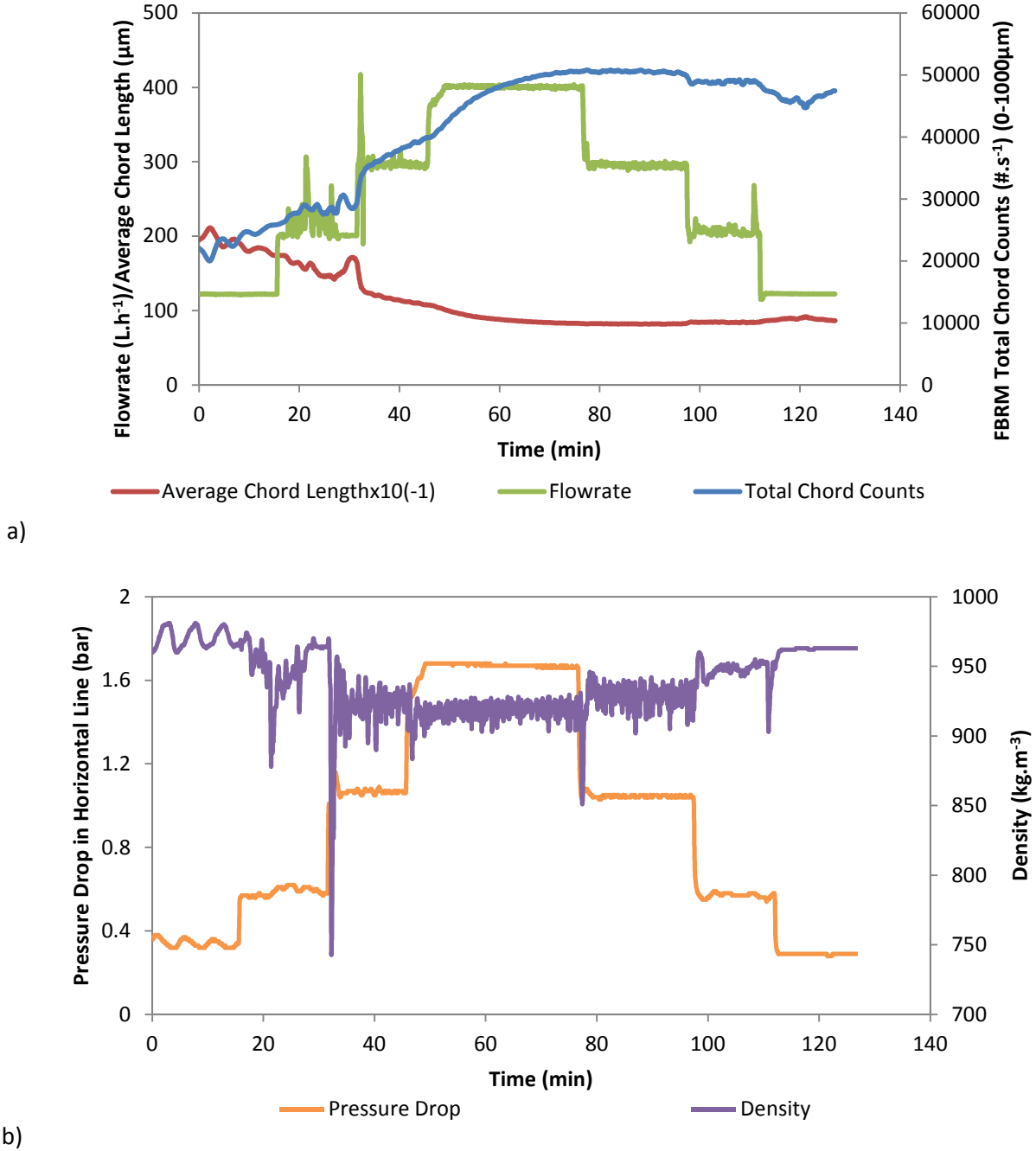


**Figure H. 3: Rheological study of the experiment with 80%WC-1%AA-LDHI-85%LV: (a) flowrate, average chord length, and FBRM total chord counts and (b) pressure drop and density.**

Importantly, the oscillations of flowrate, FBRM total chord counts, average chord length, pressure drop, and density in the experiment with AA-LDHI were higher than those in the experiment without AA-LDHI (Figure H. 1 and Figure H. 3). This is probably due to addition of AA-LDHI lowered the viscosity of dispersion.

PVM images (Figure H. 4) supported again the evidence of dispersion behavior as stated above with more and smaller droplets at higher flowrate. Moreover, the mixture with 80%WC-1%AA-LDHI showed more and smaller droplets than the one without AA-LDHI (Figure H. 2).

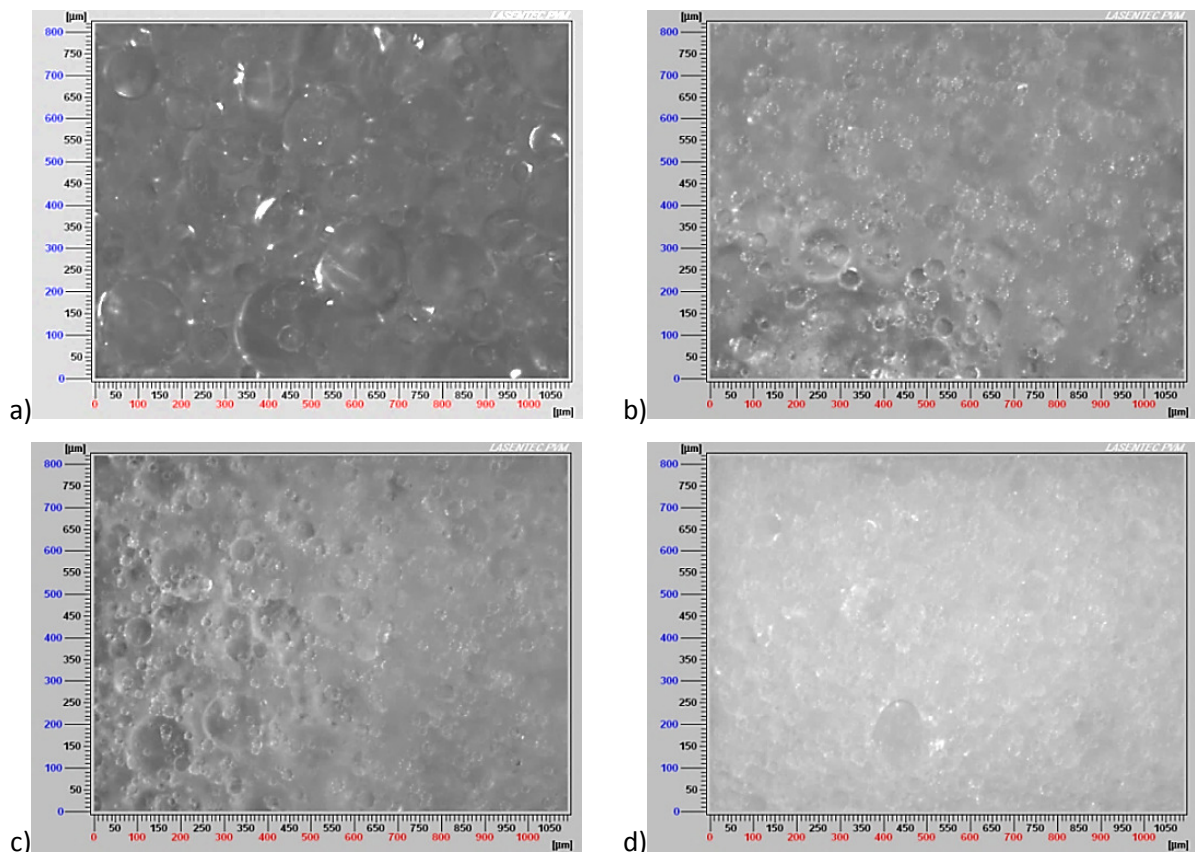
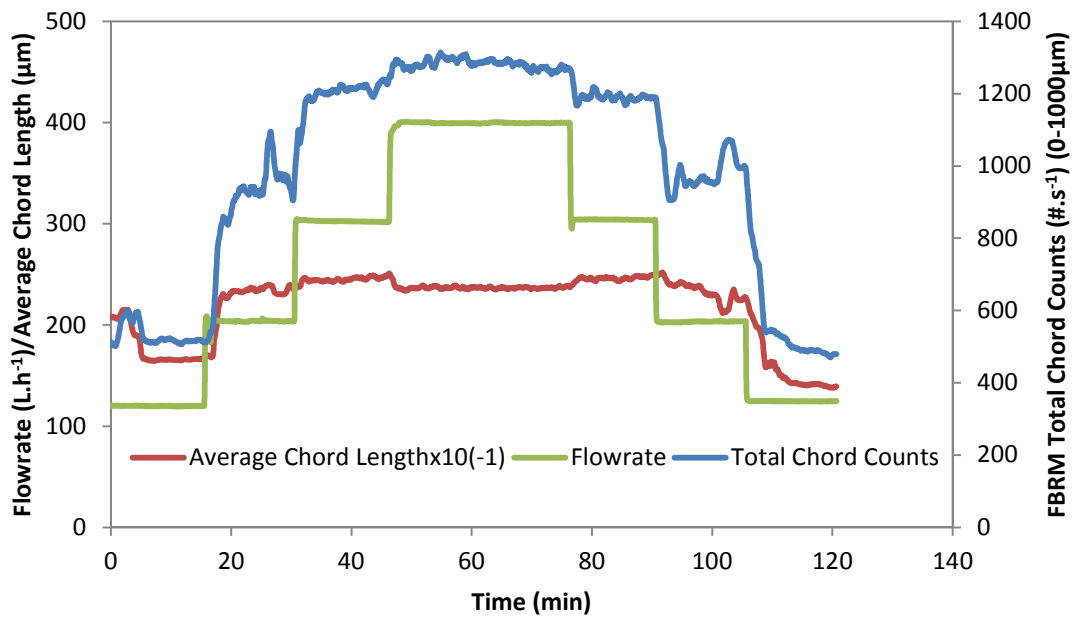
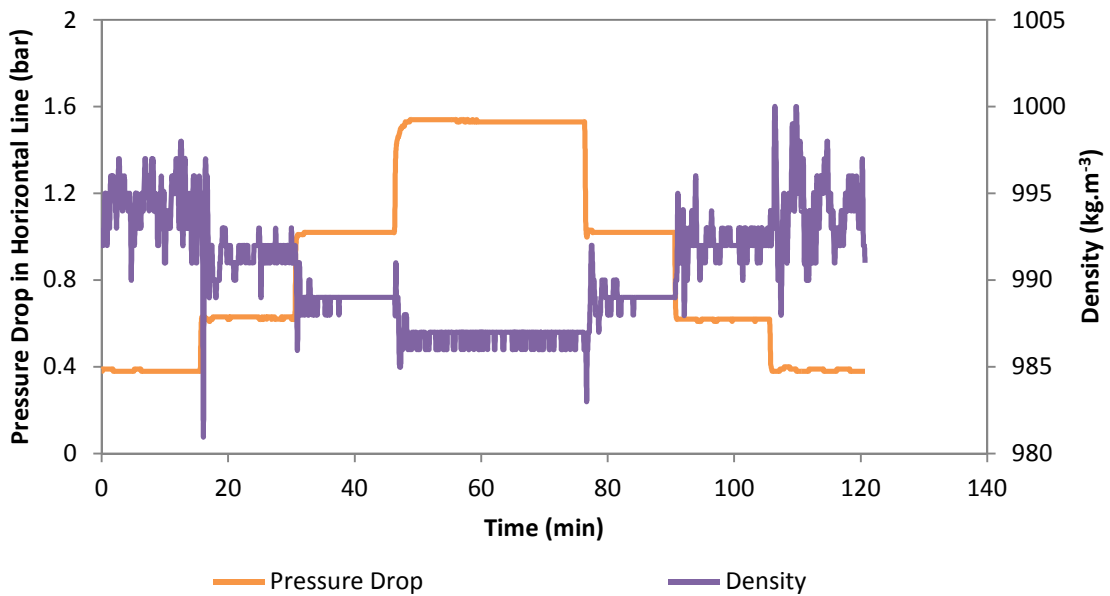


**Figure H. 4: PVM images of dispersion in the rheological study of the experiment with 80%WC-1%AA-LDHI-85%LV: (a) 120L.h<sup>-1</sup>; (b) 200L.h<sup>-1</sup>; (c) 300L.h<sup>-1</sup>; and (d) 400L.h<sup>-1</sup>.**

In Figure H. 5, because of higher IFT between water and oil in presence of salt, lower FBRM total chord counts and a disturbing trend of the average chord length of dispersion were observed with the change of flowrate. This is because of random (less) dispersion and/or (more) coalescence under flowing in the presence of salt. The decrease in flowrate lowered the FBRM total chord counts. The density profile was the same as that with and without AA-LDHI.



a)



b)

**Figure H. 5: Rheological study of the experiment with 80%WC-NaCl-85%LV: (a) flowrate, average chord length, and FBRM total chord counts and (b) pressure drop and density.**

PVM images (in Figure H. 6) confirmed the conclusion that less dispersion occurred in addition of salt with bigger droplets. In this case, few droplets were also observed by PVM measurement.

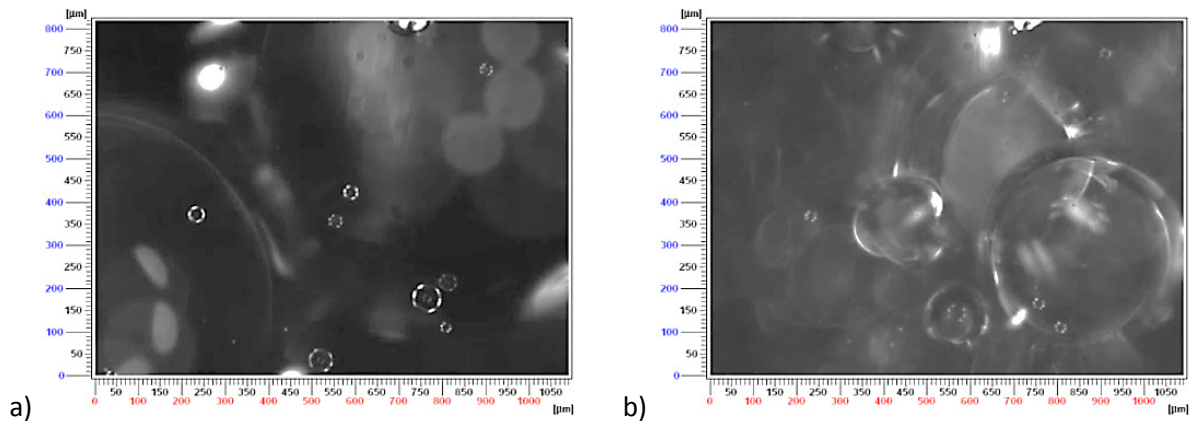
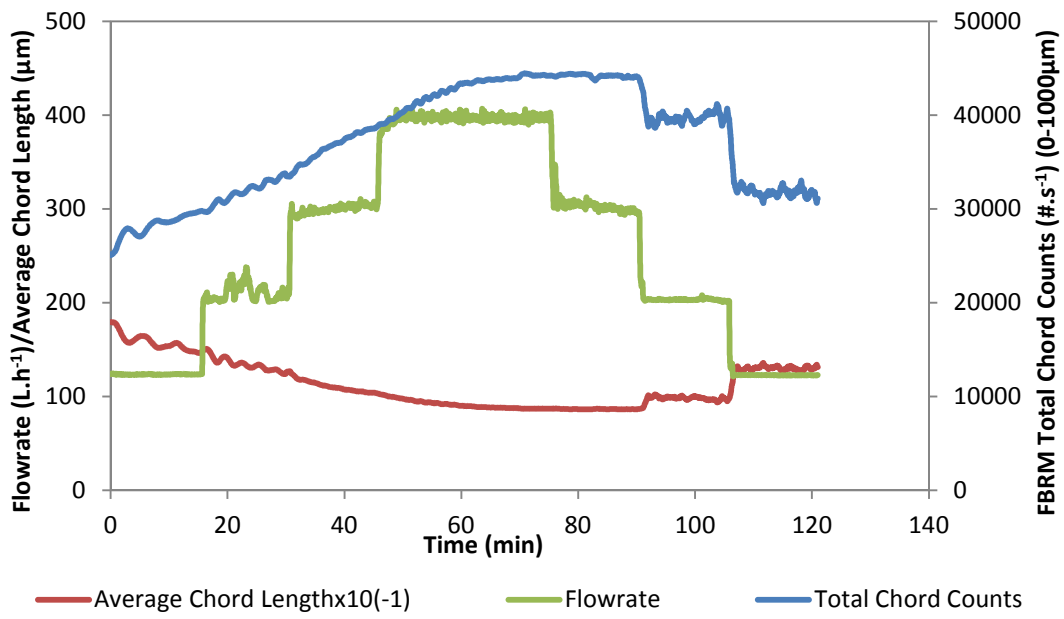


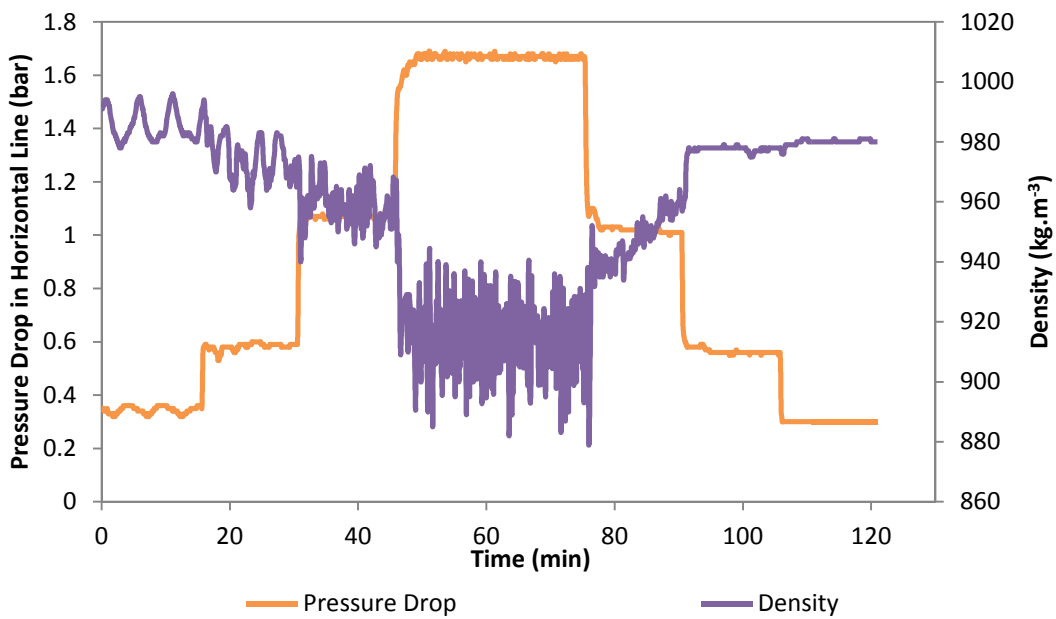
**Figure H. 6: PVM images of dispersion in the rheological study of the experiment with 80%WC-NaCl at 85%LV: (a) 120L.h<sup>-1</sup> and (b) 400L.h<sup>-1</sup>.**

The trend of FBRM total chord counts and average chord length of dispersion for the mixture with 80%WC-NaCl-1%AA-LDHI (Figure H. 7) was the same as the mixtures with and without AA-LDHI (Figure H. 1 and Figure H. 3) but different from that with only salt. This is also due to lower IFT between salt water and oil when adding AA-LDHI, leading to the easier dispersion of droplets. The higher flowrate led to the higher FBRM total chord counts of dispersion. Compared to the mixture with 80%WC-NaCl (Figure H. 5 and Figure H. 7), the addition of AA-LDHI increased the FBRM total chord counts of dispersion. However, compared to the mixture with 80%WC-1%AA-LDHI, the addition of salt decreased the FBRM total chord counts of dispersion (in the presence of AA-LDHI, see Figure H. 3 and Figure H. 7). The same explanation mentioned above can be applied to this case. The density was the same as those with and without AA-LDHI and salt.

In the presence of salt, addition of AA-LDHI might also lower the viscosity of dispersion. The fact that the fluctuations of flowrate, FBRM total chord counts, average chord length, pressure drop, and density in the experiment with AA-LDHI were higher than those in the experiment without AA-LDHI, as seen in Figure H. 5 and Figure H. 7.



a)



b)

**Figure H. 7: Rheological study of the experiment with 80%WC-NaCl-1%AA-LDHI-85%LV: (a) flowrate, average chord length, and FBRM total chord counts and (b) pressure drop and density.**

PVM images demonstrated more dispersion and smaller droplets at higher flowrate (in Figure H. 8). This also matched with total chord counts and average chord length measurement. Additionally, smaller droplets and more dispersion in the experiment with both salt and AA-LDHI compared to the experiment with only salt were witnessed (Figure H. 6).

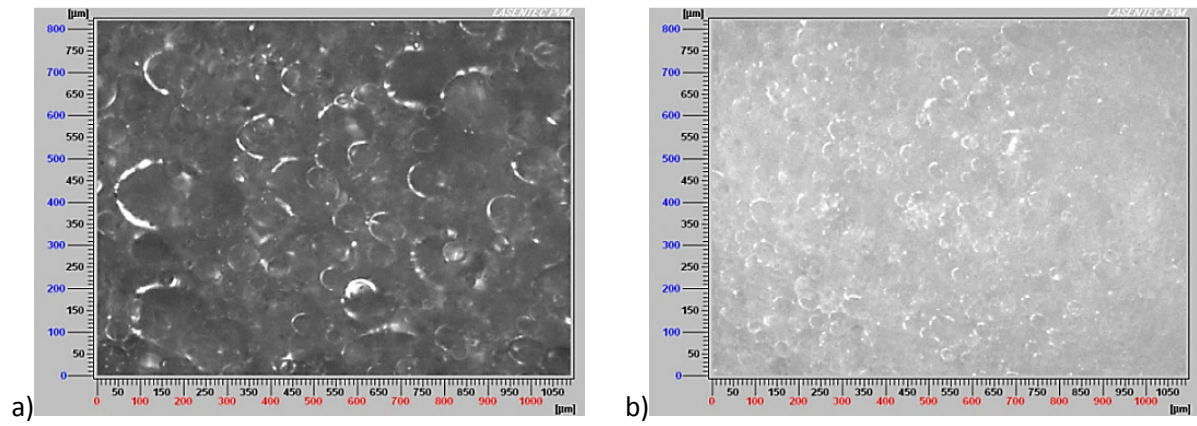
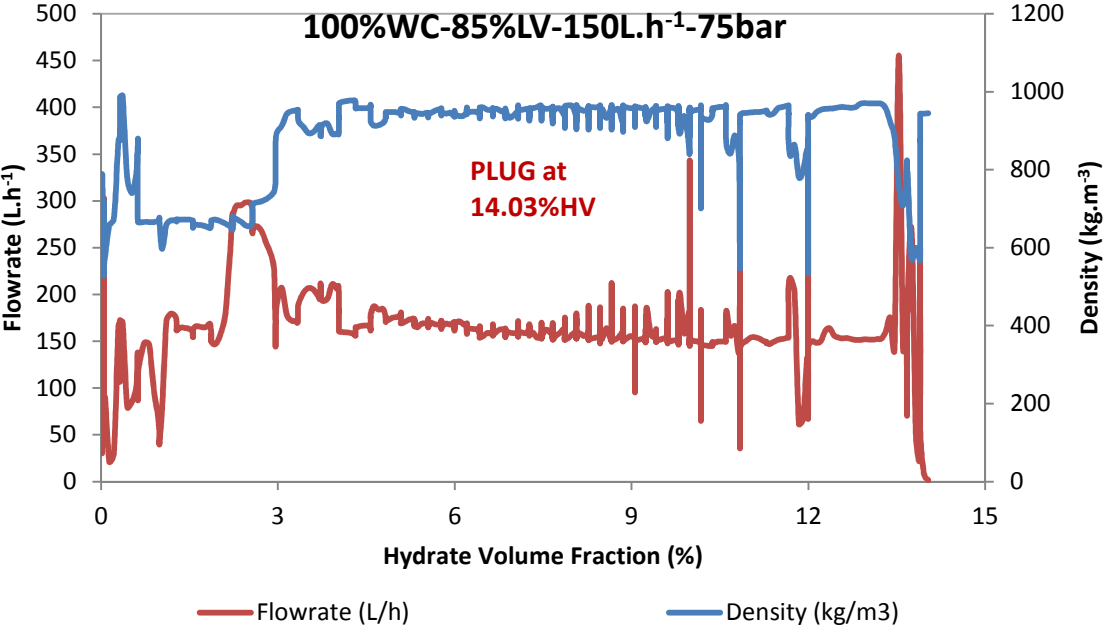


**Figure H. 8:** PVM images of dispersion in the rheological study of the experiment with 80%WC-NaCl-1%AA-LDHI-85%LV: (a)  $120\text{L}\cdot\text{h}^{-1}$  and (b)  $400\text{L}\cdot\text{h}^{-1}$ .

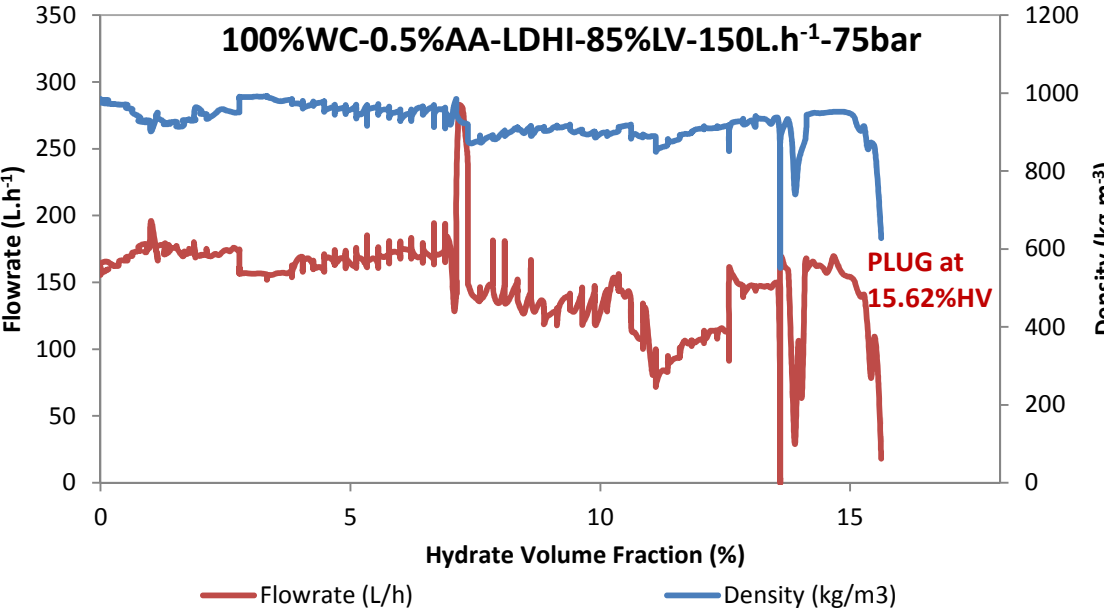
**Appendix I – Experimental results (density & flowrate) with Moineau pump protocol (with and without gas-lift system)**

**I.1. Experiments with 100%WC**

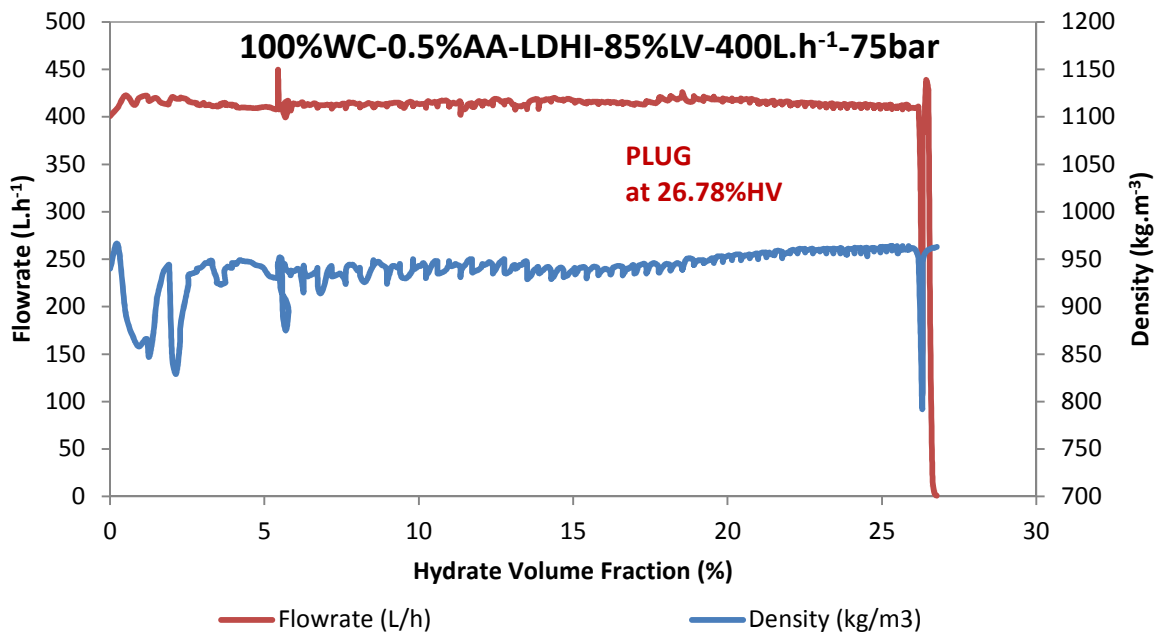
The experimental results (density & flowrate) at 100%WC with the Moineau pump protocol are shown in Figure I. 1.



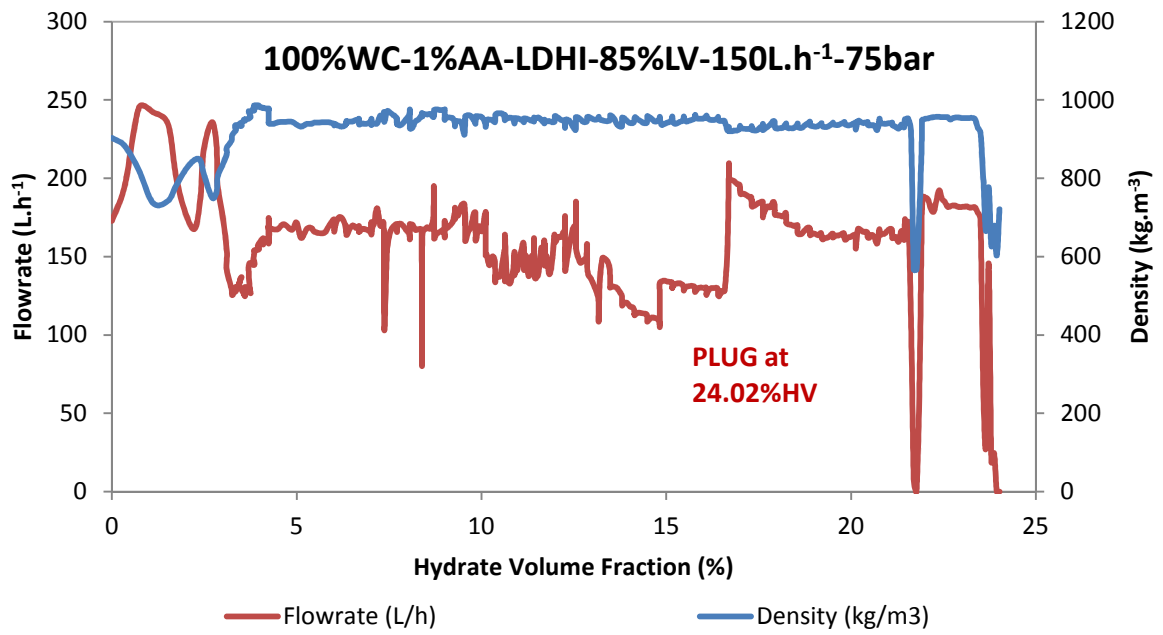
a)



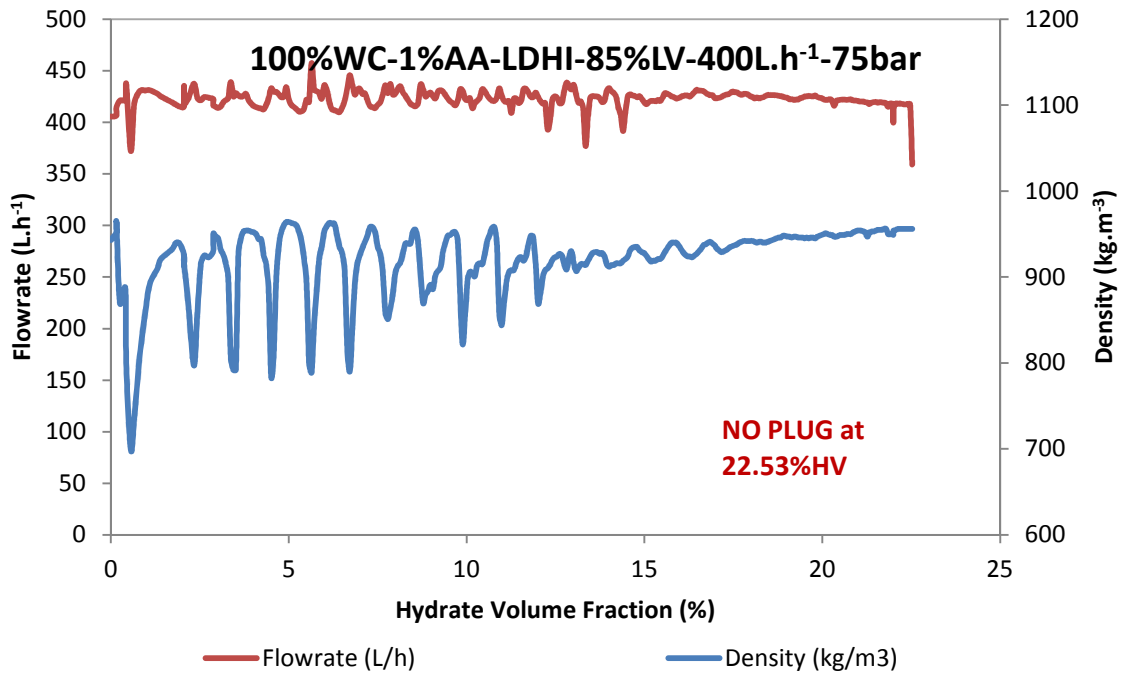
b)



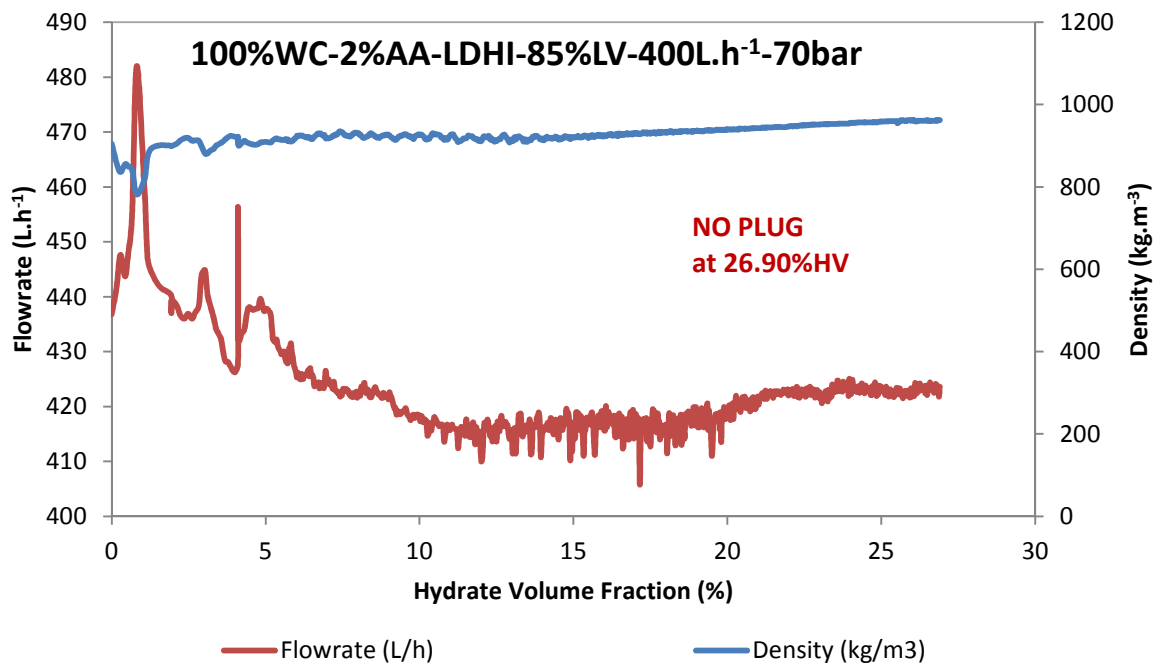
c)



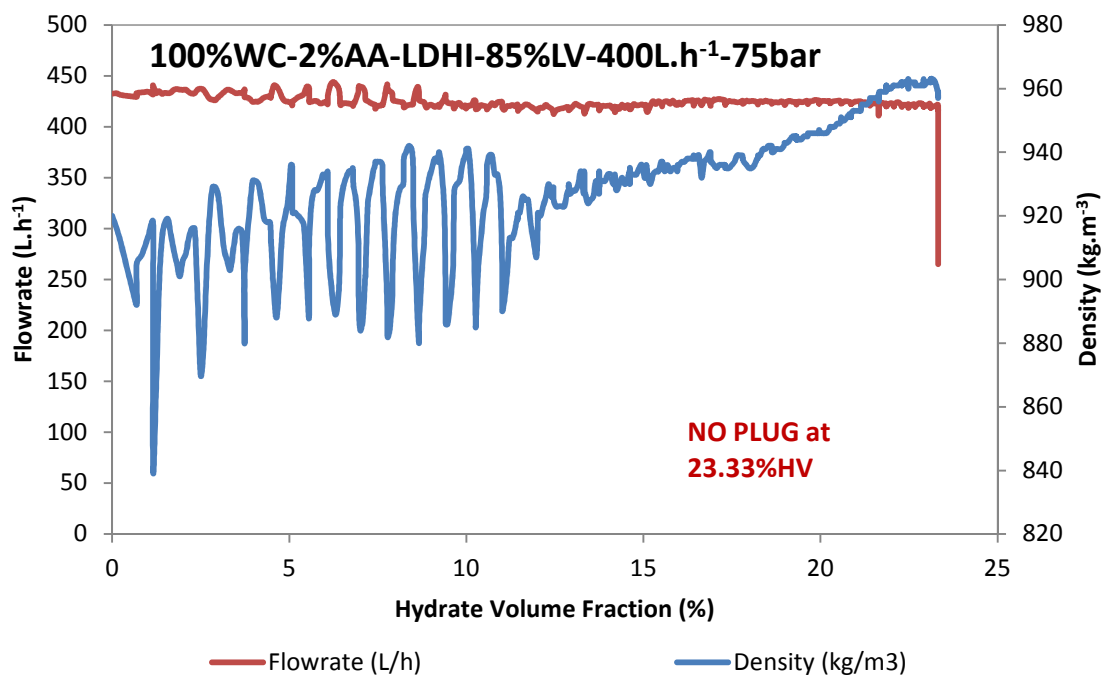
d)



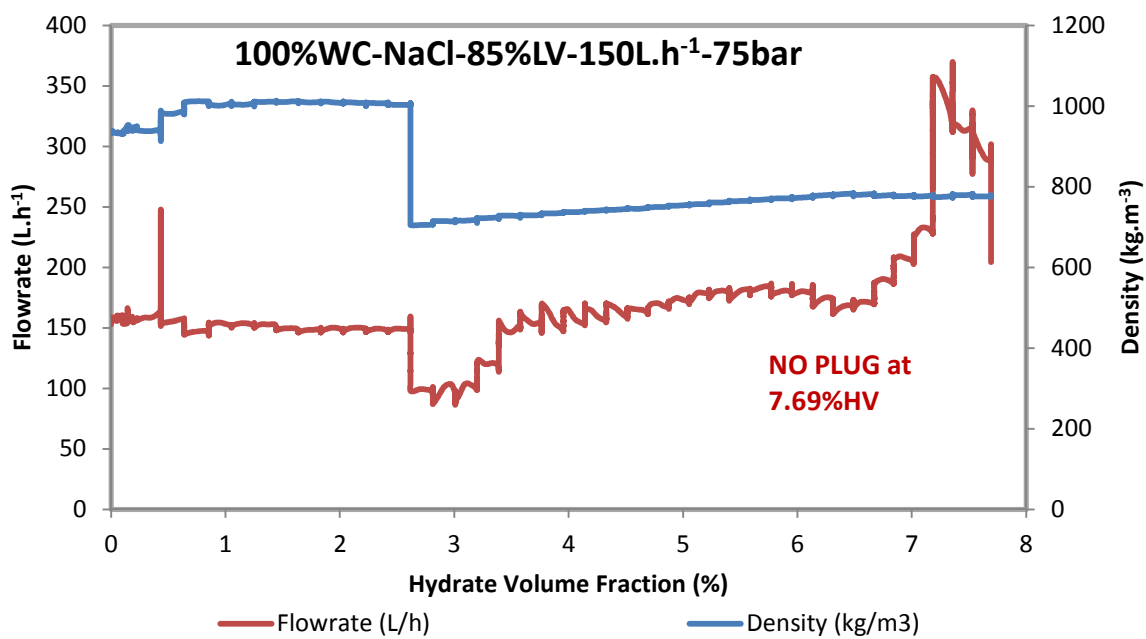
e)



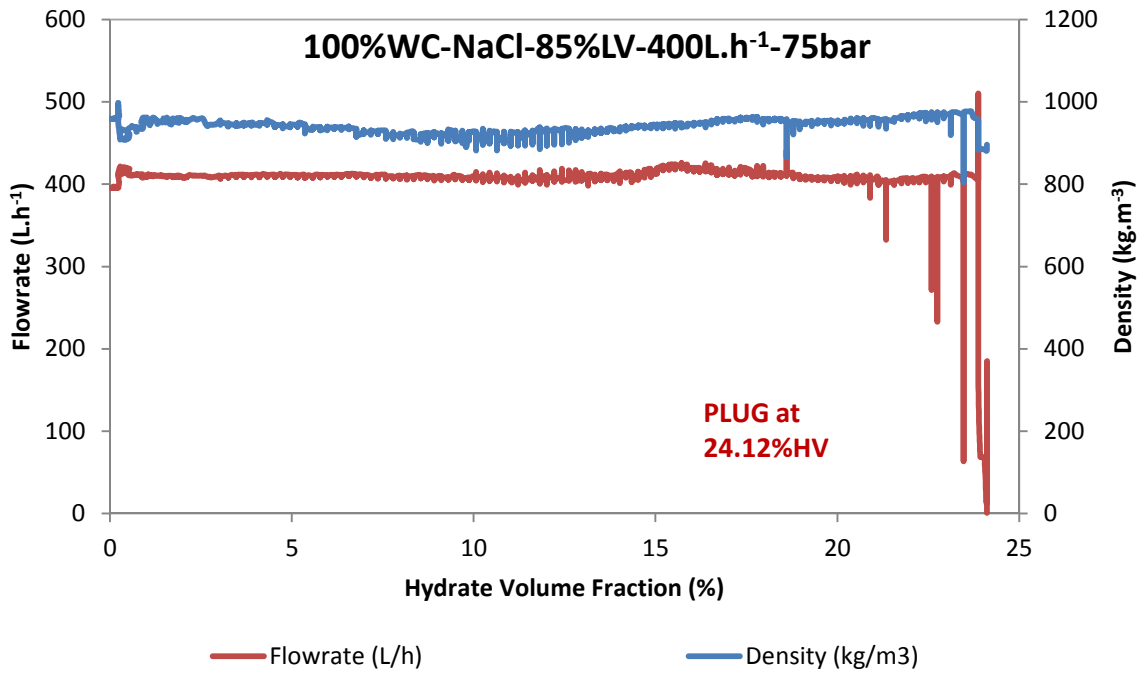
f)



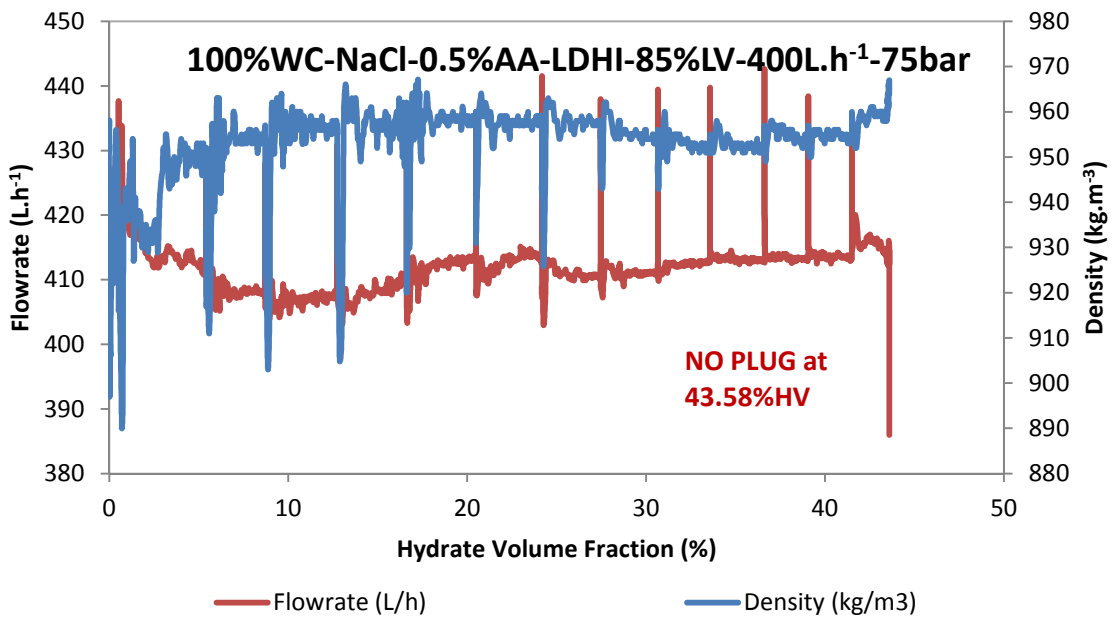
g)



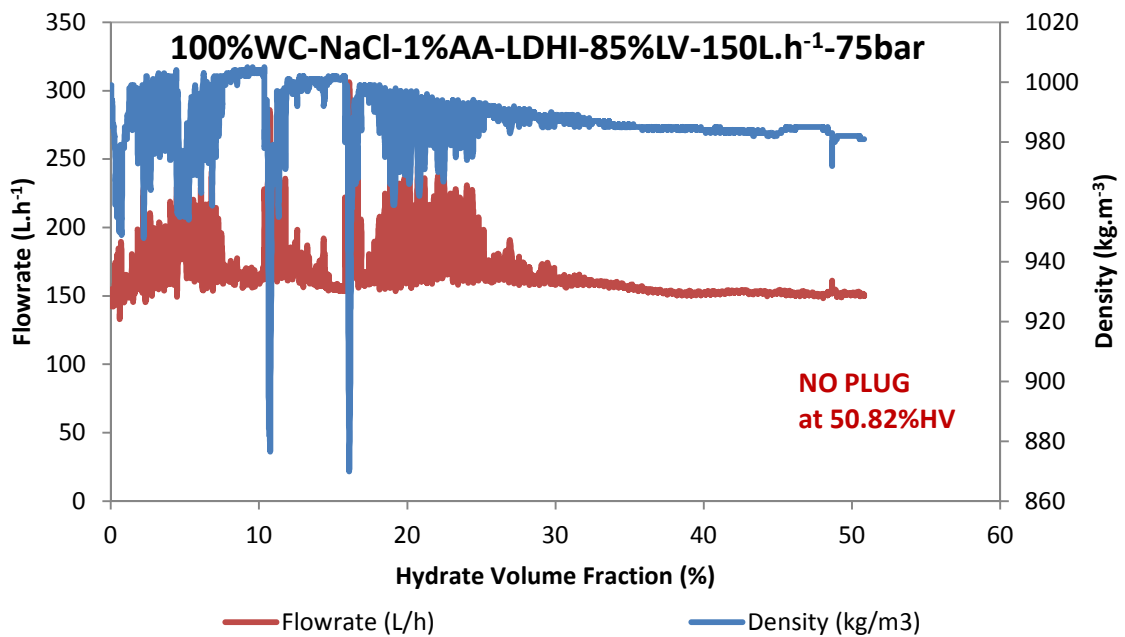
h)



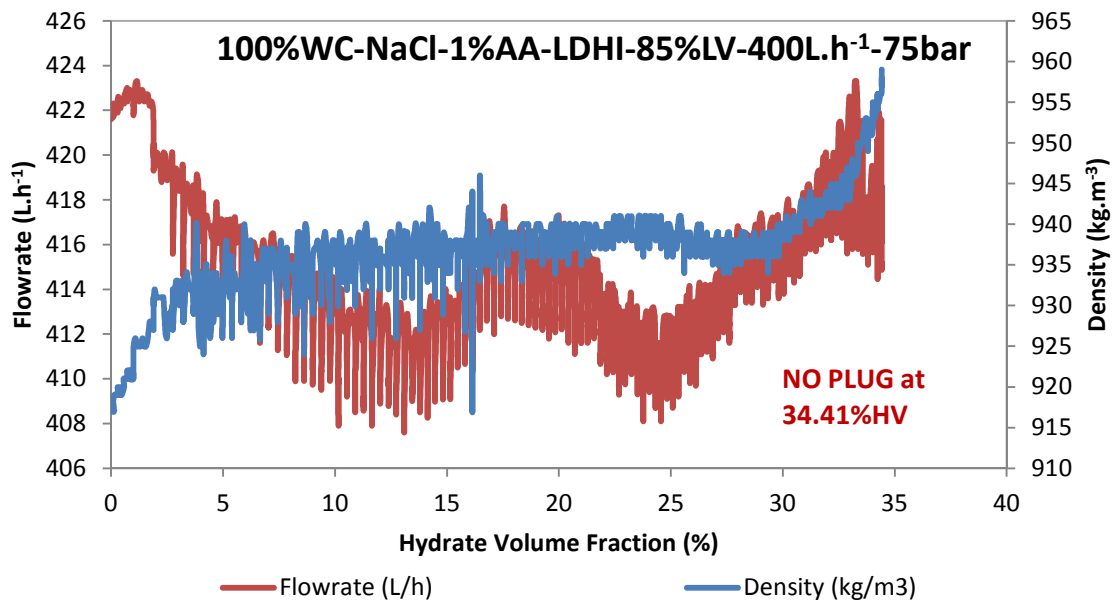
i)



j)



k)

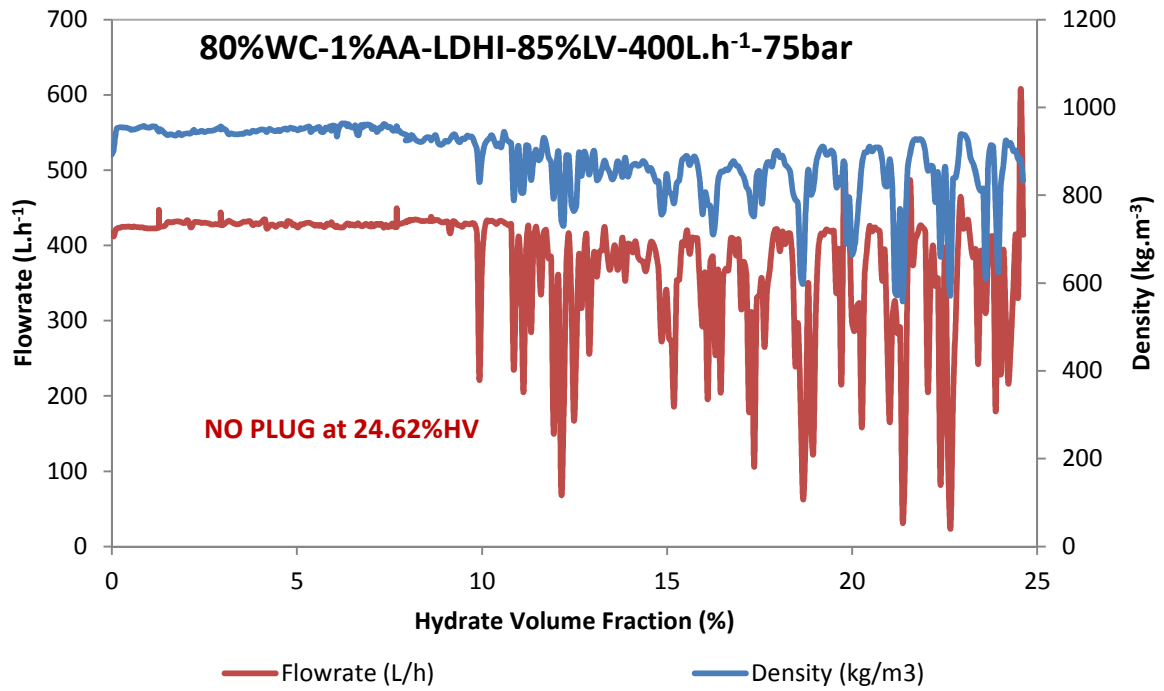


l)

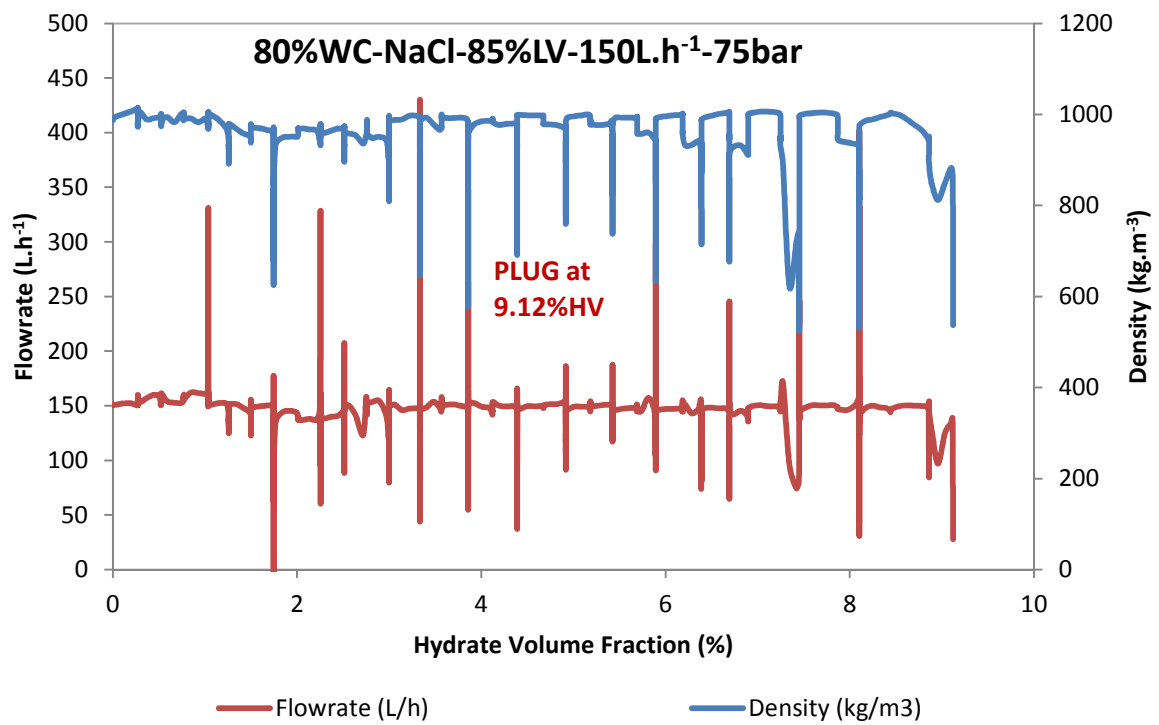
Figure I. 1: Experimental results (a-l) with the Moineau pump protocol (density and flowrate as a function of hydrate volume fraction) with 100%WC.

## I.2. Experiments with 80%WC

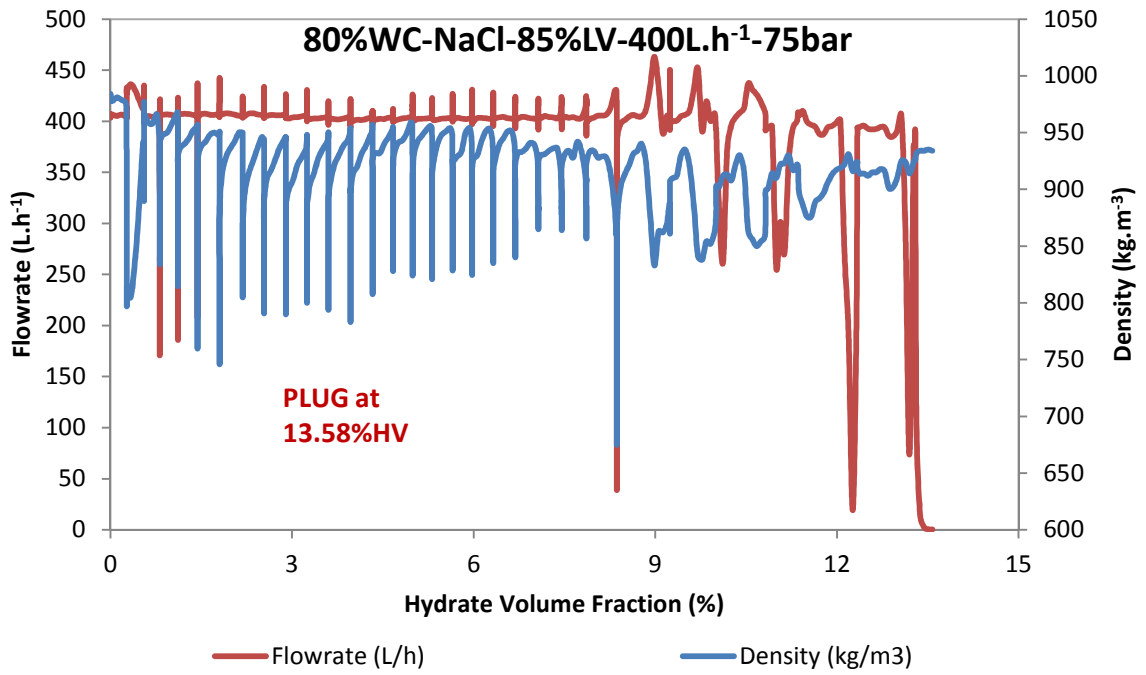
The experimental results (density & flowrate) at 80%WC with the Moineau pump protocol are shown in Figure I. 2.



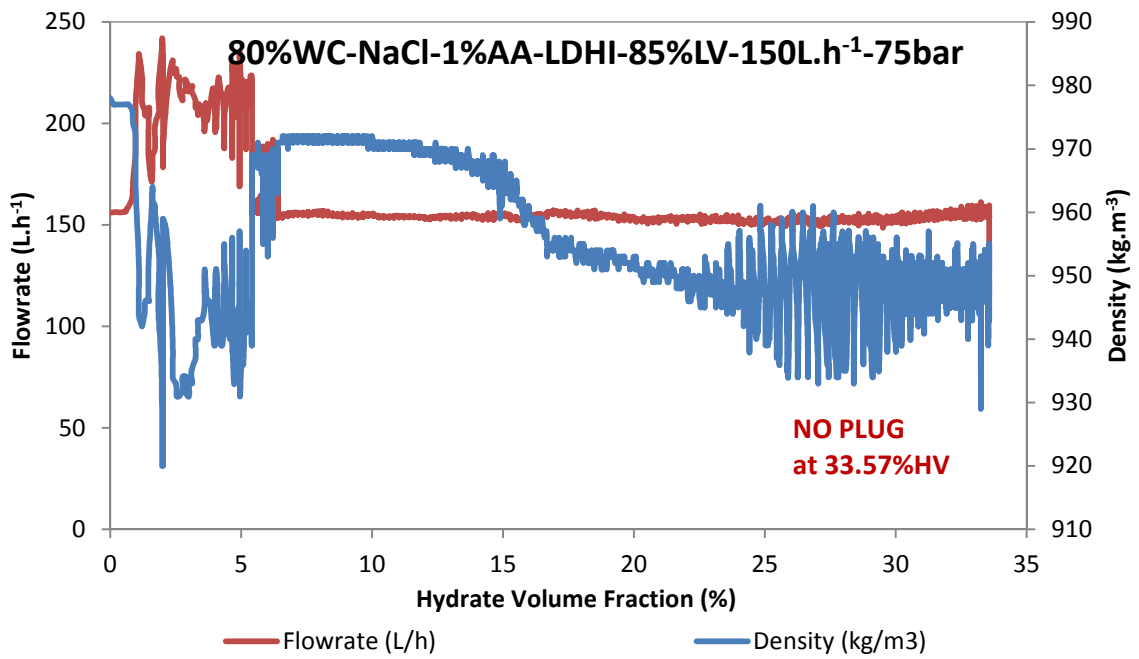
a)



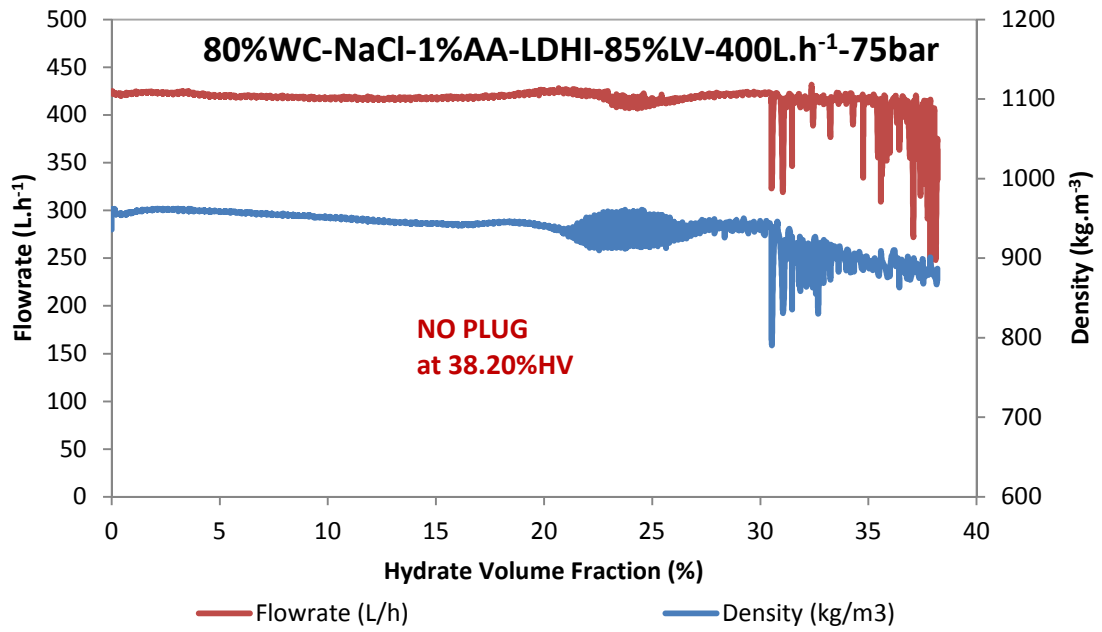
b)



c)



d)



e)

Figure I. 2: Experimental results (a-e) with the Moineau pump protocol (density and flowrate as a function of hydrate volume fraction) with 80%WC.

## Appendix J – Gas transfer coefficient ( $k_L a$ )

The rate of gas transfer into the liquid of all tests at 50-60-66-70-75-80 bar,  $4.5 \pm 0.5^\circ\text{C}$  (before gas hydrate formation) with the Moineau pump protocol is shown in Table J. 1.

**Table J. 1: Gas transfer coefficients at different pressures and  $4.5 \pm 0.5^\circ\text{C}$  with the Moineau pump protocol (before crystallization).**

WC	Flowrate	Liquid Volume	Pressure	AA-LDHI	NaCl	$k_L a$	Coefficient of multiple determination
(%)	(L.h <sup>-1</sup> )	(%)	(bar)	(wt.% of water)	(g.L <sup>-1</sup> (H <sub>2</sub> O))	(s <sup>-1</sup> )	(R <sup>2</sup> )
100	150	100	50	0	0	0.0573 (GL)	0.9778
	150	100	60	0	0	0.0323 (GL)	0.3204
	150	85	66	0	0	0.0551	0.8191
	150	85	75	0	0	0.0441	0.9566
	150	85	75	0.01	0	0.0526	0.9449
	150	85	75	0.05	0	0.0476	0.9514
	150	90	75	0.05	0	0.055	0.9164
	150	100	75	0.05	0	0.0213	0.7059
	150	85	75	0.50	0	0.0537	0.9354
	400	85	75	0.50	0	-	-
	150	85	75	1	0	-	-
	400	85	75	1	0	0.0470	0.9656
	150	85	75	2	0	0.0520	0.9350
	400	85	70	2	0	-	-
	400	85	75	2	0	0.0491	0.9278
	150	85	75	0	30	0.0547	0.9710
	150rp(1)*	85	75	0	30	0.0482	0.9597
	400	85	75	0	30	0.0519	0.9370
	150	85	75	0.50	30	0.0436	0.9322
	400	85	75	0.50	30	0.0473	0.9427
150	85	75	1	30	0.0552	0.9170	
150rp(1)*	85	75	1	30	0.0456	0.9584	
400	85	75	1	30	0.0573	0.9394	
80	150	85	75	0	0	0.0495	0.9652
	400	85	75	0	0	0.0536	0.9491
	150	85	75	1	0	0.0543	0.9198
	400	85	75	1	0	0.0532	0.9375
	150	85	75	0	30	0.0558	0.9479
	400	85	75	0	30	0.0574	0.9541
	150	85	75	1	30	-	-
	400	85	75	1	30	0.0570	0.9158
	200rp(2)*	100	80	0	0	0.0554	0.8707

WC	Flowrate	Liquid Volume	Pressure	AA-LDHI	NaCl	$k_L a$	Coefficient of multiple determination
(%)	(L.h <sup>-1</sup> )	(%)	(bar)	(wt.% of water)	(g.L <sup>-1</sup> (H <sub>2</sub> O))	(s <sup>-1</sup> )	(R <sup>2</sup> )
80	400rp(2)*	100	80	0	0	0.0580	0.9571
70	200rp(3)*	100	80	0	0	0.0437	0.9553
	400rp(7)*	100	80	0	0	0.0462	0.9604

\*rp(x): the repeated experiments, x: number of repeats; GL: Gas-Lift.

This was observed that the  $k_L a$  of the experiments with 100%WC and 150L.h<sup>-1</sup> with the gas-lift was not much different from that without gas-lift. This was explained by lower pressure and higher liquid volume. Generally, experimental results showed that the higher the flowrate, the higher value of  $k_L a$ . This was explained by higher contact surface between gas and liquid in the separator at higher flowrate. Moreover, addition of AA-LDHI improved gas transferring into liquid for all experiments (an increase in  $k_L a$ ). This was probably due to AA-LDHI changed surface properties of liquid (lowered the interfacial tension between gas and liquid phase) (C. Y. Sun et al., 2004) which enhanced gas transfer (Albal, 1983). The increase in the amount of oil increased the  $k_L a$ . This was interpreted by oil phase consumed (dissolved) gas better than water phase leading to an increase in  $k_L a$  once oil was added.

École Nationale Supérieure des Mines de Saint-Étienne

NNT: 2018LYSEM012

Trung-Kien PHAM

## **EXPERIMENTAL STUDY AND MODELLING ON METHANE HYDRATES CRYSTALLIZATION UNDER FLOW FROM A WATER-OIL DISPERSION AT HIGH WATER CUT**

Speciality: Process Engineering

**Keywords:** Dispersion, Gas bubble, Multiphase flow, Gas hydrate formation, Agglomeration, Deposition, Plug, Anti-agglomerants, Suspension, and Hydrate slurry transport.

### **ABSTRACT**

Production of crude oil with natural gas and water at low temperature and high pressure favors conditions for gas hydrate formation which might cause many troubles in flow assurance, up to blockage of pipelines. To prevent plugging, varieties of methods are applied to flowlines by addition of thermodynamic inhibitors (THIs), kinetic hydrate inhibitors (KHIs) and anti-agglomerants (AAs). Recently, AAs are more widely used due to not only their high performance under severe conditions but also the reduction in costs of operation at low dosage (AA-LDHIs). Mostly, previous studies on gas hydrate formation and transport have focused on low water cuts and without anti-agglomerants. On the contrary, at high water cuts, the gas hydrate formation and transport in the presence of AA-LDHI and/or salt in pipelines are not widely understood.

The principal objective of this study is a better understanding of hydrate formation and plugging by testing the role of commercial additives to avoid plugging. In details, this work deals with the hydrate kinetics of crystallization and agglomeration together with hydrate slurry transport and deposition under flowing conditions (especially at high water cuts). Effects of various parameters were studied, including the amount of commercial anti-agglomerants (AA-LDHIs), water volume fraction, and water salinity in a mixture of Kerdane<sup>®</sup> oil and water. The experiments were performed in the "Archimède" 80 bar - pilot scale flowloop which reproduces the conditions in oil and gas transport in subsea pipelines. The experimental apparatus is equipped with a FBRM (Focused Beam Reflectance Measurement) and a PVM (Particle Video Microscope) probe and temperature, pressure drop, flowrate and density sensors. The flow was induced through a Moineau pump and/or a "gas-lift" system. The results revealed that with the gas-lift protocol; hydrates formed on the surface of gas bubbles and water droplets and they were transported in oil and water continuous phases. Generally, the hydrates tend to deposit at high water cut and agglomerate at low water cut. Mechanisms of hydrate formation and transport with and without AA-LDHI in bubble conditions were proposed. With Moineau pump protocol; effects of hydrate formation, agglomeration, deposition and plugging on multiphase flow and vice versa were identified, analyzed and evaluated at high water cuts. Several mechanisms of hydrate formation and transport were also proposed. A model was developed in order to predict the relative pressure drop in flowlines once hydrate formed.

Trung-Kien PHAM

## **ETUDE EXPERIMENTALE ET MODELISATION DE LA CRISTALLISATION D'HYDRATES DE METHANE EN ECOULEMENT A PARTIR D'UNE DISPERSION EAU-HUILE A FORT POURCENTAGE D'EAU**

Spécialité: Génie des Procédés

Mots clefs : Dispersion, Bulle de gaz, Ecoulement multiphasique, Formation d'hydrates de gaz, Agglomération, Déposition, Bouchage, Anti-agglomérants, Suspension, et Transport de sorbets d'hydrate.

### **RÉSUMÉ (IN FRENCH)**

La production de pétrole brut avec du gaz naturel et de l'eau à basse température et à haute pression favorise les conditions de formation d'hydrates de gaz qui peuvent causer de nombreux problèmes d'écoulement jusqu'au blocage des pipelines. Pour éviter le bouchage, diverses méthodes sont appliquées aux pipelines par addition d'inhibiteurs thermodynamiques (THIs), cinétiques (KHIs) et d'antiagglomérants (AAs). Récemment, l'utilisation des AAs est devenue plus courante car non seulement à cause de leur haute performance dans des conditions sévères, mais aussi grâce à la réduction du coût d'opération dû à avec une faible dose d'AAs utilisée (AA-LDHIs). La plupart des études antérieures sur la formation et transport d'hydrates de gaz se limitent à de faibles fractions d'eau et sans antiagglomérants. Pour des fortes fractions d'eau, la formation et le transport d'hydrates de gaz en présence d'AA-LDHI et/ou de sel dans les conduites d'écoulement restent mal compris.

L'objectif principal de cette étude est une meilleure compréhension de la formation et de l'agglomération des hydrates, en testant l'influence des additifs commerciaux pour éviter le colmatage. Ce travail traite plus précisément de la cinétique de cristallisation et d'agglomération des hydrates, ainsi que du transport et du dépôt des suspensions en fonction des conditions d'écoulement (en particulier dans les systèmes à haute fraction d'eau). Les effets de divers paramètres sont étudiés, notamment : à faible dose d'antiagglomérant (AA-LDHI), et fraction volumique d'eau et de salinité dans l'eau variables dans un mélange avec du Kerdane®. Des expériences ont été menées dans la boucle "Archimède". Cet appareillage, capable de fonctionner à plus de 80 bar, permet de reproduire les conditions de transport de pétrole et de gaz dans les pipelines sous-marins. Il est équipé d'une sonde FBRM (Focused Beam Reflectance Measurement) et d'une sonde PVM (Particle Video Microscope) ainsi que de capteurs de température, de perte de charge, de débit et de masse volumique. La mise en circulation du fluide est assurée par une pompe Moineau et/ou un système dit de "gaz-lift". Les résultats ont révélé que dans le protocole avec gaz-lift, les hydrates se forment à la surface des bulles de gaz et des gouttelettes d'eau et leur transport a lieu dans les phases continues d'huile ou d'eau. Généralement, les hydrates ont tendance à se déposer à haute fraction d'eau et à s'agglomérer à une faible fraction d'eau. Des mécanismes de formation et transport des hydrates en présence de bulles ont été proposés. Dans le protocole avec pompe Moineau, les effets de la formation des hydrates, de l'agglomération, du dépôt et du colmatage dans le cadre d'un écoulement multiphasique et vice-versa ont été identifiés, analysés et évalués à fort pourcentage d'eau. Quelques mécanismes de formation et transport d'hydrates dans des conditions expérimentales différentes sont aussi proposés. Un modèle a été développé pour prédire la perte de charge relative dans les pipelines une fois l'hydrate formé.